AN ABSTRACT OF THE DISSERTATION OF

Arijit Sinha for the degree of Doctor of Philosophy in Wood Science and Civil Engineering presented on September 10, 2010.

Title: The Effect of Elevated Temperature on Mechanical Behavior of Structural Wood and Wood-based Composites.

Abstract approved:

_____

John A. Nairn Rakesh Gupta

Engineers, in practice, are often faced with the challenge of evaluating a fire-damaged structure and developing a rehabilitation and retrofit plan. In order to decide on a rehabilitation and retrofit plan, information on thermal degradation of building materials and connections are vital. A critical knowledge gap exists in terms of thermal degradation of materials and connections with respect to light-frame wood construction. Along with solid sawn lumber (SSL), various wood-based composites such as plywood, oriented strand board (OSB) and laminated veneer lumber (LVL) are also used in wood-frame construction. Characterization of the thermal degradation of strength of these structural materials will help assess the service life and strength of the damaged structure. This study addressed the thermal degradation of material strength and connection strength by conducting tests on wood, wood-based composites and connections after subjecting them to elevated temperatures, hence studying the post-fire residual strength in wood and wood composite construction. The properties evaluated in this study were bending strength (MOR), bending stiffness (MOE), lateral nail capacity, dowel bearing strength, fracture toughness and bond strength (IB) after exposing the materials to elevated temperature for various exposure times. In addition, the bending strength of OSB and plywood was studied in great detail as a function of additional temperatures and exposure times.

A general trend of degrading bending properties, fracture toughness, dowel bearing strength of materials and yield strength of the connections of various configurations with high temperature and duration of exposure was observed and confirmed by statistical analysis. A statistical regression based model incorporating the effects of temperature,

time of exposure and thier interaction and a model based on first-order kinetics were developed and evaluated for predicting the strength loss. The kinetics-based model was better than the regression-based approach. Using the kinetics analysis along with time-temperature superposition for OSB and plywood, a master curve was generated at a reference temperature of 150^{o}C that can be used for residual strength estimates and failure time predictions. A reasonable prediction of connection design values was made using National Design Specifications (NDS) yield models for thermally degraded materials. Conventional tests for bond strength provided excessive scatter which renders any statistical comparison highly difficult. An alternative to IB and bond classification could be fracture testing using energy methods for wood bond strength evaluation.

The various analytical models developed will help for characterizing the thermal degradation of material properties. Models specified in design codes were evaluated against the thermal degradation of materials. This knowledge of thermal degradation and the models will help engineers and architects in recommending categorical improvement, rehabilitation and retrofit of structures.

THE EFFECT OF ELEVATED TEMPERATURE ON MECHANICAL BEHAVIOR OF STRUCTURAL WOOD AND WOOD-BASED COMPOSITES

by
Arijit Sinha

A DISSERTATION

submitted to

Oregon State University

in partial fulfillment of
the requirements for the
degree of

Doctor of Philosophy

Presented September 10, 2010
Commencement June 2011

Doctor of Philosophy dissertation of Arijit Sinha presented on September 10, 2010

APPROVED:

_____

Co-major Professor, representing Wood Science

_____

Co-major Professor, representing Civil Engineering

_____

Head of the Department of Wood Science and Engineering

_____

Head of the School of Civil and Construction Engineering

_____

Dean of the Graduate School

I understand that my dissertation will become part of the permanent collection of Oregon State University libraries. My signature below authorizes release of my dissertation to any reader upon request.

_____

Arijit Sinha, Author

ACKNOWLEDGMENTS

I would like to express my sincere gratitude and appreciation to the following Individuals and organizations for their support in helping me complete this project:

- Dr. Rakesh Gupta and Dr. John Nairn – for the opportunity to learn from them and develop as an engineering researcher. Moreover, for their invaluable support, guidance and understanding throughout the project.
- Special thanks and sincere gratitude to Dr. Rakesh Gupta for his contribution to both my professional and personal development. His guidance and patience has really motivated me to persevere through difficult periods.
- Wood Based Composite Center – for supporting me and showing the faith in me to endow me as their fellow
- Boise Cascades Company for donating LVL and plywood used in the project
- Milo Clauson – for his help, guidance and support. I have really enjoyed working with Milo, particularly because of his extremely unique and diverse knowledge, sense of humor, and his unflappable optimism.
- Dr. Fred Kamke and Dr. John Simonsen – for their support, encouragement and guidance throughout the project.
- Dr. John Gambatese – I am grateful to him for his patience, understanding and support during testing times.
- Dr. Jason Ideker and Dr. Tona Rodriguez-Nikl – for their help and support.
- Dr. Thomas McLain – has been very supportive and I really enjoyed the interaction with him on career and life in general
- Dr. Mike Milota and Dr. Lech Muszynski – for allowing me to use their lab space and equipments
- Dr. Claire Montgomery – for her participation in my committee
- Rand Sether – for his help in sample preparation
- WSE faculty and Staff – for making my stay at OSU memorable
- Department of Statistics, OSU – for their guidance during the experimental design stage
- Fellow Graduate Students – for the invaluable support and their help in the lab.
- All of my family and friends.

CONTRIBUTION OF AUTHORS

Dr. Rakesh Gupta and Dr. John A. Nairn were involved in all aspects of the work leading to this dissertation including advising on data collection, analysis and help in writing the manuscripts.

TABLE OF CONTENTS

Page

Chapter 1. General Introduction 1

Chapter 2: Thermal Degradation of Bending Properties of Structural Wood and Wood-Based Composites 6

Abstract 6

Keywords 6

Introduction 7

Background 8

Material and Methods 10

Results and Discussion 12

Static bending Test 12

Analytical Models 13

Regression Model 14

Kinetics-Based Model 15

Validation and Comparisons of Models 17

Conclusion 18

References 19

Chapter 3: Thermal Degradation of Bending Strength of Plywood and Oriented Strand Board: A Kinetics Approach 29

Abstract 29

Introduction 29

Materials and Methods 31

Results and Discussion 32

Bending Tests 32

Degradation Kinetics Modeling 35

Master Curve Analysis 36

Conclusions 41

Acknowledgements 41

References 41

Chapter 4: Thermal Degradation of Lateral Yield Strength of Nailed Wood Connections 52

Abstract 52

Introduction 53

Materials and Methods 55

TABLE OF CONTENTS (Continued)

Page

Design of Experiment 55
Test Specimen 56
Test Procedures 58
Lateral Load Tests 58
Dowel Bearing Strength (Embedment strength of Wood) 59
Results and Discussion 59
Design Values Using Yield Models 61
Yield Modes 63
Conclusions 65
Acknowledgements 65
References 66
Chapter 5: Fracture toughness of wood and structural wood-based composites using R curve analysis 81
Abstract 81
Introduction 82
Material and Methods 82
Materials 87
Testing Methods 88
Internal Bond 88
Bond Classification for Plywood 88
Fracture 88
R curve Analysis 89
Results and Discussion 90
Steady State Strain Energy Release Rate (G_{SS}) 90
Solid Sawn Lumber 90
Wood Composites 91
Failure Modes and R Curves 93
Effect of Elevated temperature 94
IB and bond Classification Test 95
Conclusions 97
References 98

TABLE OF CONTENTS (Continued)

Page

Chapter 6: General Conclusions 111
Implications 114
Limitations and Pitfalls 115
Recommendations for future research 117
Bibliography 119
Appendices 128
Appendix A 129
Appendix B 150
Appendix C 178
Appendix D 244

LIST OF FIGURES

Figure Page

2.1. Static Third point bending test set-up 26
2.2. ln(k) vs. inverse of absolute temperature plot for all the materials. 27
3.1. Third Point Bending set-up 45
3.2. MOR of OSB as a function of exposure time at 191^{o}C 45
3.3. Summary of all bending test 46
3.4. The calculated strength loss after 8 h of exposure 47
3.5. Arrhenius activation energy plot for ln $k(T)$ as a function of 1/T 47
3.6. Shift factors, log a_T, vs. T (C) 48
3.7. Master curve for degradation in strength (MOR) of plywood 49
3.8. Master curve for degradation in strength (MOR) of OSB 50
4.1. Typical Load deflection diagram 73
4.2. Connection Geometries 74
4.3. Lateral Nail connection test set up 75
4.4. Dowel Bearing Test Set up 76
4.5. Variation in yield strength (N) 77
4.6. Weight loss (%) for various members 78
4.7. Observed yield modes of laterally loaded nail connections 79
5.1. R curve analysis procedure 105
5.2. Fracture test set up 106
5.3. R curves (G_{IC}) as a function of crack length 107
5.4 Failure modes for wood and wood composites 108
5.5. G_{IC} as a function of time 109
5.6. Internal bond and Bond classification values after different treatments 110

LIST OF TABLES

Tables Page

2.1. List of materials, their respective symbols, species, specific gravity and specimen sizes 22
2.2. Summary of average MOR and MOE 23
2.3. Regression Models for various materials 24
2.4. Kinetics based model for degradation of MOR 24
2.5. Goodness-of-fit chi square statistic for regression and kinetics based models 25
3.1. Predicted MOR values and weight loss values after 8 hours of exposure 43
3.2. Log at values used to produce the master curve for plywood and OSB 44
4.1. Experimental design matrix with description of various materials 69
4.2. Yield strength (N) of edge and plate connection geometry for various connections .. 70
4.3. Effect of exposure to elevated temperature on specific gravity 71
4.4. Effect of exposure to elevated temperature on Dowel Bearing Strength 71
4.5. Solid lumber-plywood (SSL-PWH) connection with observed and predicted strength 72
5.1. Details of various materials 103
5.2. G_{SS} (N/m) of all the materials as calculated by R curve analysis 103
5.3. % wood failure in bond classification test for plywood 103

LIST OF APPENDIX FIGURES

Figure Page

A1 Load Deflection curve in bending test for PWO control 130
A2. Load Deflection curve in bending test for PWO 100^{o}C -1hr 130
A3. Load Deflection curve in bending test for PWO 100^{o}C -2hr 131
A4. Load Deflection curve in bending test for PWO 200^{o}C -1hr 131
A5. Load Deflection curve in bending test for PWO 200^{o}C -2hr 132
A6. Load Deflection curve in bending test for PWH Control 132
A7. Load Deflection curve in bending test for PWH 100^{o}C -1hr 133
A8. Load Deflection curve in bending test for PWH 100^{o}C -2hr 133
A9. Load Deflection curve in bending test for PWH 200^{o}C -1hr 134
A10. Load Deflection curve in bending test for PWH 200^{o}C -2hr 134
A11. Load Deflection curve in bending test for OSBO Control 135
A12. Load Deflection curve in bending test for OSBO 100^{o}C -1hr 135
A13. Load Deflection curve in bending test for OSBO 100^{o}C -2hr 136
A14. Load Deflection curve in bending test for OSBO 200^{o}C -1hr 136
A15. Load Deflection curve in bending test for OSBO 200^{o}C -2hr 137
A16. Load Deflection curve in bending test for OSBH Control 137
A17. Load Deflection curve in bending test for OSBH 100^{o}C -1hr 138
A18. Load Deflection curve in bending test for OSBH 100^{o}C -2hr 138
A19. Load Deflection curve in bending test for OSBH 200^{o}C -1hr 139
A20. Load Deflection curve in bending test for OSBO 200^{o}C -2hr 139
A21. Load Deflection curve in bending test for SSL Control 140
A22. Load Deflection curve in bending test for SSL 100^{o}C -1hr 140
A23. Load Deflection curve in bending test for SSL 100^{o}C -2hr 141
A24. Load Deflection curve in bending test for SSL 200^{o}C -1hr 141
A25. Load Deflection curve in bending test for SSL 200^{o}C -2hr 142
A26. Load Deflection curve in bending test for LVL Control 142
A27. Load Deflection curve in bending test for LVL 100^{o}C - 1hr 143
A29. Load Deflection curve in bending test for LVL 200^{o}C - 1hr 144
A30. Load Deflection curve in bending test for LVL 200^{o}C - 2hr 144
B1. Load deflection curves for OSBH at 50^{o}C 151
B2. Load deflection curves for OSBH at 75^{o}C 152
B3. Load deflection curves for OSBH at 100^{o}C 153

LIST OF APPENDIX FIGURES (Continued)

Figure Page

B4. Load deflection curves for OSBH at 125°C 154
B5. Load deflection curves for OSBH at 150°C 155
B6. Load deflection curves for OSBH at 175°C 156
B7. Load deflection curves for OSBH at 183°C 157
B8. Load deflection curves for OSBH at 191°C 158
B9. Load deflection curves for OSBH at 200°C 159
B10. Load deflection curves for PWH at 50°C 160
B11. Load deflection curves for PWH at 75°C 161
B12. Load deflection curves for PWH at 100°C 162
B13. Load deflection curves for PWH at 125°C 163
B14. Load deflection curves for PWH at 150°C 164
B15. Load deflection curves for PWH at 175°C 165
B16. Load deflection curves for PWH at 183°C 166
B17. Load deflection curves for PWH at 191°C 167
B18. Load deflection curves for PWH at 200°C 168
C1. Various connection configurations. 178
C2. Load displacement diagram Edge SSL-OSBO control 179
C3. Load displacement diagram Edge SSL-OSBO 100°C -1hr 179
C4. Load displacement diagram Edge SSL-OSBO 100°C -2hr 180
C5. Load displacement diagram Edge SSL-OSBO 200°C -1hr 180
C6. Load displacement diagram Edge SSL-OSBO 200°C -2hr 181
C7. Load displacement diagram Edge SSL-PWO Control 181
8 Load displacement diagram Edge SSL-PWO 100°C -1hr 182
C9. Load displacement diagram Edge SSL-PWO 100°C -2hr 182
C10. Load displacement diagram Edge SSL-PWO 200°C -1hr 183
C11. Load displacement diagram Edge SSL-PWO 200°C -2hr 183
C12. Load displacement diagram Edge SSL-OSBH Control 184
C13. Load displacement diagram Edge SSL-OSBH 100°C -1hr 184
C14. Load displacement diagram Edge SSL-OSBH 100°C -2hr 185
C15. Load displacement diagram Edge SSL-OSBH 200°C -1hr 185
C16. Load displacement diagram Edge SSL-OSBO 200°C -2hr 186
C17. Load displacement diagram Edge SSL-PWH Contol 186

LIST OF APPENDIX FIGURES (Continued)

Figure Page

C18. Load displacement diagram Edge SSL-PWH 100°C -1hr 187
C19. Load displacement diagram Edge SSL-PWH 100°C -2hr 187
C20. Load displacement diagram Edge SSL-PWH 200°C -1hr 188
C21. Load displacement diagram for Edge SSL-PWH 200°C -2hr 188
C22. Load displacement diagram for Plate SSL-OSBO Control 189
C23. Load displacement diagram for Plate SSL-OSBO 100°C-1hr 189
C24. Load displacement diagram for Plate SSL-OSBO 100°C-2hr 190
C25. Load displacement diagram for Plate SSL-OSBO 200°C-1hr 190
C26. Load displacement diagram for Plate SSL-OSBO 200°C-2hr 191
C27. Load displacement diagram for Plate SSL-PWO Control 191
C28. Load displacement diagram for Plate SSL-PWO 100°C-1hr 192
C29. Load displacement diagram for Plate SSL-PWO 100°C-2hr 192
C30. Load displacement diagram for Plate SSL-PWO 200°C-1hr 193
C31. Load displacement diagram for Plate SSL-PWO 200°C-2hr 193
C32. Load displacement diagram Plate SSL-OSBH Control 194
C33. Load displacement diagram for Plate SSL-OSBH 100°C-1hr 194
C34. Load displacement diagram for Plate SSL-OSBH 100°C-2hr 195
C35. Load displacement diagram for Plate SSL-OSBH 200°C-1hr 195
C36. Load displacement diagram for Plate SSL-OSBH 200°C-2hr 196
C37. Load displacement diagram for Plate SSL-PWH Control 196
C38. Load displacement diagram for Plate SSL-PWH 100°C-1hr 197
C39. Load displacement diagram for Plate SSL-PWH 100°C-2hr 197
C40. Load displacement diagram for Plate SSL-PWH 200°C-1hr 198
C41. Load displacement diagram for Plate SSL-PWH 200°C-2hr 198
C42. Load displacement diagram for Edge LVL-OSBO Control 199
C43. Load displacement diagram for Edge LVL-OSBO 100°C-1hr 199
C44. Load displacement diagram for Edge LVL-OSBO 100°C-2hr 200
C45. Load displacement diagram for Edge LVL-OSBO 200°C-1hr 200
C46. Load displacement diagram for Edge LVL-OSBO 200°C-2hr 201
C47. Load displacement diagram for Edge LVL-PWO Control 201
C48. Load displacement diagram for Edge LVL-PWO 100°C-1hr 202
C49. Load displacement diagram for Edge LVL-PWO 100°C-2hr 202

LIST OF APPENDIX FIGURES (Continued)

Figure Page

C50. Load displacement diagram for Edge LVL-PWO 200°C-1hr 203
C51. Load displacement diagram for Edge LVL-PWO 200°C-2hr 203
C52. Load displacement diagram for Edge LVL-OSBH Control 204
C53. Load displacement diagram for Edge LVL-OSBH 100°C-1hr 204
C54. Load displacement diagram for Edge LVL-OSBH 100°C-2hr 205
C55. Load displacement diagram for Edge LVL-OSBH 200°C-1hr 205
C56. Load displacement diagram for Edge LVL-OSBH 200°C-2hr 206
C57. Load displacement diagram for Edge LVL-PWH Control 206
C58. Load displacement diagram for Edge LVL-PWH 100°C-1hr 207
C59. Load displacement diagram for Edge LVL-PWH 100°C-2hr 207
C60. Load displacement diagram for Edge LVL-PWH 200°C-1hr 208
C61. Load displacement diagram for Edge LVL-PWH 200°C-2hr 208
C62. Load displacement diagram for Plate LVL-OSBO Control 209
C63. Load displacement diagram for Plate LVL-OSBO 100°C-1hr 209
C64. Load displacement diagram for Plate LVL-OSBO 100°C-2hr 210
C65. Load displacement diagram for Plate LVL-OSBO 200°C-1hr 210
C66. Load displacement diagram for Plate LVL-OSBO 200°C-2hr 211
C67. Load displacement diagram for Plate LVL-PWO Control 211
C68. Load displacement diagram for Plate LVL-PWO 100°C-1hr 212
C69. Load displacement diagram for Plate LVL-PWO 100°C-2hr 212
C70. Load displacement diagram for Plate LVL-PWO 200°C-1hr 213
C71. Load displacement diagram for Plate LVL-PWO 200°C-2hr 213
C72. Load displacement diagram for Plate LVL-OSBH Control 214
C73. Load displacement diagram for Plate LVL-OSBH 100°C-1hr 214
C74. Load displacement diagram for Plate LVL-OSBH 100°C-2hr 215
C75. Load displacement diagram for Plate LVL-OSBH 200°C-1hr 215
C76. Load displacement diagram for Plate LVL-OSBH 200°C-2hr 216
C78. Load displacement diagram for Plate LVL-PWH Control 216
C78. Load displacement diagram for Plate LVL-PWH 100°C-1hr 217

LIST OF APPENDIX FIGURES (Continued)

Figure Page

C79. Load displacement diagram for Plate LVL-PWH 100°C-2hr 217
C80. Load displacement diagram for Plate LVL-PWH 200°C-1hr 218
C81. Load displacement diagram for Plate LVL-PWH 200°C-2hr 218
C82. Dowel Bearing load deflection diagram for OSBH Control 219
C83. Dowel Bearing load deflection diagram for OSBH 100°C – 1hr 219
C84. Dowel Bearing load deflection diagram for OSBH 100°C – 2hr 220
C85. Dowel Bearing load deflection diagram for OSBH 200°C – 1hr 220
C86. Dowel Bearing load deflection diagram for OSBH 200°C – 2hr 221
C87. Dowel Bearing load deflection diagram for OSBO Control 221
C88. Dowel Bearing load deflection diagram for OSBO 100°C – 1hr 222
C89. Dowel Bearing load deflection diagram for OSBO 100°C – 2hr 222
C90. Dowel Bearing load deflection diagram for OSBO 200°C – 1hr 223
C91. Dowel Bearing load deflection diagram for OSBO 200°C – 2hr 223
C92. Dowel Bearing load deflection diagram for PWH Control 224
C93. Dowel Bearing load deflection diagram for PWH 100°C – 1hr 224
C94. Dowel Bearing load deflection diagram for PWH 100°C – 2hr 225
C95. Dowel Bearing load deflection diagram for PWH 200°C – 1hr 225
C96. Dowel Bearing load deflection diagram for PWH 200°C – 2hr 226
C97. Dowel Bearing load deflection diagram for PWO Control 226
C98. Dowel Bearing load deflection diagram for PWO 100°C – 1hr 227
C99. Dowel Bearing load deflection diagram for PWO 100°C – 2hr 227
C100. Dowel Bearing load deflection diagram for PWO 200°C – 1hr 228
C101. Dowel Bearing load deflection diagram for PWO 200°C – 2hr 228
C102. Dowel Bearing load deflection diagram for SSL Control 229
C103. Dowel Bearing load deflection diagram for SSL 100°C – 1hr 230
C104. Dowel Bearing load deflection diagram for SSL 100°C – 2hr 231
C105. Dowel Bearing load deflection diagram for SSL 200°C – 1hr 232
C106. Dowel Bearing load deflection diagram for SSL 200°C – 1hr 233
C107. Dowel Bearing load deflection diagram for LVL Control 234
C108. Dowel Bearing load deflection diagram for LVL 100°C – 1hr 234
C109. Dowel Bearing load deflection diagram for LVL 100°C – 2hr 235
C110. Dowel Bearing load deflection diagram for LVL 200°C – 1hr 235

LIST OF APPENDIX FIGURES (Continued)

Figure Page

C111. Dowel Bearing load deflection diagram for LVL 200^{o}C – 2hr 236

D1. Load Deflection Curves in fracture test for SSL 248

D2. Load Deflection curves in fracture tests for LVL 249

D3. Load Deflection Curves in fracture for OSBH 250

D4. Load deflection curves in fracture tests for OSBO 251

D5. Load Deflection Curves in fracture for PWH 252

D6. Load Deflection Curves in fracture for PWO 253

LIST OF APPENDIX TABLES

Table Page

A1. Test Matrix for manuscript 1 and 4 129
A2. Data for Bending Tests for control 145
A3. Data for bending tests 100^{o}C -1h 146
A4. Data for bending tests 100^{o}C -2h 147
A5. Data for bending tests 200^{o}C -1h 148
A6. Data for bending tests 200^{o}C -2h 149
B1. Test Matrix for Chapter 3 150
B2. 50^{o}C Bending Data 169
B3. 75^{o}C Bending Data 170
B4. 100^{o}C Bending Data 171
B5. 125^{o}C Bending Data 172
B6. 150^{o}C Bending Data 173
B7. 175^{o}C Bending Data 174
B8. 183^{o}C Bending Data 175
B9. 191^{o}C Bending Data 176
B10. 200^{o}C Bending Data 177
C1. Test data for all connection using framing member SSL 237
C2. Test data for all connection using framing member LVL 238
C3. Dowel Bearing Strength Data 239
C4. ANOVA table for yield strength 240
C5. Family-wise comparison of treatment for yield strength 240
C6. Design Load predictions using NDS yield models equations 241
D1. Internal Bond Results for OSBH 244
D2. Internal Bond Results for OSBO 245
D3. Bond Classification Test results for PWH 246
D4. Bond Classification Test results for PWO 247
D5. G_{SS} (N/m) for various materials and treatment 248

Effect of Elevated Temperature on Mechanical Behavior of Structural Wood and Wood-based Composites

Chapter 1. General Introduction

Wood is an important building material. Most low-rise single family residential dwellings in the United States are wood frame construction. In contemporary wood frame construction, the main system resisting lateral force as well as vertical forces is a shear wall framed of solid sawn lumber (SSL). Due to an increasing demand for high quality and uniform structural lumber, many engineered wood composites developed in recent years, such as laminated veneer lumber (LVL) are also used for framing. Wood-based composites, such as oriented strand board (OSB) and plywood are the main structural composite panels in both residential and commercial timber construction. OSB is also widely used as the web in I-joists. The use of wood-based composites in low-rise, single-family dwellings is increasing. As a result, they represent an increasing share of the wood products market (White and Winandy 2006). OSB has taken a major market share from plywood during the last two decades and still is driven by strong demand (APA 2005).

Fire results in approximately 8 billion dollars in structural losses each year in residential structures. Additionally, it results in an average of 3500 civilian casualties (NFPA 2010). Most (92%) of these losses occur in single and two-family residential dwellings, which are predominantly wood-frame structures (NFPA 2010). It is highly important to examine the fire design of these wood-frame structures. Fire is a special design case because it is not a direct loading. Instead, fire is a condition that can have drastic impact on load carrying capacity of a structure (Cramer and White 1997). The main objective of fire resistant structural design is to ensure that structural integrity is maintained to provide for a means of egress for the inhabitants. Another objective of fire resistant design deals with rehabilitation of the partially burnt structure. When encountering a fire damage building, engineers are faced with the challenge to evaluate and design a rehabilitation plan. Knowledge of residual strength of the damaged material is required to decide between reuse and replacement.

Limited information is available regarding the thermal degradation of strength of building materials as a result of exposure to elevated temperatures (Buchanan 2002). Understanding and predicting material behavior after exposure to elevated temperatures is important to ultimately developing a post-fire rehabilitation plan. The information available is limited to solid wood. Solid wood performs well during fire and maintains a substantial part of its load-bearing

capacity and stability during exposure to fire. Its excellent properties are due to its low conductivity and formation of char on initial exposure to fire which prevents further burning. Several studies have modeled (White 1988, White and Nordheim 1992, AFPA 2003) and experimentally verified (White and Tran 1996, White 2006) the residual strength of solid wood based on the reduced cross sectional area. Studies have also suggested that strength of solid sawn lumber decreases when subjected to elevated temperature (Green et al. 1999, Buchanan 2002). On the other hand, the fire performance and post fire integrity of various engineered wood composite products has been continuously challenged (Grundahl 1992) and less studied. Questions have been raised by the fire research community on the performance of these products, because they are less massive and hence, less likely to resist a rapid temperature increase as compared to solid timber (Cramer and White 1997). As the use of wood-based composites in building construction is increasing, it is important to categorize their response when exposed to elevated temperatures (White and Winandy 2006). Hence more studies on the effect of fire and elevated temperature on various properties of wood-based composites are needed.

Fire-design is moving towards performance-based fire safety regulations and away from prescriptive codes, which are predominantly used in United States. New Zealand was one of the pioneers in performance based fire safety code (Buchanan and Barnett 1995). Other countries such as Japan, United Kingdom and Australia have followed New Zealand and incorporated performance-based fire safety regulations in their design process (Buchanan 2002). In performance-based design (PBD), performance criterions need to be agreed upon and then the structure is designed to achieve needed minimum results. The performance-based codes empower the designer with the possibility of a wide array of solution strategies for providing fire safety (Bukowski and Babrauskas 1994). However, such an array of solution strategies only comes from an understanding of fire performance and development of reliable calculation procedures to predict fire performance. The only way to predict performance is by simulation of the building behavior, using integrated data models. This requires a database of structural testing on various components of buildings, which will be used in developing and validating fire endurance models and numerical models for simulation of post-fire building performance. Knowledge of the thermal degradation of materials represents one of the most critical gaps in the development of fire endurance models (Cramer and White 1997).

The wood structural fire research community has emphasized the need for research on fire endurance. The fire endurance research is twofold. First, it deals with calculation of survival

time of the structure. Second, it deals with post-fire residual strength of the structure. Determination of residual strength of structure is based on information available on all components of structure, mainly, thermal degradation of materials and thermal degradation of connections. Knowledge of both is required to assess whether the damaged structure has to be rebuilt completely, or if some part of it can be reused. There is a significant interest worldwide in better understanding of the thermal degradation of strength of materials and connections, particularly, with the economics involved in rehabilitating and retrofitting of damaged structures. Characterization of the thermal degradation of strength of a structural material will help assess the service life and strength of the structure. Additionally, this knowledge will be the basis of recommending categorical improvement, rehabilitation or retrofit of the structure.

This study addressed specifically the aspect of thermal degradation of material strength and connection strength by conducting various tests on wood and wood-based composites and connections between them, after subjecting them to various temperatures, hence studying the post-fire residual strength in wood and wood composite construction. The properties evaluated in this study were bending strength, bending stiffness, lateral nail capacity, dowel bearing strength, fracture toughness and bond strength, after exposing the materials to elevated temperature for various exposure times. The specific objectives of this study were to:

1. investigate the changes in bending properties of wood and various wood-based composites due to exposure to elevated temperature for different exposure times,
2. develop prediction models using either multiple linear regressions or a kinetics based approach and compare the prediction capabilities of the two models,
3. study the effect of various exposure time on bending strength, modulus of rupture (MOR) of OSB and plywood at additional elevated temperatures,
4. interpret relationships between different temperature and time of exposure using a kinetics model for thermal degradation of strength,
5. develop a master curve representing temporal behavior of OSB and plywood at any reference temperature,
6. study the effect on the yield strength of laterally loaded framing to sheathing nailed connections after exposure to elevated temperatures for various time periods,
7. determine whether existing yield models can be used to predict the nominal design capacity for the exposed connections,

8. use energy methods with crack propagation (rather than initiation) and a rising R curve analysis to characterize and compare the fracture properties of wood and various wood-based composites,
9. study the effect of elevated temperature on fracture properties of these materials and
10. assess whether fracture test can be used as an alternative to convention bond strength test such as IB and bond classification.

ORGANIZATION

The results of this study are presented in four manuscripts. Supporting data and tables for these manuscripts are presented in series of supporting appendices. The first manuscript (Chapter 2) is “Thermal degradation of bending properties of wood and wood-based composites.” It presents the results from the static bending tests conducted on wood, plywood, OSB and LVL after subjected to elevated temperatures. Two methods to determine the residual strength and stiffness of these materials are discussed and compared. The second manuscript (Chapter 3) is “Thermal Degradation of Bending Strength of OSB and plywood: A kinetics approach.” It presents the results from static bending test conducted as a function of exposure time and elevated temperature on OSB and plywood. A first-order kinetics based thermal degradation model is presented and used along with the principles of time temperature superposition to develop predictive master plots. These master plots serve as predictive tools to predict thermal degradation of strength. The third manuscript (Chapter 4) is “Thermal Degradation of Lateral yield Strength of nailed wood connections.” It describes the results from monotonic tests of two different geometries of sheathing-to-framing nailed connections at increasing levels of thermal degradation. A comparison is made to existing yield models and their adequacy is discussed. The fourth manuscript (Chapter 5) is “Fracture toughness of wood and structural wood-based composites using R curve analysis.” It characterizes the fracture toughness of wood and various wood composites. It further presents the effects of increasing thermal degradation on bond strength and energy release rate for crack propagation. Whether a fracture mechanics approach is a better way to evaluate bond strength is discussed. The appended information is intended to supplement the manuscripts.

Thermal Degradation of Bending Properties of Structural Wood and Wood-Based Composites

Arijit Sinha, Rakesh Gupta and John A Nairn

Holzforschung
Walter de Gruyter GmbH & Co. KG
Genthiner Straße 13
D-10785 Berlin / Germany

Accepted for publication on July 27, 2010
Published Online: DOI 10.1515/HF.2011.001

Chapter 2: Thermal Degradation of Bending Properties of Structural Wood and Wood-Based Composites

Arijit Sinha[1*], Rakesh Gupta[2] and John A. Nairn[2]

Abstract

Wood and wood-based composites are being used heavily in single family residential dwellings. Therefore, it is important to categorize their response when exposed to elevated temperatures for a sustained period of time. In fire resistant design for wood structures, the main goal is to ensure that enough structural integrity is maintained, during and after a fire, to prevent collapse and to maintain means of egress. Another goal is an ability to assess post-fire structural integrity and residual strength of an existing structure. The objectives of this study were (a) to study the effect of temperature and exposure time on bending strength (MOR) and stiffness (MOE) of solid sawn lumber (SSL), laminated veneer lumber (LVL), oriented strand board (OSB) and plywood and (b) to develop predictive relations between different temperatures and times of exposure and the thermal degradation of strength. A total of 1080 samples were tested in static bending under various heat treatments. The results indicated that exposure to elevated temperature caused significant degradation of bending strength and stiffness. A statistical regression based model and a kinetics based model were developed and evaluated for predicting the strength loss of wood and wood-based composites as a function of thermal exposure temperature and time of exposure. The kinetics based model fit the data better and predictions consistently matched the observed values, making the model preferred over the regression approach.

Keywords

Bending Strength; Thermal Degradation of Strength; Wood and wood-based composites

[1]Wood-based Composite Center Fellow and Graduate Research Assistant, Email: arijit.sinha@oregonstate.edu
119 Richardson Hall, Department of Wood Science and Engineering, Oregon State University, Corvallis, OR 97331, USA
[2] Professor. Department of Wood Science and Engineering, Oregon State University, Corvallis, OR, USA

Introduction

A majority of low rise single family residential dwellings in the United States are timber frame construction. Various wood-based composites, along with solid sawn lumber (SSL) are increasingly used in these dwellings. Walls and partitions are usually framed with SSL. Wood composites such as plywood or oriented strand board (OSB) are used as sheathing and are nailed to the framing. Due to an increasing demand for quality and more uniform structural lumber, many engineered wood composites developed in recent years, such as laminated veneer lumber (LVL), are also used for framing.

As the use of wood-based composites in building construction is increasing, it is important to categorize their response when exposed to elevated temperatures (White and Winandy 2006). Fire is a special design case because it is not a direct loading, but instead a condition that can have drastic impact on load carrying capacity of a structure (Cramer and White 1997). The main objective of fire resistant structural design is to ensure that enough structural integrity is maintained during a fire to allow for a means of egress for the inhabitants. Another objective of fire resistant design deals with rehabilitation of a partially burnt structure. When encountering a fire damaged building, engineers are faced with the challenge to evaluate and design a rehabilitation plan. Knowledge of residual strength of the damaged material is required to decide between reuse and replacement. Understanding and predicting material behavior after exposure to elevated temperatures is important to developing rehabilitation plans.

Fire-design is moving towards performance-based fire safety regulations and away from prescriptive codes, which are predominantly used in United States. New Zealand was one of the pioneers in performance-based fire safety code (Buchanan and Barnett 1995). Other countries, such as Japan, the United Kingdom and Australia, have followed New Zealand and incorporated performance-based fire safety regulations in their design process (Buchanan 2002). In performance-based design (PBD), a performance criterion is agreed upon and then the structure is designed to achieve needed minimum results. The performance-based codes empower the designer with the possibility of a wide array of solution strategies for providing fire safety (Bukowski and Babrauskas 1994). However, the development of solution strategies only comes from an understanding of fire performance and an availability of reliable calculation procedures for predicting fire performance. The only way to predict performance is by simulation of the building behavior, using integrated data models. This requires a database of structural testing on various components of buildings which will be used in developing and validating fire endurance models and numerical models for simulation of post-fire building

performance. Knowledge of the thermal degradation of materials represents one of the most critical gaps in the development of fire endurance models (Cramer and White 1997).
This study addresses the thermal degradation of materials by conducting various tests on wood and wood- based composites after subjecting them to elevated temperatures, hence studying the post-fire residual strength in wood and wood composites. Specific objectives of this work were:

1. investigate the changes in bending properties of wood and various wood-based composites due to exposure to elevated temperature for different exposure times,
2. develop prediction models using either multiple linear regressions or a kinetics based approach and
3. compare the prediction capabilities of the two models.

Background

Solid wood performs well during fire and maintains a substantial part of its load-bearing capacity and stability after exposure to fire. Its excellent properties are due to its low conductivity and formation of a char layer on initial exposure to fire that prevents further burning. Several studies have modeled (White 1988; White and Nordheim 1992; AFPA 2003) and experimentally verified (White and Tran 1996; White 2006) the residual strength of solid wood based on the reduced cross sectional area. The effect of temperature on various mechanical properties of lumber such as modulus of elasticity (MOE), modulus of rupture (MOR), and compressive strength (Young and Clancy 2001) has been well studied and compiled by Green et al. (1999). They observed that strength of lumber decreases as the temperature increases. The variation of mechanical properties with temperature is linear to 150^{o}C. Repeated exposure to elevated temperature has a cumulative effect on wood properties (Green et al. 1999). Buchanan (2002) validated the findings of Green et al. (1999) and quantified the effect of temperature on MOE and MOR relative to ambient temperature properties (20^{o}C). The effect of elevated temperature on strength of wood was extensively studied by Buchanan (2002). A stress strain relationship at various temperatures was established by Buchanan (2002) using computer modeling of bending tests. Green and Evans (2008a) reported a 40% loss of MOR for Douglas-Fir wood after exposure to 82^{o}C for 30 months. The authors (Green and Evans 2008b) also characterized the immediate effect of temperature on MOE of wood. However, no attempt was made to characterize permanent change in MOE with exposure to temperature. Several studies (Bekhta and Niemz 2003; Kocaefe et al. 2008) have investigated the effect of heat treatment on mechanical properties of solid lumber. Many studies have also been done on the degradation of strength of lumber

following treatment by fire-retardants (MacLean 1953; Winandy and Lebow 1996). Winandy and Lebow (1996) studied degradation in strength using a kinetics based approach and calculated an activation energy of 93 kJ mol^{-1} required for thermal degradation of wood below 200^{o}C. Stamm (1956) observed activation energy for thermal degradation of various softwoods to be between 104-121 kJ mol^{-1}. These studies report significant degradation in MOR of solid lumber as temperature increases, while MOE does not show significant degradation. All these studies either investigated the immediate change in MOR and MOE at the elevated temperature or the effect of heat treatment; limited attempts were made to characterize the irreversible changes in properties of lumber following exposure to elevated temperature.

Wood composites such as OSB and plywood are also extensively used in construction but their response to elevated temperature is less studied than solid wood. Elevated temperature performance of these wood-based composites has been continuously challenged (Grundahl 1992). Their bending properties at ambient temperature are well studied and reviewed (Younquist 2000), but few studies at elevated temperature are found (Bekhta and Neimz 2003; Paul et al. 2006). A 15% reduction in MOR of OSB was observed by Bekhta and Neimz (2003) at 100^{o}C while a 30% loss in strength was observed at 140^{o}C, each after exposure of 1 h at that temperature followed by testing at that same elevated temperature. There is a lack of literature on ambient properties of OSB and plywood after exposure to elevated temperature which quantifies the irreversible changes in strength caused by exposure to elevated temperature.

A number of roof failures have occurred in structures having some type of fire retardant treated (FRT) plywood as the roof sheathing (APA 1989a). Winandy et al. (1991) concluded that the roof failures were due to the thermal degradation of FRT plywood at service temperatures, which can go up to 80^{o}C (APA 1989b). Gerhards (1982) and Winandy et al. (1988) identified temperature to be a primary factor in strength loss of FRT wood. In these tests, both FRT plywood and untreated controls were exposed to temperatures ranging from 0^{o}C to 80^{o}C. The test results for controls showed an initial slight increase (4%) in bending strength value as exposure time increased (Winandy et al. 1991). At 77^{o}C, MOR degrades, but does not degrade much on exposure beyond 21 days. In contrast, the FRT plywood loses about half its bending strength when exposed to 77^{o}C for 63 days. The rate of strength degradation depends on exposure temperature and generally decays at a constant rate for

fixed exposure conditions (Winandy et al. 1991). The highest temperatures in these studies were 88^{o}C; hence, more data is needed to study exposure at higher temperatures.

Sinha et al. (2010) studied the MOR degradation of OSB and plywood at 9 different temperatures ranging from 50^{o}C to 200^{o}C for various exposure times and observed the increase in the strength degradation rates as the temperature increased. Using a kinetics based analysis along with time-temperature superposition a master curve was developed which predicts degradation of strength with time on exposure at a reference temperature. The master curves showed that although plywood had a higher initial strength, OSB performed better in terms of strength degradation after exposure to elevated temperature. Measurement and evaluation of mechanical properties of individual materials of a structural assembly, such as SSL, LVL, OSB and plywood are critical. This study characterized the thermal degradation of strength and stiffness of these structural materials. In addition to OSB and plywood, which was studied in great detail in Sinha et al. (2010), (chapter 3) this work studied strength loss of solid lumber, laminated veneer lumber (LVL) and two different thicknesses of OSB and plywood. Characterization of mechanical properties of these materials after exposure to elevated temperatures will lead to more informed decision making between rehabilitation or retrofit for fire damaged structures.

Material and Methods

Static third-point bending tests were carried out to study the effect of elevated temperature and exposure time on MOR and MOE of the wood and wood based composites listed in Table 2.1. The specimen dimensions for various materials, along with their species, specific gravity and symbols are also listed in Table 2.1. The plywood and LVL were bonded with phenol formaldehyde (PF) resin, while the OSB panels were bonded with PMDI in the core and PF on face. The bending specimens were cut along the major axis (parallel to the fiber direction) of each panel according to ASTM D 3043-00 (ASTM 2006) and cut into desired specimen size. Third-point bending tests (fig.2.1) were conducted on an INSTRON 5582 universal testing machine. A constant span to depth ratio of 24 was maintained for all the materials as recommended by ASTM D3043, except SSL where a span to depth ratio of 14 was used. The specimens were simply supported and loaded on the wide face by two equal, concentrated forces spaced equidistant between the supports. The specimens were loaded at a rate of 8 mm min^{-1} (0.315 in. min^{-1}) and continued until failure. The MOR and MOE were calculated by the equations in ASTM D198 (ASTM 2009). For each of the six different materials (SSL, LVL, OSBH, OSBO, PWH and PWO), 180 specimens were prepared. These 180 specimens were

randomly divided into 5 exposure time-temperature groups consisting of 36 specimens each. Hence, for the six different material types a total of 1080 bending tests were conducted.

This study investigated the ambient residual bending MOR and MOE of wood and wood-based composites after exposure to elevated temperatures. The temperatures chosen were 25^{o}C (controls), 100^{o}C and 200^{o}C. The elevated temperatures were chosen to correspond with pre-charring temperatures that might occur in a protected timber frame structure. Moreover, the structural design code for timber construction (AFPA 2007) requires a structure to meet either 1 h or 2 h fire ratings. This implies that the structure will neither collapse nor allow the flame or higher temperature to pass through for the rating period of time. Hence, five different treatments were considered, namely, control (CTRL), 100^{o}C-1h (100C1), 100^{o}C-2 h (100C2), 200^{o}C-1 h (200C1) and 200^{o}C-2 h (200C2) of exposure. All tests specifically measured ambient temperature properties after exposure to elevated temperatures, hence, characterizing residual MOR and MOE of the materials at room temperature. The test program did not include characterization of the mechanical properties at elevated temperatures and did not include conditions that caused charring.

The samples were heat treated in a conventional convection oven. A separate oven run was scheduled for each treatment. The oven was preheated to the desired temperature, as monitored by internal as well as external thermocouples. Once the desired temperature was attained, the samples were inserted in the oven for the designated exposure time. The process was repeated for all the temperatures and all the materials. Once the specimens were taken out of the oven, they were allowed to cool to room temperature before testing. All specimens were conditioned to equilibrium moisture content (EMC) in a standard room maintained at 20^{o}C and 65% relative humidity, prior to exposure to temperature. The measured average EMCs were 6.7% for plywood, 4.9% for OSB, 12% for SSL and 5.3% for LVL. After exposure to elevated temperature, the specimens were cooled to room temperature for 24 h, but were not re-equilibrated with moisture. As a result, our strength changes may represent the combined effects of strength changes due to moisture change and due to high temperatures. Slight reductions in moisture tend to increase strength (Gerhards 1982) of wood. Therefore, any observed degradation in strength was likely caused by elevated temperature exposure and not by moisture effects.

Comparison of bending properties between the treatments was conducted using analysis of variance (ANOVA). A regression model was constructed to characterize the effect of time and

temperature on the measured responses (MOR and MOE). Assumptions of ANOVA and regression such as normality and homogeneity of variance were evaluated using Shapiro-Wilk test and Levene's test, respectively. The alpha level for test of significance in this study was set to 0.05. A goodness-of-fit chi square test was conducted to assess how well the data sets fit the proposed models.

Results and Discussion

Static bending Test

Table 2.2 summarizes the bending tests data for all materials and all treatments. The values of MOE and MOR and their respective standard deviations (Table 2.2) are comparable to those reported in the literature (MacLean 1953; Winandy et al. 1988; Winandy and Lebow 1996; Wang and Rao 1999; Biblis 2001; Green and Evans 2008a; b; Kocaefe et al. 2008). Statistical analysis (ANOVA) on the data set for one material at a time indicates that there were highly significant differences in MOR for all the materials between treatments. Various studies have reported loss of MOR for SSL and wood-based composites after exposure to heat from 5% to 70% (MacLean 1953; Winandy and Lebow 1996; Paul et al. 2006; Green and Evans 2008a; Sinha et al. 2010) depending on the exposure time, temperature and material. In these results, exposure to 200^{o}C for 2 h caused an 18% drop in bending strength for SSL compared to control samples. For all the materials, the drop in MOR ranged from 18-61% after exposure to 200^{o}C for 2 h. The maximum drop in MOR was observed for plywood (PWH) which was around 61%. The minimum drop was observed for SSL (18% after exposure to 200^{o}C for 2 h). The drop in MOR for OSB, observed in this study, was 34% after 2 h of exposure at 200^{o}C which was consistent with the findings of Sinha et al. (2010). Paul et al. (2006) heat treated strands before manufacturing OSB panels for 30 minutes at 220^{o}C and observed a 50% drop in MOR. This difference in the degradation compared to Paul et al. (2006) is due to the difference in the materials on which treatments were applied and also a difference in exposure temperature. Paul et al. (2006) heat treated the strands before manufacturing OSB at 220^{o}C for 30 min, while in this study the OSB panels were heated at 200^{o}C for a maximum of two hours.

MOE showed highly significant ($p<0.05$, F test ANOVA) differences between treatments for all the materials except for SSL and OSBH. This is consistent with the findings of MacLean (1953), Green and Evans (1994), Bekhta and Niemz (2003) and Kocaefe et al. (2008) where they observed no significant change in MOE after heat treatments for SSL. MacLean (1953) further reported that MOE is the least affected mechanical property by heat treatment for solid

lumber. Some wood composites in this study did show significant degradation in MOE after exposure to elevated temperatures. Paul et al. (2006) reported 10% loss in MOE of OSB after the strands have been exposed to 220^{o}C for 30 min, while in this study the drop in MOE after exposure to 200^{o}C for 2 h was 8%. MOE of plywood (11.2 mm thickness) dropped 37% after exposure to 200^{o}C for 2 h. Winandy et al. (1988) reported a slight but not-significant drop in MOE after several days of exposure at 77^{o}C. At a similar, but higher temperature of 100^{o}C after 2 h of exposure, a drop of 3% in MOE was observed in the present study.

Analytical Models

Two models, one based on statistical regression and the other based on kinetics analysis were constructed to investigate the effect of elevated temperature and exposure time on bending properties of wood and wood-based composites. Regression analysis is a statistical tool to investigate relationships between two or more variables. In this study the variables were time (t) and temperature of exposure (T). The effect of these variables and their interactions on the bending properties such as MOE and MOR, for each material was studied using a multiple linear regression model. The general form of the model is as follows:

$$MOR\,or\,MOE = \beta_0 + \beta_1 t + \beta_2 T + \beta_3 Tt \qquad (2.1)$$

where β_i are the regression coefficients associated with various terms, temperature (T in Celsius) and time of exposure (t in hours). The effect of temperature on bending properties of wood is a time dependent phenomenon (Winandy and Lebow 1996). Hence, it becomes important to include an interaction between time and temperature in our model, which is present in the β_3 term.

Various kinetics based models for thermal degradation of strength have been proposed (Millet and Gerhards 1972; Woo 1981; Winandy et al. 1991; Winandy and Lebow 1996; Branca and De Blasi 2003; Sinha et al. 2010). Generally, models using degradation kinetics are developed for MOR as it is more susceptible to temperature changes in wood based materials than is MOE (MacLean 1953). Kinetics based degradation models are based on the assumption that degradation kinetics follows an Arrhenius activation energy model. The assumption is twofold. First, at a constant temperature (T) the rate of change of bending properties is dependent on the time of exposure (t). So, at a constant T:

$$d\sigma \propto t \quad \text{or} \quad \frac{d\sigma}{dt} = -k(T) \qquad (2.2)$$

This part is similar to linear regression, where at constant temperature (T) the bending property degrades linearly with time of exposure (t). Second, at a given time, the change in property follows an activation energy theory assumption which can be represented as

$$k(T) = Ae^{-E_a/(RT)} \text{ or } \qquad \frac{d\sigma}{dt} = -Ae^{-\frac{E_a}{RT}} \tag{2.3}$$

This equation is more commonly expressed in logarithmic form as:

$$\ln k(T) = \ln A - \frac{E_a}{RT} \tag{2.4}$$

Here, E_a is activation energy, R is the gas constant and T is the absolute temperature (K) and A is a constant. This non-linear dependence of rate with temperature is what distinguishes the kinetics-based model from the linear regression model. MOR is found by integrating over any applied thermal history, T(t). In summary, first, the degradation is modeled to vary linearly with time at a constant temperature (T). The rate of degradation at a constant temperature is k(T). Then, various rates of degradation for different temperatures are fitted using eq. (2.3) based on Arrhenius activation theory. Sinha et al. (2010) applied Arrhenius activation energy theory to its strength degradation model and then used the principles of time-temperature superposition to construct master curves for the thermal degradation of strength for OSB and plywood at a given reference temperature. The methodology of kinetics modeling is explained in great detail in Winandy and Lebow (1996) and Sinha et al. (2010) where the reader is directed for more background.

The kinetics-based model evaluates the change in strength or relative strength loss, while the regression approach gives an equation for predicting a mean value of the bending property under the given set of conditions (t and T). A statistical analysis such as the regression approach is a mathematical tool to analyze and compare various factors within the current data set and develop a predictive mechanism based on the trends observed. On the other hand, the kinetics-based approach follows the Arrhenius activation energy theory, where rate of degradation at each temperature k(T) for each material is calculated from experimental observations.

Regression Model

The linear regression models relating MOR and MOE with temperature and time of exposure for all the materials used in this study are presented in Table 2.3. A total of 36 samples were tested for each heat treatment for each material. The regression was based on 30 tests after each heat treatment and the remaining were used to validate the regression models. The

results indicated that bending parameters such as MOR and MOE decreased as the exposure time increased at a given temperature. Increasing the exposure temperature also caused a decrease in MOR and MOE. Their relations could be represented by a linear regression formula (Table 2.3). The F statistic represents how well the model represents the data. An F value of 2.66 or greater (Ramsey and Schafer 2002) represents a good fit for the data set because it provides a corresponding p-value of 0.05 or less. On the other hand, an F value less than 2.66 implies that the model poorly represents the data. All the relations studied were significant ($F > 2.66$; $p < 0.05$) except for MOE for SSL (marked with *). As explained in the previous section, a change in temperature did not have much effect on MOE of SSL. This was also evident from the non-significance of the regression equation.

The R^2 for the linear regression relations were generally weak, especially for MOE. The low R^2 values could be due to many reasons (R^2 =1 is ideal for linear fits). The goal of regression is to explain the variability in the measured responses as a function of some controlled variables. Wood as an engineering material has highly variable properties within a species and within a tree as well. This inherent variability in wood as a material induces a lot of variation in the tested parameters such as MOR and MOE and poses a challenge for any regression model involving wood. The presence of knots, for example, can cause variations. Similarly, for composites such as plywood and OSB, manufacturing processes may cause variability in the material properties. Wang and Rao (1999) analyzed MOE and MOR of FRT plywood using a regression model to establish a relation between strength loss and time of exposure at one temperature of exposure. The R^2 values of Wang and Rao (1999) were higher than that of this study. This difference can be attributed to the fact that the model proposed here also takes into account both exposure temperature and time, whereas, the one proposed by Wang and Rao (1999) only regressed time of exposure. The R^2 values are comparable to other regression models proposed in the literature for MOR of wood (Winandy and Lebow 1996; Brancheriau and Bailleres 2003; Ikonen et al. 2008) and other parameters related to wood, such as knot diameter (Vestol and Hoibo 2001).

Kinetics-Based Model

Degradation of composites after exposure to elevated temperature follows a two phase regime (Sinha et al. 2010). The first phase is below 100^{o}C and the second phase being degradation after exposure to 100^{o}C and above. Historically, wood does not degrade in strength after exposure to temperature less than 100^{o}C (Green et al. 1999). However, there is ample research (Winandy et al. 1988; 1991; Wang and Rao 1999) that suggests wood composites,

such as plywood and OSB degrade in strength after exposure to temperatures of 100^{o}C and below, however, they degrade slowly. This could be due to complex interactions between wood and resin in a composite, where if the resin deteriorates it can lead to degradation of strength. Moreover, as the material is exposed to 100^{o}C, the moisture from the material is driven out, which may cause the strength to increase. The total degradation at 100^{o}C is therefore a combination of influences for moisture-change effects and for degradation of the resin. For degradation to be observed below 100^{o}C, the exposure time at that temperature needs to be long enough for resin effect to exceed moisture-change effects. Winandy et al. (1988; 1991) did observe room-temperature strength loss in plywood exposed to temperatures below 100^{o}C, but the degradation occurred only after an exposure time spanning a few months.

The second regime of degradation of bending strength is at exposure above 100^{o}C. After exposure to temperature higher than 100^{o}C, both wood and wood composites show degradation in strength (Buchanan 2002, Green et al. 1999; Sinha et al. 2010).
Our observation also suggested no degradation in strength of wood (SSL) after exposure to 100^{o}C (Table 2.4). When strength degradation with time was observed for various wood composites at 100^{o}C, the rate of degradation (k) was positive for both varieties of plywood (PWH and PWO) and LVL (Table 4). While for OSBH and OSBO along with SSL, the rate of degradation was negative or the MOR increased. We observed positive degradation rates below 100^{o}C (Table 2.4) for plywood (PWH and PWO) and LVL. On the other hand, all the materials showed positive rates of degradation in strength when exposed to 200^{o}C. The temperature of 200^{o}C is high enough to counter all the moisture effects and moreover causes both, wood and resin to degrade. As a result, all the materials exhibited positive rates of degradation in strength (Table 2.4).

For all the materials that degraded with time at a given temperature, the rate of degradation k(T) was obtained from the change in strength per unit time $k(T) = \frac{\Delta\sigma}{\Delta t}$, and is presented in table 2.4. From these calculated k(T) values, the Arrhenius parameter E_a/R was calculated by plotting ln k(T) vs. 1/T (K^{-1}). Fig. 2.2 plots ln k(t) vs. 1/T (K^{-1}) for all materials. All experimental results with positive degradation rates in the study (black symbols) are plotted, which are all materials at 200^{o}C and LVL, PWH and PWO at 100^{o}C. Data from Sinha et al. (2010) for OSBH and PWH and data from Winandy and Lebow (1996) for SSL (other softwood species, Southern Yellow Pine) are overlaid on the graph at various temperatures for comparison

(open symbols). For materials showing positive rate of degradation, the Arrhenius parameter is the slope of the fits to the Arrhenius equation (eq. 2.4). For materials showing negative rate of MOR degradation (SSL, OSBH and OSBO) the Arrhenius parameter (E_a/R) was calculated using data available in the literature. Data from Winandy and Lebow (1996) and Sinha et al. (2010) were used to calculate the rate of degradation as well as Arrhenius parameter for SSL and OSBH, respectively, using the Arrhenius activation energy model. No study involving thermal degradation of OSB with a thickness in the range of 20-24 mm was found; hence, the second stage of the kinetics model for OSBO was not calculated. Table 2.4 summarizes the kinetics-based modeling results i.e. k(T) and E_a/R, along with their standard errors. The rate of degradation for OSBH and PWH at 200^{o}C is consistent with the rate of degradation observed by Sinha et al. (2010). The difference in duration of exposure for the two studies can possibly account for the slight variations in the degradation rates. Exposure times for the current study were 1 h or 2 h at each temperature, while it ranged from 1 through 8 h for Sinha et al. (2010). Winandy and Lebow (1996) proposed kinetics based degradation models for solid lumber. Their exposure times ranged from 200 to 600 days for the study which was long enough to detect some degradation in strength after exposure to low temperature, 65^{o}C or 82^{o}C.

Validation and Comparisons of Models

A total of 36 tests per material per heat treatment were conducted. 30 of these tests were used to build the models i.e. to get the parameters β_i (Table 3) for regression-based model and k(t) (Table 2.4) for kinetics-based model. The remaining 6 tests for elevated temperature (100^{o}C and 200^{o}C) were used to validate the models, hence, a total of 24 data points were used to validate the models. A goodness-of-fit chi square (χ^2) statistic as sum of squares of difference between the observed and expected results normalized over expected results was calculated for each model and is presented in Table 2.5. The formula for χ^2 for n data points is as follows:

$$\chi^2 = \sum_{i=1}^{n} (E_i - O_i)^2 / E_i \quad (5)$$

The relations between MOR degradation, temperature and time of exposure for PWH and OSBH were also validated using data from Sinha et al. (2010) and χ^2 was calculated (Table 5). For direct comparison, the degrees of freedom were kept constant by selecting same number of data points (24) from Sinha et al. (2010). The critical χ^2 value for a probability level of 0.05 and 24 data points was 35 (Ramsey and Schafer 2002). A χ^2 value of 35 or less indicated a good fit. Moreover, the lower the χ^2 value, the better is the fit.

It was evident from the χ^2 values (Table 2.5) that both the proposed models, i.e. regression-based and kinetics-based models provided good fits to the independent data sets used for validation, except for the regression based model for LVL (χ^2 = 97.9). Comparing the chi-square values for kinetics and regression models; all the values were lower for the kinetics model than for the regression models, except for plywood. The regression-based model consistently predicted the MOE and MOR values for exposure temperature of 100^{o}C, but it tended to under-predict the MOE and MOR values for plywood after exposure to 200^{o}C. However, the predictions were consistent with observed values for OSB at 200^{o}C temperature exposure. For example, the regression models predicted the MOR for plywood (11.2 mm thickness) to be 25% lower than actual value, while for OSB the predictions were 5% lower than the observed values. The predictions with the kinetics-based model were more consistent with the observed values. The predictions were within 0.1-12% of the observed values. The lower χ^2 values suggest that the kinetics-based model is preferred over the regression models.

Conclusion

After exposure to elevated temperature, the ambient MOR of wood and wood based composites, such as plywood, OSB and LVL were lower than that of the control specimens. Exposure to elevated temperature caused degradation in strength for all tested materials. Modulus of elasticity was also affected by exposure to elevated temperature for the wood based composites, but no degradation in MOE was observed for solid sawn lumber after exposure to these elevated temperatures.

A statistical linear regression based model incorporating the effects of temperature, time of exposure and interaction between the two, and a model based on the assumption that strength degradation follows first-order kinetics were developed and evaluated for predicting the strength loss of wood and wood-based composites as a function of thermal exposure temperature and time. The kinetics-based model was better than the linear regression-based approach. The kinetics based models fit the data better and the prediction consistently matched the observed values. The predictive models can serve as a tool to provide engineers with more comprehensive information on thermal degradation of structural wood and composites, and will help guide the rehabilitation and retrofit of fire damaged structures. The measured k(T) and the Arrhenius parameters here can be used to predict the degradation in strength of these structural wood composites at various temperatures and further used to calibrate new models.

Acknowledgement

The author would like to acknowledge the support of Wood based Composite Center for funding the project.

References

American Forest & Paper Association (AFPA). (2003) Calculating the fire resistance of exposed wood members. Technical Report 10. American Wood Council. Washington, D.C., USA

American Forest & Paper Association (AFPA). (2007) Design for Code Acceptance: Fire rated wood floor and wall assemblies. Washington, D.C., USA

APA. (1989a) Fire-retardant-treated plywood roof sheathing: Field failures. American Plywood Association, Tacoma, WA

APA. (1989b) Fire-retardant-treated plywood roof sheathing: General information. American Plywood Association, Tacoma, WA

American Society for Testing and Materials (ASTM) (2009) D 198. Standard Test Methods of Static Tests of Lumber in Structural Sizes

American Society for Testing and Materials (ASTM) (2006) D3043.Standard test methods for structural panel in flexure

Bekhta P., Niemz, P. (2003) Effect of high temperature on the change in color, dimensional stability and mechanical properties of spruce wood. Holzforschung 57(5):539–546

Biblis, E.J. (2001) Edgewise flexural properties and modulus of rigidity of different sizes of southern pine LVL and plywood. Forest Products Journal 51(1):81-84

Branca, C., Di Blasi, C. (2003) Kinetics of the isothermal degradation of wood in the temperature range 528–708 K. Journal of Analytical and Applied Pyrolysis, 67:207–219

Brancheriau, L., Baillères, H. (2003) Use of the Partial Least Squares Method with Acoustic Vibration Spectra as a New Grading Technique for Structural Timber. Holzforschung 57(6):644-652.

Buchanan, A.H. Structural design for fire safety. John Wiley and Sons, West Sussex, England, 2002

Buchanan, A.H., Barnett, J. (1995) Performance-based design for fire in New Zealand. Restructuring: America and Beyond, Proceedings of Structures Congress XIII, 1995, April 2-5, Boston, MA, ASCE, NY, 1106-1121

Bukowski, R.W. Babrauskas, V. (1994) Developing rational, performance-based fire safety requirements in model building codes. Fire and Material 18:173-191.

Cramer, S.M.,White, R.H. (1997) Fire performance issues. Wood Engineering in the 21st century: research needs and goals: proc. Workshop offered in conjunction with SEI/ASCE structures congress *XV*, Portland, OR. 75-86

Gerhards, C.C. (1982) Effect of moisture content and temperature on mechanical properties of wood: an analysis of immediate effects. Wood and Fiber 14(1):4-36

Green, D.W., Evans, J.W. (1994) Effect of ambient temperatures on the flexural properties of lumber. *PTEC 94* Timber shaping the future: Proceedings, Pacific Timber Engineering Conference, Timber research development and advisory council, Fortitude Valley, Queensland, Australia*,* 2:190-197.

Green, D.W., Evans, J.W. (2008a) Effect of cyclic long-term temperature exposure on bending strength of lumber. Wood and Fiber Science 40(2):288-300

Green, D.W., Evans, J.W. (2008b) The immediate effect of temperature on the modulus of elasticity of green and dry lumber. Wood and Fiber Science 40(3):374-383

Green, D.W., Winandy, J.E., Kretschmann, D.E. (1999) Mechanical Properties of wood- Wood as an engineering material. General Technical Report FPL-TR 113, U.S. Department of Agriculture, Forest Service, Forest Products Laboratory, Madison, WI

Grundahl, K. (1992) National Engineered Lightweight Construction Fire Research Project. Technical Report: Literature Search and Technical Analysis. National Fire Protection Research Foundation, Quincy, MA, USA

Ikonen, V., Peltola, H., Wilhelmsson, L., Kilpelainen, A., Vaisanen, H., Nuutinen, T., Kellomaki, S.(2008) Modelling the distribution of wood properties along the stems of Scots pine (Pinus sylvestris L.) and Norway spruce (Picea abies (L.) Karst.) as affected by silvicultural management. Forest Ecology and Management 256:1356-1371

Kocaefe, D., Poncsak, S., Boluk, Y. (2008) Effect of thermal treatment on the chemical composition and mechanical properties of Birch and Aspen. BioResources 3(2):517-537

MacLean, J.D. (1953) Effect of steaming on strength of wood. Proceedings of American wood –preservers' Association, Washington D.C. 88-112

Millet, M.A., Gerhard, C.C. (1972) Accelerated Aging: Residual weight and flexural properties of wood heated in air at 115 to 175^{o}C. Wood Science 4(4):193-201.

Paul, W., Ohlmeyer, M., Boonstra, M.J., Pizzi, A. (2006) Optimising the properties of OSB by a one-step heat pre-treatment process. Holz als Roh- und Werkstoff 64: 227–234

Ramsey, F.L., Schafer, D. W. The Statistical Sleuth: A Course in Methods of Data Analysis. Duxbury/Thompson Learning, Pacific Grove, California, USA, 2002

Sinha, A., Nairn, J.A., Gupta, R. (2010) Thermal Degradation of the bending strength of plywood and oriented Strand Board: A Kinetics approach. Wood Science and Technology, in print (DOI 10.1007/s00226-010-0329-3).

Stamm, A.J. (1956) Thermal degradation of wood and cellulose. Industrial and Engineering Chemistry 48(3):413-417

Vestol, G.I., Hoibo, O.A. (2001) Prediction of knot diameter in Picea abies (L.) Karst. Holz als Roh- und Werkstoff 59:129–136

Wang, S., Rao, Y. (1999) Structural performance of fire-retardant treated plywood: effect of elevated temperature. Holzforschung 53(5):547-552

White, R.H. (1988) Charring rates of different wood species Ph.D. thesis. University of Wisconsin-Madison, WI, USA.

White, R.H. (2006) Fire resistance of Structural Composite lumber *Research paper FPL-RP 633*, U.S. Department of Agriculture, Forest Service, Forest Products Laboratory, Madison, WI.

White, R. H., Nordheim, E.V. (1992) Charring rate of wood for ASTM E 119 Exposure Fire Technology 28(1):5–30

White, R.H., Tran, H.C. (1996) Charring rate of wood exposed to a constant heat flux Proceedings of Wood and Fire Safety Conference. Zvolen, Slovak Republic, 175–183

White, R.H., Winandy, J.E. (2006) Fire performance of Oriented Strandboard Proc. Seventeenth Annual BCC Conference on Flame Retardancy, Norwalk, CT, USA, 297-309

Winandy, J.E., Lebow, P.K. (1996) Kinetics models for thermal degradation of strength of fire-retardant treated wood. Wood and Fiber Science 28(1):39-52

Winandy, J.E., LeVan, S.L., Schaffer, E.L., Lee, P.W. (1988) Effect of fire-retardant treatment and redrying on the mechanical properties of Douglas-fir and aspen plywood. Research Paper FPL-RP 485. U.S. Department of Agriculture, Forest Service, Forest Products Laboratory. Madison, WI

Winandy, J.E., LeVan, S.L., Ross, R.J., Hoffman, S.P., McIntyre, C.R. (1991) Thermal degradation of fire-retardant-treated plywood: Development and evaluation of test protocol *Research Paper FPL-RP 501*, U.S. Department of Agriculture, Forest Service, Forest Products Laboratory. Madison, WI.

Woo, J.K. (1981) Effect of thermal exposure on strength of wood treated with fire retardants. Ph.D. Thesis. Berkeley, CA: University of California, CA

Young, S.A., Clancy, P. (2001) Compression mechanical properties of wood at temperatures simulating fire conditions. Fire and Material, 25:83-93

Younquist, J.A. (2000) Wood based composites and panel products. Wood as an engineering material. General Technical Report 113, U.S. Department of Agriculture, Forest Service, Forest Products Laboratory, Madison, WI

Table 2.1. List of materials, their respective symbols, species, specific gravity (coefficient of variation, n = 36) and specimen sizes used in the study to test for MOE and MOR.

	Material	Symbols	Species	SG (COV %)	Specimen Size (mm x mm)	depth (mm)	Span to Depth Ratio (l/d)
M1	Solid Sawn Lumber	SSL	Douglas-Fir	0.487 (14.3)	25.4 x 25.4	25.4	12
M2	Laminated Veneer Lumber	LVL	Douglas-Fir	0.512 (3.1)	1016 x 89	38	24
M3	Oriented Strand Board	OSBH	Aspen	0.592 (4.0)	406 x 76	11.9	24
M4	Oriented Strand Board	OSBO	Aspen	0.563 (3.2)	762 x 76	22	24
M5	Plywood	PWH	Douglas-Fir	0.553 (6.4)	406 x 76	11.2	24
M6	Plywood	PWO	Douglas-Fir	0.468 (3.4)	762 x 76	24	24

Table 2.2. Summary of average MOR and MOE along with their respective standard deviations of various materials after subjected to five different treatments involving elevated temperature and exposure time. P-values are the probability calculated form ANOVA F-test to test whether means of MOR and MOE were different for different heat treatments within a material (N = 36)

Material	SSL				LVL			
Treatment	MOR	SD	MOE	SD	MOR	SD	MOE	SD
CTRL	96.86	16.30	12.47	1.97	63.38	9.93	12.85	1.26
100C1	98.83	17.14	12.64	2.08	52.22	8.35	11.32	0.81
100C2	101.61	17.77	12.74	1.71	57.11	9.20	13.59	0.93
200C1	83.93	21.07	12.32	2.14	50.55	8.65	13.18	1.10
200C2	78.93	20.57	12.21	2.19	42.03	6.84	12.33	0.71
p-value	**<0.001**		0.79		**<0.001**		**<0.001**	

Material	PWH				PWO			
Treatment	MOR	SD	MOE	SD	MOR	SD	MOE	SD
CTRL	46.30	12.50	10.01	2.08	35.84	7.26	6.98	1.04
100C1	44.87	12.22	9.41	3.12	28.90	6.75	6.71	1.03
100C2	41.13	11.93	9.75	2.00	31.30	7.76	6.72	1.10
200C1	31.40	10.07	9.18	2.32	20.86	5.56	6.25	1.06
200C2	18.26	6.17	6.34	2.11	18.21	4.77	6.12	0.94
p-value	**<0.001**		**<0.001**		**<0.001**		**0.002**	

Material	OSBH				OSBO			
Treatment	MOR	SD	MOE	SD	MOR	SD	MOE	SD
CTRL	32.37	6.79	6.86	1.27	31.47	4.66	8.19	1.39
100C1	29.24	7.95	6.44	1.38	31.33	3.44	8.44	0.61
100C2	33.08	5.82	6.88	1.31	31.86	5.00	8.27	0.79
200C1	26.48	6.28	6.87	1.40	27.13	4.48	7.77	0.88
200C2	21.31	6.27	6.30	1.73	23.08	9.40	7.26	2.26
p-value	**<0.001**		0.25		**<0.001**		**0.002**	

Table 2.3. Regression Models for various materials depicting MOR and MOE as a function of time of exposure (t), temperature of exposure (T) and their interaction. R^2 and F values of respective models are presented (*non significant)

Material	Analytical Model for MOR (MPa) and MOE (GPa)	R^2	F values
SSL	MOR = 79 + 0.07T + 22.2t - 0.1489Tt	0.170	12.24
	MOE = 11.89 + 0.0034T + 0.69t - 0.0043Tt	0.007	0.46*
LVL	MOR = 53.79 + 0.10T + 9.21t - 0.08Tt	0.374	35.09
	MOE = 9.45 + 0.02T + 2.70t-0.02Tt	0.159	11.06
PWH	MOR = 36.75 + 0.05T + 13.63t - 0.14Tt	0.474	52.96
	MOE = 6.91 + 0.0249T + 3.12t - 0.0295Tt	0.226	16.06
PWO	MOR = 31.16 - 0.0.98T + 6.6136t - 0.0456Tt	0.510	61.15
	MOE = 6.875 - 0.0024T + 0.224t - 0.0018Tt	0.089	5.77
OSBH	MOR = 22.26 + 0.0494T + 10.68t - 0.0805Tt	0.280	40.35
	MOE = 6.29 + 0.0096T + 1.2811t - 0.0112Tt	0.060	7.42
OSBO	MOR = 24.88 + 0.0364T + 7.8765t - 0.062Tt	0.255	19.95
	MOE = 7.56 + 0.0096T + 0.915t - 0.012Tt	0.080	5.11

Table 2.4. Kinetics based model for degradation of MOR with temperature and exposure time for all the materials.

Material	T (Kelvin)	Intercept	SE	k (T)	SE	Ea/R
SSL	373	96.73	2.59	---		
	473	95.54	2.95	8.97	2.29	*728.61*
LVL	373	60.71	1.51	3.13	1.16	
	473	62.66	1.31	10.68	1.01	2163.30
PWH	373	46.69	1.59	2.59	1.43	
	473	46.09	1.50	14.02	1.66	2981.70
PWO	373	34.28	1.15	2.27	0.89	
	473	33.79	1.01	8.82	0.78	2393.30
OSBH	373	31.21	1.08	---		
	473	32.25	0.98	5.53	0.76	*7892.90*
OSBO	373	31.36	0.67	---		
	473	31.42	0.99	4.20	0.77	--

--- refers to negative rate of strength degradation.

The italicized numbers means the second step of kinetics modeling is conducted using data available in the literature.

Table 2.5. Goodness-of-fit chi square statistic for regression and kinetics based models for strength degradation

Material	Model Type	
	Regression	Kinetics
SSL	32.2	26.1
LVL	97.9	32.5
PWH	24.7	26.8
PWH*	33.1	33.8
PWO	10.9	14.4
OSBH	20.7	18.8
OSBH*	21.9	14.2
OSBO	17.7	16.8

**Sinha et al. data*

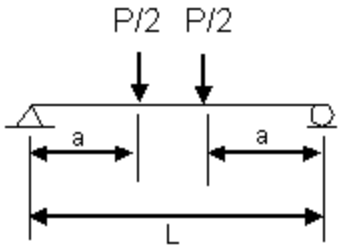

$$E = \frac{23PL^3}{108bd^3\Delta} \qquad MOR = \frac{2P_{\max}L}{bd^2}$$

Figure 2.1. Static Third point bending test set-up. All specimens were tested in third-point bending (a = L/3). Modulus (E or MOE) and strength (σ or MOR) were calculated from the above equations where Δ = deflection at L/2, P = applied load and P_{max}= Maximum Load.

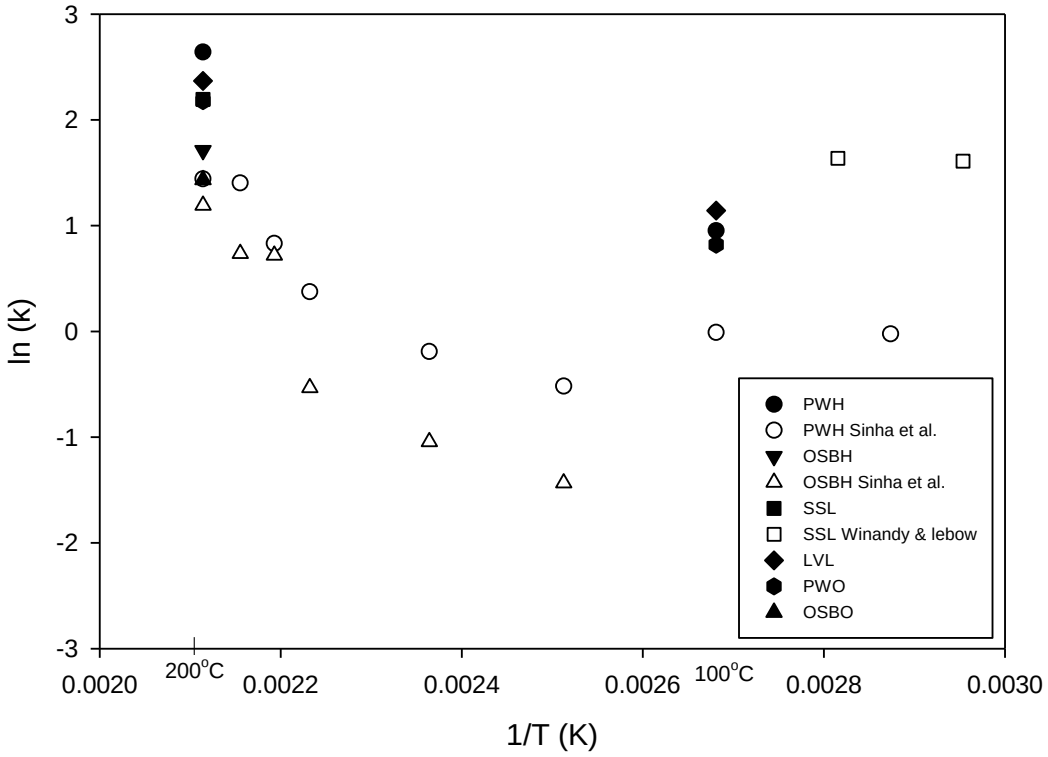

Figure 2.2. ln(k) vs. inverse of absolute temperature plot for all the materials. Data from Winandy and Lebow (1996) and Sinha et al. (2010) (chapter 3) are overlaid with the current data.

Thermal Degradation of Bending Strength of Plywood and Oriented Strand Board: A Kinetics Approach

Arijit Sinha, John A. Nairn and Rakesh Gupta

Wood Science and Technology
Springer Heidelberg
Haberstrasse 7
69126 Heidelberg
Germany
Published online on April 10, 2010
DOI:10.1007/s00226-010-0329-3

Chapter 3: Thermal Degradation of Bending Strength of Plywood and Oriented Strand Board: A Kinetics Approach

Abstract

The construction industry has relied heavily on wood and wood-based composites such as oriented strand board (OSB) and plywood for timber frame construction. Therefore, it is highly imperative to categorize the response of wood-based composites when exposed to elevated temperatures for a sustained period of time. The essence of fire resistant structural design is to ensure that structural integrity be maintained during and after the fire, prevent collapse and maintain means of egress. Another aspect is to assess post fire structural integrity and residual strength of existing structure. The objective of this project was (a) to study the effect of exposure time on bending strength (MOR) of OSB and plywood at elevated temperatures, (b) to interpret any relationships between different temperature and time of exposure using a kinetics model for thermal degradation of strength, and (c) to develop a master curve representing temporal behavior of OSB and plywood at a reference temperature. A total of 1152 samples were tested in static bending as a function of exposure time and several temperatures. Strength (MOR) of both OSB and plywood decreased as a function of temperature and exposure time. These results were fit to a simple kinetics model, based on the assumption of degradation kinetics following an Arrhenius activation energy model. The apparent activation energies for thermal degradation of strength were 54.1 kJ/mole for OSB and 62.8 kJ/mole for plywood. Furthermore, using the kinetics analysis along with time-temperature superposition, a master curve was generated at a reference temperature of 150^{o}C which predicts degradation of strength with time on exposure at that reference temperature. The master curves show that although plywood has a higher initial strength, OSB performs better in terms of strength degradation after exposure to elevated temperature.

Introduction

Wood-based composites, such as oriented strand board (OSB) and plywood are the main structural composite panels in both residential and commercial timber construction. Walls and partitions are usually framed with solid sawn lumber (SSL) studs. Plywood and OSB are used as structural sheathings. OSB is also widely used as the web in I-joists. The use of wood-based composites in low-rise, single-family dwellings is increasing. As a result, they represent an increasing share of the wood products market (White and Winandy 2006). OSB has taken a major market share from plywood during the last two decades and still is driven by strong demand (APA 2005). With this increased use of wood composites, it becomes important to assess their fire performance and integrity after exposure to elevated temperatures (Grundahl

1992). Because they are less massive than solid timber, they are less likely to resist a rapid temperature rise (Cramer and White 1997). Hence, more study on the effect of elevated temperature on various properties of wood-based composites is needed. Such thermal degradation studies involve understanding and predicting wood-based materials' behavior during and after exposure to elevated temperatures.

Untreated plywood has a long history in service as roof sheathings. The introduction of fire retardant treated (FRT) plywood for roof sheathings allowed the building codes to accept FR-treated plywood roof sheathing as a replacement for noncombustible decking in some multifamily structures. In the past decade, however, a number of roof failures have occurred in structures using FRT plywood (APA 1989a). These failures were attributed to thermal degradation (Winandy *et al*. 1991) at service temperatures, which can reach up to 80^{o}C (APA 1989b). Temperature has been shown to be a primary factor in strength loss of FRT wood (Gerhards 1982; Winandy *et al*.1988). In these tests, both FRT plywood and untreated controls were exposed to temperatures ranging from 0^{o}C to 80^{o}C. The test results for controls showed an initial slight increase (4%) in bending strength value as exposure time increased (Winandy *et al.* 1991; Winandy and Lebow 1999). At 77^{o}C, the strength degrades, but does not degrade much on exposure beyond 21 days. In contrast, FRT plywood loses about half its bending strength when exposed to 77^{o}C for 63 days. This study reported that an increase in moisture content causes the degradation rate to increase. The strength degradation rate depends on exposure temperature and generally decays at a constant rate for fixed exposure conditions (Winandy *et al*.1991). The strength degradation rates at higher temperatures are expected to be higher, but have not been investigated.

Other than FRT plywood, few studies have been conducted on changes in mechanical properties of OSB or untreated plywood at or after exposure to elevated temperatures (100-200^{o}C). Due to the increased use of OSB and plywood in construction, it is important to undertake such studies. Fire is a special design case as it is not a loading condition for structures, but instead an environmental condition that can have dramatic effects on the load carrying capacity of a structure (Cramer and White 1997). The main objective of fire resistant structural design is to ensure that structural integrity is maintained during and after the fire. Furthermore, post fire concerns include whether the structure has enough residual capacity to withstand the stresses in service during the course of its lifetime and can be reused, or whether all or part of the structure has to be rebuilt. Evaluation of the post fire structural integrity and residual strength capacity will facilitate this decision-making process.

This study addresses these questions by testing OSB and plywood in bending after subjecting them to various temperatures for different exposure times, hence characterizing the time dependence of strength as a function of temperature. More specifically, the objectives were to:

1. study the effect of exposure time on bending strength, modulus of rupture (MOR) of OSB and Plywood at elevated temperatures,
2. interpret relationships between different temperature and time of exposure using a kinetics model for thermal degradation of strength, and
3. develop a master curve representing temporal behavior of OSB and plywood at any reference temperature.

The master curve provides a predictive tool for residual strength and time to failure at a given reference temperature. By shifting the master curve reference temperature, it would be possible to predict residual strength following exposure at a wide range of temperatures for any amount of time.

Materials and Methods

Commercially available aspen OSB and Douglas-fir Plywood were selected for this study. The panels were rated C-D exposure 1, 32/16 span rated with thickness of 11.90 mm (15/32 in.) for plywood and 11.12 mm (7/16 in.) for OSB, respectively. The measured specific gravity of the phenol formaldehyde (PF) bonded plywood and OSB (PMDI in core; PF on the face) were 0.51 and 0.60, respectively.

Static third point bending tests were carried out to study the effect of temperature and exposure time on MOR of OSB and plywood. The bending specimens were cut along the major axis of each panel according to ASTM D 3043-00 (American Society for Testing and Materials 2006). The material was cut into specimens of size 406 x 76 mm (16 x 3 in.). This study being a part of a larger project, half of each panel was used for bending samples (this study). The other half of the panel was reserved for future tests for properties like Internal bond (IB), lateral nail connection strength and fracture toughness, which will be part of future publications. Therefore, for this study each panel yielded 45 bending samples. 576 specimens each from OSB and plywood (1152 in total) were prepared. The 576 OSB specimens were randomly divided into 72 exposure time-temperature groups with each group consisting of 8 specimens. The 72 groups allowed testing after exposure to 9 different temperatures (50^{o}C, 75^{o}C, 100^{o}C, 125^{o}C, 150^{o}C, 175^{o}C, 183^{o}C, 191^{o}C and 200^{o}C) and eight exposure time increments at each temperature ranging from 1 hour to 8 hours at 1 hour increments.

Additionally, a set of control specimens was tested at room temperature. A similar randomized selection was done for plywood. For each temperature and each material a separate oven run was scheduled. 64 samples for one temperature were placed in the oven, 8 samples were taken out of the oven every hour up to 8 hours. The process was repeated for all the temperatures and both the materials. Once the specimens were taken out of the oven, they were allowed to cool to room temperature before testing.

All specimens were conditioned to equilibrium moisture content (EMC) prior to exposure to temperature. The measured EMCs were 6.7% for plywood and 4.9% for OSB. After exposure to elevated temperature, the specimens were cooled to room temperature for 24 hours, but were not re-equilibrated with moisture. As a result, our strength changes may represent the combined effects of strength changes due to moisture change and due to the prior high temperature exposure. Separating these effects would require a control experiment determining strength as a function of moisture content below equilibrium moisture content in samples that were never exposed to high temperature. Because the only way to reduce moisture content below equilibrium is to heat the specimens, such control experiments are not possible. Instead, we assumed that slight increases in strength that might result from reduced moisture content were negligible compared to the observed decreases in strength due to high temperature exposure. Justification of this assumption follows by noting that low temperature results showed little or no increase in strength (where moisture effects might be expected to be more important and cause an increase) while high temperature results showed significant strength reductions.

Third-point bending tests (fig.3.1) were conducted on an INSTRON 5582 machine. A constant span of 304.8 mm (12 in.) was used, which resulted in a span to depth ratio of 24 as recommended by ASTM D3043. The specimens were simply supported and loaded on the wide face by two equal, concentrated forces spaced equidistant between the supports. The specimens were loaded at a rate of 8 mm/minute (0.314 in./min) and continued until failure. The Modulus of Rupture (MOR) and Modulus of Elasticity (MOE) were calculated by the equations in figure 1.

Results and Discussion

Bending Tests

The bending tests were conducted as function of exposure time and temperature. All lower temperatures (100^{o}C and lower) showed little change in strength over 8 hours; at higher

temperatures (125°C and above), the strength decreased with time. As explained later in the modeling section, all results were fit to straight lines based on an assumption of a constant, but temperature dependent, degradation rate for strength:

$$\frac{d\sigma(t,T)}{dt} = -k(T) \quad \text{or} \quad \sigma(t,T) = \sigma(0) - k(T)t \qquad (3.1)$$

where σ is MOR, $k(T)$ is the temperature-dependent degradation rate (MPa/hour), and σ(0) is the MOR of control specimens. The straight line fits were constrained to go through the σ(0) control value. The MORs after 8 hours of exposure along with their respective weight losses are listed in Table 1 along with their R squared (R^2) values for the fit to Eq. (3.1). The 8-hour strengths were calculated from the fit results rather than quoting the one result at 8 hours, to provide a better representation of the complete set of data at each temperature. The R^2 values at higher temperatures (125°C and higher) suggest a good fit to the linear strength degradation assumption, however, the low R^2 values for lower temperature data are lower indicating a poor fit. These data hardly changed in strength and thus only scatter in the strength results remain and scatter was not related to exposure time. At 200°C, the linear fits predicted that plywood will have no residual strength after 8 hours of exposure, while OSB will show a drop of 76% from its initial strength. At 191°C, decreases in strength of 70% and 47% are predicted after eight hours of exposure for plywood and OSB, respectively. This Figure 3.2 shows one set of data for OSB at 191°C with its fit for degradation. Figure 3.3 shows MOR as a function of exposure time at all temperatures for plywood (3a) and OSB (3b), respectively. The results at high temperature (150°C and higher) clearly showed degradation; these experimental points are the filled symbols and their linear fits are the labeled, solid lines. The results at lower temperature (100°C and lower) had little or no degradation and their linear fits had small slopes, some of which were positive. This can also be observed from their respective R^2 values. Table 3.1 also shows that the bending strength slightly increased for plywood after eight hours of exposure to 50°C and also increased for OSB at 50°C, 100°C and 125°C, respectively, but decreased at 75°C. These increases could be the result of two factors. First, all increases were within experimental scatter from the control values. In other words, there may be no increase. Second, at the lowest temperatures, the exposure may not cause any degradation of strength, but it might drive some moisture out of the specimen. Because moisture has an inverse relation with strength, if some moisture was removed, the low-temperature results could show an increase in strength. These experiment results are in open symbols in Fig. 3.3 and their fits are shown as the dashed lines. The results at 125°C were mixed. For plywood, degradation could be detected and is plotted in Fig. 3.3a as filled symbols and a solid line. For OSB, the constrained fit had a positive slope and is plotted in

Fig. 3.3b as open symbols and a dashed line. By relaxing the constraint that the OSB results for 125^{o}C must go through the control value, we determined a degradation rate consistent with other results; this adjusted rate was used in the modeling below.

Figure 3.3 shows that with an increase in exposure time at sufficient temperature, there is a decrease in bending strength for both materials. However, there was little or no consistent effect on bending strength after exposure to temperatures 100^{o}C or less, even for 8 hours of exposure. Our strength loss results hence can be described using two regimes. The first regime is where the temperature of exposure is less than or equal to 100^{o}C and the second is where the exposure temperature is 125^{o}C and higher. There is evidence in the literature (Green et al 1999) that wood does not deteriorate at sustained exposure to 100^{o}C. Plywood and OSB, however, are composites that contain of wood and resin as adhesive. Even if the wood does not deteriorate at 100^{o}C, the resins used in OSB and plywood might deteriorate which would in turn cause degradation in strength of the composite. A 15% reduction in strength of OSB was observed by Bekhta *et al*. (2003) at 100^{o}C while a 30% loss in strength was observed at 140^{o}C, each after exposure of 1 hour at that temperature followed by testing at that same elevated temperature. As their tests were conducted at the exposure temperature rather than after cooling down to room temperature, there is bound to be some difference in results compared to the present study. Winandy *et al*. (1988; 1991) did observe room-temperature strength loss in plywood exposed to temperatures below 100^{o}C, but the degradation took much longer than 8 hours. Apparently, degradation does occur below 100^{o}C, but the amount of degradation compared to scatter or compared to moisture-change effects was too small to detect in our 8-hours tests.

The second regime occurs at 100^{o}C and higher, where the degradation in strength of the composite is the combined effect of degradation of the wood and degradation of the resin. As seen in figure 3, there is a decrease in MOR at every temperature above 100^{o}C for both OSB and plywood. Figure 4 summarizes the results by plotting the strength loss from the curve fits after 8 hours of exposure as a function of temperature. At 200^{o}C, the samples were not able to sustain the heat exposure and caught fire at 7 hours and 5 hours of exposure for plywood and OSB, respectively. Plywood lost 71% of its initial strength after 7 hours of exposure at 200^{o}C while, OSB lost 47% after 5 hours of exposure at the same temperature. Figure 4 plots the strength loss after 8 hours by extrapolating the degradation rate from the first 7 or 5 hours of results. The 125^{o}C results for OSB used an unconstrained fit rather than the fit given in Fig.

3.3. The dashed vertical line divides the results into regime 1 for 100°C and lower and regime 2 for 125°C and higher. The data in regime 2 were used for the modeling in the next section.

Degradation Kinetics Modeling

The measured strengths were used to model thermal degradation as a function of temperature and exposure time. Strength of solid wood has two-stages of degradation. Below 200°C there is a slow decline in strength, but as temperature increases beyond 200°C, a rapid decrease in strength is observed (Schaffer 1970) due to degradation of hemicelluloses at 200°C (Beall and Eickner 1970). Strength loss can be predicted from exposure time at elevated temperature, based on kinetics modeling (Mitchell *et al.* 1953; Winandy and Lebow 1996; Gao *et al.* 2006). Similarly, the strength data here were evaluated using kinetics methods. Since all results were below 200°C, a single-degradation process was assumed. Stamm (1964) also supports this approach.

The thermal degradation model assumed that the strength degradation follows the constant degradation rate in Eq. (3.1). Modeling of such first-order kinetics requires an equation for the temperature dependence of the rate constant (Winandy *et al*. 1991). For cellulosic materials, this rate constant can represent rate of change in concentration of a chemical constituent. For mechanical properties, it can be rate of change in any measured property, such as strength (Millett and Gerhards 1972). Here the temperature dependence was assumed to follow an Arrhenius activation energy equation:

$$k(T) = Ae^{-E_a/(RT)} \tag{3.2}$$

where A is constant, E_a is activation energy, R is the gas constant and T is the absolute temperature (K).

For all exposure temperatures, $k(T)$, was found from the slopes of the linear fits in Fig. 3.3 (for OSB at 125°C, $k(T)$ was found for a fit that was not constrained to go through the control value). Next, the model parameters ($k(T)$) for each temperature were fit to the Arrhenius activation energy theory model. The Arrhenius activation energy model can be represented in logarithmic form as follows:

$$\ln k(T) = \ln A - \frac{E_a}{RT} \tag{3.3}$$

Fig. 3.5 plots ln $k(T)$ for temperatures above 100^{o}C and for both plywood and OSB. The straight lines are the fits to Arrhenius equation in Eq. (3.3). For plywood, the 77^{o}C degradation rate from Winandy *et al*. (1991) was included in the fitting process. The rate constants for both plywood and OSB closely followed the Arrhenius equation. Furthermore, extrapolation of our high temperature results to low temperature was consistent with the one low-temperature result from Winandy *et al*. (1991). From the slopes, the apparent activation energies were 54 kJ/mole and 65 kJ/mole for OSB and plywood, respectively. These values are lower than that of solid wood, which has activation energy for degradation below 200^{o}C of 74-107 kJ/mol (Gao *et al*. 2006). Winandy and Lebow (1996) calculated an activation energy of 93 kJ/mol required for thermal degradation of wood below 200^{o}C. This value falls within the range of values calculated by Gao *et al.* (2006). We are not aware of a similar study on plywood or OSB for comparison to these new results.

The quality of the fits and the consistency with the Winandy *et al*. (1991) results suggest that a single Arrhenius activation energy can model degradation of wood composites from low temperature up to 200^{o}C. Our experiments could measure $k(T)$ for 125^{o}C and above. For 100^{o}C and lower, however, there was too much scatter in strength experiments to detect the small amount of degradation that would occur in 8 hours. Even at 125^{o}C, the measured rates deviated to faster degradation than expected (*i.e.*, above the fits), suggesting that the short-term, 125^{o}C results may be unreliable. All results 150^{o}C and higher, however, were consistent. Measuring $k(T)$ at 125^{o}C and lower, requires long-term experiments. An alternative to long-term tests is to find degradation rates by extrapolation of short-term, high-temperature results using the Arrhenius equation. This approach is described in the next section to construct master curves for degradation or plywood and OSB over a wide range of reference temperatures.

Master Curve Analysis

Time-temperature superposition (TTSP), is a common extrapolation technique for experiments involving both temperature and time. It is most frequently used for studying viscoelastic properties of polymers (Aklonis and MacKnight 1983), but it can have application in other properties as well. Here it will be used to study degradation in strength. The principle of TTSP is that a property measured over a short time at a higher temperature is equivalent to that property measured over a long time at a lower temperature (Aklonis and MacKnight 1983). The superposition is guided by the kinetics of the underlying mechanisms of the studied process. Here the kinetics described by the Arrhenius equation guides the superposition. First,

short-term experimental data for successively increasing temperature levels (accelerated data) are plotted against log-time. Next, a reference temperature is chosen and data at other temperatures are shifted until they overlap the results at the reference temperature. Experimental curves at temperatures above the reference temperature are shifted right, and those below the reference temperature are shifted left along a log-time axis. The resulting master curve predicts the behavior of the measured property at the reference temperature over a much wider time scale. An experimental output of TTSP is the temperature dependence of the shift factor, a_T, defined by

$$\log t_{ref} = \log t(T) - \log a_T \tag{3.4}$$

In other words, the effective time at the reference temperature, t_{ref}, is shifted along a log scale from the measured time at the test temperature, $t(T)$. The shift factor, log a_T, is negative for temperatures below the reference temperature and positive for temperatures above the reference temperature.

The above shifting process requires data with sufficient changes over the time scale of the experiments to detect overlap and usually requires relatively low scatter. These criteria are commonly met by visco-elasticity data of polymers, but are not met by our strength data. If the kinetics of the underlying process are known, however, that kinetics analysis, rather than experimental data overlap, can be used to construct the master plot. Using our assumption of a linear decay rate, the condition to obtain equivalent strength loss at two different temperatures is when

$$k(T_{ref})t_{ref} = k(T)t(T) \tag{3.5}$$

Comparing to equation (3.4), the experimental shift factor from temperature T to any reference temperature can be found from

$$\log a_T = \log\left(\frac{k(T_{ref})}{k(T)}\right) \tag{3.6}$$

This shift factor can be determined directly from linear fits to degradation experiments without any kinetics modeling (*i.e.*, directly from $k(T)$ without any use of Arrhenius activation energy fits). If the kinetic modeling is used to express $k(T)$, however, it is possible to calculate the expected shift factor from the measured activation energy:

$$\log a_T = \frac{E_a}{R \ln 10}\left(\frac{1}{T} - \frac{1}{T_{ref}}\right) \tag{3.7}$$

Shift factors for a reference temperature of T_{ref} = 150°C were calculated from our experimental results for $k(T)$ above 100°C and are plotted in figure 3.6 for plywood (3.6a) and OSB (3.6b), respectively. These results are plotted as solid symbols. For results 100°C and lower, the results are plotted in figure 3.6 as open symbols. The only low-temperature results that could be plotted, however, were the ones that had positive $k(T)$. Finally the shift factor for plywood from the results of Winandy *et al*. (1991) for an exposure time of 63 days at 77°C for N grade Southern pine plywood 15.9 mm (0.625 in) in thickness, is plotted in figure 6a. The smooth curves plotted in fig. 3.6 are the predicted shift factors from the Arrhenius equation (Eq. 3.7) found using the activation energies determined in the kinetics modeling section. For both plywood and OSB, the Arrhenius shift factor agreed well for results 150°C and higher. At 125°C, the experimental shift factors deviated below the curves. For results 100°C and below, our data could not determine $k(T)$ and thus could not determine a shift factor. The theoretical curve increases rapidly at lower temperatures. Because it is close to the Winandy *et al*. (1991) results, we claim that the Arrhenius rate constant accurately represents the degradation of plywood from 200°C down to at least 77°C. Winandy *et al*. (1991) also studied the degradation of strength at 66°C for 63 days, but the strength increased, hence providing a negative rate for degradation of strength. This result indicates that while an Arrhenius extrapolation down 77°C seems reasonable, there are no experimental results confirming that the extrapolating can continue to even lower temperatures. Similarly for OSB, only experimental data above 100°C were used to obtain the shift factors, as they showed degradation in strength over time when exposed to elevated temperature. At or below 100°C, degradation was in regime 1 and too small to detect in the 8-hour time frame of the experiments. One experimental result decreased in strength and the result is plotted as an open symbol. The curve is prediction of the shift factor from the Arrhenius equation (see Eq. 3.7) using the activation energy determined in the kinetics modeling.

We next used the shift factors to transform experimental data into master degradation plots at a reference temperature of 150°C. The master curves are shown in Fig. 3.7 and 3.8 for plywood and OSB, respectively. The curves indicate that TTSP can be used to develop long-term thermal strength degradation curves. Such master curves convert a series of short-term tests into a prediction of long-term behavior at the reference temperature. The 150°C curve now spans four decades in time while the input data was only one decade. Experimental data

points in the master curve from different temperatures are represented by different symbols. The initial horizontal portion of the curve refers to the data obtained after exposure to temperatures below 100^{o}C; these data were shifted using theoretical shift factors and are represented by open symbols. In contrast, the experimental results 125^{o}C and above were shifted according to actual shift factors (from Eq. 3.6) and are represented by filled symbols. The shift factors and methods used for generating the master curves are tabulated in table 3.2. The smooth curve through the points was a least-square cubic spline smoothing of the experimental data.

Figure 3.7 and 3.8 plot the master curve for degradation of strength on exposure to 150^{o}C over time on a log scale for plywood and OSB, respectively. Although, the initial strength of plywood is higher than that of OSB, plywood degrades faster than OSB. The strength of plywood at 150^{o}C decreases by around 70% in approximately 19 hours, while it takes 100 hours for the strength of OSB to drops to 59%. Another contrasting aspect in the behavior of OSB and plywood at 150^{o}C is that the strength of OSB does not vary much for the first 10 hours, after which the strength starts to degrade. However, for plywood the strength remains constant for only about 1 hour of exposure before starting to degrade. As plywood has a layered structure, the strength of the plywood is highly dependent on glue between the layers. OSB, on the other hand is comprised of densely packed flakes and glue is applied as droplets. The structure of OSB is such that it distributes defects more efficiently. If the glue starts to deteriorate, one might expect plywood to deteriorate faster since it is more dependent on the integrity of its fewer glue bonds. One interpretation of our results is that plywood has higher room-temperature strength because of it more regular structure, more highly aligned plies, and efficient load transfer between plies through the resin. But, when exposed to elevated temperature, the degradation of the integral glue lines causes more rapid degradation in strength. In contrast, OSB distributes resin throughout the composite. The less-oriented structure and perhaps less-efficient glue bonds results in lower room temperature strength, but when exposed to elevated temperature, the strength is less sensitive to early stages of glue degradation. In brief, the elevated temperature strength performance of OSB is better than that of plywood.

Master curves provide predictive estimates of failure time and residual strength of a material for prolonged exposure at the reference temperature. Considering the 150^{o}C master plot for plywood (Fig. 3.7), the smoothed curve predicts a residual strength after 10 hours of exposure to be 36 MPa. Similarly, the residual strength can be obtained from the master plot for any

given exposure time. By defining failure at a certain percentage of initial strength, one can predict the time to failure at 150^{o}C. For example, if failure is defined as 50% strength loss, then the failure time at 150^{o}C is approximately 12 hours. Similarly, analyses could be done for OSB at the reference temperature of 150^{o}C (Fig. 3.8). Compared to plywood, the 50% strength reduction time for OSB is approximately 90 hours at 150^{o}C.

Time-temperature superposition can be carried out for any reference temperature. The generic shape of the curve remains the same for each reference temperature, only the time scale changes or shifts as the reference temperature changes. The shift to any new reference temperature can be determined from experimental shift factors. As an example, a master plot for plywood at a reference temperature of 77^{o}C was generated using the plywood shift factors and the scale is shown as an inset in fig. 3.7. First, we used Eq. (3.2) to calculate $k(T_{ref})$. Next our experimental results below 100^{o}C were shifted by again finding $k(T)$ by Arrhenius activation energy and shifting according to Eq. (3.6). As expected, the shape of the curve is the same while the only time scale has shifted. Our results above 100^{o}C where shifting using measured $k(T)$ and Eq. (3.6). This new master plot predicts a 16% loss in strength in approximately 41 days, which is similar to the observed 16% loss in strength in 63 days (Winandy *et al*. 1991). This result further suggests that an Arrhenius rate constant accurately represents the degradation of plywood from 200^{o}C down to at least 77^{o}C.

Post-fire residual strength of structural composites that were not affected by direct fire, but were exposed to elevated temperature is a critical piece of information. Knowledge of response to high-temperature exposure can lead to more informed decisions on whether a structure needs to be deconstructed completely or just partly. For modest exposure temperatures (<100^{o}C), long-term tests would be required if those tests had to be carried out at the exposure temperature. An alternative to long-term tests is to obtain degradation rates from several short-term experiments at several higher temperatures. The results in this section show that such short-term test can be shifted by experiment results or by analysis with simple Arrhenius activation energy theory to construct a master plot. The master plot provides an accelerated test method for long-term results. By shifting the master plot to any exposure temperature of interest, the resulting strength of plywood or OSB can be predicted. All results here used strengths determined from small specimens cut from the panel. Since the accelerated methods can obtain results in shorter tests, one recommendation of this study is to repeat the higher-temperature results for full-scale panels.

Conclusions

Strength (MOR) of both OSB and plywood decreased as a function of temperature and exposure time. The degradation results were divided into two regimes. The rate of change of strength was greater at higher temperature than at lower temperature. A kinetics analysis and Arrhenius activation energy theory of the strength degradation data was valid for temperatures above 100^{o}C. The degradation rate $k(T)$ follows the relation $k(T) = 40E6e^{-7549/T}$ for plywood and $k(T) = 2E6e^{-6510/T}$ for OSB. The apparent activation energies were 54.1 kJ/mole for OSB and 62.8 kJ/mole for plywood. Using the kinetics analysis along with time-temperature superposition, a master curve was generated at a reference temperature of 150^{o}C. The master curve can be used for residual strength estimates and failure time predictions. The master curves show that although plywood has a higher initial strength, OSB performs better in terms of strength degradation after exposure to elevated temperature. After longer-term exposures, the strength of OSB is higher than plywood.

Acknowledgements

The author would like to acknowledge the support of Wood based Composite Center for funding the project.

References

Aklonis JJ and MacKnight WJ (1983) Introduction to polymer viscoelasticity. 2nd ed. John Wiley and Sons, New York.

APA (1989a) Fire-retardant-treated plywood roof sheathing: Field failures. American Plywood Association, Tacoma, WA.

APA (1989b) Fire-retardant-treated plywood roof sheathing: General information. American Plywood Association, Tacoma, WA.

APA (2005) APA Economics Report E171. American Plywood Association, Tacoma, WA.

American Society of Testing & Materials (ASTM) (2006) Standard test methods for structural panel in flexure. ASTM D 3043-00, West Conshohocken, PA.

Aynlmis N, Kartel SN, Laufenberg TL, Winandy JE and White RH (2005) Physical and mechanical properties and fire, decay, and termite resistance of treated oriented strand board. Forest Products Journal 55(5):74-81.

Beall FC and Eickner HW (1970) Thermal degradation of wood components: A literature review. Research Paper FPL-RP-130. U.S. Department of Agriculture, Forest Service, Forest Products Laboratory. Madison, WI.

Bekhta P, Lecka J and Morze Z (2003) Short-term effect of the temperature on the bending strength of wood-based panels. Holz als Roh- und Wekstoff 61(2003):423-424.

Cramer SM and White RH (1997) Fire performance issues. Wood Engineering in the 21st century: research needs and goals: proc. Workshop offered in conjunction with SEI/ASCE structures congress XV, Portland, OR. pp 75-86.

Gao M, Sun CY and Wang CX (2006) Thermal degradation of wood treated with flame retardants. Journal of Thermal Analysis and Calorimetry 85(3):765-769.

Gerhards CC (1982) Effect of moisture content and temperature on mechanical properties of wood: an analysis of immediate effects. Wood and Fibre 14(1):4-36.

Green DW, Winandy JE and Kretschmann DE (1999) Wood Handbook-Wood as an engineering material. General technical report FPL-GTR-113, U.S. Department of Agriculture, Forest Service, Forest Products Laboratory. Madison, WI.

Grundahl K (1992) National Engineered Lightweight Construction Fire Research Project. Technical Report: Literature Search and Technical Analysis. National Fire Protection Research Foundation, Quincy, MA, USA.

Millett MA and Gerhards CC (1972) Accelerated aging: Residual weight and flexural properties of wood heated in air at 115 to 175°C. Wood Science 4(4):193-201.

Mitchell RL, Seborg RM and Millett MA (1953) Effect of heat on the properties and chemical composition of Douglas-fir wood and its major components. Forest Products Journal 3(11):38-42.

Schaffer EL (1970) Elevated Temperature Effect on the Longitudinal Mechanical Properties of Wood. Ph.D. Thesis, Department of Mechanical Engineering, Univ. Wisconsin, Madison, WI, USA.

Stamm AJ (1964) Wood and Cellulose Science. Ronald Press, New York, USA. pp 308-311.

White RH and Winandy JE (2006) Fire performance of Oriented Strandboard. Proc. Seventeenth Annual BCC Conference on Flame Retardancy, Norwalk, CT, USA, pp 297-309.

Winandy JE and Lebow PK (1996) Kinetics models for thermal degradation of strength of fire-retardant treated wood. Wood and Fiber Science 28(1):39-52.

Winandy JE, LeVan SL, Ross RJ, Hoffman SP and McIntyre CR (1991) Thermal degradation of fire-retardant-treated plywood: Development and evaluation of test protocol. Research Paper FPL-RP 501. U.S. Department of Agriculture, Forest Service, Forest Products Laboratory. Madison, WI.

Winandy JE, LeVan SL, Schaffer EL and Lee PW (1988) Effect of fire-retardant treatment and redrying on the mechanical properties of Douglas-fir and aspen plywood. Research Paper FPL-RP 485. U.S. Department of Agriculture, Forest Service, Forest Products Laboratory. Madison, WI.

Table 3.1. Predicted MOR values and weight loss values after 8 hours of exposure for plywood and OSB at various temperatures with their root mean square error (R^2) values

	Plywood				OSB			
	$\sigma_{(0)}$ = 46.2 MPa				$\sigma_{(0)}$ = 32.4 MPa			
Temp (^oC)	σ_f (MPa)	% loss	R^2	Weight Loss (%)	σ_f (MPa)	% loss	R^2	Weight Loss (%)
50	46.8	-1	0.00	1.40	36.20	-12	0.20	0.57
75	39.4	15	0.38	3.26	29.34	9	0.02	2.73
100	33.9	27	0.23	5.17	33.47	-3	0.05	4.12
125	39.4	15	0.07	6.28	34.77	-7	0.00	4.13
150	38.6	17	0.20	6.46	29.73	8	0.01	4.96
175	27.2	41	0.21	7.13	27.93	14	0.33	5.56
183	26.7	42	0.50	8.83	17.41	46	0.82	6.81
191	13.6	71	0.78	9.61	17.22	47	0.87	7.48
200	0.0	100	0.65	NA	7.80	76	0.84	NA

$\sigma_{(0)}$ – MOR of control specimens

σ_f – Predicted MOR after 8 hours of exposure

NA – The samples caught fire prior to eight hours of exposure

Table 3.2. Log a_t values used to produce the master curve for plywood and OSB for a reference temperature of 150^{o}C

Temperature (^{o}C)	Log (a_t)		Method
	Plywood	OSB	
50	1.658	2.069	Arrhenius
75	1.154	1.440	Arrhenius
100	0.718	0.896	Arrhenius
125	0.142	0.169	Actual k
150	0.000	0.000	Actual k
175	-0.246	-0.222	Actual k
183	-0.444	-0.765	Actual k
191	-0.693	-0.773	Actual k
200	-0.710	-0.971	Actual k

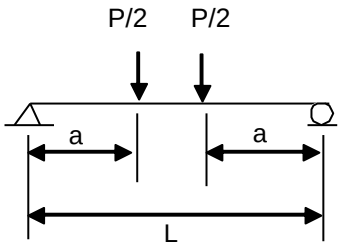

$$E = \frac{23PL^3}{108bd^3\Delta}$$

$$MOR = \frac{2P_{max}L}{bd^2}$$

Figure 3.1: Third Point Bending set-up. All specimens were tested in third-point bending (a = L/3). Modulus (E or MOE) and strength (σ or MOR) were calculated from the above equations where Δ = deflection at L/2, k = slope of load-deflection curve in the linear region, P = applied load, P_{max}= Maximum Load and I = bending moment of inertia (bd^3/12).

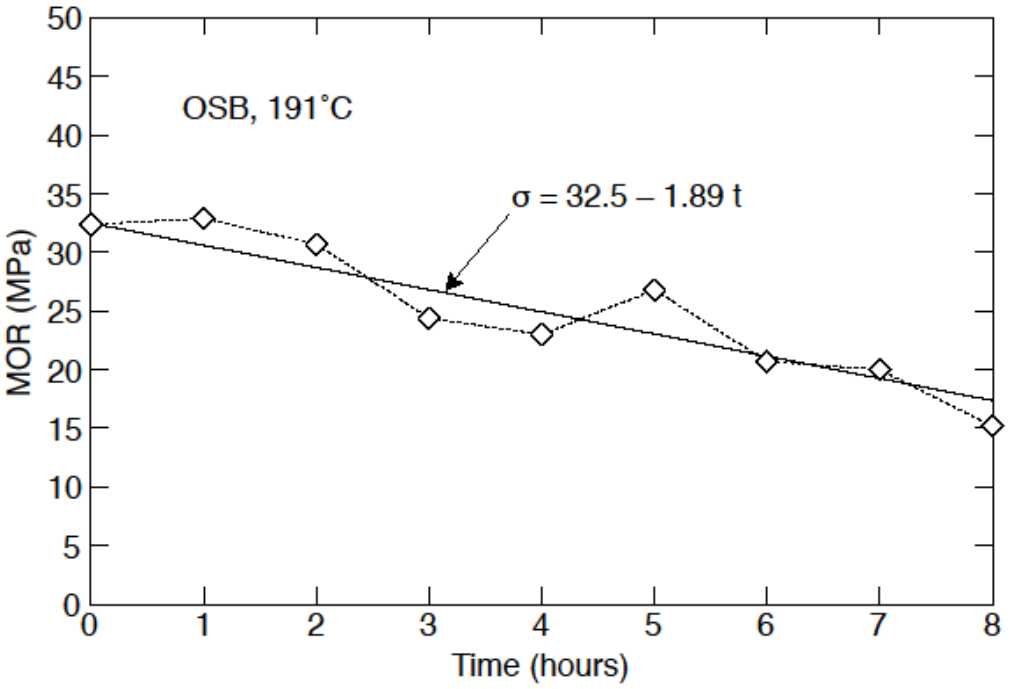

Figure 3.2: MOR of OSB as a function of exposure time at 191°C. The linear fit assumes a constant degradation rate and was constrained to go through the control value at time zero.

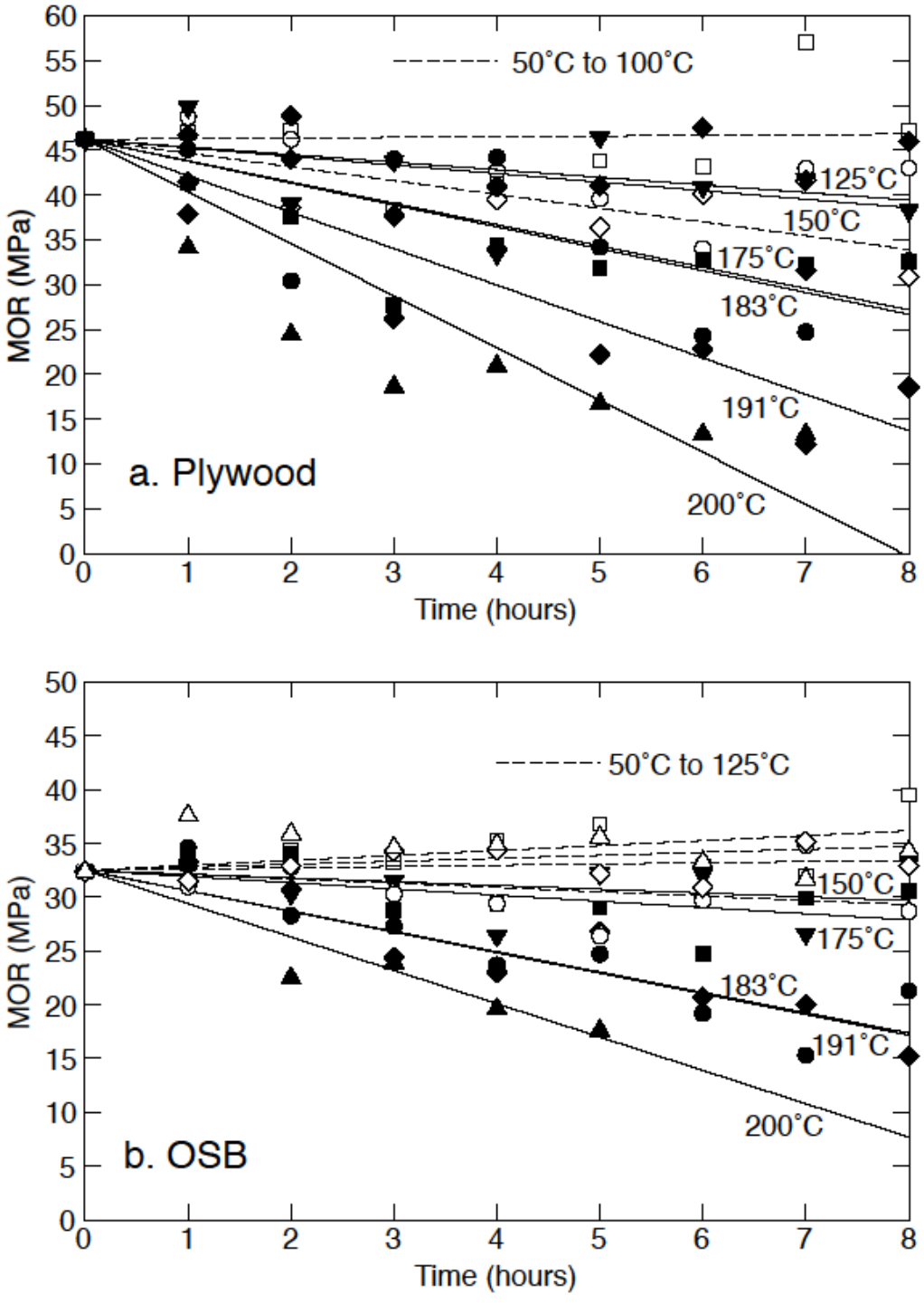

Figure 3.3. Summary of all bending test conducted as function of exposure time and temperatures for plywood (a) and for OSB (b). The experimental results are the symbols; the straight lines are fits assuming a constant degradation rate.

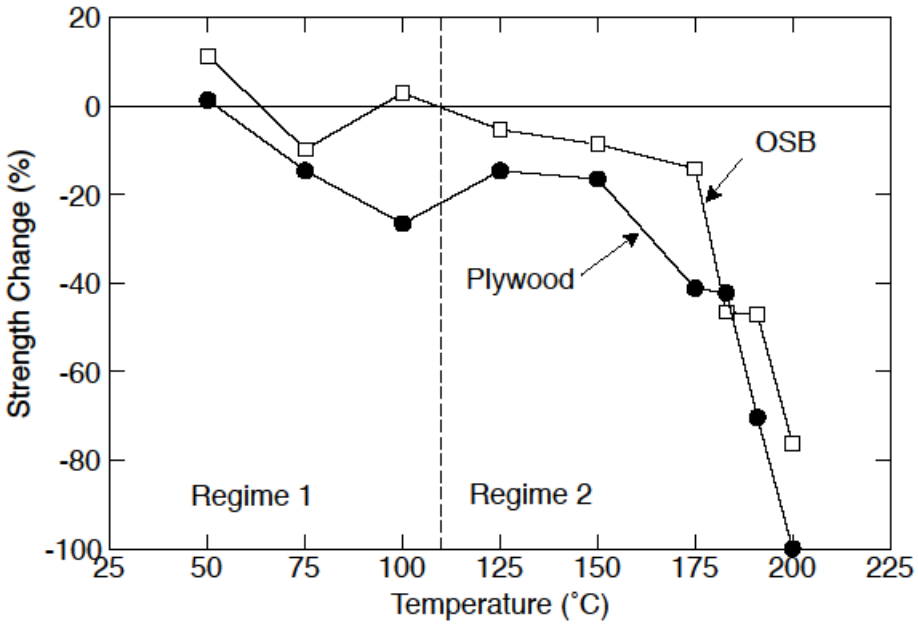

Figure 3.4: The calculated strength loss after 8 hours of exposure as a function of exposure temperature for Plywood (filled symbols) and OSB (open symbols).

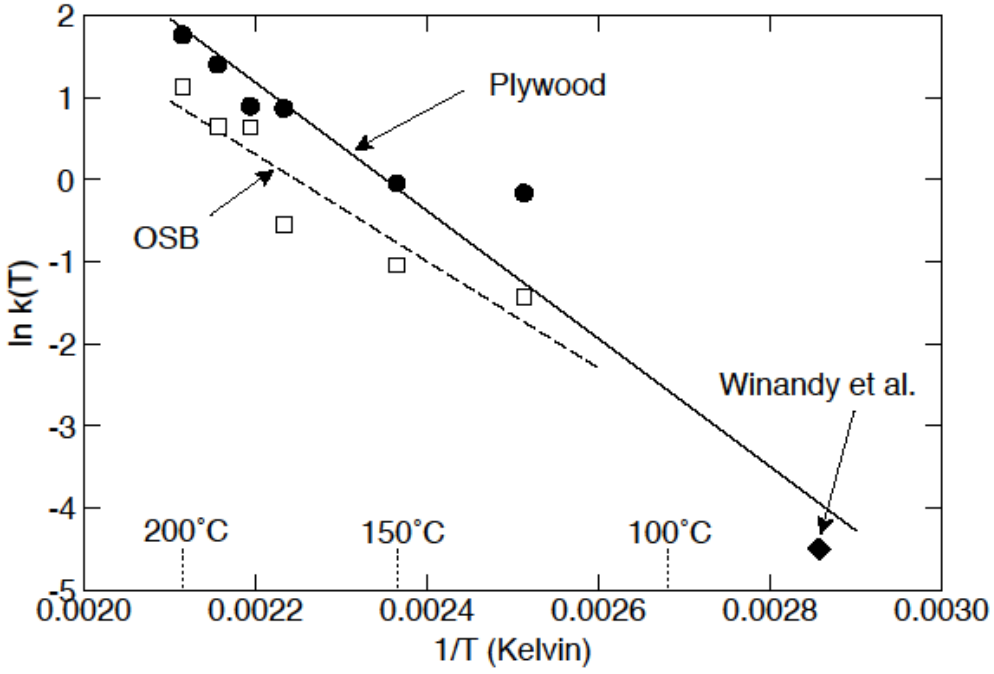

Figure 3.5. Arrhenius activation energy plot for ln $k(T)$ as a function of 1/T for plywood (filled symbols) and OSB (open symbols) including only results above 100^{o}C. The “Winandy et al.” result at 77^{o}C for plywood is plotted as the filled diamond.

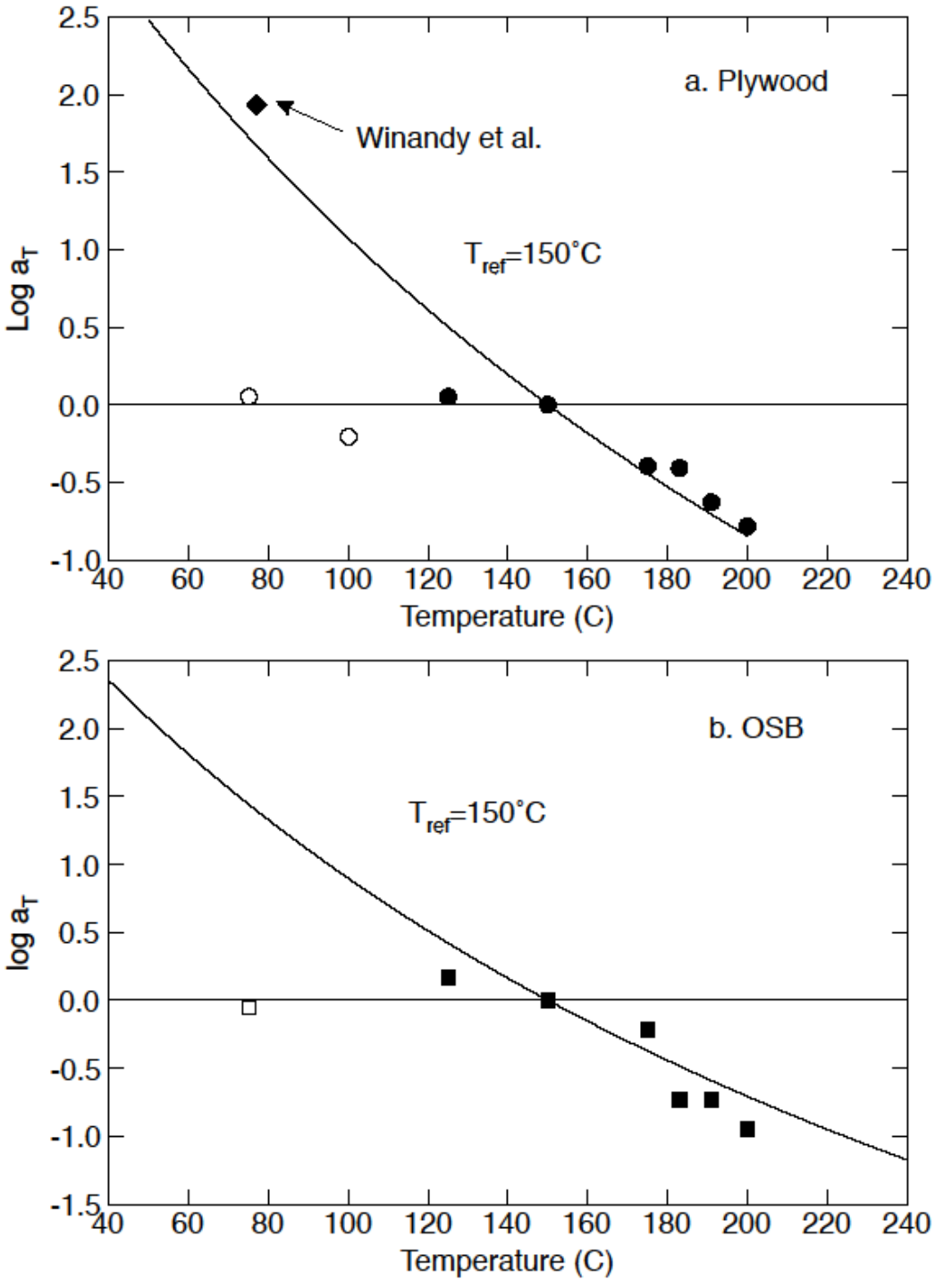

Figure 3.6: Shift factors, log a_T, calculated from experiment results for $k(T)$ (symbols, Eq. (6)) and by Arrhenius activation energy (curves, Eq. (7)) for (a) plywood and (b) OSB.

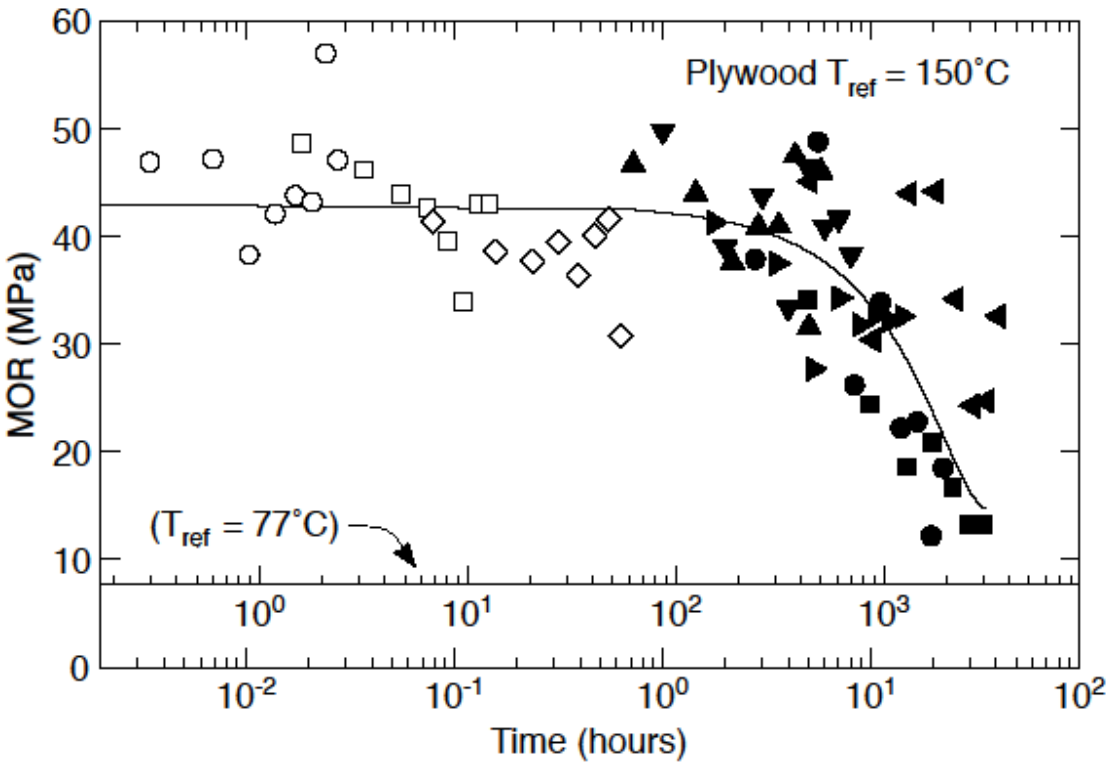

Figure 3.7. Master curve for degradation in strength (MOR) of plywood. The main axis references a reference temperature of 150^{o}C. The inset x-axis is the time axis for a reference temperature of 77^{o}C

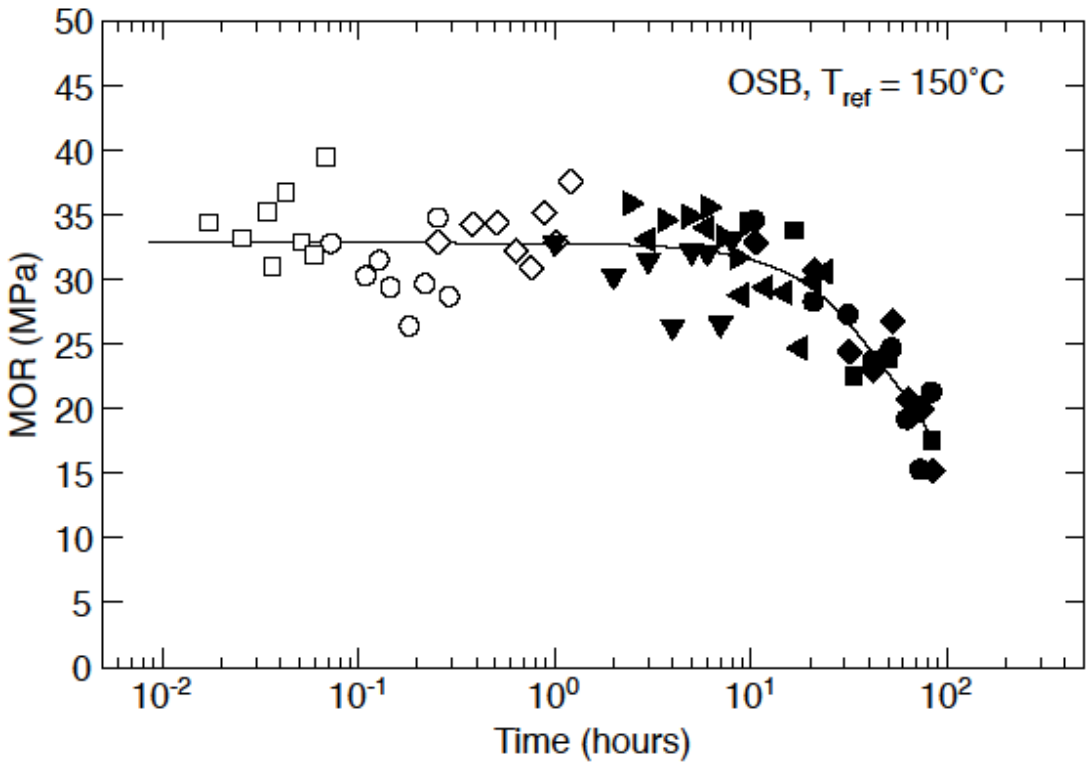

Figure 3.8. Master curve for degradation in strength (MOR) of OSB. The main axis references a reference temperature of 150°C.

Thermal Degradation of Lateral Yield Strength of Nailed Wood Joints Connections

Arijit Sinha, Rakesh Gupta and John A Nairn

ASCE Journal of Materials in Civil Engineering
ASCE Publications
1800 Alexander Bell Drive
Reston, VA 20191
USA

Accepted for publication on November 16, 2010.

Chapter 4: Thermal Degradation of Lateral Yield Strength of Nailed Wood Connections

Arijit Sinha, M. ASCE[1], Rakesh Gupta, M. ASCE[2] *and* John A. Nairn[3]

Abstract

This study investigated the effect of exposure to elevated temperature on the yield strength of single shear nail connections when subjected to lateral loading. Solid sawn lumber and laminated veneer lumber were used as framing members while two different thicknesses of both, oriented strand board and plywood were used as the sheathing members. The connection geometries evaluated were typical of those encountered in lateral force resisting systems such as shear walls or roof diaphragms. Data collected from monotonic tests on 480 nail connections, after exposure to elevated temperatures, were analyzed for yield strength. In addition, 210 dowel bearing strengths were evaluated for the same treatments. The results indicated that exposure to elevated temperature caused significant degradation in lateral yield strength after exposure. The highest degradation occurred when exposed to 200^{o}C for 2 hours. For example, plywood (11.2 mm) and solid lumber connections, the decrease in yield strength after exposure to 200^{o}C for 2 hours was 26% for edge connections and 56% for plate connections. The results further indicated that given thermal degradation of the dowel bearing capacity of a material, the existing yield models stipulated in National Design Specifications (NDS) can predict yield load values for nailed connections for a given sheathing and framing member combination under those thermal degradation conditions. Additionally, the yield models predicted a predominant yield mode (III_s) consisting of a single plastic hinge being formed just beneath the surface of the thicker member. These predictions were fairly consistent with observed yield modes.

Keywords: Laterally loaded connections; Yield models; Dowel Bearing Strength; Wood-based composites

[1] Graduate Research Assistant and Wood-based Composite Center Fellow, 152 Richardson Hall, Email: arijit.sinha@oregonstate.edu

[2]Professor, 114 Richardson Hall, E-mail: rakesh.gupta@oregonstate.edu

[3]Richardson Chair and Professor, 112 Richardson Hall, E-mail: john.nairn@oregonstate.edu

Dept. of Wood Science and Engineering, Oregon State University, Corvallis, OR 97331-5751

Introduction

In contemporary wood frame construction, the main structural system resisting lateral force is a shear wall. A shear wall predominantly consists of solid sawn lumber (SSL) or laminated veneer lumber (LVL) framing, anchored to the foundation, with engineered structural panels, such as plywood or oriented strand board (OSB), as sheathing connected to the framing by dowel type mechanical fasteners, such as nails, staples, or screws. The weakest link in a shear wall assembly is often the connections (Kalkert and Dolan 1997) between the sheathing and framing member, especially the ones on the perimeter of the sheathing panel (Sinha and Gupta 2009). Many studies (Foschi 1974, McLain 1975, Foschi and Bonac 1977, Price and Gromala 1980, Aune and Patton-Mallory 1986b, Theilen *et al.* 1998, Kent *et al.* 2004, Anderson *et al.* 2007) have tested and modeled (Kuenzi 1955, Aune and Patton-Mallory 1986 a, Pellicane 1991, Smith *et al.* 2001, Nishiyama and Ando 2003) the failure, strength and slip characteristics of nailed joints. Most tests and analytical or numerical models for nail-slip characteristics have been for ambient temperature conditions. Our knowledge about behavior of nailed joints in timber structures after exposure to elevated temperature is limited. Elevated temperatures are caused in service as a result of fire in the structure. Fire in itself is not a loading condition for structures, but it changes the load carrying capacity of the structure (Cramer and White 1997). There are two aspects to fire-resistant design. First, the structural assembly should have the ability to withstand a given exposure to fire for a specified time while maintaining its structural integrity. Second, the structural assembly should retain post-fire integrity. In other words, will the structure have enough residual capacity to withstand in service stresses, and thereby be reusable, or will all or part of the structure have to be rebuilt. This study focused on the second aspect. Engineers are faced with the need to evaluate post-fire structural integrity and residual strength capacity in order to facilitate the decision-making process to rehabilitate a wood structure following a fire. Hence, there is a need for research on thermal degradation of wood and on connection properties after exposure to elevated temperature.

The effect of heat and elevated temperature on wood connections, especially in light-frame timber construction, has received little attention in the literature. Noren (1996) tested wood-to-wood nailed joints for endurance under fire exposure to determine failure load and time to failure under fire. The failure loads ranged from 0.1-0.6 times the load under ambient circumstances. The predicted mode of failure consistently matched the observed mode of failure of the joints. Earlier work on elevated temperature properties of a connection focused on wood-to-gypsum connection (Fuller 1990) and metal plate connectors (Shrestha et al.

1995). Their main focus was on finite elements for heat transfer to get a temperature profile and very few connections were tested at elevated temperature to verify their models. They did not try to characterize the properties at ambient temperature after exposure to elevated temperature in order to determine the residual strength capacity of connections. Peyer and Cramer (1999) tested plywood to wood joints at elevated temperatures (30^{o}C, 120^{o}C, 200^{o}C and 265^{o}C) and concluded that elevated temperatures decrease the strength and connection stiffness even at low temperature (120^{o}C). Slip modulus reduced by a greater percentage than strength. The largest percentage decrease in strength (13%) and connection stiffness (47%) occurred between ambient (30°C) and 120°C. Peyer and Cramer (1999) predicted the failure of assemblies at elevated temperature. Residual strength at ambient temperature after exposure to elevated temperature, however, has not been investigated.

The National Design Specification (NDS) for wood construction (American Forest and Paper Association, AFPA 2005) stipulates yield models for design of nailed connections that will encounter lateral loads. Yield models, popularly referred to as European Yield Models (EYM) were first developed by Johansen (1949) in Switzerland to provide a predictive mechanism for assessing the load carrying capacity of a mechanical connection involving wood. Aune and Patton-Mallory (1986 a, b) introduced and popularized yield models in North America. Yield strength and mode of yielding of a laterally loaded nail connection are predicted using EYM. The yield modes of laterally loaded connections involve bending of the nail, wood crushing, or a combination of the two. The NDS defines six modes of yielding depending on which component of the connection yields. The yield models identify three reasons for the failure of connections: (1) wood yielding in the side member, (2) wood yielding in both the main member and the side member along with yielding of the nail in one member and (3) wood and nail yielding in both members. The EYM analysis, consequently, is based on the embedment strength of the wood (dowel bearing strength) which is determined according to ASTM 5764 (ASTM 2007d), the bending yield strength (f_{yb}) of the nail (dowel), which is calculated using ASTM F 1575 (ASTM 2007a) and the joint geometry using an engineering mechanics based approach (AFPA 1999). Wilkinson (1991) documented the dowel bearing strength for wood products, while its use for the design of laterally loaded wood connections is provided by AFPA (1999), where the reader is directed for more background. Using these parameters and the equations associated with the six yield modes (AFPA 1999) the yield loads are calculated. The predicted yield mode and predicted yield load are then decided as the mode which resulted in the smallest load value out of the calculated six modes. NDS (AFPA 2005) adopted the original EYM however the yield limit load is defined distinctively. The NDS yield limit load

refers to the 5% diameter offset load (Fig.4.1), defined as the intersection of load–slip (P-Δ) curve and a line parallel to the initial linear portion of the P-Δ curve offset by 0.05 times the shank diameter of the dowel in the positive direction. The NDS mentions six possible yield modes in a laterally loaded connection for single shear joints. These modes are dependent on various material and geometric parameters of the connections (Pellicane 1993). The yield mode is highly dependent on the member thickness (Blass *et al.* 1999), particularly, side member or sheathing thickness. Mode IV yielding, which involves formation of two plastic hinges due to bending of the fastener, one in each of the members, framing and sheathing, will only occur if the side member has adequate thickness to develop that failure mode. Exposure to elevated temperatures causes a change in mechanical properties of wood (Knudsen and Shniewind 1975, Winandy and Lebow 1996, Green *et al.* 1999, Buchanan 2002, AFPA 2005) and wood-based composites (Winandy *et al.* 1988, Winandy *et al.* 1991, Sinha *et al.* 2010). Exposure to elevated temperature may also have an effect on the strength of laterally loaded nail connections as the dowel bearing capacity is reduced as a result of thermal degradation. As a result, the NDS uses a temperature factor C_t, to reduce design values when the member or the connection is subjected to elevated temperature for a sustained period of time (AFPA 2005). This study investigated the residual strength of laterally loaded nail connections by testing them after exposing them to various temperatures for various exposure times. This study also tested whether existing yield models could be used to predict yield strength of the connections after accounting for thermal degradation of dowel bearing strength due to exposure to elevated temperature. Specifically the objectives of this study were:

1. to study the effect on the yield strength of laterally loaded framing to sheathing nailed connections after exposure to elevated temperatures for various time periods, and
2. to determine whether existing yield models can be used to predict the nominal design capacity for the exposed connections.

Materials and Methods

Design of Experiment

This study investigated the residual strength of laterally loaded nail connections at room temperature after exposure to elevated temperatures using a randomized split plot design (Table 4.1). The temperatures chosen were 25^{o}C (controls), 100^{o}C and 200^{o}C with two different exposure times of 1hr and 2hr at elevated temperatures. Therefore, there were five different treatments in the experimental design, namely, control (CTRL), 100^{o}C-1 hr, 100^{o}C-2 hr, 200^{o}C-1 hr and 200^{o}C-2 hr. These temperatures were chosen to correspond with pre-

charring temperatures that might occur in a protected joint assembly. The times of exposure were chosen to represent the 1 hr and 2 hr fire ratings for wall assemblies. The test program was not designed to characterize nail connection properties at elevated temperatures, nor was it designed to characterize post-charring or post-combustion residual strength. The tests specifically measured ambient temperature properties after exposure to elevated temperatures, hence, characterizing residual strength of the connections at room temperature. The samples were divided into two groups depending on the connection geometry (CG) as shown in Fig. 4.2. They were further divided into two sub samples based on the type of framing member (FM), solid sawn lumber (SSL) or laminated veneer lumber (LVL). For each of the framing types, 4 different sheathing types were used namely, Oriented Strand Board (OSB) 11.9 mm thickness, OSB 22 mm thickness, Plywood (PW) 11.2 mm thickness and PW 24 mm thickness. The next factor applied to each of the sheathing-to-framing connection types was a combination of elevated temperature and exposure time with a structured factorial arrangement of heat treatments at 5 levels as shown in Table 1. Six replicates were assessed per treatment combination providing 240 samples for each connection geometry and 480 samples in total.

Analysis of Variance (ANOVA) was used to determine the effect of treatment, geometry, framing material and sheathing material on the mean yield strength of the connection. Assumptions of ANOVA such as normality and homogeneity of variance were evaluated using Shapiro-Wilk test and Levene's test, respectively. A preliminary ANOVA was conducted to check the significance level for the main effects which were treatment, geometry, framing and sheathing. Insignificance of the main effects would have required an ANOVA including all the interactions and further refinement depending on the level of significance for the interactions. Since the main effects were significantly influencing the yield strength only a main effect analysis was required and performed. Hence, the final ANOVA compared the differences in means due to the main effects. Mean comparisons within a factor were achieved using a Tukey's family wise comparisons. The alpha level for the test of significance in this study was set to 0.05. Additionally, within each geometry-framing-sheathing combination the effect of treatment was analyzed using ANOVA.

Test Specimen

Standard wood-frame construction has three different sheathing-to-framing nail joint configurations. The connection geometries are (1) panel edge connection – nail positioned 19 mm from the panel edge, loaded parallel to the grain of the main member; (2) field connection

– nail with edge and end distances of 50 mm, loaded parallel to the grain of the main member; (3) plate connection – nail positioned 19 mm from the panel end, loaded perpendicular to grain of the main member. The first two configurations, panel edge and field have similar ultimate strengths, yield strength, and yield modes (Kent 2004) which our preliminary results also supported (Sinha 2010). Hence, only edge and plate geometries were included in this study as shown in Fig. 4.2 and are referred to as CG1 and CG2, respectively.

The framing members (FM) were 38 mm x 89 mm (2x4) stud grade Douglas-fir (*pseudotsuga menzeisii*) (FM1) and laminated veneer lumber (LVL) (FM2). The framing members selected for the nailed connections were almost free from knots. Two different types of sheathing members (SM) were used with two different thicknesses as listed in Table 4.1. One sheathing thickness is typical shear wall sheathing (AFPA 2005), while the thicker thickness of OSB and plywood is often used in flooring and diaphragms (SBA 2009). The symbols for each type of sheathings are also listed in Table 4.1 and hereafter these will be used in text to describe different sheathing types. A single-shear nail connection was constructed using smooth-shank nails [3.2 mm diameter, length = 75 mm, f_{yb} = 690 MPa (100 ksi)], pneumatically driven. The nails were driven with a Senco pneumatic nail gun such that the head of the nails stuck out slightly. The heads were then made flush with the surface of the sheathing using a hammer. The nails were centered in the thickness of the framing member.

All the framing and sheathing members were conditioned to equilibrium moisture content (EMC) in standard room maintained at 20^{o}C and 65% relative humidity, prior to exposure to temperature. The measured average EMCs were 6.7% for plywood, 4.9% for OSB, 10.2% for SSL and 5.3% for LVL. After the connections were constructed, they were exposed to elevated temperatures (100^{o}C or 200^{o}C) for two different exposure times, 1 hr or 2 hr, at each temperature. A vented convection oven was used to heat treat the samples. A separate oven run was scheduled for each treatment (TR). The oven was preheated to the desired temperature and monitored by internal as well as external thermocouples but not embedded on the surface of samples. Once the designated temperature was attained, the samples were inserted in the oven for the designated exposure time. After exposure to elevated temperature, the specimens were cooled to room temperature, but were not re-equilibrated with moisture. As a result, our strength changes may represent the combined effects of strength changes due to moisture change and due to high temperatures. Separating these effects would require a control experiment determining yield strength as a function of moisture content below equilibrium moisture content in samples that were never exposed to high temperature.

Because the only way to reduce moisture content below equilibrium is to heat the specimens, such control experiments are not possible. Instead, we assumed that slight increases in strength that might result from reduced moisture content (Gerhards 1982) were negligible compared to the observed decreases in strength due to high temperature exposure (Sinha et al. 2010). After the heat treatments and testing of the connections, part of the samples were used to measure specific gravity of the materials based on oven-dry dimensions and weight (ASTM 2007c).

Test Procedures

Lateral Load Tests

The nails were laterally loaded using a Universal Testing Machine (UTM, Instron 5582) at constant displacement rate of 5 mm/ min. Two set-ups were used to hold the two loading geometries, namely edge and plate as shown in Fig. 4.3 (a and b). The connections were designed by modifying ASTM D 1761 (ASTM 2007b). The edge distance of 50 mm was used as recommended in ASTM D1761. The standard does not require testing plate geometry (CG2), hence, there were no edge distance requirement specified. However, the standard mentions about minimum edge distance requirements for connection test to be 19 mm. Hence, an edge distance of 19mm was decided based on Kent (2004) after due consideration such that the nail is in the center of the framing member thickness to avoid the end effects. Compression clamps gripped the sheathing on top for both geometries. The framing was clamped to a right angle metal bracket for the edge geometry (CG1), while for the plate geometry (CG2); the framing was clamped to the floor of the UTM as shown in Fig. 4.3. This apparatus kept the specimen straight and in-plane to reduce eccentricities caused by nail withdrawal. Furthermore, the slip surface was specifically centered on the centerline of the load head to reduce eccentricity (Fig. 4.3 a, b insets). Load slip curves (P-Δ) were recorded for each test. The test was stopped after a plateau had been reach in the P-Δ curve. Yield strength was calculated from the P-Δ curves by the 5% diameter offset method as shown in Fig. 4.1. Here, the 5% offset was 0.16 mm. Ultimate load from P-Δ curve, is the maximum load the connection can withstand without failure. However, the yield models suggest that for a connection, the yield strength is considered to be the ultimate strength for the connection (Aune and Patton-Mallory 1986a, Peyer and Cramer 1999). Moreover, design of connections is based on this assumption. Hence, for the present study only yield strength was evaluated.

Dowel Bearing Strength (Embedment strength of Wood)

Dowel bearing strength was evaluated based on ASTM D 5764 for each of the materials and for each of the treatments with six replicates each. After heat treatment, a half hole of 3.2 mm diameter was machined in one face of each sheathing and framing member by drilling a hole first followed by a 3.2 mm router bit to finish the holes. This is slight deviation from ASTM D 5764 procedure, which requires drilling a pilot hole with diameter between 75 and 90% of the nail shank diameter, then driving a fastener perpendicular to, and through, the pilot hole to produce the half hole. However, for this study nails were not driven through the pilot holes. This was done to reduce the possibility of damage to the high heat treated specimen as those became brittle and flaky after the heat treatment. The set-up for the dowel bearing test is shown in Fig. 4.4. The test sample was placed in a vice to provide lateral support and centered under the load head carrying the load cell. A nail (3.2 mm diameter, 75 mm length) was then placed in the half hole. The load head was lowered at a constant velocity of 2 mm/min to press the nail shank, while the load cell measured the applied load at the top surface of nail shank. The P-Δ curve was recorded for the test and the test was stopped when the load head touched the wood surface. NDS defines the yield point using the 5% offset method. The same definition is applied to determine the yield point in a dowel bearing strength test and is stipulated in NDS (AFPA 2005). Thus, the dowel bearing strength is also defined by yield strength.

Results and Discussion

The mean yield strengths along with their coefficients of variation (COV) for each treatment group for all connection configurations are listed in Table 4.2. The observed yield strength for Douglas-fir framing and Douglas-fir plywood were within the experimental variation of literature reported values for similar nails (Pellicane 1993). Kent *et al.* (2004) tested SSL-OSB connections and the yield strength capacities were less than that observed in this study. Different nail types used in both the studies may be the reason for this variation. Kent et al. (2004) used 2.87 mm diameter and 63.5 mm long nails, while, the nails used in this study were of 3.2 mm diameter and 75 mm in length. Peyer and Cramer (1999) observed a 15% drop in strength when tested at 200^{o}C for plywood-to-wood double shear connection of aspen plywood and southern pine lumber, with interlayer gaps. In contrast, this study tested single shear connection of Douglas-fir plywood and lumber without any interlayer gaps and observed a strength drop of 26% after exposure to 200^{o}C for 2hr. Although, Fuller (1990) and Noren (1996) tested some connections at elevated temperature but their connections differed vastly in terms of configuration to the connections tested in this study. Due to a lack of studies which

tested similar connections after exposure to elevated temperature, no direct comparison of the results obtained in this study could be made with existing literature.

There is a general trend of degrading yield strength of the connections of various configurations with high temperature and duration of exposure confirmed by statistical analysis. The yield strength of a connection was influenced by all the main effects, which were the framing member ($p=0.009$), sheathing members ($p<0.001$), connection geometry ($p<0.001$) and treatments ($p<<0.001$). Hence, the statistical evidence suggests that mean yield strengths for the four classifications groups (FM, SM, TR and CG) were significantly different from each other. Table 4.2 presents the p-value for a statistical test whether the elevated temperature treatments (TR1-5) caused any change in mean yield strength within one connection configuration (e.g. Edge-SSL-PWH). The comparison summary of the mean yield strengths from all the tests for each of the connection configurations (CG-FM-SM) and geometries are presented in Fig. 4.5. The yield strengths in Fig. 4.5 are presented as a function of exposure time at the temperature of exposure. To this general trend of degrading strength with heat treatment there were a few exceptions, namely, Edge-SSL-PWO, Plate-LVL-PWO and Plate-LVL-OSBH configuration ($p>0.05$, Table 4.2). Although, there was degradation in yield strength for these configuration (Fig. 4.5), but it was not statistically significant. This can be attributed to the high variability in mechanical properties of wood and wood composites (Green *et al.* 1999), which poses a great challenge for any statistical analysis. The treatments at 100^{o}C, expectedly, did not cause much degradation of yield strength for the connections [Fig. 4.5 (a,c,e,g)] as the temperature is not high enough to cause significant irreversible changes in the strength of the materials. A consistent decrease in yield strength was observed [Fig. 4.5 (b,d,f,h)] for all the connection geometries and for different sheathing and framing members after exposure to 200^{o}C. Furthermore, as the exposure time increased at 200^{o}C the lateral connection yield strength capacity decreased for all the combinations. This is due to the degradation of wood as well as the resin in the composite, which causes an overall degradation in properties of wood or wood composites (Sinha *et al.* 2010).

A greater decrease in yield strength was observed for plate geometry (CG2) than for edge geometry (CG1) (Fig. 4.5 and Table 4.2). For example, comparing the connection with 11.2 mm plywood (SSL-PWH) to control samples, the decrease in yield strength was 53% for plate geometry as opposed to 26% for edge geometry after exposure to 200^{o}C for 2 hours (Table 4.2). Greater degradation in yield strength for the plate geometry than the edge geometry was further observed as a general trend for every sheathing and framing material (Fig. 4.5). The

difference in yield strength of edge (CG1) and plate (CG2) geometry was expected because of the smaller edge distance for CG2 in the direction of loading of sheathing, and the fact that the assembly is loaded perpendicular to grain direction of the main member in the case of plate geometry (CG2). Moreover, dowel bearing tests (discussed in the next section) revealed (Table 4.4) that the decrease in embedment strength for wood perpendicular to grain (34%) was greater than wood parallel to the grain (18%) after 2 hours of exposure at 200^{o}C, which also reduced the capacity of laterally loaded connections as per the yield models. Both framing materials, LVL and SSL had a higher decrease in yield strength with higher exposure time and temperature, in the plate geometry than in the edge geometry. However, the magnitude of the differences varied for LVL and SSL. The decreases were much higher in magnitude for SSL when compared to LVL for the 200^{o}C 2hr treatment.

The specific gravity and its coefficient of variation for all sheathing and framing members are presented in Table 4.3. The values in the Table are mean of all replications in edge and plate connection geometry and all the treatments. Average weight loss values for all the framing and sheathing members for various treatments are shown in Fig. 4.6. The weight loss values in Fig. 4.6 are aggregate values of all connection geometries, calculated based on weight loss data compared to average initial weight of the control group. The sheathing elements after 2 hours of exposure at 200^{o}C showed slightly less damage in terms of weight loss than the framing members. However, between various types of sheathing elements, all of them experienced relatively similar weight loss. The weight loss for both the 100^{o}C treatments with exposure time one hour and 2 hour were minor as compared to 200^{o}C treatments. SSL lost more weight as compared to LVL for all the treatments. LVL being a composite started off with lower moisture content than SSL, and as they were heat treated, SSL lost more moisture as compared to LVL. The specific gravity and weight loss is correlated to structural properties of wood and connections (AFPA 2005). Higher reduction in specific gravity at exposures at 200^{o}C (Table 4.3), results in higher reduction in yield strength of the connections (Fig. 4.5).

Design Values Using Yield Models

The dowel bearing yield strengths for various framing and sheathing materials after exposure to elevated temperatures are presented in Table 4.4. Dowel bearing strength calculations were based on the panel thicknesses mentioned in Table 4.1 for the sheathing elements. Exposure at 200^{o}C for two hours caused a reduction in mean dowel bearing yield strength of the materials. However, the reduction was more prominent for thinner sheathing elements such as plywood 11.2 mm (PWH) and OSB 11.9 mm (OSBH). The degradation of dowel

bearing strength was also higher in OSBH and PWH than in solid sawn lumber or LVL, while the thicker sheathing material, showed resistance to thermal degradation of dowel bearing capacity. Consequently, the damage in the lateral load capacity of connections will be driven by the dowel bearing strength loss of OSB (11.9 mm) and plywood (11.2 mm).

The SSL-PWH connection showed significant reduction in yield strength (Table 4.2) for both edge and plate geometry. This presents a scenario of significant degradation and if the yield models can reasonably predict the design values in this scenario, the results can be generalized over other connection configurations. Hence, the discussion of predicted design yield strength will focus on the SSL-PWH connections. Although, the discussion on yield modes is predominantly on this connection type it mentions other connections as well. Prediction of design yield strength for all other connection types and their respective failure modes has been studied in more detail in Sinha (2010). The dowel bearing yield strengths of SSL and plywood from Table 4.4 were used to predict the yield load for the connections and the predicted mode of yielding; the results are presented in Table 4.5. The predicted yield load incorporated a reduction factor (R_d) stipulated in NDS (AFPA 2005). The reduction factor is based on dowel diameter and for this study an R_d of 2.2 was used. These values thus calculated are nominal design values. To compare the calculated design values to actual test values, these values need to be adjusted for 10 min duration of load (C_d = 1.6). Additionally, for the connections exposed to elevated temperature (all connections except controls) a temperature factor (C_t) was included in the evaluation of predicted design value. A C_t of 0.7 was used in this study as per NDS (AFPA 2005). Table 4.5 further compares predictions to the experimental yield strengths for the connections obtained from lateral nail tests.

The NDS yield models predicted the yield strength of connections (Table 4.5) adequately. The models do take into account the thermal degradation of the materials as it predicts a low value for yield strength for 200^{o}C-2 hr of exposure. The estimate provided by the yield models predicts a drop of 20% in yield strength when compared to control value for the edge connection after exposure to 200^{o}C for 2 hours. This drop in yield strength is due to the thermal degradation of dowel bearing strength of both the sheathing and the framing member which is accounted for in the yield models. The observed drop in yield strength was around 25% but the predicted yield strength value was lower than the observed yield strength value. The dowel bearing strength perpendicular to the grain of the wood is highly variable (Table 4.4) and lower than of parallel to the grain. As a result, the predicted drop in yield strength for plate connections was higher than the edge geometry (47% for 200^{o}C 2hr exposure) but

comparable to the observed drop in yield strength (51%). NDS yield models using the dowel bearing yield strength of materials reasonably predicts the observed yield strength. The estimation index, which is the ratio of the observed yield strength to adjusted predicted yield strength, is a good indicator of the adequacy of NDS yield models to estimate the nominal design capacity of the connections after incorporating the effect of exposure to elevated temperature. The estimation index exceeded 1.0 for all the treatments indicating that the NDS yield models are a good indicator of the expected design loads even after exposure to elevated temperatures for a period of time. Kent *et al.* (2007) also reported that the NDS models do reasonably predict the yield strength values. Aune and Patton-Mallory (1986b) also validated the models using experimental data with various sheathing members and different nail types. Theilen *et al.* (1998), however, reported that the NDS yield model approach overestimates the observed yield strength of connections. This could be due to the uncertainty in determining the yield strength of connections. The yield model does not dictate how connection yield strength is determined. The NDS yield model approach, is thus a reasonable indicator of the yield strength of connections and does tend to predict lower yield strength values for connections using materials which were exposed to elevated temperatures for a period of time, provided the dowel bearing strength of the framing and sheathing member is known. The dowel bearing yield strength or embedment strength of materials and their degradation due to exposure to elevated temperature is thus crucial. Knowledge of this dowel bearing strength and its degradation can be used in the NDS yield models to predict the yield strength of the connections between the framing and sheathing member.

Yield Modes

The predominant yield mode observed for SSL-PWH (Table 4.5) was III_s (Fig. 4.7 a-c), which implies yielding by bending of the nail (Fig. 4.7a) in the main member. There was a high level of consistency in the predicted yield mode and the observed yield mode for all the connections. The predicted yield mode for SSL-PWO was IV (Fig. 4.7 d and e) irrespective of the treatments. 80% of the SSL-PWO samples did show mode IV yield where bending of the fasteners took place in both the main member and the side member, while others showed a III_s mode of yielding. The yield models predicted either a mode III_s (Fig. 4.7c) or a mode IV (Fig. 4.7f) yielding for SSL-OSBO connections for different treatments depending on the dowel bearing strength of the materials, which consistently matched with the observed yield mode (Fig. 4.7c and f). For connections to yield by mode IV, they must have adequate member thicknesses to allow bending of the metallic fastener and to facilitate formation of plastic hinge in both the members as illustrated by Blass *et al.* (1999). PWO had a nominal thickness of 24

mm, which facilitated formation of plastic hinge within the main and side member to yield by mode IV. The thickness used in calculation was nominal thickness, the actual thicknesses varied due to manufacturing variability. Some samples had thicknesses less than 24 mm as well, hence, not all the samples showed mode IV yielding. For SSL-OSBH geometry, the prediction consistently matched the observed yield mode, except for 200^{o}C 2hr exposure where the predominant yield mode was I_s (Fig. 4.7 g and h), and not III_s, as predicted by yield models. The connections when exposed to 200^{o}C for 2hr cause the OSB to degrade in strength due to degradation in wood as well as resin. This degradation in resin also caused some flakes near the fastener to loosen and this might have led to crushing of flakes in the side member (I_s) as opposed to predicted III_s failure.

Predicted yield modes were consistent with the observed yield modes for the plate geometry (CG2). However, the extent of consistency was less than that for the edge geometry (CG1), especially for thinner sheathing materials (PWH and OSBH) and after exposure to 200^{o}C. For example, for SSL-PWH plate connection predicted yield modes were III_s for all the treatment groups. In observation, several connections for TR4 and TR5 tested in this configuration failed due to tear out at the edge (Fig. 4.7i) before any of the yield modes could be observed. In other words, the connections failed due to edge tear out before they yielded. The reason for the observed edge tear out failure could be a combination of smaller sheathing thickness (11.2 mm) and proximity of the nail to the edge of the sheathing in the direction of loading. Moreover, with exposure to high heat, the wood gets brittle, which in turn induces the tear out failure mode. The connections with thicker sheathing materials such as OSBO and PWO, yielded in accordance to the predicted modes and no edge tear out was observed.
These results suggest that with knowledge of the dowel bearing capacity of the connected members, the lateral load yield strength and failure mode of sheathing to framing nailed connections can be adequately predicted. A coherent on-site protocol can be developed to calculate and quantify the dowel bearing strength of constitutive components of a timber frame construction to provide an estimate of the residual capacity of the connection. This knowledge will help in assessing the post-fire residual capacity of a connection which was not affected by direct fire, but was exposed to elevated temperature. This is a very critical piece of information in the decision making process on rebuilding vs. rehabilitation of a structure. More data for longer exposure times would be helpful to fully characterize the temporal behavior of a material at a given temperature.

Conclusions

Data from lateral tests of 480 nailed joints connecting conventional sheathing and framing member suggests that yield strength of a connection is affected by the type of framing and sheathing member used and is different for different connection geometries (edge and plate). Furthermore, the data suggests that with exposure to elevated temperature for a sustained period of time significant degradation in the yield strength of the nail joints occurs. The degradation is greater for plate connections than for edge connections, irrespective of the sheathing and framing member. Moreover, the lateral connection capacities of the nailed joints do not show much degradation after exposure to 100^{o}C, but do show significant degradation in yield strength after 1 hour or 2 hours of exposure at 200^{o}C. For plywood (11.2 mm) and solid lumber connections, the decrease in yield strength after exposure to 200^{o}C for 2 hours was 26% for edge connections, and 56% for plate connections.

The dowel bearing strength of various materials also decreased following exposure to elevated temperatures. The greatest degradation was observed in thinner sheathing materials (OSBH and PWH). Hence, the degradation in lateral load carrying capacity of the nailed connections is governed by the thermal degradation of the dowel bearing strength of OSB and plywood for thinner sheathing materials. Using dowel bearing strength of control and exposed materials, a reasonable prediction of design values were made. In addition, the predicted yield modes were consistent with observed yield modes. However, tear-out for connections with thinner sheathing and after exposure to high temperature was deviations from the yield models. Hence, the yield models performed reasonably while predicting the yield modes of connections after exposure to elevated temperature. The models must be based on the dowel bearing strength determined after exposure to elevated temperature for expected exposure time. It thus appears that yield models are a rational approach to estimate the strength and residual capacity of the connections.

Acknowledgements

The authors gratefully acknowledge the financial support provided by Wood-Based Composite Center for this research. The experimental assistance of Milo Clauson at Oregon State University is highly appreciated.

References

AFPA. (1999). General dowel equations for calculating lateral connection values. *Technical Report 12*. American Forest and Paper Association. Washington, D.C.

AFPA. (2005). National design specification® for wood construction. *American Forest and Paper Association*. Washington, D.C.

ASTM. (2007a). Standard test method for determining bending yield moment of nails, F 1575. American Society for Testing and Materials, West Conshohocken, PA.

ASTM. (2007b). Standard test method for mechanical fasteners in wood, D 1761. American Society for Testing and Materials, West Conshohocken, PA.

ASTM. (2007c). Standard test method for specific gravity of wood and wood-based materials, D 2395. American Society for Testing and Materials, West Conshohocken, PA.

ASTM. (2007d). Standard test method for evaluating dowel-bearing strength of wood and wood-base products, D 5764. American Society for Testing and Materials, West Conshohocken, PA.

Anderson, E.N., Leichti, R.J., Sutt Jr., E.G. and Rosowsky, D.V. (2007). "Sheathing nail bending-yield stress: Effect of cyclic performance of wood shear walls." *Wood and Fiber Science*, 39(4) 536-547.

Aune, P. and Patton-Mallory, M. (1986 a). "Lateral load bearing capacity of nailed joints based on the yield theory: Theoretical development." *Research Paper FPL 469*. USDA, Forest Serv. Forest Prod. Lab., Madison, WI.

Aune, P. and Patton-Mallory, M. (1986b). "Lateral load-bearing capacity of nailed joints based on the yield theory: Experimental verification." *Research Paper FPL 470*. USDA, Forest Serv. Forest Prod. Lab., Madison, WI.

Blass, H.J., Ehlbeck, J. and Rouger, F. (1999). "Simplified design of joints with dowel-type fasteners." *Proc. Pacific timber engineering conference*, 14-18th March, Rotorua, New Zealand. Forest Research institute Limited, Rotorua, New Zealand (3), 275-279.

Buchanan, A.H. (2002). *Structural design for fire safety*. John Wiley and Sons, West Sussex, England.

Cramer, S.M. and White, R.H. (1997). "Fire performance issues." *Wood Engineering in the 21st century: research needs and goals: proc. Workshop offered in conjunction with SEI/ASCE structures congress XV*, Portland, OR. 75-86.

Foschi, R.O. (1974). "Load-slip characteristics of nails." *Journal of Wood Science,* 7(1), 69-76.

Foschi ,R.O. and Bonac, T. (1977). "Load-slip characteristics for connections with common nails." *Wood Science*, 9(3), 118-123.

Fuller, J.J. (1990). "Predicting the thermo-mechanical behavior of a gypsum-to-wood nailed connection." MS Thesis, Oregon State University, Corvallis, OR

Gerhards, C.C. (1982). Effect of moisture content and temperature on the mechanical properties of wood: An analysis of immediate effects. *Wood and Fiber Science*, 14(1), 3-36.

Green, D.W., Winandy, J.E. and Kretschmann, D.E. (1999). “Mechanical Properties of wood-Wood as an engineering material.” *General Technical Report FPL-TR 113*, U.S. Department of Agriculture, Forest Service, Forest Products Laboratory, Madison, WI.

Johansen, K.W. (1949). “Theory of timber connectors.” *Publication No. 9, International Association of Bridges and Structural Engineering*, Bern, Switzerland, 249–262.

Kalkert, R.E. and Dolan, J.D. (1997). “Behavior of 8-D nailed stud-to-sheathing connections.” *Forest Prod. J.,* 47(6),95–102.

Kent, S. (2004). “The effect of biological deterioration on the performance of nailed oriented strand board sheathing to Douglas-fir framing member connections.” PhD Thesis, Oregon State University, Corvallis, OR.

Kent, S.M., Leichti, R.J., Rosowsky, D.V., and Morrell J.J. (2004). “Effect of wood desay by Postia Placenta on the lateral capacity of nailed oriented strandboard sheathing and douglas-fir framing members.” *Wood and Fiber Science*. 36(4) 560-572.

Knudsen, R.M and Schniewind, A.P. (1975). “Performance of structural wood members exposed to fire. *Forest Products Journal*, 25(2), 23-32.

Kuenzi, E.W. (1955). “Theoretical design of a nailed or bolted joint under lateral load.” *Rep. No. Dl951*. U.S. Dept. of Agriculture, Forest Products Laboratory, Madison, WI.

McLain,T.E. (1975). “Curvilinear load-slip relations in laterally loaded nail joints.” PhD Thesis, Colorado State University, Fort Collins, Colorado.

Nishiyama, N. and Ando, N. (2003). “Analysis of load-slip characteristics of nailed wood joints: application of a two-dimensional geometric nonlinear analysis.” *J. Wood Science,* (49), 505-512.

Noren, J. (1996). “Load-bearing capacity of nailed joints exposed to fire.” *Fire Material,* (20), 133-143.

Pellicane, P.J. (1991). “Application of the European yield model to nailed joints in southern hardwoods.” *J. Testing Eval.,* 19(5), 385-393.

Pellicane, P.J. (1993). “Plywood-Solid-wood nailed joints under lateral loading.” *Journal of material in Civil Engineering*, 5(2), 226-236

Peyer, S.M. and Cramer, S.M. (1999). “Behavior of nailed connection at elevated temperature.” *Wood and Fiber Science*, 31(3), 264-276

Price, E.W. and Gromala, D.S. (1980). “Racking strength of walls sheathed with structural flakeboards made from southern species.” *Forest Products Journal*. 30(12), 19-23.

SBA (2009). “OSB: A flooring panel that stands on its own.” S*pecifications EL809*, Structural Board Association, Ontario, Canada.

Shrestha, D. Cramer, S and White, R. (1995). “Simplified models for the properties of dimension lumber and metal- plate connections at elevated temperatures. *Forest Products Journal*, 45(7/8), 35-42.

Sinha, A. (2010). “Effect of Heat on mechanical properties of wood and wood-based composites.” PhD Thesis, Oregon State University, Corvallis, OR. (in progress)

Sinha, A. and Gupta, R. (2009). “Strain distribution in OSB and GWB in wood-frame shear walls.” *Journal of Structural Engineering*, 135(6), 666-675

Sinha, A., Nairn, J.A. and Gupta, R. (2010). “Thermal Degradation of the bending strength of plywood and oriented strandboard: A Kinetics approach.” *Wood Science and Technology*, Accepted.

Smith, I., Craft, S.T. and Quenneville, P. (2001). “Design capacities of joints with laterally loaded nails.” *Can. J. Civil Engineering,* (28), 282-290.

Theilen, R.D., Bender, D.A, Pllock, D.G. and Winistorfer, S.G. (1998). “Lateral Resistance of ring-shank nail connections in Southern Pine lumber.” *Transactions of the ASAE*, 41(2), 465-472.

Wilkinson, T. L. (1991). “Dowel bearing strength.” *FPL-RP-505*. USDA Forest Service, Forest Products Laboratory, Madison, WI.

Winandy, J.E. and Lebow, P.K. (1996). “Kinetics models for thermal degradation of strength of fire-retardant treated wood.” *Wood and Fiber Science*, 28(1), 39-52.

Winandy, J.E., LeVan, S.L., Ross, R.J., Hoffman, S.P. and McIntyre, C.R. (1991). “Thermal degradation of fire-retardant-treated plywood: Development and evaluation of test protocol.” *Research Paper FPL-RP 501*. U.S. Department of Agriculture, Forest Service, Forest Products Laboratory. Madison, WI.

Winandy, J.E., LeVan, S.L., Schaffer, E.L. and Lee, P.W. (1988). “Effect of fire-retardant treatment and redrying on the mechanical properties of Douglas-fir and aspen plywood*.” Research Paper FPL-RP 485. U.S*. Department of Agriculture, Forest Service, Forest Products Laboratory. Madison, WI.

Table 4.1. Experimental design matrix with description of various materials used and their symbols.

Variable	Quantity	Description	Symbols
Connection Geometry (CG)	2	Edge (CG1) and Plate (CG2)	
Framing member (FM)	2	FM1- SSL (38 x 89mm), Douglas-Fir	SSL
		FM2- LVL (38 x 89mm), Douglas-Fir	LVL
Sheathing member (SM)	4	SM1- OSB 11.9 mm, Aspen	OSBH
		SM2- OSB 22 mm, Aspen	OSBO
		SM3- Plywood 11.2 mm, Douglas Fir	PWH
		SM4-Plywood 24 mm, Douglas Fir	PWO
Fastener	1	SENCO (3.2 x 75 mm)	
Treatments (TR)	5	TR1- CTRL, TR2- 100C-1hr, TR3- 100C-2hr, TR4- 200C-1hr, TR5- 200C-2hr	
Replication	6		
Total	**480**	(2 x 2 x 4 x 1 x 5 x 6)	

SSL – Solid Sawn Lumber; LVL- Laminated Veneer Lumber; OSBH – Oriented strand board (t=11.9 mm); OSBO – Oriented strand board (t=22 mm); PWH- Plywood (t= 11.2 mm); PWO- Plywood (t = 24 mm); CTRL – Control Treatment

Table 4.2. Yield strength (N) of edge and plate connection geometry for various sheathing and framing member combinations tested, along with their coefficients of variation (COV %) and p-values for an analysis of variance F-test for comparison of means within the same groups. Abbreviations of various materials explained in table 1.

Treatment	Geometry	Edge							
	Framing	SSL				LVL			
	Sheathing	PWH	PWO	OSBH	OSBO	PWH	PWO	OSBH	OSBO
Control	Load	710	809	678	723	717	608	680	731
	COV	16.6	22.5	19.3	18.0	13.4	10.2	18.1	12.5
100C-1hr	Load	584	791	610	702	616	593	549	615
	COV	13.6	4.2	11.8	7.5	12.1	13.4	11.9	14.8
100C-2hr	Load	604	731	569	719	610	597	585	625
	COV	11.2	6.7	7.4	10.3	13.3	11.9	8.1	10.2
200C-1hr	Load	635	707	474	652	581	649	467	503
	COV	16.2	8.3	8.1	12.1	16.4	13.2	6.3	11.7
200C-2hr	Load	526	651	468	542	437	489	346	484
	COV	13.4	14.7	9.4	11.9	12.8	19.6	13.7	17.2
p-value		0.020	0.060	0.000	0.005	0.000	0.026	0.000	0.000

Treatment	Geometry	Plate							
	Framing	SSL				LVL			
	Sheathing	PWH	PWO	OSBH	OSBO	PWH	PWO	OSBH	OSBO
Control	Load	749	724	486	655	689	510	421	669
	COV	21.7	23.1	15.3	11.2	14.2	18.2	19.2	10.8
100C-1hr	Load	534	693	506	599	713	422	491	621
	COV	5.6	13.6	17.1	10.5	14.8	21.7	15.9	14.0
100C-2hr	Load	509	515	467	523	498	530	498	689
	COV	14.7	25.9	13.1	10.4	15.2	22.3	14.6	14.8
200C-1hr	Load	391	672	392	500	382	404	502	500
	COV	27.0	9.4	16.2	15.0	16.5	17.4	16.1	12.0
200C-2hr	Load	355	309	322	568	292	462	412	421
	COV	16.2	12.4	13.3	19.8	17.3	22.3	14.1	15.3
p-value		0.000	0.000	0.000	0.010	0.000	0.130	0.256	0.000

Table 4.3. Effect of exposure to elevated temperature on specific gravity of various materials with their coefficients of variation (COV %). Abbreviations of various materials explained in table 1.

Treatments		Specific Gravity					
		SSL	**LVL**	**PWH**	**PWO**	**OSBH**	**OSBO**
CTRL	Mean	0.487	0.508	0.553	0.462	0.592	0.563
	COV	*14.3*	*3.1*	*6.4*	*3.3*	*4.0*	*3.2*
100C-1hr	Mean	0.496	0.512	0.564	0.458	0.572	0.565
	COV	*11.1*	*2.7*	*8.1*	*3.7*	*6.4*	*3.6*
100C-2hr	Mean	0.483	0.517	0.566	0.461	0.594	0.560
	COV	*8.4*	*2.8*	*5.4*	*3.2*	*6.2*	*5.1*
200C-1hr	Mean	0.465	0.500	0.500	0.468	0.581	0.543
	COV	*10.6*	*2.4*	*9.3*	*3.8*	*5.1*	*3.4*
200C-2hr	Mean	0.421	0.470	0.503	0.437	0.549	0.542
	COV	*10.2*	*3.2*	*6.1*	*3.1*	*7.2*	*4.2*

Table 4.4. Effect of exposure to elevated temperature on Dowel Bearing Strength of various materials with their coefficient of variation (parentheses) in % (n=6, for each cell). Abbreviations of various materials explained in table 1.

Treatment	Nominal Dowel Bearing Strength (MPa)													
	SSL $_{parallel}$		**SSL $_{perp}$**		**LVL $_{parallel}$**		**PWH**		**PWO**		**OSBH**		**OSBO**	
Control	44.22	(11.8)	16.80	(25.1)	44.33	(9.6)	51.65	(9.1)	41.55	(9.1)	36.43	(23.5)	25.46	(9.2)
100C 1hr	48.56	(9.1)	13.90	(24.1)	38.40	(17.1)	60.56	(16.6)	48.34	(10.9)	37.98	(26.2)	33.18	(15.4)
100C 2hr	58.48	(13.6)	14.03	(18.7)	56.35	(20.6)	56.45	(12.6)	45.19	(13.1)	36.01	(23.9)	27.07	(22.3)
200C 1hr	50.23	(7.9)	14.50	(24.4)	47.75	(16.1)	52.36	(8.6)	38.32	(12.9)	37.21	(16.1)	27.46	(6.2)
200C 2hr	36.34	(11.0)	11.05	(30.3)	42.20	(5.9)	35.18	(21.7)	37.59	(10.9)	25.64	(24.0)	26.08	(23.7)

Table 4.5. Solid lumber-plywood (SSL-PWH) connection with observed and predicted strength comparison using yield models.

Treatment	Predicted Yield Load [Z(N)]	Adjusted Predicted Yield Loads (N)	Predicted Mode	Actual Yield Load (N)	Observed Mode	Estimation Index
Edge Geometry (CG1)						
CTRL*	404	646	III_s	710	III_s	1.10
100C-1hr	446	500	III_s	584	III_s	1.17
100C-2hr	447	501	III_s	604	III_s	1.21
200C-1hr	417	467	III_s	635	III_s	1.36
200C-2hr	324	363	III_s	526	III_s	1.45
Plate Geometry (CG2)						
CTRL*	312	500	III_s	749	III_s	1.50
100C-1hr	314	352	III_s	534	III_s	1.52
100C-2hr	306	342	III_s	509	III_s	1.49
200C-1hr	300	336	III_s	391	Edge Tear out	1.17
200C-2hr	236	264	III_s	355	Edge Tear out	1.34

*Control values were not adjusted by temperature factor $C_t = 0.7$

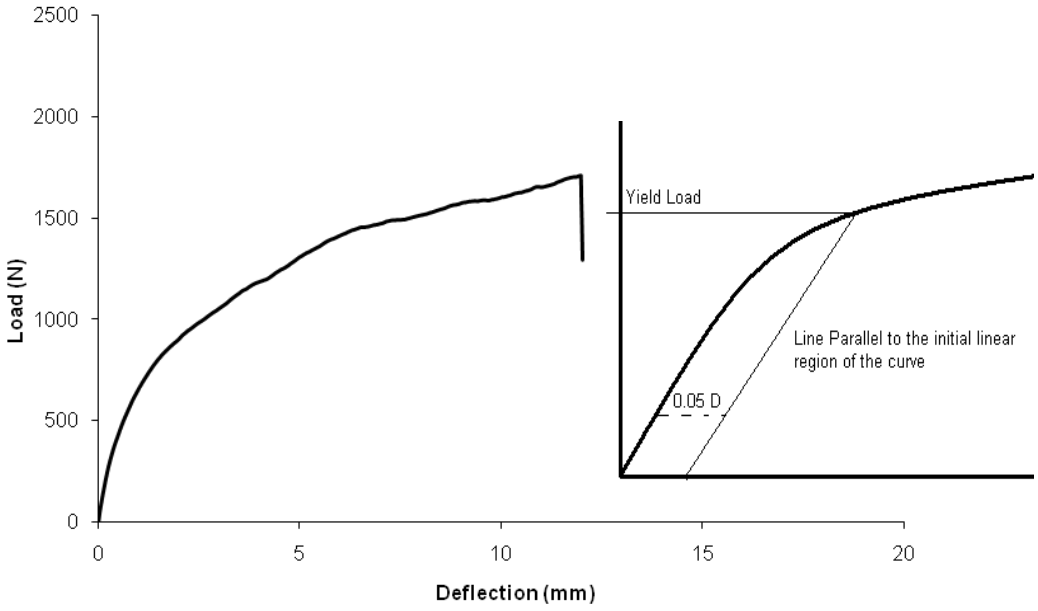

Figure 4.1. Typical Load deflection diagram; inset depicting the 5% offset yield point.

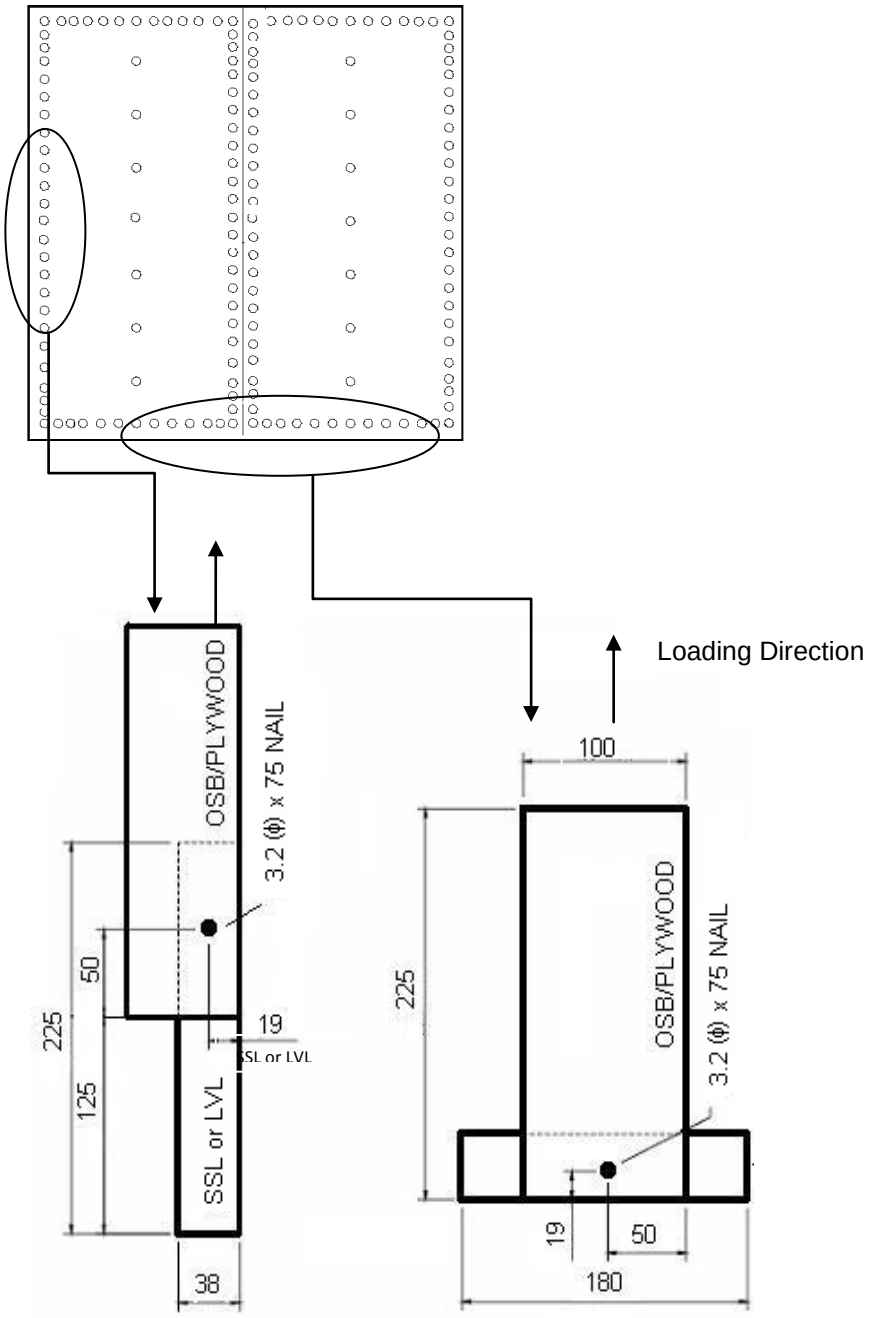

(a) Edge Connection Geometry (b) Plate Connection Geometry (All dimension in mm)

Figure 4.2. Connection Geometries

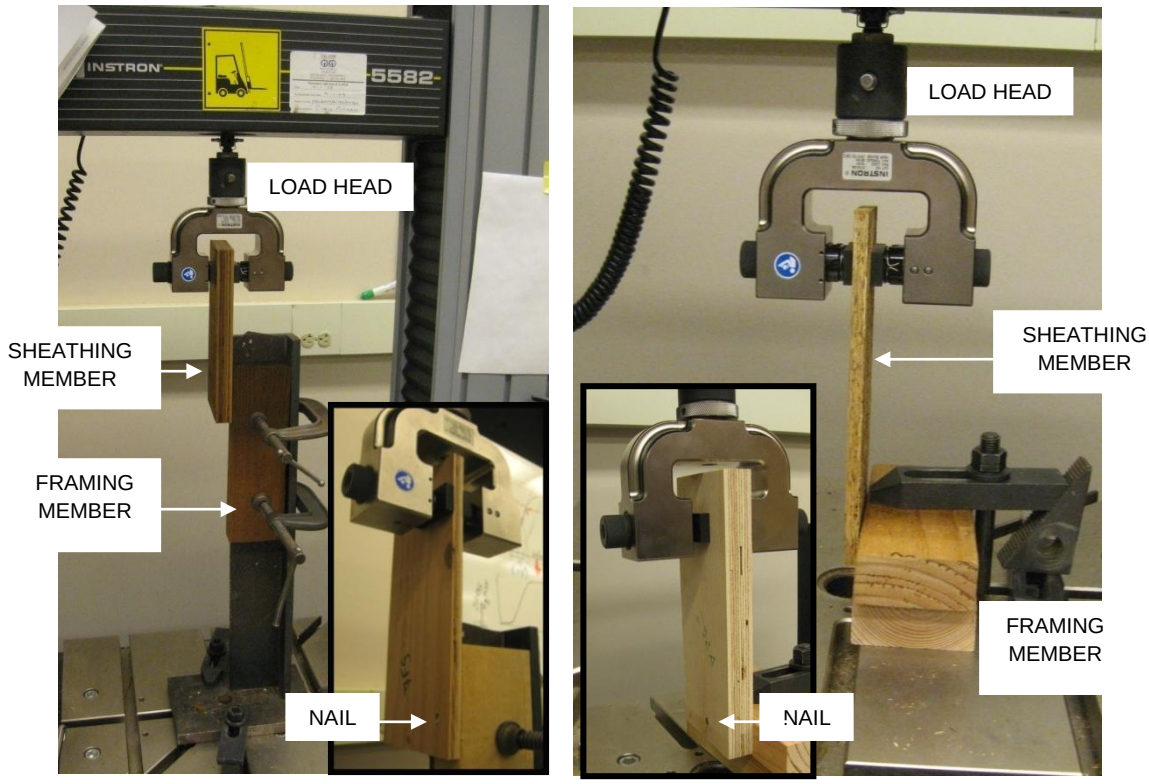

(a) Edge Connection set up (b) Plate Connection set up

Figure 4.3. Lateral Nail connection test set up. Inset showing the position of grips with respect to nail.

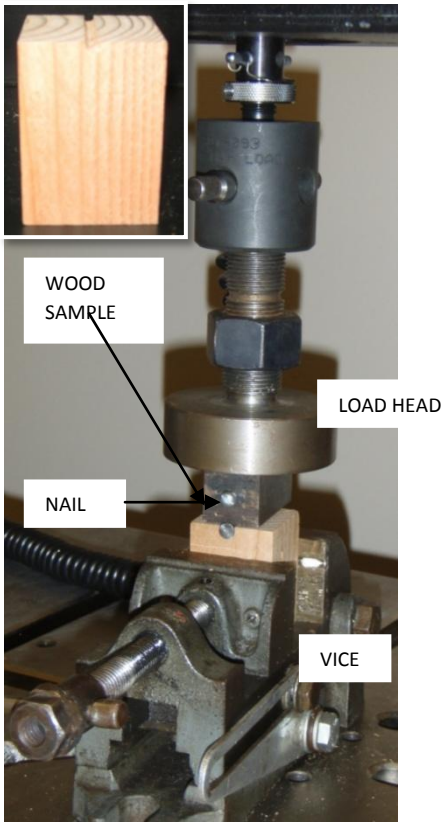

Figure 4.4. Dowel Bearing Test Set up; SSL sample (inset)

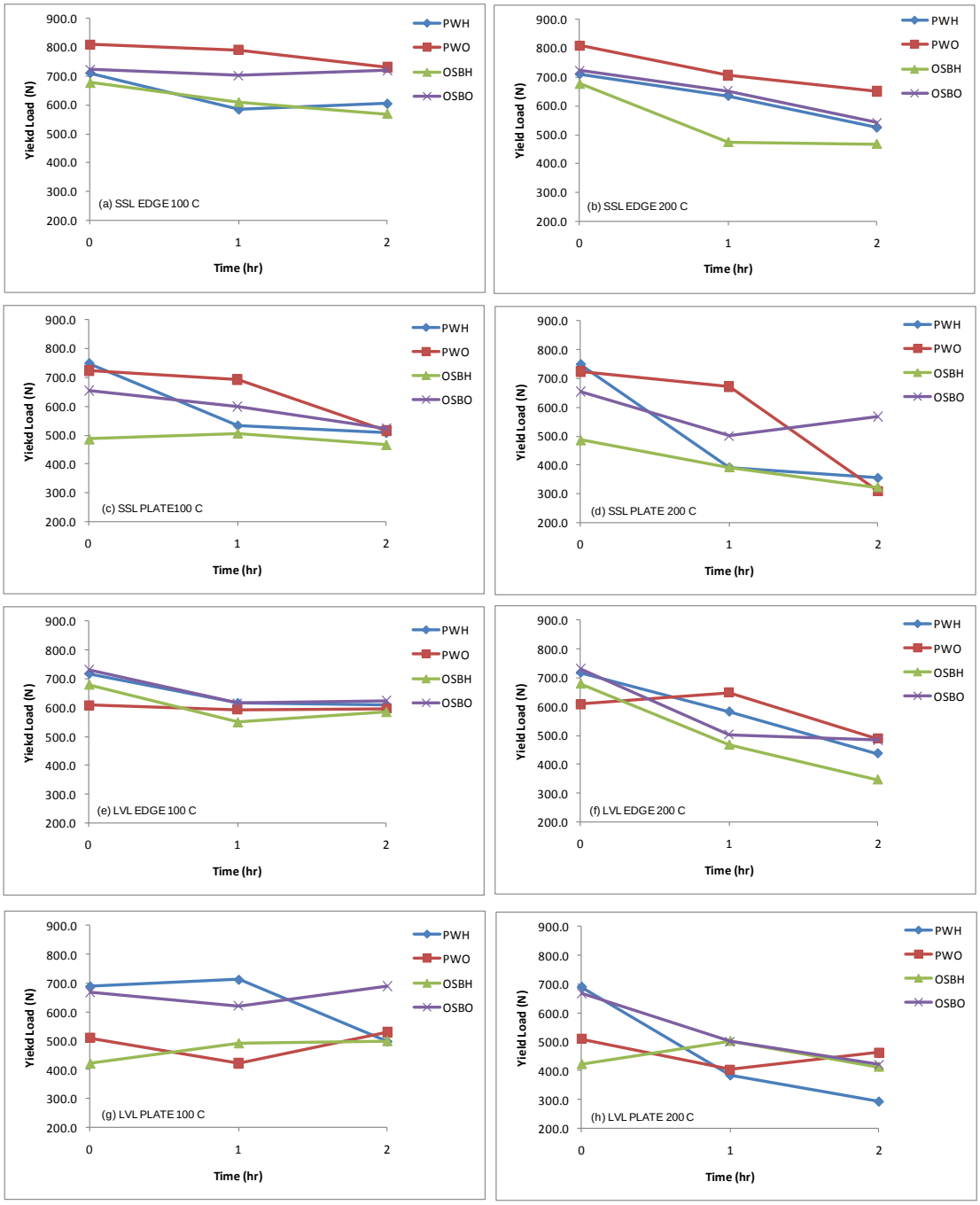

Figure 4.5. Variation in yield strength (N) of various sheathing – framing combinations tested when tested after exposure to elevated temperatures shown as function of exposure time.

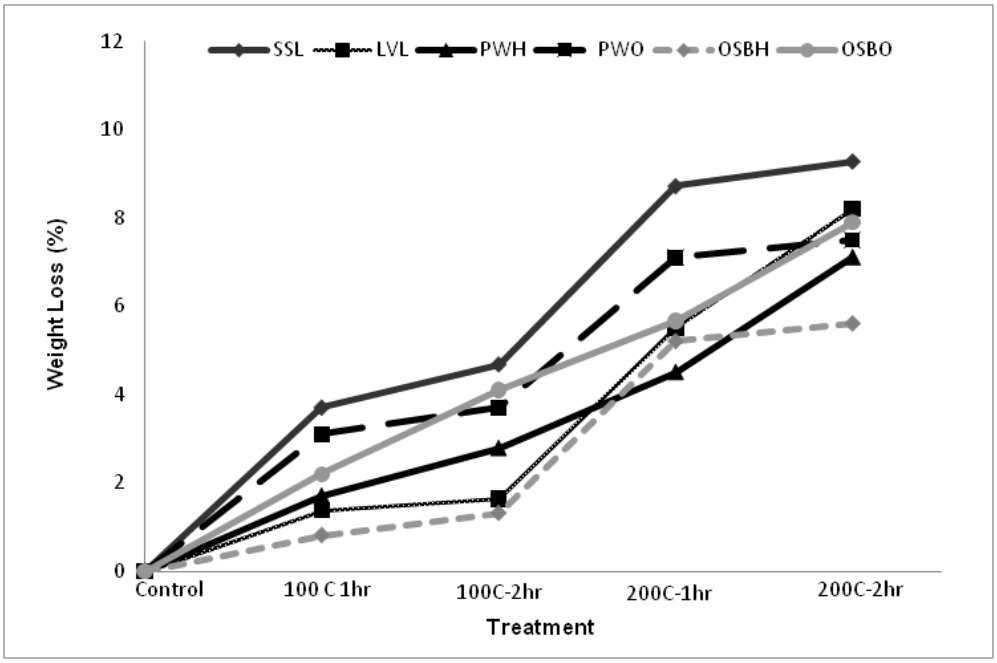

Figure 4.6. Weight loss (%) for various members on exposure to elevated temperature.

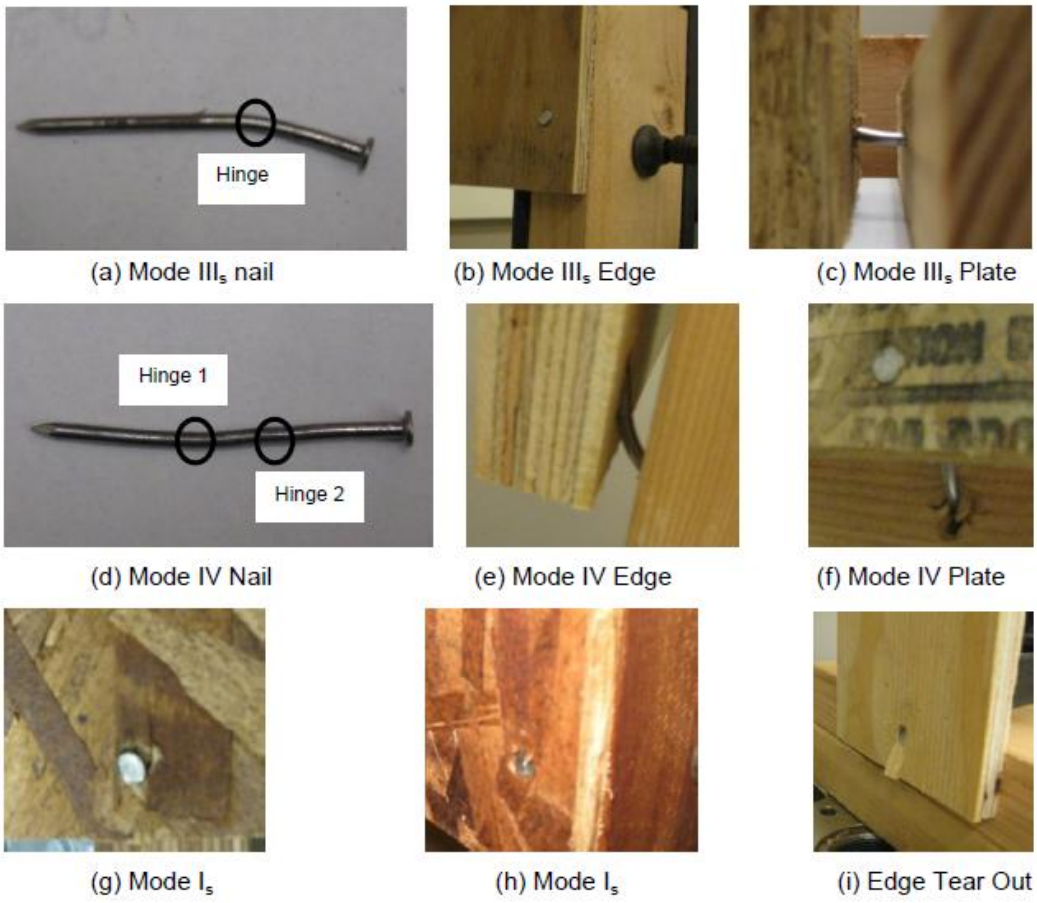

Figure 4.7. Observed yield modes of laterally loaded nail connections.

Fracture Toughness of Wood and Structural Wood-based Composites Using R Curve Analysis

Arijit Sinha, John A. Nairn and Rakesh Gupta

To be Submitted to:
Engineering Fracture Mechanics
Elsevier

Chapter 5: Fracture toughness of wood and structural wood-based composites using R curve analysis

Arijit Sinha, John A. Nairn and Rakesh Gupta

Abstract

Fracture toughness of wood and wood composites has traditionally been characterized by a stress intensity factor, an initiation strain energy release rate (G_{init}) or a total energy to fracture (G_f). These parameters provide incomplete fracture characterization for these materials because the toughness changes as the crack propagates. Thus for materials such as wood, oriented strand board (OSB), plywood and laminated veneer lumber (LVL), it is essential to characterize the fracture properties during crack propagation by measure a full crack resistant or R curve. The objectives of this study were to use energy methods during crack propagation to measure full R curves and then to compare the fracture properties of wood and various wood-based composites such as, OSB, LVL and plywood. The effect of exposure to elevated temperature on fracture properties of these materials was also studied. The steady state energy release rate (G_{SS}) of wood was lower than that of wood composites such as LVL, plywood and OSB. The resin in wood composites provides them with the higher magnitude of fracture toughness as compared to solid lumber. Depending upon the internal structure of the material the mode of failure also varied. With exposure to elevated temperatures, G_{SS} all materials decreased while the failure mode remained the same. The scatter associated with conventional bond strength tests such as internal bond (IB) and bond classification renders any statistical comparison difficult. In contrast, fracture tests with R curve analysis may provide an improved tool for characterization of bond quality in wood composites.

Introduction

Traditionally, designs involving timber are based on stress or strain criteria derived by strength analysis (AFPA 2005) and have performed fairly well in practice. However, the presence of a flaw (which induce stress concentrations) can lead to failure before the ultimate load capacity derived from stress criteria is reached (Anderson 2005); this effect can cause traditional stress design methods to give poor predictions of load-bearing capacity. The flaws may be due to natural features such as, knots, checks, shakes, and cracks that form during drying or may be a result of construction and handling such as notches and holes in beams or columns, holes due to dowel type fasteners (Daudeville et al. 1999) and bond lines in adhesive joints (Conrad et al. 2004). An alternative approach to failure analysis is to use fracture mechanics. Fracture is important in wood, especially mode I fracture in which tensile stresses are perpendicular to grain direction. The resulting cracks parallel to the longitudinal direction of wood, Glulam or laminated veneer lumber (LVL) are of great concern may lead to failure of the member. The stresses that cause these cracks are applied on the member either by mechanical load or by drying stresses. These types of cracks can be analyzed by fracture mechanics.

Fracture mechanics deals with characterization of fracture properties of a material. Fracture properties can be determined through two methods - stress intensity factor or energy release rate methods (Anderson 2005). The stress intensity method provides information on the stress state near the tip of a sharp crack. On the other hand, the energy method provides great deal of insight into the fracture process (Roylance 2001) and crack growth. The energy required to develop and propagate the crack is called the fracture energy and can be determined through stable crack growth tests. In many materials, resistance to fracture increases as the crack grows. This resistance to crack growth is due to the development of a process zone (Morel et. al 2003, Smith and Vasic 2003, Nairn 2009). Materials that develop process zone include wood (Smith and Vasic 2003), wood-based composites (Matsumoto 2009), fiber reinforced composites (Nairn 2009) and cement based composites (Li et al. 1987). A process zone in wood and wood composites is usually the result of fiber bridging. When a crack propagates, some non-fractured fibers cross the crack surface in the wake of the crack; these bridged fibers continue to carry stress and will increase the failure load compared to a material with stress-free fracture surfaces. In other words, when a process zone is present, some of the energy required to propagate a crack is needed to overcome the process zone while the remaining energy is used for crack tip propagation (Stanzl-Tschegg and Navi, 2009). As a result, the toughness increases as a function of crack length. Experimental observation of this

increase is known as the material's fracture resistance or R curve. A fiber-bridging zone leads to a rising R curve.

The *R* curve is defined as the actual amount of energy released as a function of the extent of crack propagation:

$$R(\Delta a) = G_{init} + G_B(\Delta a) \qquad \text{(eq. 5.1)}$$

where G_{init} is the initiation toughness and $G_B(\Delta a)$ is the toughness due to bridging, which depends on the amount of crack growth, Δa. In materials with fiber bridging, *R* starts at $R(0) = G_{init}$ and $G_B(0)=0$. As the crack propagates, *R* increases because the fiber bridging zone develops, which causes $G_B(\Delta a)$ to increase. If the crack propagation is sufficient long (e.g., in large specimens) or the bridging zone is sufficient short, $G_B(\Delta a)$ may reach a constant value denoted here as G_B or the total toughness associated with a fully-developed bridging zone. When this constant value is reached the R curve will plateau at a constant toughness denoted here as steady state toughness or $G_{SS} = G_{init} + G_B$. The rising part of the *R* curve corresponds to crack tip propagation edge of the process zone at the initial crack tip (the notch root) remains stationary. During the phase, the process zone is increasing in length. Steady-state crack propagation occurs when the crack tip and notch root propagate simultaneously and about the same rate. In this regime, the fiber-bridging zone is fully developed and remains constant in length (Nairn 2009). Fig. 5.1c shows a typical R curve for experiments described below. This *R* curve for LVL rises from G_{init} of about 700 J/m^2 for about 15 mm if crack growth where it reaches G_{SS} of about 1200 J/m^2, which implies G_B of about 500 J/m^2.

Conventional fracture mechanics methods have been applied to wood starting in 1960s (Wu 1963, 1967) and has been comprehensively reviewed by Vasic (2000), Smith et al. (2003) and Stanzl-Tschegg and Navi (2009). Most studies have focused on either initial fracture toughness or G_{init} (Stanzl-TSchegg and Navi 2009, Aicher 2010) or total energy (G_f) at fracture (Frühmann et al. 2003). Neither of these methods provide a full fracture characterization. G_{init} is a useful material property, but the initiation toughness ignores contributions to material properties from fiber-bridging zones. G_f is approximately an average under and the *R* curve, but it provides no information about the shape of the *R* curve. For example, some specimens may never reach G_{SS} and such materials are not well characterized by an average value or an unknown extent of process zone development. An additional complication is that edge effects can lead to artifacts in total fracture energies (Matsmoto and Nairn, 2009). The best way to characterize fracture properties of wood and wood composite is to record the complete *R* curve. If a material reaches G_{SS}, the results provided G_{init}, G_B, G_{SS}, and the size of the bridging

zone. If a specimen does not reach G_{SS}, the shape of the rising *R* curves still provides information about fiber bridging processes (Nairn and Matsumoto 2010).

Wood is an orthotropic material, with three axes of symmetry namely longitudinal (L), tangential (T) and radial (R) over which the properties differ significantly (Green et al. 1999).The direction parallel to the fiber direction called the longitudinal direction (L); a direction perpendicular to (L) is called the tangential direction (T), while radial direction (R) is perpendicular to growth rings. Crack propagation properties can be characterized in each of two directions in the three planes of symmetry, namely, RL, TL, RT, LR, LT and TR. The second letter represents the direction of crack propagation, while the first letter indicates the direction normal to the crack plane. Prior work has looked at crack propagation in all 6 directions (although testing in LR and LT are suspect because cracks generally will not propagate through the wood fibers in these directions) (Frühmann et al. 2003, Stanzl-TSchegg and Navi 2009). It is interesting to focus on crack growth along the wood fibers, namely the RL and TL directions. Schneiwind and Centano (1973) and Johnson (1973) measure K_{Ic} for initiation of RL and TL cracks in Douglas fir. Schneiwind and Centano (1973) found that K_{Ic} for RL to be higher than for TL (409 MPa √m *vs*. 309 MPa √m). They concluded that radial ray cells, which are perpendicular to the crack plane in RL specimens, are arresting crack growth in the RL direction, but are not available to arrest crack growth in the TL direction. Johnson (1973) found the opposite or that TL toughness is higher than RL (374 MPa √m *vs*. 324 √m). He concluded, however, that the results were too close to draw conclusions. Fruhman *et al*. (2002) and Reiterer *et al*. (2002) used total fracture energy instead and compared RL and TL toughness for various species. Again, the results differ. Fruhman *et al*. (2002) found TL toughness higher than RL in both beech and spruce. They concluded the late wood zones, which are perpendicular to crack growth in TL specimens, are contributing to increased TL toughness. In contrast, Reiterer *et al*. (2002) found RL toughness to be higher than TL toughness. Like Schneiwind and Centano (1973), they attributed the difference to rays cells inhibiting RL crack growth. These prior results are conflicting because the conclusions were based on incomplete fracture information – either initiation alone or total fracture energy alone. A much clearer picture emerges when a complete *R* curve is used instead. Nairn and Matsumoto (2010) looked at RL and TL *R* curves in Douglas fir. The initiation values are similar and probably the same within experimental uncertainty (G_{init} = 158 J/m^2 for RL and 215 J/m^2 for TL). The *R* curves, however were dramatically different. The RL *R* curve was essentially flat (G_B = 0) while the TL *R* curve increased to G_{SS} = 620 J/m^2, which implies G_B = 405 J/m^2. Our new R curves for DF (described below and including new results after exposure

to high temperature) agree with these recent *R* curves. The results indicate that latewood zones provide bridging that enhances TL toughness. This conclusion is based on much larger differences (G_B = 0 *vs*. 405 J/m^2) than seen in prior work that did not record the full *R* curve.

Wood composites have also been studied by fracture mechanics methods (Conrad et al. 2004), although they have been studied less often than solid wood. A misconception in both synthetic and wood composites is that fracture mechanics may not apply. Because fracture mechanics is simply energy balance during crack growth (*i.e.*, thermodynamics), it must apply. The use of fracture mechanics, however, requires a material that can grow a crack and experiments that can monitor that crack growth; that situation may not always exist in composites or many only exist for a few crack paths. Composites, like medium density fiberboard (MDF) and particle board (PB) can propagate either in-plane (crack surface normal to the plane of the panel) or through-the–thickness (crack surface parallel to the plane of the panel) cracks (Matsumoto and Nairn 2007, 2010). It is a challenge to see these cracks but that issue can be solved with advanced imaging methods (Matsumoto 2009). In composites, such as OSB and plywood, only through-the-thickness crack propagation is possible. For LVL, crack propagation is easiest in the wood fiber direction. The crack surface may be parallel to the veneers (through-the-thickness cracks) or perpendicular, but most work has focused on the former. As in solid wood, most prior fracture work has used either conventional fracture mechanics for crack initiation or looked at total fracture energy. Niemz et al. (2006) measure K_{Ic} for initiation in chip board, MDF, PB, OSB, and plywood. They looked only at initiation. Ehart *et al*. (1996, 1998, 1999) studied PB and parallam (PSL) by total work of fracture. They tried to construct an *R* curve, but they needed numerical calculations to determine an *effective* crack length rather than using the actual crack length. When fracture results on interpreted using *effective* cracks lengths, the results have to be termed as *effective* toughness or *effective R* curve rather than actual amount of energy required to propagate the crack. Frühmann *et al*. (2002) studied the fracture behavior of LVL in mode I. Their energy analysis looked only at initiation and total area under the force-displacement curve, rather than a full *R* curve analysis. Mihashi and Hoshino (1989) supported the use of *R* curve analysis in fracture mechanics of LVL to verify their experimental results with analytical solutions. Recently, Matsumoto and Nairn (2007, 2010) characterized fracture properties of MDF and PB with a full *R* curve analysis. They observed large fiber-bridging effects; thus the characterization of wood composites, like solid wood, requires a full *R* curve analysis (Nairn 2009). The results here extended the methods of Matsumoto and Nairn (2007, 2010) to experiments on OSB, plywood, LVL, and solid wood. We are not aware or prior *R* curve studies on OSB or plywood.

Fracture properties of these wood composites will depend upon the fracture properties of the adhesive bond as well as the wood phases. Many wood composites, like OSB, may also contain void spaces, which can alter their fracture behavior (Conrad et al. 2004).

The evaluation of bond strength in plywood is commonly done in the industry by using a lap shear strength test called the bond classification test (NIST 2007). For OSB, the common bond strength test is called the Internal bond (IB) test (ASTM D 1037). Both these methods have shortcomings. In the bond classification test, wood is loaded in shear parallel to grain while in IB wood it is loaded in tension perpendicular to grain. These are wood's two weakest orientations (Green et al. 1999). Both these tests typically have high scatter in the results, which is due to inherent variations in wood (River 1994) and to drawbacks in the testing procedures (Gagliano and Frazier, 2001). It is hard to find statistical significance in changes, unless the changed are very large. These conventional tests fail at statistically random weakest links. The weakest link in IB tests could be within the OSB itself or could be in the adhesion of testing block to the wood surface. Similarly, the bond classification test for plywood is influenced by a multitude of factors such as lathe checks and veneer roughness (DeVallance et. al. 2007). Because, both these tests look only at final failure and average stress over the bonded area, they provide no information about the amount of stress necessary to initiate failure (River and Okkonen 1993). This is crucial, as it has been reported that the most common mode of failure for laminated composites is by the propagation of an inter-laminar crack (Hashemi et al. 1990). Perhaps through-the-thickness crack propagation of plywood, OSB, MDF *etc*. would be a better test for bound quality? A fracture test is likely to have less scatter (because the crack is controlled rather than at a random weakest link) and the results may provide a more fundamental material property for internal bonds (toughness instead of strength). Fracture testing of wood composites for the evaluation of wood adhesion is not a new concept (Gagliano and Frazier 2001, Ebewele et al., 1979, 1980, 1982, and 1986). Most prior work, however, has looked at crack growth along an adhesive bond line between two layers of wood. This study explores whether fracture analysis of crack propagation within a single composite material (OSB, plywood, LVL, etc.) can be an alternative to conventional bond strength testing.

The objective of this study was to use energy methods during crack propagation to measure the full *R* curves to characterize and compare the fracture properties of solid wood and various wood-based composites such as, OSB, LVL and plywood. The application of these R curves was to study the effect of exposure to elevated temperature on the fracture properties. The

materials were exposed to 100˚C or 200˚C for one or two hours and the fracture properties before and after exposure were measured. An second object was to study in fracture testing is a preferred test over convention bond strength tests such as IB and bond classification is presented. We thus also looked at bond strength tests before and after exposure to elevated temperatures. The observed changes to the fracture properties *vs*. bond strength properties helped to assess the efficiency and sensitivity of the two methods for wood composites.

Material and Methods

Materials

The fracture toughness of six different materials were evaluated. The materials included Douglas fir (*Pseudotsuga menziesii*) solid sawn lumber, laminated veneer lumber (LVL), and plywood (2 thicknesses) and Aspen oriented strand board (2 thicknesses) as listed in Table 5.1. To observe whether exposure to elevated temperature changes the material properties, two different temperatures, 100 and 200^{o}C were chosen. At each temperature, the materials were exposed for two different exposure times, 1h and 2h. There were, therefore, five different heat treatments for the materials namely, control (CTRL), 100^{o}C-1h (100C1), 100^{o}C-2 h (100C2), 200^{o}C-1 h (200C1) and 200^{o}C-2 h (200C2). All specimens were conditioned to equilibrium moisture content (EMC) prior to exposure to temperature. The samples were heat treated in a conventional convection oven. A separate oven run was scheduled for each treatment. The oven was preheated to the desired temperature, as monitored by internal as well as external thermo-couples. Once the desired temperature was reached, the samples were inserted in the oven for the designated exposure time. The process was repeated for all the temperatures. Once the specimens were taken out of the oven, they were allowed to cool to room temperature before testing. After exposure to elevated temperature the specimens were not re-equilibrated with moisture. As a result, the property changes may represent the combined effects of property changes due to moisture change and exposure to elevated temperatures.

A sample size of 25 for each treatment for IB and Bond classification were chosen based on pilot study, such that an alpha priori level of 0.05 may be achieved in statistical tests for comparison between treatments. Due to lack of study in R curve analysis of wood, coupled with the facts that fracture propagation experiments generate many data points from each specimen and the image processing and subsequent R curve analysis is time intensive, 2 samples for each material were chosen per treatment, making it a total of 60 fracture tests.

Testing Methods

Internal Bond

Internal bond strength for OSB (OSO and OSH) was determined according to ASTM Standard D-1037. The OSB was cut into 50 mm square sample. Both surfaces were glued to aluminum alloy loading blocks designed to hold the blocks securely in the testing apparatus as a tensile force was applied at a speed of 1 mm/minute until failure. The peak stress at failure and the peak force in MPa were used to assess the internal bond strength. At each treatment 25 samples were tested, giving a total of 125 samples for one material.

Bond Classification for Plywood

The typical bond classification test for plywood, as outlined in PS-1 (NIST 2007) involves testing 25.4 mm square test area in the center of the specimen. The specimens were cut to specification of PS-1 to be 82.6 mm long by 25.4 mm wide and saw-kerfed one-third of the length of the specimen from each end, to provide the desired test area. Kerfing extended two-thirds of the way through the ply to be tested and care was taken not to penetrate the next bond line. Specimens were oriented so that the grain direction of the ply under test runs at a 90° angle to the length of the specimen. These specimens were gripped and pulled at a rate of 2 mm/min. PS-1 only uses visual inspection of the percentage wood failure in the sample. Here both the % wood failure and maximum load at failure were recorded. A total of 250 samples were tested for two materials (PWH and PWO) consisting of 25 samples per material per treatment.

Fracture

A total of 60 samples were tested encompassing 2 samples each for the 6 materials and 5 different treatments. The fracture test was conducted on double cantilever beam (DCB) specimens. The specimen size and thickness for all the materials are listed in Table 5.1. The fracture set up is sown in Fig.5.2. An L-shape steel channel connected to compression grips were used to load the DCB specimens at a rate of 2 mm/min. The DCB was supported at the end using a metal plate. A notch was created for the L channels to fit into the DCB specimen. The notch length on either arm of the DCB was 25.4 mm. The notch was followed by a pre-defined crack of 76mm length. The load, deflection and time data were recorded using the Instron 5582 data acquisition system. One important aspect of the energy method, and especially the R curve analysis, is tracking and knowledge of crack growth during the test. This was achieved by optical methods.

A pair of CCD cameras was used to track the crack propagation and image capturing was automated using ViC Snap software. Images were captured at a rate of 2 images per second. Vic Snap provides with analog data relating image number and a time stamp. Similar analog data was obtained from the Instron 5582, providing with load deflection data and a time stamp. As the test and image capturing were started simultaneously, the two time stamps coincided with each other allowing correlation between load, deflection and image number. The images were then analyzed using ImageJ, by first, calibrating each sets of images against measured dimension in pixel coordinates. Then, the crack growth was visually tracked in pixel coordinates and then converted to units of length (mm). An advantage of using two cameras is that it provides a stereoscopic view and verification for the results obtained from one camera can be performed by processing the images from the second camera. The second camera was used to verify the results and it matched the crack length calculation from the set of images using the first camera. The final results were plotted for load and crack length vs. deflection, which were analyzed to measure the R curve.

R curve Analysis

During fracture experiments, a specimen is loaded; energy is released during crack propagation through the material. A typical load deflection curve as obtained from Instron 5582 universal testing machine is shown in Fig. 5.1a. Till peak load P_{max} the crack growth has occurred till a critical crack length value. The critical crack length is dependent on initial crack length or notch and specimen thickness (Aicher 2010). Beyond P_{max}, the load deflection curve is descending. In this phase the process zone is fully developed and a stable crack growth is assumed. The energy release rate for fracture is a constant for ideal brittle material called the critical energy release rate (G_{IC}). In wood and other fiber bridging material, the energy becomes constant once steady-state crack propagation is achieved. Generally, G_{IC} is represented as:

$$R = G_{IC}(a) = \frac{\Delta U_f(a)}{t.\Delta a} \tag{5.2}$$

where t is the thickness of the material, Δa is the crack growth and ΔU_f (a) is the energy released for the crack increment. Effectively, each increment in crack length can be treated as a separate test providing with a different data point. The calculation of G_{IC} requires division by Δa (eq. 5.2), which may be of very small magnitude. Division by a small number results in high scatter in the data. As a crack propagates towards the edge at the end of specimens, Δa between two successive data points diminishes rapidly and causes scatter in the resultant R

curve. In this study a new method developed by Nairn (2009) was used to analyze R curves. Nairn (2009) proposed a new method to develop R curve called the revised area method which helps in reducing the scatter. Here, all the increments of ∆a are taken into account, but it is treated or reduced by a single analysis as explained. The method is a three step process. First, load and crack length vs. displacement data sets are obtained using load displacement data obtained from the testing machine and correlating it with the image acquisition software. This is followed by integrating the force displacement data up to some displacement, d provides the cumulative energy, U(d), released per unit specimen thickness t. This is shown in Fig. 5.1a and represented by:

$$U(d) = \frac{1}{t}\left(\int_0^d F(x).dx - \frac{1}{2} F(d).d \right) \qquad (5.3)$$

Secondly, the cumulative energy is re-plotted as a function of crack length, treating U(d) and a(d) as functions of displacement (Fig. 5.1b). This step converts energy which was earlier a function of displacement [U(d)] to energy as function of crack length, U(a). Fig. 5.1b also shows the J vs. Crack opening displacement curve (displacement of the load head). Lastly, numerically differentiating U(a) with respect to a provides the R curve:

$$R = \frac{dU(a)}{da} \qquad (5.4)$$

Various smoothing techniques are applied on U(a) to reduce the scatter. After this step R can be plotted as a function of crack length and is presented in Fig. 5.1c. The steady state region of the R curve is the G_{SS} value for that material. This analysis is based on the most unambiguous definition of change in energy required for crack growth. Analysis to calculate G_{SS} requires crack length to be tracked during the testing process. If crack length can be tracked at various points during a test, energy methods and R curve analysis can be a useful tool for characterizing fracture properties of a fiber bridging material such as wood. With the augment of visual data acquisition systems and sophisticated image processing software, an R curve analysis is highly feasible and practical way to characterize fracture property of a fiber bridging material.

Results and Discussion

Steady State Strain Energy Release Rate (G_{SS})

Solid Sawn Lumber

Average calculated results of G_{SS} for all the materials and respective treatments are shown in Table 5.2. Each value represents an average of two values, unless otherwise noted. These are obtained from R curve from one test at each treatment. The G_{SS} values for solid sawn lumber are comparable to ones available in literature. The average value for G_{SS} at ambient temperature was 195 N/m for Douglas-Fir. Matsumoto and Nairn (unpublished) reported G_{init} of 170 N/m in TL direction and G_{SS} of 210 N/m in RL directions. Yeh and Schneiwind (1992) reported a G_f of 280 N/m for Douglas-Fir in TR direction. Our tests for controls were conducted for fracture in RL direction. Our values were within experimental range of that presented by Matsumoto and Nairn (unpublished). The specimens for other treatments were a mixture of either pure TL direction fracture or mixed RL and TL direction fracture. Fracture toughness is higher in TL direction than in RL direction as can be observed from Table 5.2 as well. Not many studies were found where G_{SS} was calculated using R curve analysis. As a result, comparison with our results was difficult. However, few studies calculated G_f for Spruce and Yew to be 290 N/m and 310 N/m, respectively (Keunecke et al. 2007). These results are for crack propagating in RT and TR planes, which are different than the planes analyzed in this study. Frühmann et al. (2003) reported G_f of spruce TR to be 300 N/m similar to Keunecke et al. (2007), while Yoshihara and Nobusue (2008) reported G_{init} of spruce to be 210 N/m and 320 N/m in TL and TR planes, respectively. Frühmann et al. (2003) also reported G_f of pine to be 550 N/m. Douglas-Fir is stronger and denser than Spruce or Yew (Green et al. 1999) and similar but higher than pine. Consequently, its fracture toughness can be expected to be higher than Spruce, Yew and pine (Gibson and Ashby 1997). These are G_f values, hence, represent the energy required to initiate, then propagate the crack and are expectedly much higher than our results for Douglas-Fir. The G_f also may include edge effects which gives very high values of G_f (Matsumoto and Nairn 2007). In critical design scenarios, a design based on G_f value will not be appropriate, because G_{SS} will be lower than G_f. Therefore, it is highly important to characterize fracture toughness using steady state strain energy release rate (G_{SS}).

Wood Composites

The G_{SS} are presented in Table 5.2 for OSB, plywood (2 thicknesses each) and LVL. The G_{SS} for wood composite is higher than that of solid sawn lumber (SSL). In case of PWH, because the material was 11.2 mm in thickness, a DCB specimen carved out of the material did not have rigid arms through which it could be loaded. As a result, after the initiation of crack the arms tend to break resulting in no further propagation of crack. The entire load applied to the

system was then used in breaking of the arm, hence, an R curve analysis tended to yield a very high value of G_{IC}. To negate this, only G_{init} is considered for PWH and are not discussed in comparison to other composites. LVL, PWO and PWH are all laminated composites, comprised of laminations running in one direction in case of LVL and alternate cross laminations for plywood. Wood composites, even though they were fabricated with same species as SSL, had higher G_{IC} than SSL for controls (Table 5.2). The G_{SS} value of LVL was 1100 N/m in this study. Frühmann et al. (2002) reported G_f value of LVL between 280-333 N/m. Frühmann et al. (2002) used Aspen, which is much lower density wood, than Douglas-fir, hence the discrepancy. Moreover, Aspen LVL used was of 12 mm thickness while the LVL used in this study were 38mm. The difference in results may also be due to the different testing protocols used in the respective studies.

Although, the fracture properties of wood composites such as LVL and plywood have not been studied, there is vast body of research in the field of fracture of laminated composites. As LVL and PWO are laminated composites they have a layer of adhesive between each ply. The G_{SS} value for LVL, PWO and PWH are five to seven times higher than SSL of the same species. Sela et al. (1989) investigated the effect of adhesive layer between the plies and observed a 7-10 fold increase in the fracture toughness of the material due to an adhesive layer. It is the adhesive which is contributing to higher toughness of the composites. As seen from Table 5.2, the control values of LVL is little lower than that of plywood (PWO). The layup sequence for the plies also has an effect on energy release rate (Davidson et al. 2000, Lee and Knauss 2000).There is a vast body of literature compiled by Anderson and Konig (2004) on the effect of layup sequence on fracture toughness. The critical energy release rate is generally higher for a multidirectional composite than a unidirectional composite (Davidson et al. 2000). The properties of adjacent plies are similar for unidirectional composites such as LVL, so their mode partitioning or delamination is the same. On the other hand in plywood has a cross ply layup. The plies bounding the crack growth or delamination are at different orientations, and it gives rise to a different directionality of force and stresses in adjacent plies near the interface. However, no directional dependence of plies on the fracture toughness at initiation was observed (Schon et al. 2000).

The G_{SS} of OSB values are generally lower than that of LVL and PWO. OSB is a strand based composites, with various process parameters such as voids and undulations affecting its strength as well as the fracture toughness. Lei and Wilson (1980,1981) found that fracture toughness of OSB was affected by void size and board densities while it was not affected by

resin content and directionality of flakes. The inter strand voids acts as flaws and aid in crack propagation. The inter-space voids can further act as a localized crack initiation point. With more compaction, higher density of board will be achieved resulting in less void space. Conrad et al. (2004) suggested LVL represents perfectly bonded OSB, therefore fracture toughness of LVL can be regarded as the upper bound for OSB. Although this argument has merit, perfectly bonded OSB, i.e. no void space, will not have all the strands oriented in one direction. The core strands are either randomly oriented or oriented in cross direction than the surface flakes. Although the low density Aspen strands are compressed to form an OSB panel with higher density than that of LVL or plywood, due to void spaces fracture toughness of OSB will be lower than that of plywood or LVL. When comparison of G_{SS} between the two OSB types is made, OSBH has a higher G_{SS} than OSBO. The density of OSBO was lower than that of OSBH (Table 5.1). This might be because of higher compaction achieved by heat transfer during manufacturing of the OSBH than OSBO, due to their thicknesses (Zambori et al. 2001). Moreover, the lower the density, the greater is the void space, which negatively affects G_{SS} values.

Failure Modes and R Curves

The R curves are shown in Fig. 5.3 while various failure modes for all the materials are shown in Fig. 5.4. The failure in SSL (Fig. 5.4a) is typically through one growth ring in the RL direction. This is also seen in the R curve where the R curve doesn't rises (Fig. 5.3a), it remains constant as the crack propagates. Similar results were observed by Matsumoto and Nairn (unpublished). The R curve for SSL in TL direction (Fig. 5.3b) has a initiation value and then continue to rise as the crack propagates and does not reach a steady state value. The failure mode for LVL was either through fracture through the wood veneer sheets, with hardly any glue line failure (Fig. 5.4 e). This can be seen from the R curve (Fig. 5.3c) which initiates, then rises and reaches a steady state. Similar failure mode was observed by Frühmann et al. (2002) on Aspen LVL. On the other hand, in plywood (PWO), fracture was a combination of ply delamination and ply fracture as shown in Fig. 5.4c and the corresponding R curve (Fig. 5.3d). The R curve is a step wise R curve representing ply delamination and ply fracture. The failure initiates at the ply and subsequent progression occurs by delamination and ply fracture. As the crack grows towards the end of the plywood specimen, it cuts across the plies and causes failure and delamination in the adjacent plies. A similar failure mode was observed by Lee and Knauss (2000) on multidirectional composites. LVL is made up of high quality thicker plies. Consequently, the crack can propagate through the ply in which initial crack was pre-defined and therefore, result in fracture through wood. Failure in OSB, started as crack

propagation along the strands with strand undulations governing the directions of crack growth (Fig. 5.4b). The void spaces acted as crack initiation points during advanced stages of loading and a discontinuous crack growth resulted, particularly in OSO. This trend is observed in the R curves, with void spaces acting as localized crack initiation point resulting in energy going down as crack propagates (Fig. 5.3e). On the other hand in OSH, due to less void spaces, a continuous crack could be identified (Fig. 5.4d) and the R curve reaches a steady state value after initiation (Fig. 5.3f). Overall, there was hardly any fracture through the strand thickness. The cracks found a plane of least energy and propagated through that, with strand undulation and specifically, void spaces helping in the process of fracture, especially for OSO.

Effect of Elevated temperature

Fig. 5.5 shows the effect of exposure time on G_{SS} at two temperatures of exposure for various materials. Solid sawn lumber (Fig. 5.3a) after exposure to 100^{o}C, does not show much change in G_{SS}. Contrastingly, after exposure to 200^{o}C, a drop in G_{IC} is observed as the exposure time is increased (Fig. 5.5b). Wood does not degrade in terms of material property at exposure to 100^{o}C, especially for the exposure times used in this study. Hence, no detectable change was observed in G_{SS} of wood. On the other hand, when exposed to 200^{o}C, wood deteriorates (Green et al. 1999, Sinha et al. 2010) in terms of its mechanical properties. The 43% decrease in G_{SS} of wood after 2 h of exposure at 200^{o}C (Fig. 5.5a) when compared to the control sample can be attributed to thermal degradation of wood. Yeh and Schneiwind (1992) tested Douglas-fir at temperatures ranging from 21^{o}C to 60^{o}C and as a function of moisture content. Although, the authors found temperature to have a statistically significant effect on fracture toughness, moisture had a more pronounced effect than temperature. The authors found a slight decrease in fracture properties with increase in temperature at one loading rate. On the other hand, when the loading rate was increased no difference in fracture toughness was observed with increase in temperature. The test was performed at a low and narrow temperature range, which should not involve the thermal degradation, which is only caused at higher temperatures.

After exposure to 200^{o}C, G_{SS} for all materials dropped as the exposure time increased (Fig. 5.5b). Wood composites are manufactured using wood and resin. Adhesives or resin contributed towards higher G_{SS} of composites for control as compared to SSL of same species. The resin is also contributing towards faster degradation in G_{SS} with exposure to elevated temperature for wood composites. The degradation in fracture toughness possibly is an influence of two factors. As the wood is heated, degradation occurs in all mechanical

properties including fracture as shown above. Second, thermal degradation of the resin can deteriorate its capacity after exposure to elevated temperature. Wood starts to degrade in mechanical properties when exposed to 200^{o}C (Sinha et al. 2010). Similarly, resin which is binding the wood into composite also tends to degrade after exposure to 200^{o}C and degrade more at longer exposure time. As a result, the fracture property is affected more after 2 h of exposure at 200^{o}C than after 1h of exposure. The drop in G_{SS}, when compared with control values, is more for wood composites such as PWO (73%), LVL (78%) and OSO (53%) as compared to a drop of 43% in SSL after exposure to 200^{o}C for 2 h. Degradation of resin can possibly cause a higher drop in wood composites than SSL. LVL and PWO are laminated composites and uses higher resin content by weight than OSO, consequently, the drop in their respective G_{SS} values are higher due to deterioration of resin after exposure to elevated temperature.

The failure characteristics were identical to those at room temperature (Fig. 5.4). The failures of all the samples of the 100^{o}C treatments were identical to controls. The magnitude of G_{SS} was much lower after exposure to 200^{o}C, but the failure modes were identical, especially for plywood and OSB. The failure in plywood was again steady crack propagation with trans-veneer cracking and subsequent delamination. The failure for LVL occurred mainly by crack propagation in veneer, however, glue failure was also visible in one of the samples. The OSB samples OSO and OSH exhibited identical failure characteristics to the control samples.

These results suggest that the materials do degrade significantly in fracture toughness after exposure to elevated temperature. The fracture test based on energy methods and R curve analysis is robust enough to detect that degradation.

IB and bond Classification Test

Standard industry test for characterizing adhesive strength for OSB and plywood are internal bond (IB) and bond classification test, respectively. The results from IB and Bond Classification tests are shown in Fig. 5.6 (a-d). For both varieties of OSB, the IB test did not show any thermal degradation in bond strength with exposure to elevated temperature. OSBO ($p=0.25$, ANOVA) and OSBH ($p=0.053$, ANOVA) showed no evidence of degradation statistically with exposure to elevated temperature for certain durations. On the other hand, plywood bond classification expectedly degraded with exposure to elevated temperature ($p < 0.01$, ANOVA), especially for both duration of 200^{o}C treatment. The reason IB could not lead to any sort of statistical power in the analysis was due to the scatter associated with IB testing

procedure. The theory of failure at weakest link holds true, but the weakest link can be anywhere from the adhesion of the loading blocks to the OSB surface to the voids in the OSB. The weakest link is not pre-defined by the test protocol; hence, a vast scatter of data resulted. The coefficient of variation (COV) for IB test ranges from 25-40% as reported in literature. In this study the COV for IB varied from 23-52%, highlighting the variability associated with the test. With so much of variability, an assessment of the bond property with ample confidence cannot be made. In contrast the fracture test did work well in detecting the thermal degradation of the materials.

For bond classification, the PS1 (NIST 2007) requires to note only percentage wood failure neglecting the maximum load at failure. However, load at failure is an important parameter as shown by Perkins (1950) and DeVallance et al. (2007). The maximum load and % wood failure was noted and presented in Table 5.3. The average % wood failure decreases after exposure to 200^{o}C for hrs. The average % wood failure, for example, for PWH reduced from 74% for control to 50% for 200^{o}C – 2h of exposure. Similarly for PWO it decreased from 57% to 19%. The conventional test interpretation is that the bonding has improved due to exposure. However, it looks like the degradation in wood was governing the failure rather than bond properties especially in the treatments including temperature of 200^{o}C. A scenario now arises where the control and 100^{o}C treatment samples has higher load and higher percentage of wood failure, while the 200^{o}C treatment samples have lower load and lower percentage of wood failure. High % of wood failure accompanied by higher load at failure may not be a measure of the adhesive bonding rather than strength of wood. Contrastingly, there could be a scenario where higher % of wood failure occurs but the load at failure is low. This will be due to lower strength of wood rather than a measure of bond adequacy (Perkins 1950). Interpretation of bond classification tests leads to ambiguity in terms of what property is being measured; whether this is measure of adhesive strength or the wood property. Fracture, on the other hand, was clearer in terms of measuring degradation in fracture toughness of the material.

IB has problems with high scatter in the data rendering a statistical evaluation difficult. As a result of the scatter, the IB test was not able to clearly detect any thermal degradation in OSB after exposure to elevated temperature. On the other hand, bond classification test has a low scatter and was able to detect degradation after exposure to elevated temperature. Bond classification, however, has its ambiguity in terms of whether it is providing a measure of shear strength of wood veneers or the bond strength of adhesive. Moreover, both these tests

load the wood to failure in two of its weakest directions, tension perpendicular (IB) and shear parallel (bond classification) and as a result only knowledge of an average stress for the bonded area is obtained. The most common mode of failure in laminated composite being inter-laminar cracking (Hashemi et al. 1990) and trans-ply failure (Lee and Knauss 2000), knowledge of stress to initiate (River and Okkonen 1993) and propagate the failure is necessary. Although these tests are well ingrained in the quality control process of manufacturing of OSB and plywood and very hard to replace, an alternative to these tests can be fracture test presented in this study which provides the energy required for steady state crack growth for the material as a whole. Fracture test provides an engineering property of the material, unlike, IB and bond classification, where ambiguity of what is being measured hampers its efficiency and power of the test. Moreover, fracture tests, unlike IB, are robust enough to detect the thermal degradation of the materials tested and does show a thermal degradation in magnitude of G_{SS} on exposure to elevated temperature.

A fracture test to characterize adhesive bonding is not, by any means, a new concept. Much work has been done in this regard and has been compiled by Conrad et al. (2004). However, fracture test on the material as a whole rather than two pieces of veneers or flakes joined together has not been extensively studied. Moreover, mostly all these studies and the fracture studies on wood used either stress intensity method or G_{init} or G_f to characterize fracture toughness. For a fiber bridging material such as wood and wood-based composites, an R curve analysis is necessary to characterize the fracture properties most unambiguously. The test on the material or the composite as a whole will provide information on engineering material characteristic of the composite rather than bond adequacy. How well the wood is bonded in a composite does have an effect on the engineering properties such as G_{SS}. To characterize G_{SS} for a fiber bridging material correctly an R curve analysis is required, which in turn requires the crack length to be tracked during the tests. This fracture method is more demanding than the IB and bond classification tests, in terms of time associated with data analysis and image processing. However, with development in technology and image processing software, this problem can be automated and expedited.

Conclusions

Fracture properties of wood and wood-based composites were studied using energy methods. Visual data acquisition and image processing solutions were used to track the crack propagation at various stages in the test. Wood being a fiber bridging material, an R curve analysis was necessary and conducted. A new analysis technique developed by Nairn (2009)

was applied to experimental data to conduct rising R curve analysis. The method proved to be simple, effective and robust enough to track thermal degradation in G_{SS}. The steady state energy release rate (G_{SS}) of wood was lower than that of wood composites such as LVL, plywood and OSB. The resin in wood composites provides them with the higher magnitude of fracture toughness as compared to solid lumber. Depending upon the internal structure of the material the mode of failure also varied. For laminated composites such as LVL and plywood, depending upon the stacking sequence next to the crack the modes of failure differed. For LVL, with unidirectional layup of veneers, the mode of failure was crack propagation through the veneers, with hardly any glue failure. While for plywood with alternate stacking of cross directional veneers, the failure was transverse ply cracking and delamination. In case of OSB the void space influenced and governed the crack propagation and failure pattern. The R curves for the composites and SSL had distinct features depending on their failure modes.

With exposure to elevated temperatures, G_{SS} of all the material decreased. In the range studied, the effect of temperature was visible in primarily lowering the magnitude of G_{SS}, while the mode of failure was unaltered. The highest drop in G_{SS}, however, was associated with the wood composites than solid lumber. The greater the resin content in the composite, the greater was the drop. Hence, LVL and plywood had a greater drop in G_{SS} than OSB. The bond strength of plywood and OSB was evaluated using IB and bond classification, respectively. The bond classification tests showed significant thermal degradation in bond strength of plywood but the IB tests were not able to detect degradation due to excessive scatter in the data. Additionally, it was unclear whether the IB or Bond classification provided a clear measure of adhesive bond strength. An alternative to IB and Bond classification is presented in the form of fracture testing. A novel analysis method, previously not applied to wood and structural wood composites proves to be effective. This method outlined in this study should enable quality control and R&D personnel to adopt energy methods in fracture for wood bond strength evaluation.

Acknowledgement

The authors would like to thank Wood-Based Composite Center for their financial support.

References

AFPA. (2005). *National design specification® for wood construction*. American Forest and Paper Association. Washington, D.C.

Aicher, S. (2010). “Process zone length and fracture energy of spruce wood in mode I from size effect.” *Wood and Fiber Science*, 42(2), 237-247.

Anderson, T.L. (2005). *Fracture Mechanics, Fundamentals and Applications*. CRC Press: Taylor and Frances Group, Boca Raton, FL, 122-125, 310-311.

Anderson, J. and Konig, M. (2004). “Dependence of fracture toughness of composite laminates on interface ply orientations and delamination growth direction.” *Composites Science and technology*, 64, 2139-2152.

ASTM (2001). “Standard test method for evaluating properties of wood-based fiber and particle panel materials.” *ASTM D 1037*, West Conshohocken, PA.

Conrad, M.P.C, Smith, G.D and Ferlund, G. (2003). “Fracture of discontinuous wood-adhesive bonds.” *International Journal of Adhesion & Adhesives,* 23(2003), 39–47

Conrad, M.P.C., Smith, G.D. and Fernlund, G. (2004). “Fracture of wood composites and wood-adhesive joints: A comparative review.” *Wood and Fiber Science*, 36(1), 26-39

Davidson, B.D., Gharibian S.J. and Yu, L. (2000). “Evaluation of energy release rate-based approaches for predicting delamination growth in laminated composites.” *Int. J. Fract*. 105,343–65.

Daudeville, L., Davenne, L., Yasumura, M. (1999). “Prediction of load carrying capacity of bolted timber joints.” *Wood Sci. Technol*. 33, 15–29.

DeVallance, D.B., Funck, J.W. and Reeb, J.E. (2007). “Douglas-fir plywood gluebond quality as influenced by veneer roughness, lathe checks, and annual ring characteristics.” *Forest products journal*, 57(1-2) 21-28.

Ebewele, R., River, B. and Koutsky, J. (1979). “Tapered double cantilever beam fracture tests of phenolic-wood adhesive joints. Part I. Development of specimen geometry: Effects of bondline thickness, wood anisotropy, and cure time on fracture energy.” *Wood Fiber,* 11(3),197-213.

Ebewele, R., River, B. and Koutsky, J. (1980). “Tapered double cantilever beam fracture tests of phenolic-wood adhesive joints. Part II. Effects of surface roughness, the nature of surface roughness, and surface aging on joint fracture.” *Wood Fiber*, 12(1),40-65.

Ebewele, R., River, B. and Koutsky, J. (1982). “Relationship between phenolic adhesive chemistry, cure and joint performance. Part I. Effects of base resin constitution and hardener on fracture energy and thermal effects during cure.” *J. Adhesion,*14, 189-217.

Ebewele, R., River, B. and Koutsky, J. (1986). “Relationship between phenolic adhesive chemistry and adhesive joint performance; effect of filler type on fraction energy.” *J.Appl. Polym. Sci.* (31), 2275-2302.

Ehart, R.J.A., Stanzl-Tschegg, S.E. and Tschegg, E.K. (1996). “Characterization of crack propagation in particleboard.” *Wood Sci. Technol.* 30,307–321.

Ehart, R.J.A., Stanzl-Tschegg, S.E. and Tschegg, E.K. (1998). “Crack face interaction and mixed mode fracture of wood composites during mode III loading.” *Eng. Fract. Mech.* 61, 253–278.

Ehart, R.J.A., Stanzl-Tschegg, S.E. and Tschegg, E.K. (1999). “Mode III fracture energy of wood composites in comparison to solid wood.” *Wood Sci. Technol.* 33, 391–405.

Frühmann, K., Tschegg, E.K., Dai, C. and Stanzl-Tschegg, S.E. (2002). “Fracture behavior of laminated veneer lumber under mode I and III loading.” *Wood Sci. Technol.* 36, 319–334

Frühmann, K., Burgert, I., Stanzl-Tschegg, S.E and Tschegg, E.K. (2003). “Mode 1 fracture behavior on the growth ring scale and cellular level of spruce and beech loaded in TR crack propagation system.” *Holzforschung*. 57, 653–660.

Gagliano, J.M and Frazier,C.E. (2001). “Improvements in the fracture cleavage testing of adhesively-bonded.” *Wood and Fiber Science*, 33(3), 377-385

Gibson, L.J. and Ashby, M.F. *Cellular Solids*. Cambridge University Press, Cambridge, England, 1997.

Hashemi, S., Kinloch, A.J. and Williams J.G. (1990). “The analysis of interlaminar fracture in uniaxial fibre-polymer composites.” *Proc. R. Soc. Lond. A* (427), 173-199.

Keunecke, D., Stanzl-Tschegg, S.E. and Niemz, P. (2007). “Fracture characterization of yew and spruce in the radial-tangential and tangential-radial crack propagation system by micro wedge splitting test.” *Holzforschung*, 61, 582-588.

Lee, S. and Knauss, W.G. (2000). “Failure of laminated composite at thickness discontinuities under complex loading and elevated temperatures.” *International Journal of Solids and Structures,* 37, 3479-3501.

Lei, Y.-K. and Wilson,J.B. (1980). “Fracture toughness of oriented flakeboard.” *Wood Science,* 12(3),154–161.

Lei, Y.-K. and Wilson, J.B. (1981). “A model for predicting fracture toughness of flakeboard.” *Wood Science*, 13(3),151–156.

Li, V.C., Chan, C.M. and Leung, C.K.Y. (1987). “Experimental determination of the tension-softening relations for cementitious composites.” *Cement and Concrete Research,* 17, 441-452

Matsumoto, N. (2009). “The Fracture Toughness of Medium Density Fiberboard and other Fiber Bridging Composites.” MS thesis, Oregon State University, Corvallis, OR.

Matsumoto, N. and Nairn, J.A. (2007). “Fracture toughness of MDF and other materials with fiber bridging.” *In: Proceedings of the 22nd Annual Technical Conference of the American Society of Composites*, September 17–19, Seattle, WA, USA.

Matsumoto, N. and Nairn, J.A. (in preparation). Fracture toughness of wood and wood composites during crack propagation.

Mihashi, H. and Hoshino, M. (1989). “Fracture toughness and tension softening properties of glued laminated timbers.” *In 8th European Conference on Fracture: Fracture Behavior and Design of Materials and Structures*, 799–804

Morel, S., Mourot, G. and Schmittbuhl, J. (2003). “Influence of the specimen geometry on R curve behavior and roughening of fracture surfaces.” *International Journal of Fracture* 121, 23-24.

Narin, J.A. (2009). “Analytical and Numerical modeling of R curves for cracks with bridging zones.” *International Journal of Fracture*, 5(2) 167-181.

NIST (2007). *Voluntary Products Standard PS 1-2007*. Construction and Industrial Plywood. Office of Standards Services, National Institute of Standard and Technology. Gaithersburg, MD.

Perkins, N.S. (1950). “Predicting exterior plywood performances.” *In. Proc.of the National annual meeting.* 4, 352-364. Forest Product Res. Soc. Portland, OR

River, B.H. (1994). “Fracture of adhesive-bonded wood joints.” *in A. Pizzi and K.L. Mittal, eds. Handbook of adhesive technology*. Marcel Dekker, New York, N.Y. 151-177

River, B.H. and Okkonen, E.A. (1993). “Contoured wood double cantilever beam specimen for adhesive joint fracture tests.” *Journal of testing and Evaluation* 21(1), 21-28.

Roylance, D. (2001). *Modules in Mechanics of Materials*. A web-based collection of educational modules developed under the auspices of the National Science Foundation.

Schon, J., Nyman, T., Blom, A. and Ansell, H. (2000). “Numerical and experimental investigation of a composite ENF-specimen.” *Engrg Fract Mech*, 65, 405–33.

Sela, N., Ishai, O. and Banks-Sills, L. (1989). “The effect of adhesive thickness on interlaminar fracture toughness of interleaved cfrp specimens.” *Composites*, 20(3), 257-264

Sinha, A., Nairn, J.A. and Gupta, R. (2010). “Thermal Degradation of Bending Strength of Plywood and Oriented Strand Board: A Kinetics Approach.” Wood Science & Technology, in press. DOI 10.1007/s00226-010-0329-3

Smith, I., Landis, E., Gong, M. (2003). *Fracture and Fatigue in Wood*. John Wiley & Sons Ltd, West Sussex PO19 8SQ, England, 161-166.

Smith, I. and Vasic, S. (2003). “Fracture behavior of softwood.” *Mech. Mater.* 35, 803–815.

Stanzl-Tschegg, S.E. and Navi, P. (2009). “Fracture behavior of wood and its composites. A review.” *Holzforschung* 63, 139-149.

Vasic, S. (2000). “Applications of fracture mechanics to wood.” PhD thesis, University of New Brunswick, New Brunswick, Canada.

Wu, E.M. (1963). “Application of Fracture Mechanics to Orthotropic Plates.” T*&AM Report No. 248*, Department of Theoretical and Applied Mechanics, University of Illinois, Urbana, Illinois.

Wu, E.M. (1967). “Application of Fracture Mechanics to Anisotropic Plates.” Journal of Applied Mechanics, 34(4), 967-974.

Yeh, B and Schniewind, A.P (1992). “Elasto-Plastic Fracture mechanics of wood using J integral method.” *Wood and fiber Science*, 24 (3) 364-376.

Yoshihara, H. and Nobusue, K. (2008). “Mode I and Mode II fracture toughness of densified Sitka spruce fabricated in an airtight atmosphere with high temperature steam.” *Holzforschung*, 62, 82-85.

Zamborie, B.G., Kamke, F.A. and Watson, L.T. (2001). “Simulation of the mat formation process.” *Wood and Fiber Science*, 33(4), 564-579.

Table 5.1. Details of various materials with their respective symbols, densities and dimensions.

Material		Symbols	Density (g/cm^3)	Specimen Size			Sample Size		
				L (mm)	B (mm)	t (mm)	Fracture	IB	Bond Class.
M1	Solid Sawn Lumber	SSL	0.487	254	25.4	25.4	10		
M2	Laminated Veneer Lumber	LVL	0.512	254	90	38	10		
M3	Oriented Strand Board	OSBH	0.592	254	76	11.9	10	130	
M4	Oriented Strand Board	OSBO	0.543	254	76	22	10	130	
M5	Plywood	PWH	0.503	254	76	11.2	10		130
M6	Plywood	PWO	0.468	254	76	24	10		130
						Total	60	260	260

Table 5.2. G_{SS} (N/m) of all the materials as calculated by R curve analysis across all treatments.

Material	Treatments				
	CTRL	100C1	100C2	200C1	200C2
SSL	195	167.5	215	205	110
LVL	1050	500	775	925	225
PWO	1175	1105	700	450	310
PWH	906	625	675	600	450
OSH	950	1300	1500	1050	800
OSO	380	250	340	381	175

Table 5.3. % wood failure in bond classification test for plywood (PWO and PWH)

Treatment	PWH (%)				PWO (%)			
	Average	St. Dev.	Min	Max	Average	St. Dev.	Min	Max
Control	74	25	0	100	57	19	20	100
100C1	70	25	20	100	53	22	20	95
100C2	65	21	20	100	53	24	10	95
200C1	48	28	5	100	42	23	5	95
200C2	50	28	5	100	19	20	0	90

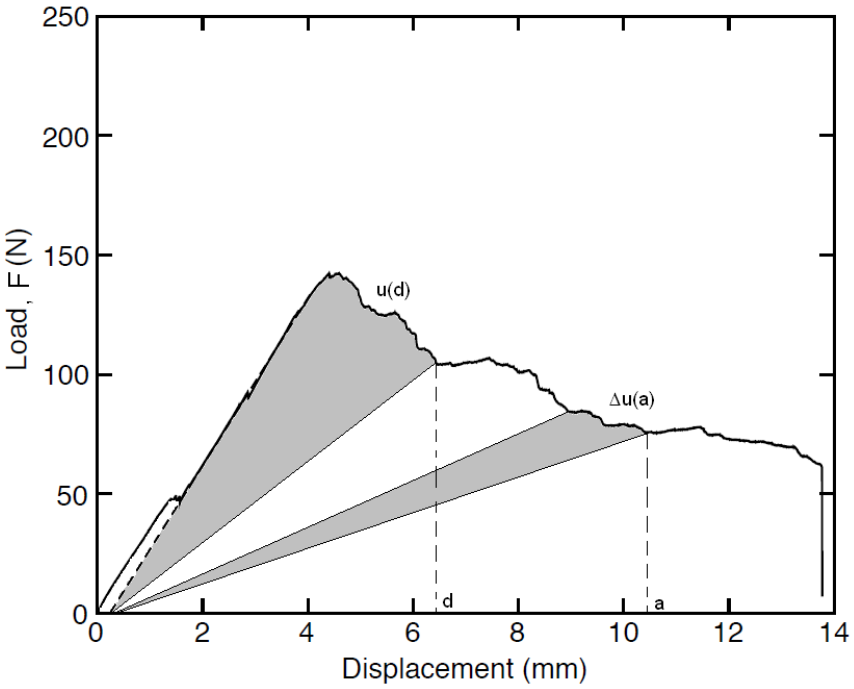

(a) Load Displacement diagram of a fracture test

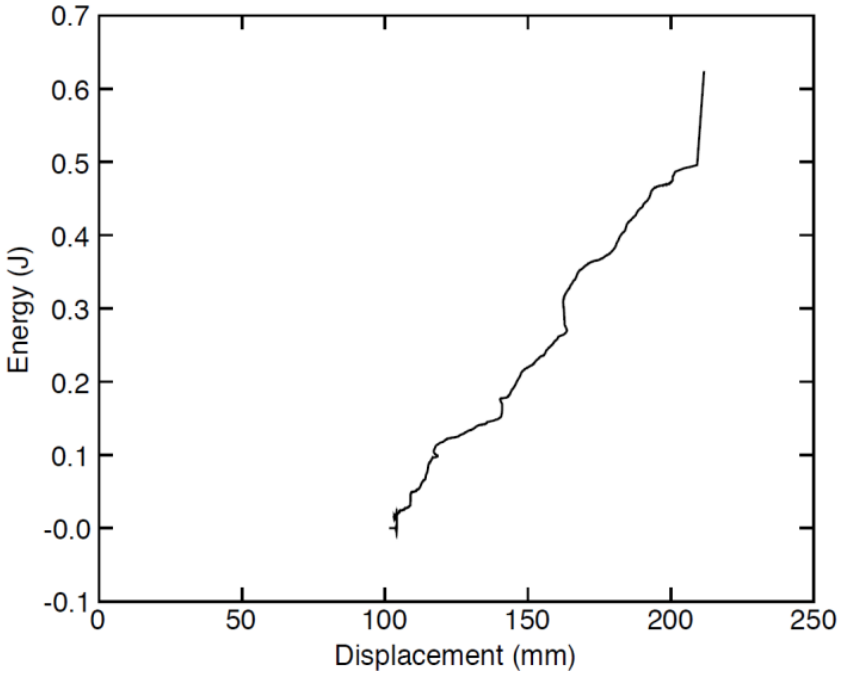

(b) Energy vs. Displacement

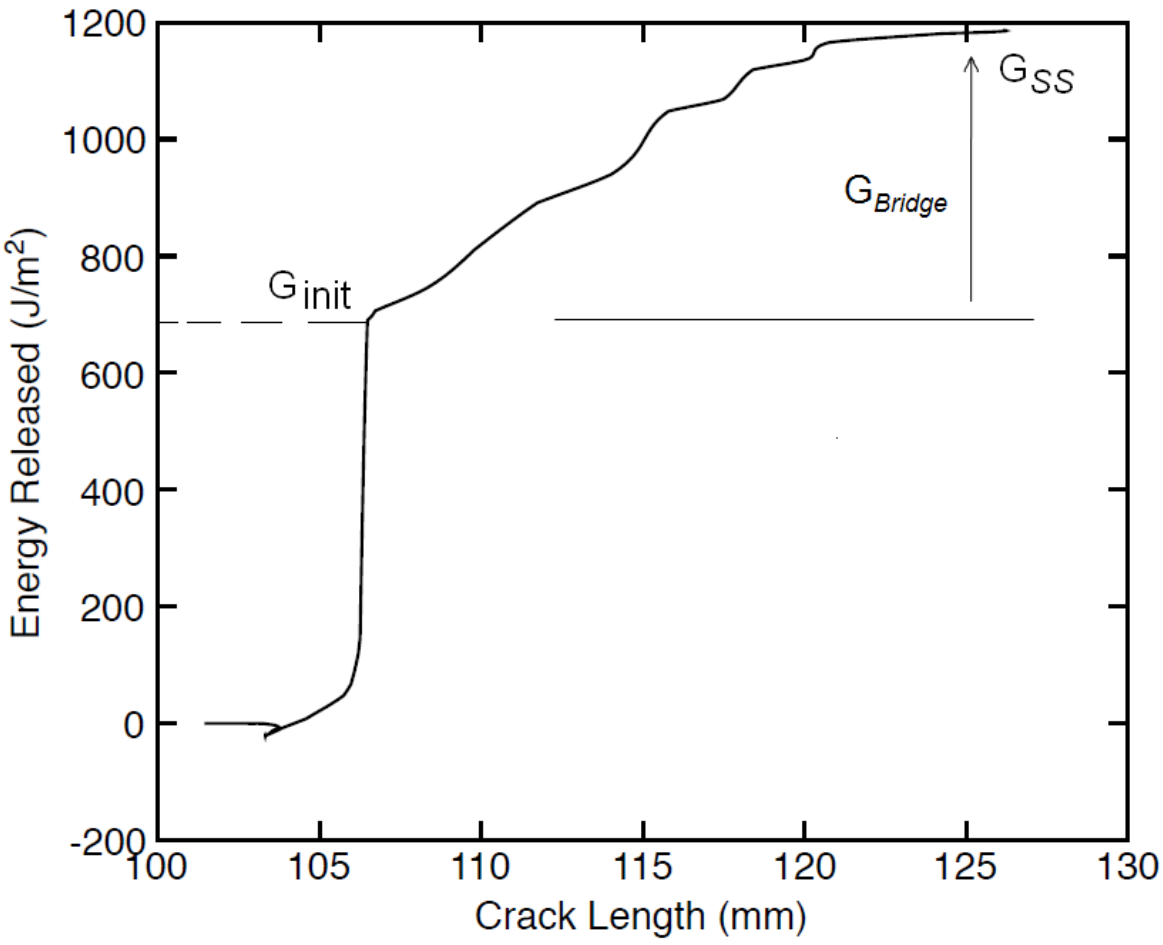

(c) R curve

Figure 5.1. R curve analysis procedure

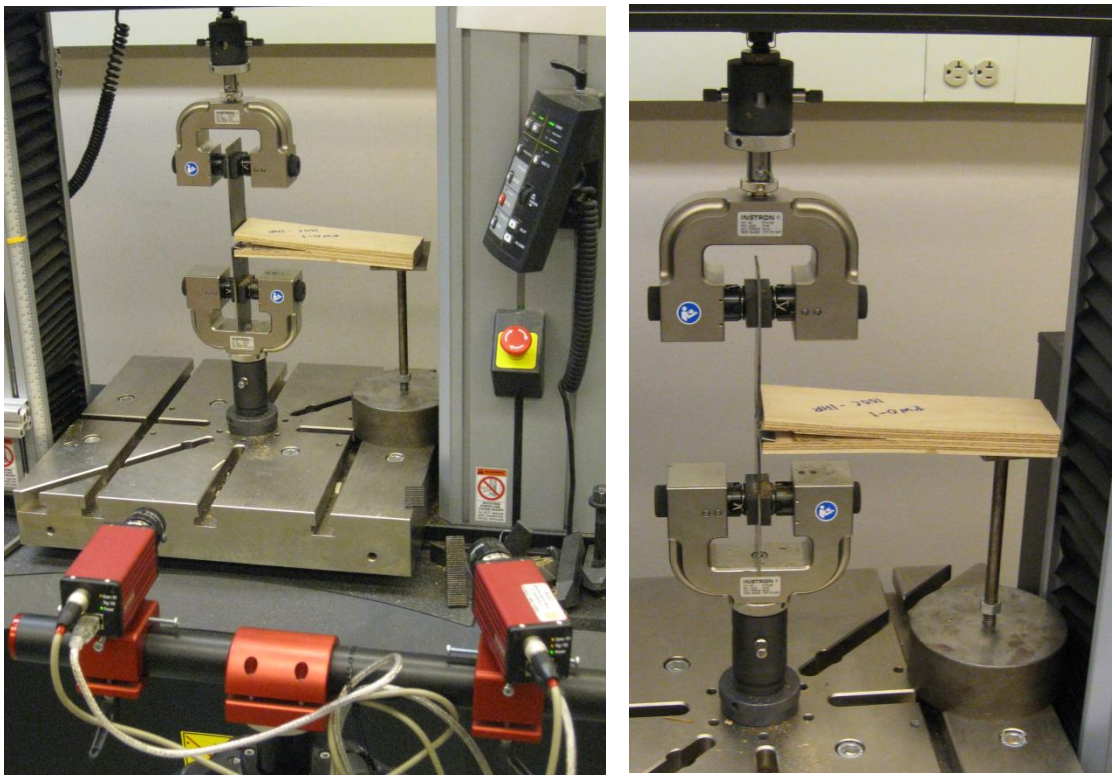

Figure 5.2. Fracture test set up

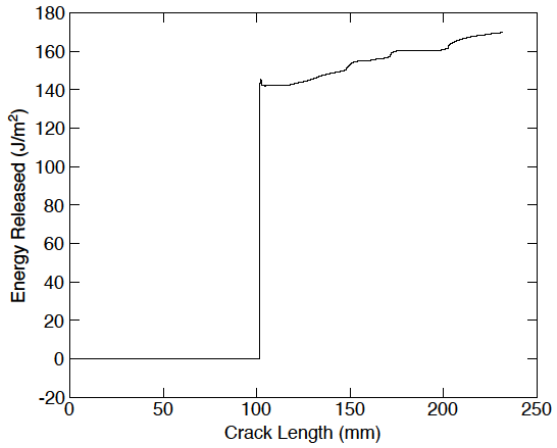

(a) SSL in RL direction

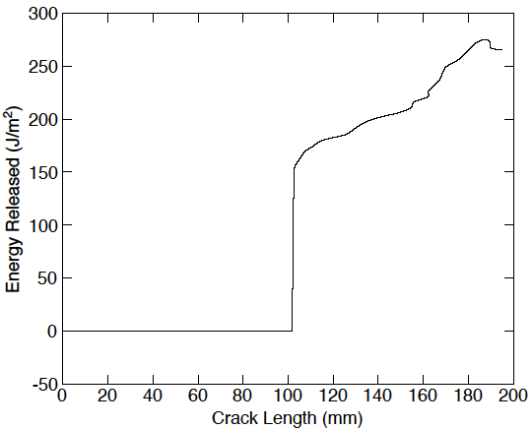

(b) SSL in TL direction

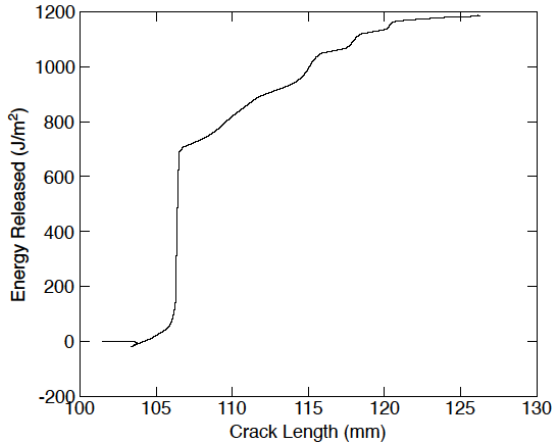

(c) LVL

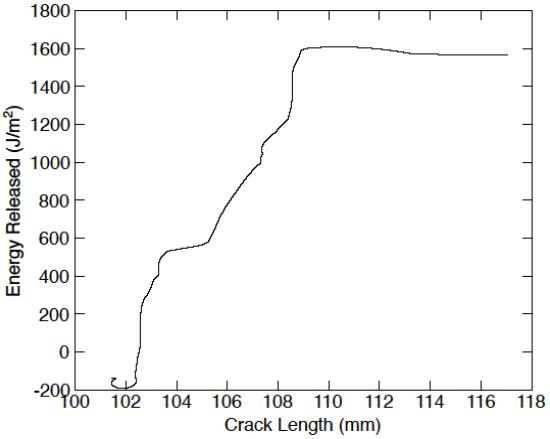

(d) PWO

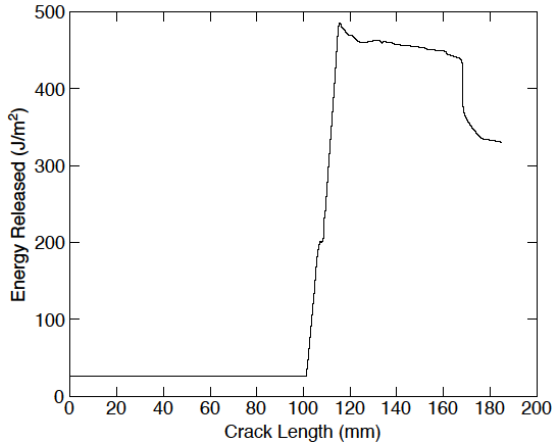

(e) OSO

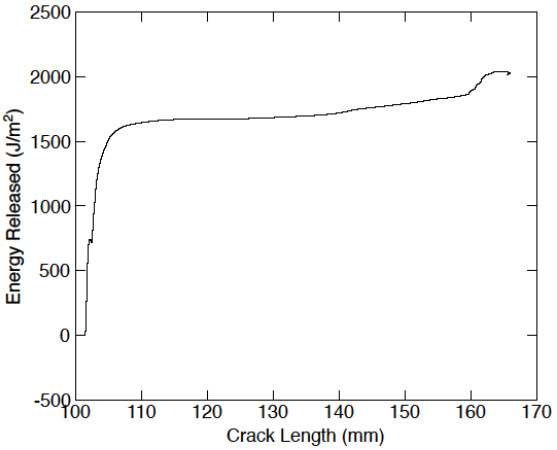

(f) OSH

Figure 5.3. R curves (G_{IC}) as a function of crack length for various materials tested.

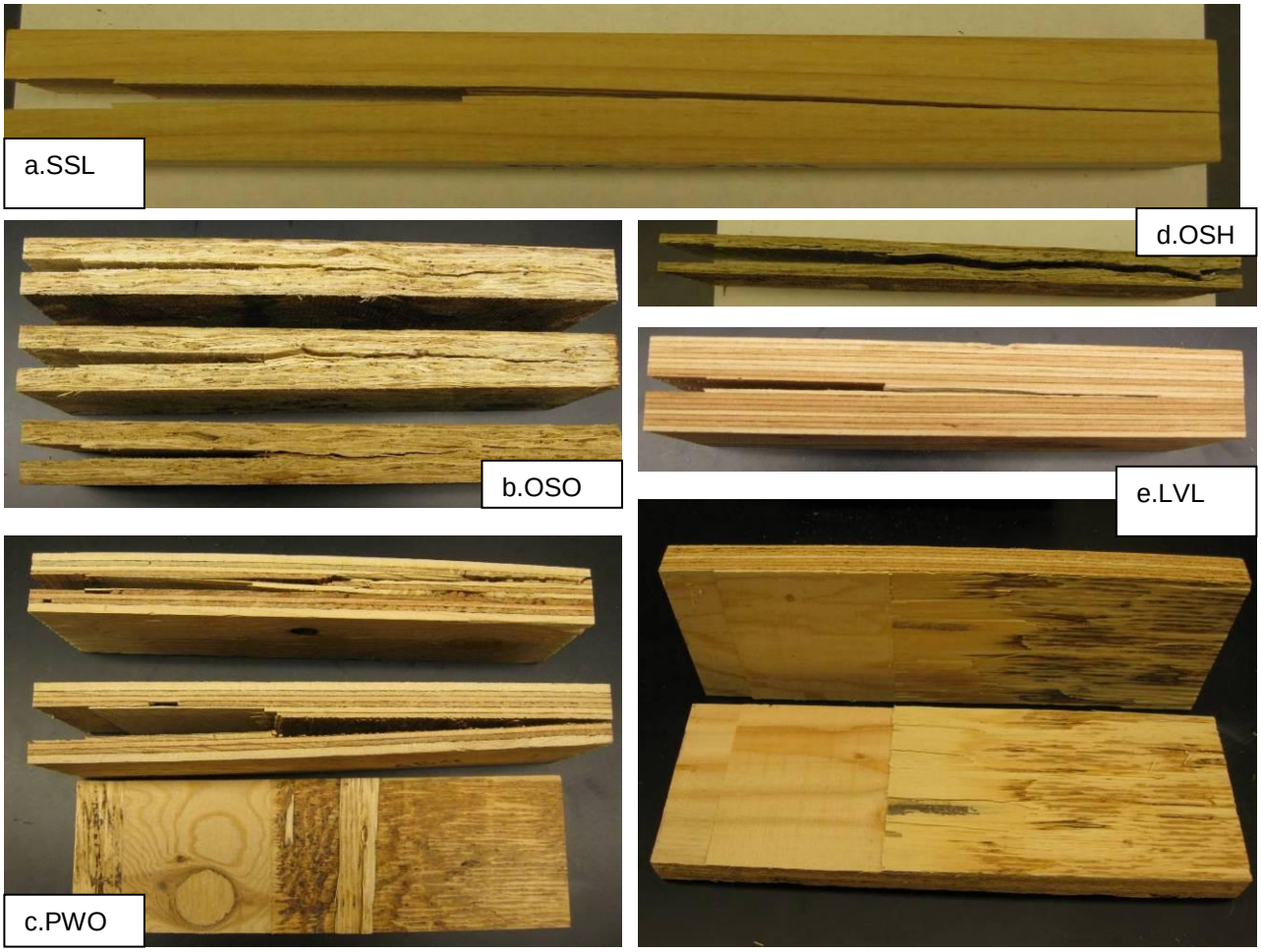

Fig. 5.4 Failure modes for wood and wood composites

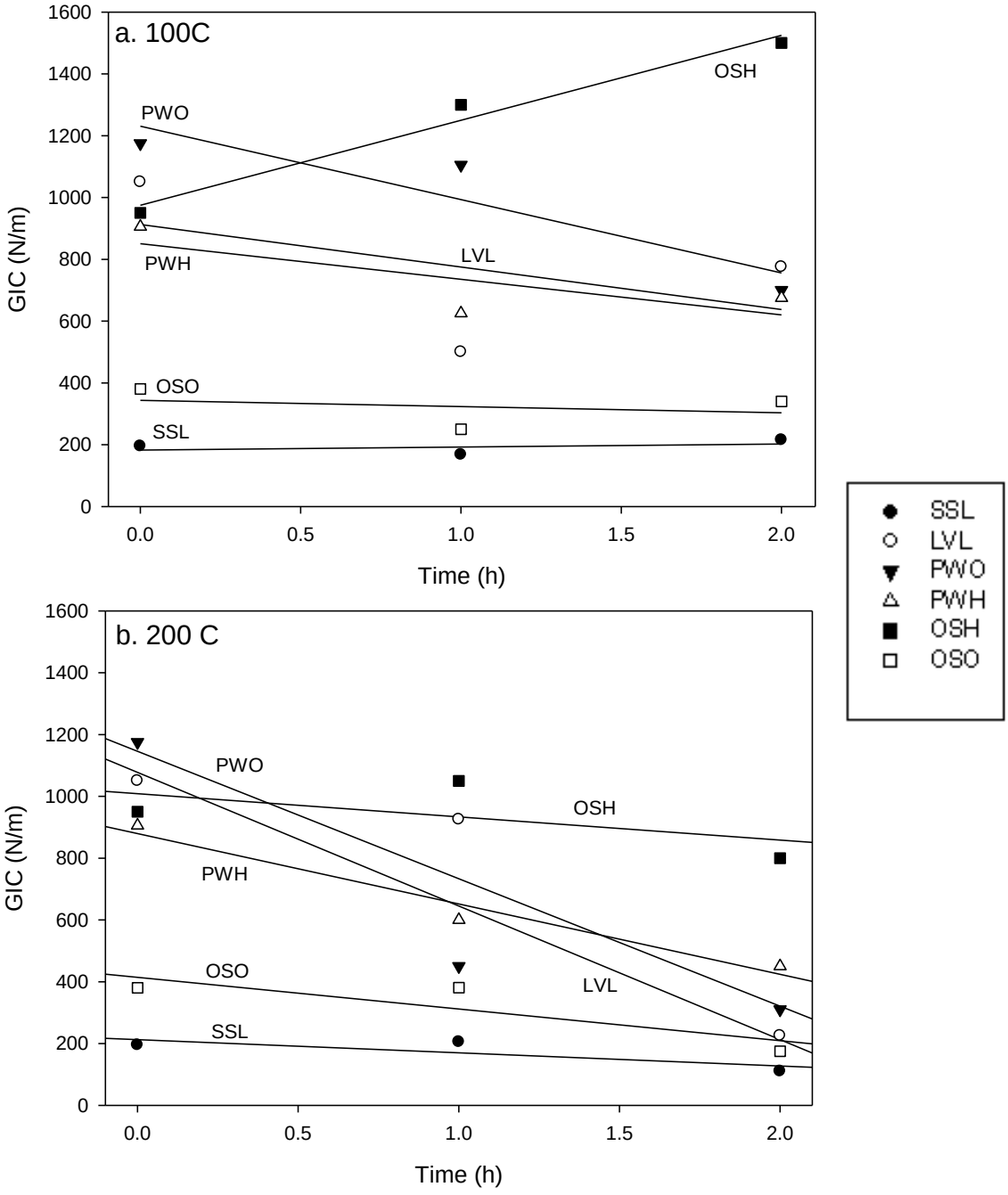

Figure 5.5. G_{IC} as a function of time at (a) 100^{o}C and (b) 200^{o}C

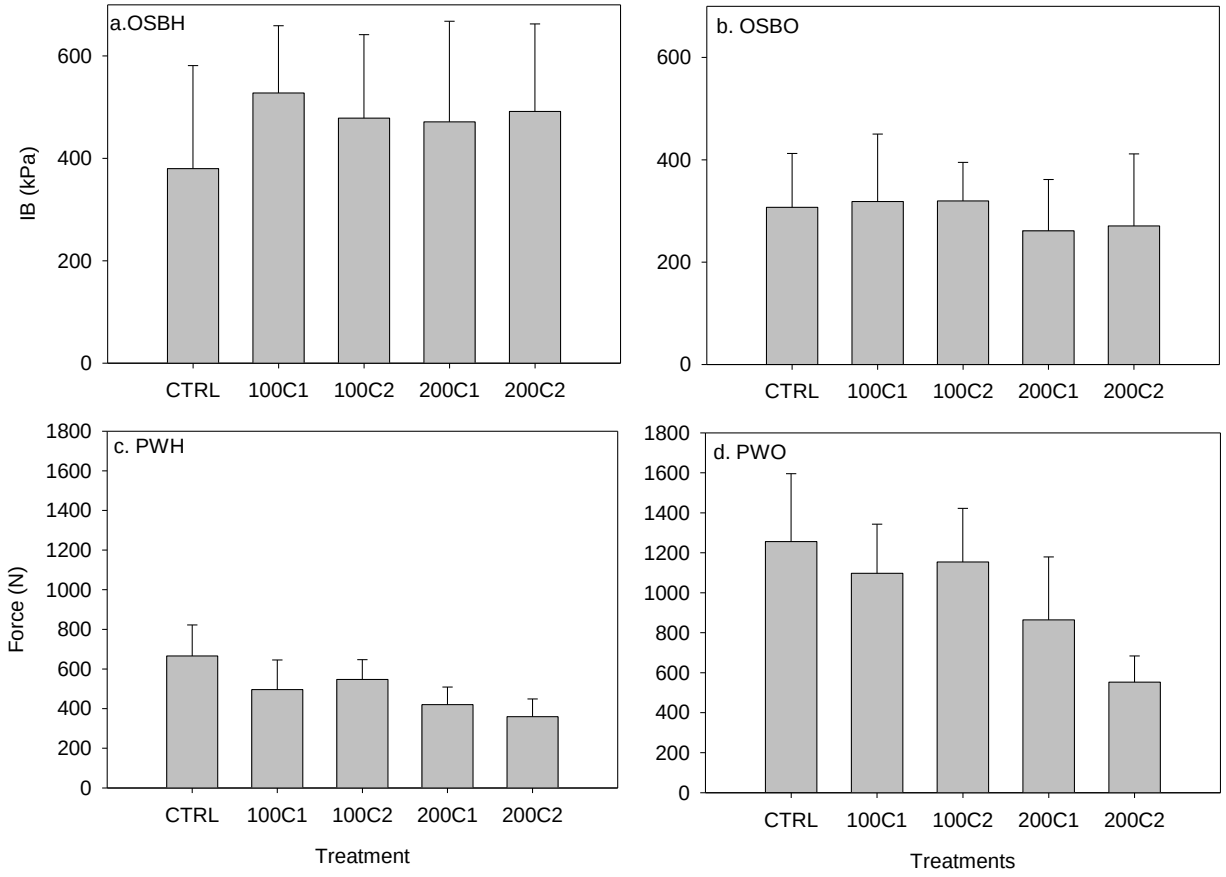

Figure 5.6. Internal bond and Bond classification values after different treatments (n=25).

Chapter 6: General Conclusions

Fire-design code is moving towards performance-based fire safety regulations in the United States. Such codes require a minimum performance criterion to be decided upon and the structure designed to achieve those minimum results. The only way to predict performance is by simulation of the building behavior, using integrated data models. This requires a database of structural testing on various components of buildings which will be used in developing and validating fire endurance models and numerical models for simulation of post-fire building performance. Knowledge of the thermal degradation of materials represents one of the most critical gaps in the development of fire endurance models, especially for wood based composites.

This research was a multidisciplinary initiative combing wood science, structural engineering and material sciences to study the thermal degradation of wood and wood-based composites commonly used in construction. Four manuscripts were compiled and are included in this dissertation. The range of applications is manifold and through this dissertation, new characterization of material and connection properties have been explored that have traditionally not been part of fire endurance research. Each one addresses pressing problems in thermal degradation of structural materials and connections.

In the first manuscript bending properties of SSL, LVL, OSB and plywood were evaluated after exposure to elevated temperature. A total of 1080 samples were tested in static bending under various heat treatments. The results indicated that exposure to elevated temperature caused significant degradation of bending strength and stiffness. For all the materials, the drop in MOR ranged from 18-61% after exposure to 200^{o}C for 2 h. The maximum drop in MOR was observed for half inch plywood (PWH), which was around 61%. A statistical regression based model and a kinetics based model were developed and evaluated for predicting the strength loss of wood and wood-based composites as a function of thermal exposure temperature and time of exposure. The kinetics based model fit the data slightly better despite having one less parameter. It's predictions consistently matched the observed values, making the kinetics model preferred over the regression approach.

Since the kinetics model was a better predictor of the strength degradation for wood and wood composites, it was studied in greater detail in the second manuscript. In this manuscript, bending strengths of OSB and plywood were evaluated as a function of various exposure times at many temperatures. The thermal degradation model assumed that the strength

degradation has a constant degradation rate. Modeling of such first-order kinetics requires an equation for the temperature dependence of the rate constant, which was provided by Arrhenius activation energy methods. Strength (MOR) of both OSB and plywood decreased as a function of temperature and exposure time. A kinetics analysis and Arrhenius activation energy theory of the strength degradation data was valid for temperatures above 100^{o}C. The degradation rate $k(T)$ follows the relation $k(T) = 40x10^{6}e^{-7549/T}$ for plywood and $k(T) = 2x10^{6}e^{-6510/T}$ for OSB. The apparent activation energies were 54.1 kJ/mole for OSB and 62.8 kJ/mole for plywood. Furthermore, using the kinetics analysis along with time-temperature superposition, a master curve was generated at a reference temperature of 150^{o}C which predicts degradation of strength with time on exposure at that reference temperature. The master curves show that although plywood has a higher initial strength, OSB performs better in terms of strength degradation after exposure to elevated temperature.

The third manuscript evaluated the yield strength of nailed sheathing (OSB or plywood) to Douglas-fir framing members (SSL or LVL) with various levels of thermal exposure under monotonic loading conditions. A general trend of degrading dowel bearing strength of materials and yield strength of the connections of various configurations with high temperature and duration of exposure was observed and confirmed by statistical analysis. With two types of geometries studied, the degradation was found to be higher in plate connections than for edge connections, irrespective of the sheathing and framing member. The degradation in lateral yield strength of the nailed connections was governed by the thermal degradation of the dowel bearing strength of OSB and plywood rather than the framing member. Using dowel bearing strength of controls and exposed materials, reasonable predictions of design values were made using National Design Specification (NDS) yield models. The yield models were found to be a rational approach to estimate the strength and residual capacity of the connections. In addition, the predicted yield modes were consistent with observed yield modes.

The fourth manuscript studied the fracture properties of wood and wood-based composites using energy methods. A new analysis technique developed by Nairn (2009) was applied to experimental data to conduct rising R curve analysis. The method proved to be simple, effective and robust enough to track thermal degradation in the steady state energy release rate (G_{SS}). G_{SS} of wood was lower than that of wood composites such as LVL, plywood and OSB. The resin in wood composites provides them with the higher magnitude of fracture toughness as compared to solid lumber. Depending upon the internal structure of the material,

the mode of failure also varied. For LVL and plywood, depending upon the stacking sequence next to the crack, the modes of failure differed. For LVL, the mode of failure was crack propagation through the veneers, with hardly any glue failure, while for plywood the failure was transverse ply cracking and delamination. For OSB the void space influenced and governed the crack propagation and failure pattern. The bond classification tests showed significant thermal degradation in bond strength of plywood but the IB tests were not able to detect degradation due to excessive scatter in the data. Additionally, it was unclear whether the IB or Bond classification provided a clear measure of adhesive bond strength. An alternative to IB and Bond classification is presented in the form of fracture testing. A novel analysis method, previously not applied to wood and structural wood composites proves to be effective.

In summary, the conclusions of this dissertation are:

1. The bending property of wood, OSB, plywood and LVL degrade with exposure to elevated temperature and was confirmed by statistical analyses.
2. A linear regression based prediction model and a kinetics based prediction model were developed and compared. The kinetic based approach was better than a statistical approach.
3. The rate of thermal degradation of MOR for OSB and plywood was higher at higher temperature.
4. The kinetics based model based on Arrhenius activation energy was valid for temperature regimes greater than $100^{o}C$.
5. A master curve representing temporal behavior of OSB and plywood at any reference temperature was developed.
6. The yield strength of connections and dowel bearing strengths degrade with exposure to elevated temperature.
7. The NDS yield models are reasonable predictors of design capacity for the exposed connections.
8. Energy methods with crack propagation (rather than initiation) and a rising R curve analysis were used to characterize and compare the fracture properties (G_{SS}) of wood and various wood-based composites. G_{SS} of wood was lower than that of wood composites such as LVL, plywood and OSB.
9. With exposure to elevated temperature, the fracture toughness of all the materials degraded.

10. Fracture tests with R curve analysis is presented as an alternative to conventional bond strength tests to assess quality of bonding.

Implications

Post-fire residual strength of structural composites that were not affected by direct fire, but were exposed to elevated temperature is a critical piece of information. Knowledge of response to high-temperature exposure can lead to more informed decisions on whether a structure needs to be deconstructed completely or just partly. Results of this study are useful to engineers and architects to assess the amount of degradation in bending strength of wood and wood-based composites used in construction. The predictive models can serve as a tool to provide engineers with more comprehensive information on thermal degradation of structural wood and composites, and will help guide the rehabilitation and retrofit of fire damaged structures. Additionally, the results are immediately useful for the engineering community for estimating the nominal design strength of sheathing to framing member connections post exposure to elevated temperature. Prior to this work, if a post-fire structural inspection revealed areas of sustained exposure to elevated temperature in shear walls or horizontal diaphragms, the only reasonable recommendation would be immediate replacement of damaged members. There are no tools to check the residual load capacity of the member or the connection. Reasonable calculation methods are now available to assist engineers with this process. However, there are opportunities for further development.

The methodology of time temperature superposition can be applied for strength and stiffness degradation of wood. This opens up various avenues where long term testing is required. An alternative to long-term tests is to obtain degradation rates from several short-term experiments at several higher temperatures. The results can be shifted by experiment results or by analysis with simple Arrhenius activation energy theory to construct a master plot. The master plot provides an accelerated test method for long-term results.

Engineering design is based on stress criteria and fracture toughness of the material is often neglected although it might govern material failure. This research used fracture mechanics of wood and wood based composites in an attempt to characterize their fracture properties as a material and its dependence on temperature. For the composite manufacturing industry an important quality control test is for bond strength. The internal bond (IB) test provides bond strength information for OSB, while for plywood, the bond classification test is used. The

scatter associated with conventional IB test and the ambiguity in interpretation of bond classification tests makes any statistical comparison of the adequacy of the bond difficult. In contrast, fracture tests provide an unambiguous definition of a material property called fracture toughness. In wood composites, fracture toughness depends significantly on the performance of the adhesive. Hence, characterizing fracture toughness will provide insight into the adhesive performance and can be used as an alternative to conventional quality control tests.

The long-term goal of this research area is to aid in development of a fire endurance and service life or time-dependent reliability model for structural systems of light-framed wood buildings. The ideal model would need empirical data and material property characterization with varying temperature and exposure time. The information presented in this study provides a significant contribution to the required volume of empirical data for such models. There is continuing research focus on evaluating performance and reliability of shear walls and horizontal diaphragms. Connection data obtained from this study adds to the testing data base required for the shear wall performance research.

Limitations and Pitfalls

This work demonstrates that wood and wood-based composites degrade in their mechanical behavior after exposure to elevated temperatures. Moreover, analytical predictive tools are presented to predict the thermal degradation in mechanical properties. These tools and some conclusions drawn in the manuscript are based on certain assumptions which are explained as follows.

In Chapters 2 and 3, a kinetics based model was presented and subsequently the mechanism of degradation was used to construct a master plot using time-temperature superposition. A linear degradation rate with temperature was assumed for the kinetics approach. The assumption was based on initial data analysis and a literature review (Lebow and Winandy 1999) also justified the assumption. Linear degradation assumption provided the best fit at all temperatures, justified by the squared residual (R^2) values. Simple plots of degradation vs. time (Fig. 3.3) can be used to visually test using the linear degradation assumption. Our degradation trends behaved according to assumptions and the chosen models fit well. However, this is an assumption; the final results based on different assumptions (non-linear degradation) may not be consistent with an analysis based on linear degradation rates. This means that the degradation mechanism depends on more than a simple continuous degradation process.

A conclusion of this study is that at lower temperature of 100^{o}C the degradation of wood and composites is driven by the resin and hence called the resin effect. The resin effect does not mean that the resin is degrading significantly, but it is somehow driving the degradation process. The chemical process of degradation was beyond the scope of this work, however a summary based on references and personal communication is presented.

The degradation in mechanical properties of wood is govenrned by degradation of hemicelluloses. Hemicellulose and its acetyl group get hydrolyzed forming acetic acid. The acetic acid is autocatalytic in nature and leads to formation of more acetic acid leading to further degradation of hemicelluloses. The acetic acid also attacks the glycosidic bonds and reduces the degree of polymerization of the glucose and hence in turn reducing the strength of wood. Elevated temperature (140-160^{o}C) conditions start this degradation process but this degradation can also occur at room temperature in presence of chemicals and moisture with an increase in temperature accelerating the entire process. In wood composites there is an interaction of highly alkaline resins at the interface. This facilitates transfer of reactants in and out of the interphase, which may lead to certain degrading chemical changes in the wood. Furthermore, the cured resin degrades as temperature increases beyond the curing temperature and may also become brittle. As the resin degrades the stiffness of the composite is affected. If the resin becomes brittle at the interphase, the composites will loose its stress transfer mechanism which is, strain entanglement, hence the strength will be affected. A wood composite has a wood phase, resin phase and an interaction between wood and resin. Any one of these phases could degrade or lead to degradation of others over time and at elevated temperature. The controls tested were for wood and composites but not for resin and hence separation of a specific degradation mechanism was beyond the scope of this study. In summary, a combination of things is driving the degradation in mechanical properties at elevated temperature. Due to more interaction with chemicals and presence of interphase, the wood-composites are more susceptible to degradation at a lower temperature than is solid wood.

In these tests, the temperature loading condition was a steady state temperature held at the temperature of exposure. However, in real fire conditions, with all the architectural features in a structure the loading condition resembles a spike rather than a steady state temperature. Exposing to a steady state temperature would lead to more deterioration and yield conservative results as compared to spike increase in temperature. Hence, the results of this study would be more conservative and it would characterize the worst case scenario.

The scope of inference of this study has to be carefully defined. Thought needs to put in addressing the scope of inference relative to the board types and thicknesses. This is mainly because there are multiple manufacturers, multiple lots per manufacturer and multiple sheets/boards within each lot and multiple resin type used for manufacturing wood composites. To reduce the variability across manufacturers, a single manufacturer was chosen. OSB or Plywood, irrespective of the manufacturer, resin type used, species of wood and process used has to meet certain basic minimum standard value for various mechanical properties stipulated in voluntary codes PS1 and PS2 for plywood and OSB, respectively. All manufacturers in North America have to manufacture boards conforming to these standards to acquire a certification. Hence, the mechanical properties for any panel have to exceed a basic value irrespective of the manufacturer, wood species and resin type. This study specifically addresses the change in mechanical properties for structural panels, hence a comparison is made and conclusions shall be drawn between plywood, OSB, LVL and wood species used in this study. Generalization of the results would be speculative at this stage. More studies are required involving various manufacturers and different species used in the wood composites before such generalizations can be attempted.

Recommendations for future research

- Verify the kinetics-based model for SSL and LVL at a broader range of temperatures and for different species of wood. Once verified, master curves can be generated for different species of wood and LVL using the principle of time temperature superposition.
- Similar studies can be repeated on other engineered wood composites commonly used in construction such as I joists and structural composite lumber.
- Since the accelerated methods can obtain results in shorter tests, one recommendation of this study is to repeat the higher-temperature results for full-scale members. Research on full size members would allow for deriving design values for thermally degraded structures.
- Study the thermal degradation in yield strength of nailed joints as a function of various temperatures and many exposure times. Then, test whether the NDS yield models are reasonable in those ranges of temperature. Nominal design strength for those connections can be estimated.

- Develop numerical models incorporating the results of this study to estimate the lateral capacity of full-scale wood-frame shear walls and horizontal diaphragms and account for thermal degradation of the materials.
- Study the degradation in bolted connections involving wood and other materials such as steel and concrete.
- Develop procedures to automate analysis and reduction of the optical data acquired during a fracture test to reduce the analysis time. For the composite industry to embrace this test for quality control purposes a significant reduction in data processing time is needed.

Bibliography

Aicher, S. (2010). “Process zone length and fracture energy of spruce wood in mode I from size effect.” *Wood and Fiber Science*, 42(2), 237-247.

Aklonis, J.J. and MacKnight W.J. (1983). *Introduction to polymer viscoelasticity*, 2nd ed. John Wiley and Sons, New York, NY.

American Forest and Paper Association. (AFPA). (1999). *General dowel equations for calculating lateral connection values*. Technical Report 12, Washington, D.C.

AFPA. (2003). *Calculating the fire resistance of exposed wood members*. Technical Report 10. Washington, D.C.

AFPA. (2005). *National design specification® for wood construction*. Washington, D.C.

AFPA. (2007). *Design for Code Acceptance: Fire rated wood floor and wall assemblies*. Washington, D.C.

American Plywood Association (APA). (1989a). *Fire-retardant-treated plywood roof sheathing: Field failures*. Tacoma, WA.

APA. (1989b). *Fire-retardant-treated plywood roof sheathing: General information*. Tacoma, WA.

APA. (2005). *APA Economics Report E171*. Tacoma, WA.

American Society for Testing of Materials (ASTM). (2000). “Standard test methods for structural panel in flexure.” *ASTM D 3043-00*, West Conshohocken, PA.

ASTM. (2001). “Standard test method for evaluating properties of wood-based fiber and particle panel materials.” *ASTM D-1037*, West Conshohocken, PA.

ASTM. (2007a). “Standard test method for determining bending yield moment of nails.” *ASTM F 1575*, American Society for Testing and Materials, West Conshohocken, PA.

ASTM. (2007b). “Standard test method for mechanical fasteners in wood.” *ASTM D 1761*, American Society for Testing and Materials, West Conshohocken, PA.

ASTM. (2007c). “Standard test method for specific gravity of wood and wood-based materials.” *ASTM D 2395*. American Society for Testing and Materials, West Conshohocken, PA.

ASTM. (2007d). “Standard test method for evaluating dowel-bearing strength of wood and wood-based products.” *ASTM D 5764*. American Society for Testing and Materials, West Conshohocken, PA.

Anderson, E.N., Leichti, R.J., Sutt Jr., E.G. and Rosowsky, D.V. (2007). “Sheathing nail bending-yield stress: Effect of cyclic performance of wood shear walls.” *Wood and Fiber Science*, 39(4) 536-547.

Anderson, J. and Konig, M. (2004). “Dependence of fracture toughness of composite laminates on interface ply orientations and delamination growth direction.” *Composites Science and technology*, 64 2139-2152.

Anderson, T.L. (2005). *Fracture Mechanics, Fundamentals and Applications.* CRC Press: Taylor and Frances Group, Boca Raton, FL, 122-125, 310-311.

Aune, P. and Patton-Mallory, M. (1986 a). “Lateral load bearing capacity of nailed joints based on the yield theory: Theoretical development.” *Research Paper FPL 469*. USDA, Forest Serv. Forest Prod. Lab., Madison, WI.

Aune, P. and Patton-Mallory, M. (1986b). “Lateral load-bearing capacity of nailed joints based on the yield theory: Experimental verification.” *Research Paper FPL 470*. USDA, Forest Serv. Forest Prod. Lab., Madison, WI.

Aynlmis, N., Kartel, S.N., Laufenberg, T.L., Winandy, J.E. and White, R.H. (2005). “Physical and mechanical properties and fire, decay, and termite resistance of treated oriented strand board.” *Forest Products Journal*, 55 (5), 74-81.

Beall, F.C and Eickner, H.W (1970). “Thermal degradation of wood components: A literature review.” *Research Paper FPL-RP-130*. U.S. Department of Agriculture, Forest Service, Forest Products Laboratory. Madison, WI.

Bekhta, P., Lecka, J. and Morze, Z. (2003). “Short-term effect of the temperature on the bending strength of wood-based panels.” *Holz als Roh- und Wekstoff,* 61(2003), 423-424.

Bekhta P. and Niemz, P. (2003). “Effect of high temperature on the change in color, dimensional stability and mechanical properties of spruce wood.” *Holzforschung* 57(5), 539–546.

Biblis, E.J. (2001). “Edgewise flexural properties and modulus of rigidity of different sizes of southern pine LVL and plywood.” *Forest Products Journal*, 51(1), 81-84.

Blass, H.J., Ehlbeck, J. and Rouger, F. (1999). “Simplified design of joints with dowel-type fasteners.” *Proc. Pacific timber engineering conference*, 14-18th March, Rotorua, New Zealand. Forest Research institute Limited, Rotorua, New Zealand (3), 275-279.

Branca, C. and Di Blasi, C. (2003). “Kinetics of the isothermal degradation of wood in the temperature range 528–708 K.” *Journal of Analytical and Applied Pyrolysis*, 67, 207–219

Brancheriau, L. and Baillères, H. (2003). “Use of the Partial Least Squares Method with Acoustic Vibration Spectra as a New Grading Technique for Structural Timber.” *Holzforschung*, 57(6), 644-652.

Buchanan, A.H. (2002). *Structural design for fire safety*. John Wiley and Sons, West Sussex, England.

Buchanan, A.H. and Barnett, J. (1995). “Performance-based design for fire in New Zealand.” *Restructuring: America and Beyond, Proceedings of Structures Congress XIII*, 1995, April 2-5, Boston, MA, ASCE, NY, 1106-1121

Bukowski, R.W. and Babrauskas, V. (1994). “Developing rational, performance-based fire safety requirements in model building codes.” *Fire and Material*, 18, 173-191.

Conrad, M.P.C, Smith, G.D and Ferlund, G. (2003). “Fracture of discontinuous wood-adhesive bonds.” *International Journal of Adhesion & Adhesives,* 23(2003), 39–47

Conrad, M.P.C., Smith, G.D. and Fernlund, G. (2004). “Fracture of wood composites and wood-adhesive joints: A comparative review.” *Wood and Fiber Science*, 36(1), 26-39

Cramer, S.M. and White, R.H. (1997). “Fire performance issues.” *Wood Engineering in the 21st century: research needs and goals: proc. Workshop offered in conjunction with SEI/ASCE structures congress XV*, Portland, OR. 75-86.

Curling, S.F., Winandy, J.E., Carll, C., Micales, J. A. and Tenwolde, A. (2003). “How variability in OSB mechanical properties affects biological durability testing.” *Holzforschung*, 57(1), 8-12.

Davidson, B.D., Gharibian S.J. and Yu, L. (2000). “Evaluation of energy release rate-based approaches for predicting delamination growth in laminated composites.” *Int. J. Fract*. 105,343–65.

Daudeville, L., Davenne, L., Yasumura, M. (1999). “Prediction of load carrying capacity of bolted timber joints.” *Wood Sci. Technol*. 33, 15–29.

DeVallance, D.B., Funck, J.W. and Reeb, J.E. (2007). “Douglas-fir plywood gluebond quality as influenced by veneer roughness, lathe checks, and annual ring characteristics.” *Forest products journal*, 57(1-2) 21-28.

Ebewele, R., River, B. and Koutsky, J. (1979). “Tapered double cantilever beam fracture tests of phenolic-wood adhesive joints. Part I. Development of specimen geometry: Effects of bondline thickness, wood anisotropy, and cure time on fracture energy.” *Wood Fiber,* 11(3),197-213.

Ebewele, R., River, B. and Koutsky, J. (1980). “Tapered double cantilever beam fracture tests of phenolic-wood adhesive joints. Part II. Effects of surface roughness, the nature of surface roughness, and surface aging on joint fracture.” *Wood Fiber*, 12(1),40-65.

Ebewele, R., River, B. and Koutsky, J. (1982). “Relationship between phenolic adhesive chemistry, cure and joint performance. Part I. Effects of base resin constitution and hardener on fracture energy and thermal effects during cure.” *J. Adhesion,*14, 189-217.

Ebewele, R., River, B. and Koutsky, J. (1986). “Relationship between phenolic adhesive chemistry and adhesive joint performance; effect of filler type on fraction energy.” *J.Appl. Polym. Sci.* (31), 2275-2302.

Ehart, R.J.A., Stanzl-Tschegg, S.E. and Tschegg, E.K. (1996). “Characterization of crack propagation in particleboard.” *Wood Sci. Technol.* 30,307–321.

Ehart, R.J.A., Stanzl-Tschegg, S.E. and Tschegg, E.K. (1998). “Crack face interaction and mixed mode fracture of wood composites during mode III loading.” *Eng. Fract. Mech.* 61, 253–278.

Ehart, R.J.A., Stanzl-Tschegg, S.E. and Tschegg, E.K. (1999). “Mode III fracture energy of wood composites in comparison to solid wood.” Wood Sci. Technol. 33, 391–405.

Foschi, R.O. (1974). “Load-slip characteristics of nails.” *Journal of Wood Science,* 7(1), 69-76.

Foschi ,R.O. and Bonac, T. (1977). “Load-slip characteristics for connections with common nails.” *Wood Science*, 9(3), 118-123.

Frühmann, K., Tschegg, E.K., Dai, C. and Stanzl-Tschegg, S.E. (2002). “Fracture behavior of laminated veneer lumber under mode I and III loading.” *Wood Sci. Technol.* 36, 319–334

Frühmann, K., Burgert, I., Stanzl-Tschegg, S.E and Tschegg, E.K. (2003). “Mode 1 fracture behavior on the growth ring scale and cellular level of spruce and beech loaded in TR crack propagation system.” *Holzforschung*. 57, 653–660.

Fuller, J.J. (1990). “Predicting the thermo-mechanical behavior of a gypsum-to-wood nailed connection.” MS Thesis, Oregon State University, Corvallis, OR

Gagliano, J.M and Frazier,C.E. (2001). “Improvements in the fracture cleavage testing of adhesively-bonded.” *Wood and Fiber Science*, 33(3), 377-385

Gerhards, C.C. (1982). “Effect of moisture content and temperature on mechanical properties of wood: an analysis of immediate effects.” *Wood and Fibre*, 14 (1), 4-36.

Gibson, L.J. and Ashby, M.F. *Cellular Solids*. Cambridge University Press, Cambridge, England, 1997.

Green, D.W. and Evans, J.W. (2008a). “Effect of cyclic long-term temperature exposure on bending strength of lumber.” *Wood and Fiber Science*, 40(2), 288-300.

Green, D.W. and Evans, J.W. (1994). “Effect of ambient temperatures on the flexural properties of lumber.” *PTEC 94 Timber shaping the future: Proceedings, Pacific Timber Engineering Conference,* Timber research development and advisory council, Fortitude Valley, Queensland, Australia, 2, 190-197.

Green, D.W. and Evans, J.W. (2008b). “The immediate effect of temperature on the modulus of elasticity of green and dry lumber.” *Wood and Fiber Science*, 40(3), 374-383.

Green, D.W., Winandy, J.E and Kretschmann, D.E. (1999). “Wood Handbook-Wood as an engineering material.” General technical report FPL-GTR-113, U.S. Department of Agriculture, Forest Service, Forest Products Laboratory. Madison, WI.

Grundahl, K. (1992). “National Engineered Lightweight Construction Fire Research Project.” *Technical Report: Literature Search and Technical Analysis*. National Fire Protection Research Foundation, Quincy, MA, USA.

Hashemi, S., Kinloch, A.J. and Williams J.G. (1990). “The analysis of interlaminar fracture in uniaxial fibre-polymer composites.” *Proc. R. Soc. Lond. A* (427), 173-199.

Ikonen, V., Peltola, H., Wilhelmsson, L., Kilpelainen, A., Vaisanen, H., Nuutinen, T. and Kellomaki, S.(2008). “Modelling the distribution of wood properties along the stems of Scots pine (Pinus sylvestris L.) and Norway spruce (Picea abies (L.) Karst.) as affected by silvicultural management.” *Forest Ecology and Management*, 256, 1356-1371.

Johansen, K.W. (1949). “Theory of timber connectors.” *Publication No. 9, International Association of Bridges and Structural Engineering*, Bern, Switzerland, 249–262.

Kalkert, R.E. and Dolan, J.D. (1997). “Behavior of 8-D nailed stud-to-sheathing connections.” *Forest Prod. J.,* 47(6),95–102.

Kent, S. (2004). “The effect of biological deterioration on the performance of nailed oriented strand board sheathing to Douglas-fir framing member connections.” PhD Thesis, Oregon State University, Corvallis, OR.

Kent, S.M., Leichti, R.J., Rosowsky, D.V., and Morrell J.J. (2004). “Effect of wood desay by Postia Placenta on the lateral capacity of nailed oriented strandboard sheathing and douglas-fir framing members.” *Wood and Fiber Science*. 36(4) 560-572.

Keunecke, D., Stanzl-Tschegg, S.E. and Niemz, P. (2007). “Fracture characterization of yew and spruce in the radial-tangential and tangential-radial crack propagation system by micro wedge splitting test.” *Holzforschung*, 61, 582-588.

Knudsen, R.M and Schniewind, A.P. (1975). “Performance of structural wood members exposed to fire. *Forest Products Journal*, 25(2), 23-32.

Kocaefe, D., Poncsak, S., and Boluk, Y. (2008). “Effect of thermal treatment on the chemical composition and mechanical properties of Birch and Aspen.” *BioResources,* 3(2), 517-537.

Kuenzi, E.W. (1955). “Theoretical design of a nailed or bolted joint under lateral load.” *Rep. No. Dl951*. U.S. Dept. of Agriculture, Forest Products Laboratory, Madison, WI.

Lebow, P.K. and Winandy, J.E. (1999). “Verification of a kinetics-based model for long term effects of fire retardants on bending strength at elevated temperatures.” *Wood and Fiber Science*, 31(3), 49-61

Le Van, S.L., Ross, R J., and Winandy, J.E. (1990). “Effects of fire retardant chemicals on the bending properties of wood at elevated temperatures.” *Research Paper FPL-RP-498*, U.S. Department of Agriculture, Forest Service, Forest Products Laboratory. , Madison, WI.

Lee, S. and Knauss, W.G. (2000). “Failure of laminated composite at thickness discontinuities under complex loading and elevated temperatures.” *International Journal of Solids and Structures,* 37, 3479-3501.

Lei, Y.-K. and Wilson,J.B. (1980). “Fracture toughness of oriented flakeboard.” *Wood Science,* 12(3),154–161.

Lei, Y.-K. and Wilson, J.B. (1981). “A model for predicting fracture toughness of flakeboard.” *Wood Science*, 13(3),151–156.

Li, V.C., Chan, C.M. and Leung, C.K.Y. (1987). “Experimental determination of the tension-softening relations for cementitious composites.” *Cement and Concrete Research,* 17, 441-452

MacLean, J.D. (1953). “Effect of steaming on strength of wood.” *Proceedings of American wood –preservers’ Association*, Washington D.C. 88-112.

Matsumoto, N. (2009). “The Fracture Toughness of Medium Density Fiberboard and other Fiber Bridging Composites.” MS thesis, Oregon State University, Corvallis, OR.

Matsumoto, N. and Nairn, J.A. (2007) Fracture toughness of MDF and other materials with fiber bridging. In: Proceedings of the 22nd Annual Technical Conference of the American Society of Composites, September 17–19, Seattle, WA, USA.

Matsumoto, N. and Nairn, J.A. (in preparation). Fracture toughness of wood and wood composites during crack propagation.

McLain,T.E. (1975). “Curvilinear load-slip relations in laterally loaded nail joints.” PhD Thesis, Colorado State University, Fort Collins, Colorado.

Mihashi, H. and Hoshino, M. (1989). “Fracture toughness and tension softening properties of glued laminated timbers.” *In 8th European Conference on Fracture: Fracture Behavior and Design of Materials and Structures*, 799–804

Millett, M.A., and Gerhards, C.C. (1972). “Accelerated aging: Residual weight and flexural properties of wood heated in air at 115 to 175°C.” *Wood Science*. 4(4), 193-201.

Mitchell, R.L., Seborg, R.M. and Millett, M.A. (1953). “Effect of heat on the properties and chemical composition of Douglas-fir wood and its major components.” *Forest Products Journal*. 3(11), 38-42.

Morel, S., Mourot, G. and Schmittbuhl, J. (2003). “Influence of the specimen geometry on R curve behavior and roughening of fracture surfaces.” *International Journal of Fracture* 121, 23-24.

Narin, J.A. (2009). “Analytical and Numerical modeling of R curves for cracks with bridging zones.” *International Journal of Fracture*, 5(2) 167-181.

National Fire Protection Agency (NFPA) (2010). “Home Structures Fires.” Tech. Report by Maty Ahrens, March 2010. National Fire andalysis and research division, NFPA, Quincy, MA.

National Institute of Standard and Technology (NIST) (2007). *Voluntary Products Standard PS 1-2007*. Construction and Industrial Plywood. Office of Standards Services, NIST, Gaithersburg, MD.

Nishiyama, N. and Ando, N. (2003). “Analysis of load-slip characteristics of nailed wood joints: application of a two-dimensional geometric nonlinear analysis.” *J. Wood Science,* (49), 505-512.

Noren, J. (1996). “Load-bearing capacity of nailed joints exposed to fire.” *Fire Material,* 20,133-143.

Paul, W., Ohlmeyer, M., Boonstra, M.J. and Pizzi, A. (2006). “Optimising the properties of OSB by a one-step heat pre-treatment process.” *Holz als Roh- und Werkstoff*, 64, 227–234

Pellicane, P.J. (1991). “Application of the European yield model to nailed joints in southern hardwoods.” *J. Testing Eval.,* 19(5), 385-393.

Pellicane, P.J. (1993). “Plywood-Solid-wood nailed joints under lateral loading.” *Journal of material in Civil Engineering*, 5(2), 226-236

Perkins, N.S. (1950). “Predicting exterior plywood performances.” *In. Proc.of the National annual meeting.* 4, 352-364. Forest Product Res. Soc. Portland, OR

Peyer, S.M. and Cramer, S.M. (1999). “Behavior of nailed connection at elevated temperature.” *Wood and Fiber Science*, 31(3), 264-276

Price, E.W. and Gromala, D.S. (1980). “Racking strength of walls sheathed with structural flakeboards made from southern species.” *Forest Products Journal*. 30(12), 19-23.

River, B.H. (1994). “Fracture of adhesive-bonded wood joints.” *in A. Pizzi and K.L. Mittal, eds. Handbook of adhesive technology*. Marcel Dekker, New York, N.Y. 151-177

River, B.H. and Okkonen, E.A. (1993). “Contoured wood double cantilever beam specimen for adhesive joint fracture tests.” *Journal of testing and Evaluation* 21(1), 21-28.

Roylance, D. (2001). *Modules in Mechanics of Materials*. A web-based collection of educational modules developed under the auspices of the National Science Foundation.

Schaffer, E.L. (1970) “Elevated Temperature Effect on the Longitudinal Mechanical Properties of Wood.” Ph.D. Thesis, Department of Mechanical Engineering, Univ. Wisconsin, Madison, WI, USA.

Schon, J., Nyman, T., Blom, A. and Ansell, H. (2000). “Numerical and experimental investigation of a composite ENF-specimen.” *Engrg Fract Mech*, 65, 405–33.

Sela, N., Ishai, O. and Banks-Sills, L. (1989). “The effect of adhesive thickness on interlaminar fracture toughness of interleaved cfrp specimens.” *Composites*, 20(3), 257-264

Shrestha, D. Cramer, S and White, R. (1995). “Simplified models for the properties of dimension lumber and metal- plate connections at elevated temperatures. *Forest Products Journal*, 45(7/8), 35-42.

Sinha, A. (2010). “Effect of Heat on mechanical properties of wood and wood-based composites.” PhD Thesis, Oregon State University, Corvallis, OR.

Sinha, A. and Gupta, R. (2009). “Strain distribution in OSB and GWB in wood-frame shear walls.” *Journal of Structural Engineering*, 135(6), 666-675

Sinha, A., Nairn, J.A. and Gupta, R. (2010). “Thermal Degradation of the bending strength of plywood and oriented Strandboard: A Kinetics approach.” *Wood Science and Technology*, published online.

Smith, I., Craft, S.T. and Quenneville, P. (2001). “Design capacities of joints with laterally loaded nails.” *Can. J. Civil Engineering,* (28), 282-290.

Smith, I., Landis, E., Gong, M. (2003). *Fracture and Fatigue in Wood*. John Wiley & Sons Ltd, West Sussex PO19 8SQ, England, 161-166.

Smith, I. and Vasic, S. (2003). “Fracture behavior of softwood.” *Mech. Mater.* 35, 803–815.

Stamm, A.J. (1964). *Wood and Cellulose Science*. Ronald Press, New York, USA. 308-311.

Stanzl-Tschegg, S.E. and Navi, P. (2009). “Fracture behavior of wood and its composites. A review.” *Holzforschung* 63, 139-149.

Structural Board Association (SBA). (2009). *OSB: A flooring panel that stands on its own. Specifications EL809.* Ontario, Canada.

Theilen, R.D., Bender, D.A, Pllock, D.G. and Winistorfer, S.G. (1998). “Lateral Resistance of ring-shank nail connections in Southern Pine lumber.” *Transactions of the ASAE*, 41(2), 465-472.

Thomas, G.C. (1997). “Fire Resistance of Light Timber Framed Walls and Floors.” *Fire Engineering Research Report 97/17*, School of Engineering, University of Canterbury, New Zealand.

Vasic, S. (2000). “Applications of fracture mechanics to wood.” PhD thesis, University of New Brunswick, New Brunswick, Canada.

Vestol, G.I. and Hoibo, O.A. (2001). “Prediction of knot diameter in Picea abies (L.) Karst.” *Holz als Roh- und Werkstoff*, 59, 129–136

Wang, S. and Rao, Y. (1999). “Structural performance of fire-retardant treated plywood: effect of elevated temperature.” *Holzforschung*, 53(5), 547-552.

White, R.H. (1988). “Charring rates of different wood species.” Ph.D. thesis. University of Wisconsin-Madison, WI, USA.

White, R.H. (2006). “Fire resistance of Structural Composite lumber.” *Research paper FPL-RP 633*, U.S. Department of Agriculture, Forest Service, Forest Products Laboratory, Madison, WI.

White, R. H. and Nordheim, E.V. (1992). “Charring rate of wood for ASTM E 119 Exposure.” *Fire Technology*, 28(1), 5–30.

White, R.H. and Tran, H.C. (1996). “Charring rate of wood exposed to a constant heat flux.” *Proceedings of Wood and Fire Safety Conference*. Zvolen, Slovak Republic, 175–183.

White, R.H. and Winandy, J.E. (2006). “Fire performance of Oriented Strandboard” *Proc. Seventeenth Annual BCC Conference on Flame Retardancy*, Norwalk, CT, USA, 297-309.

Wilkinson, T. L. (1991). “Dowel bearing strength.” *FPL-RP-505*. USDA Forest Service, Forest Products Laboratory, Madison, WI.

Winandy, J.E. and Lebow, P.K. (1996). “Kinetics models for thermal degradation of strength of fire-retardant treated wood.” *Wood and Fiber Science*, 28(1), 39-52.

Winandy, J.E., LeVan, S.L., Ross, R.J., Hoffman, S.P. and McIntyre, C.R. (1991). “Thermal degradation of fire-retardant-treated plywood: Development and evaluation of test protocol.” *Research Paper FPL-RP 501*. U.S. Department of Agriculture, Forest Service, Forest Products Laboratory. Madison, WI.

Winandy, J.E., LeVan, S.L., Schaffer, E.L. and Lee, P.W. (1988). “Effect of fire-retardant treatment and redrying on the mechanical properties of Douglas-fir and aspen plywood*.” Research Paper FPL-RP 485. U.S*. Department of Agriculture, Forest Service, Forest Products Laboratory. Madison, WI.

Woo, J.K. (1981). “Effect of thermal exposure on strength of wood treated with fire retardants.” Ph.D. Thesis. Berkeley, CA: University of California. 112 p.

Wu, E.M. (1963). “Application of Fracture Mechanics to Orthotropic Plates.” T*&AM Report No. 248*, Department of Theoretical and Applied Mechanics, University of Illinois, Urbana, Illinois.

Wu, E.M. (1967). “Application of Fracture Mechanics to Anisotropic Plates.” Journal of Applied Mechanics, 34(4), 967-974.

Yeh, B and Schniewind, A.P (1992). “Elasto-Plastic Fracture mechanics of wood using J integral method.” *Wood and fiber Science*, 24 (3) 364-376.

Yoshihara, H. and Nobusue, K. (2008). “Mode I and Mode II fracture toughness of densified Sitka spruce fabricated in an airtight atmosphere with high temperature steam.” *Holzforschung*, 62, 82-85.

Young, S.A. and Clancy, P. (2001). “Compression mechanical properties of wood at temperatures simulating fire conditions.” *Fire and Material*, 25, 83-93.

Younquist, J.A. (2000). “Wood based composites and panel products. Wood as an engineering material.” *General Technical Report 113,* U.S. Department of Agriculture, Forest Service, Forest Products Laboratory, Madison, WI.

Zamborie, B.G., Kamke, F.A. and Watson, L.T. (2001). “Simulation of the mat formation process.” *Wood and Fiber Science*, 33(4), 564-579.

Appendices

Appendix A

Load Deflection Diagrams for Bending Tests

This Appendix provides the supporting materials for manuscript 1 (chapter 2). All the load deflection diagrams are presented in the subsequent pages followed by MOR and MOE values of all the samples tested. The sample size was 36 per treatment per material. As a result, each graph represents 36 load deflection curves.The axes of the graphs are identical for structural panels i.e. OSBO, OSBH, PWH and PWO. As SSL and LVL failed at much higher load than these materials the axes for SSL and LVL are different.

Table A1. Test Matrix for manuscript 1 and 4

Temperature (^{o}C)	20						100												200									
Exposure time (min)							60						120						60						120			
Materials	OSB		PW		LVL	SSL	OSB		Plywood		LVL	SSL	OSB		PW		LVL	SSL	OSB		PW		LVL	SSL	OSB		PW		LVL	SSL
Thickness (mm)	12	25	12	25	25	25	12	25	12	25	25	25	12	25	12	25	25	25	12	25	12	25	25	25	12	25	12	25	25	25
Response																														
MOE/MOR	36	36	36	36	36	36	36	36	36	36	36	36	36	36	36	36	36	36	36	36	36	36	36	36	36	36	36	36	36	36
Weight Loss	36	36	36	36	36	36	36	36	36	36	36	36	36	36	36	36	36	36	36	36	36	36	36	36	36	36	36	36	36	36
Fracture Toughness	2	2	2	2	2	2	2	2	2	2	2	2	2	2	2	2	2	2	2	2	2	2	2	2	2	2	2	2	2	2
IB	25	25	25	25			25	25	25	25			25	25	25	25			25	25	25	25			25	25	25	25		

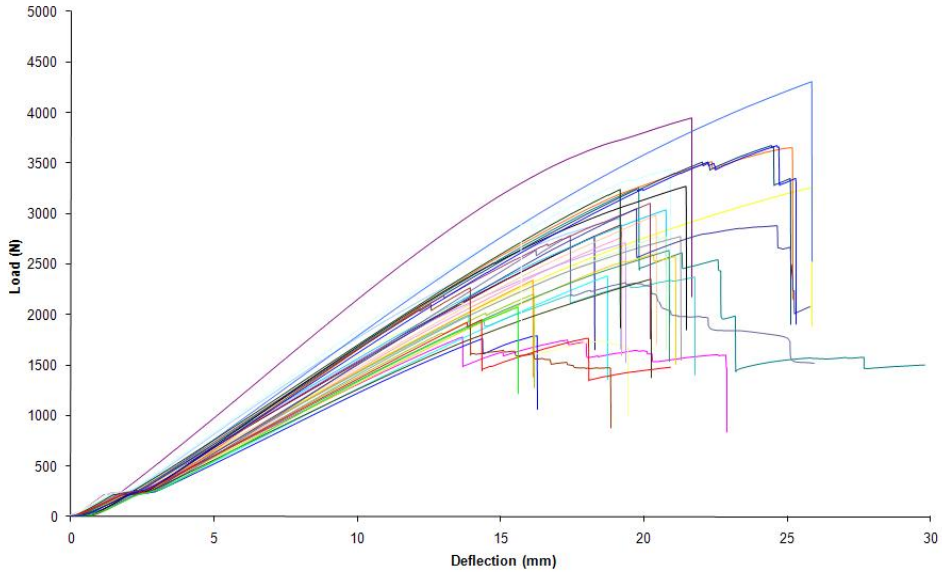

Fig. A1 Load Deflection curve in bending test for PWO control

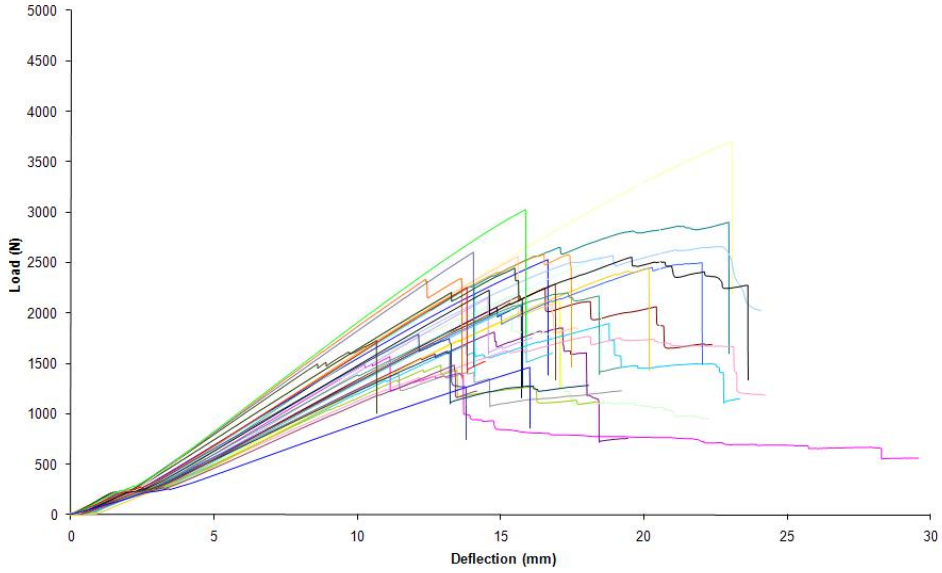

Fig. A2. Load Deflection curve in bending test for PWO 100^{o}C -1hr

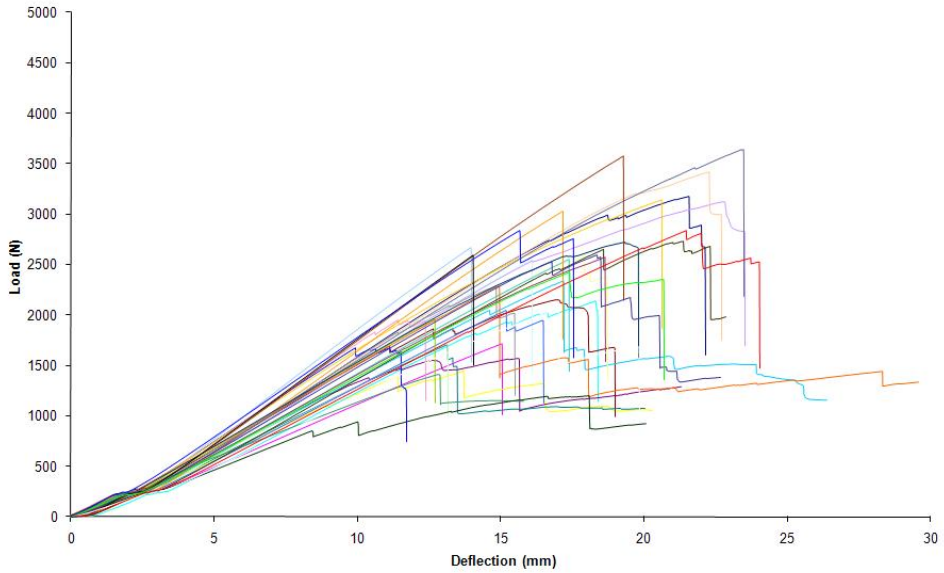

Fig. A3. Load Deflection curve in bending test for PWO 100^{o}C -2hr

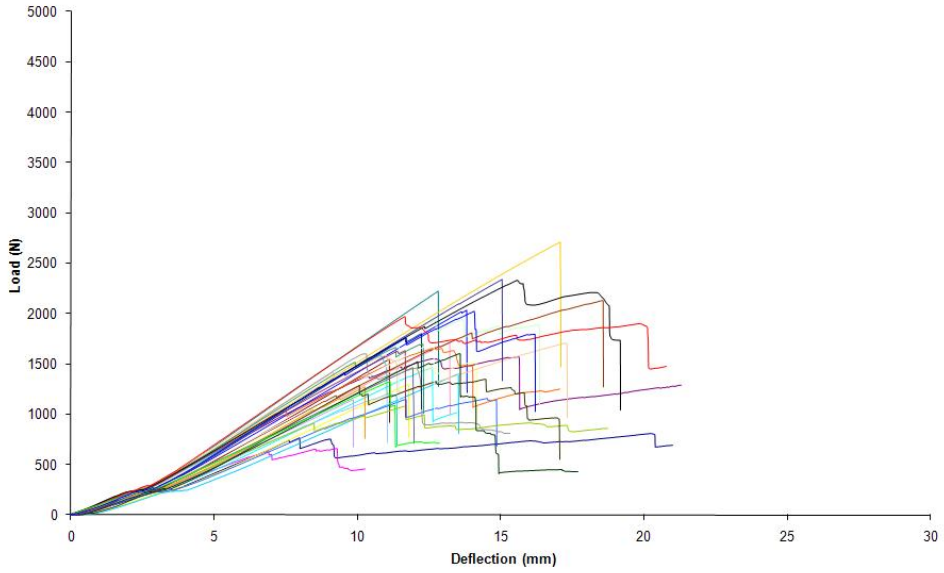

Fig. A4. Load Deflection curve in bending test for PWO 200^{o}C -1hr

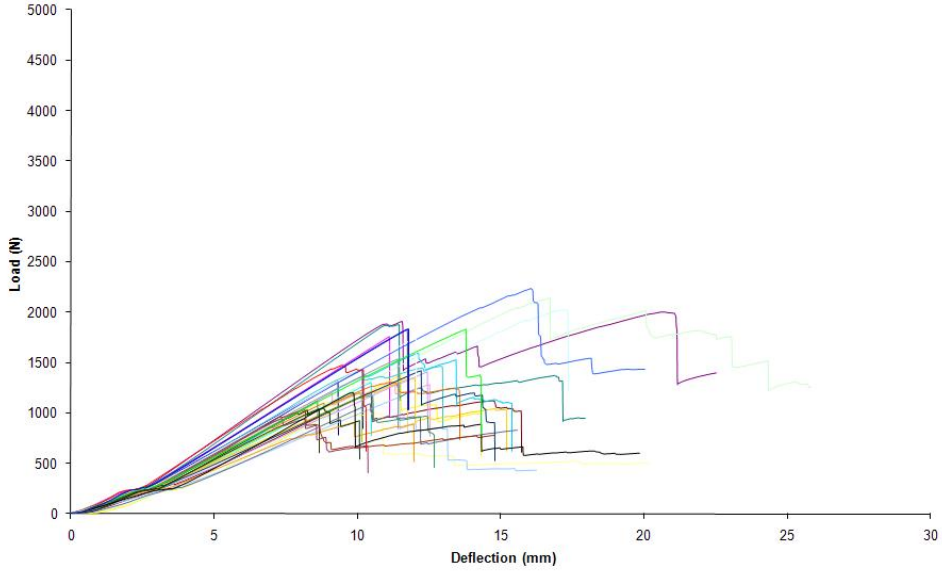

Fig. A5. Load Deflection curve in bending test for PWO 200^{o}C -2hr

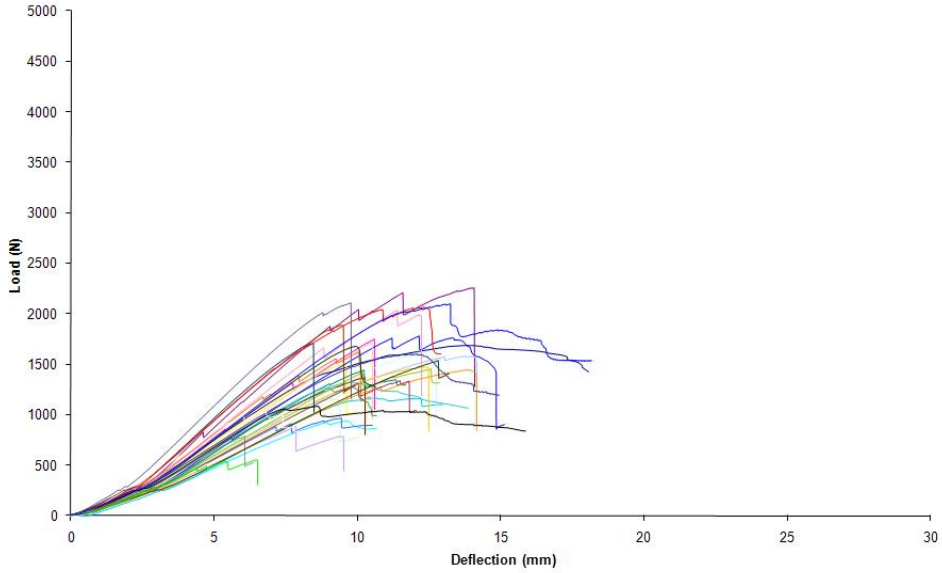

Fig. A6. Load Deflection curve in bending test for PWH Control

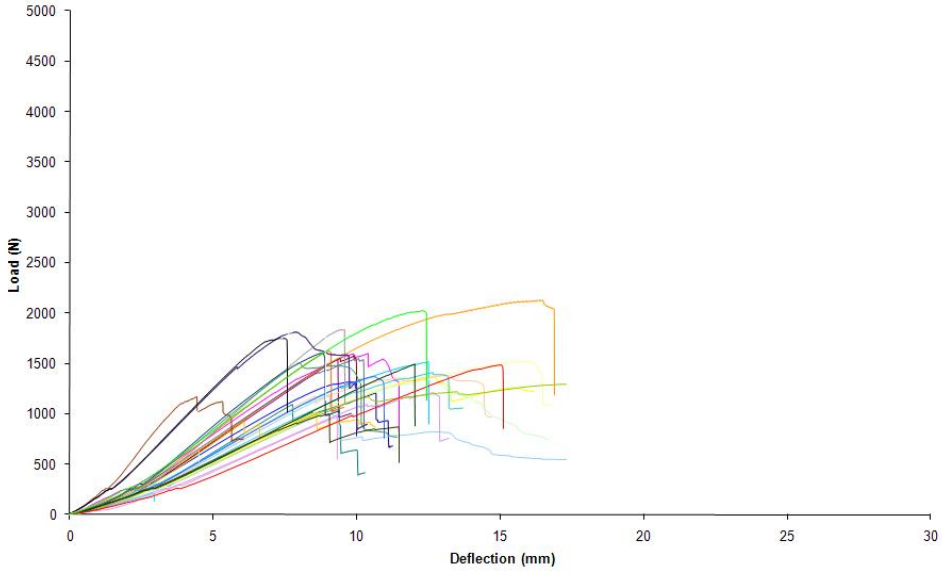

Fig. A7. Load Deflection curve in bending test for PWH 100^{o}C -1hr

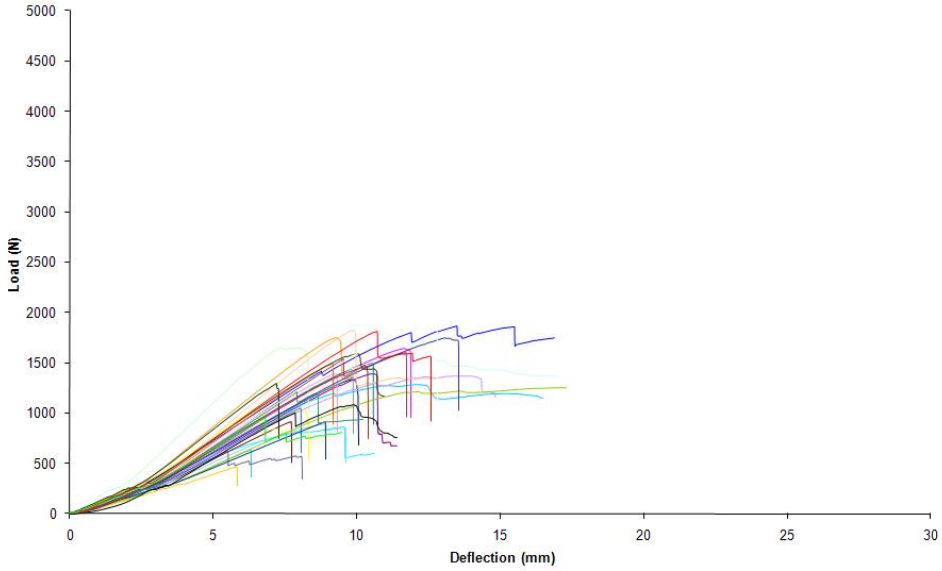

Fig. A8. Load Deflection curve in bending test for PWH 100^{o}C -2hr

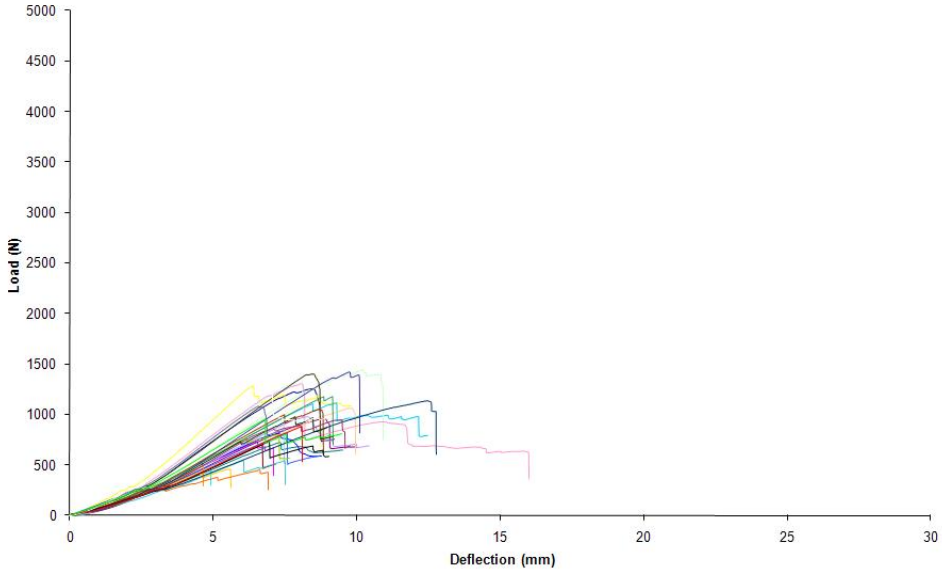

Fig. A9. Load Deflection curve in bending test for PWH 200^{o}C -1hr

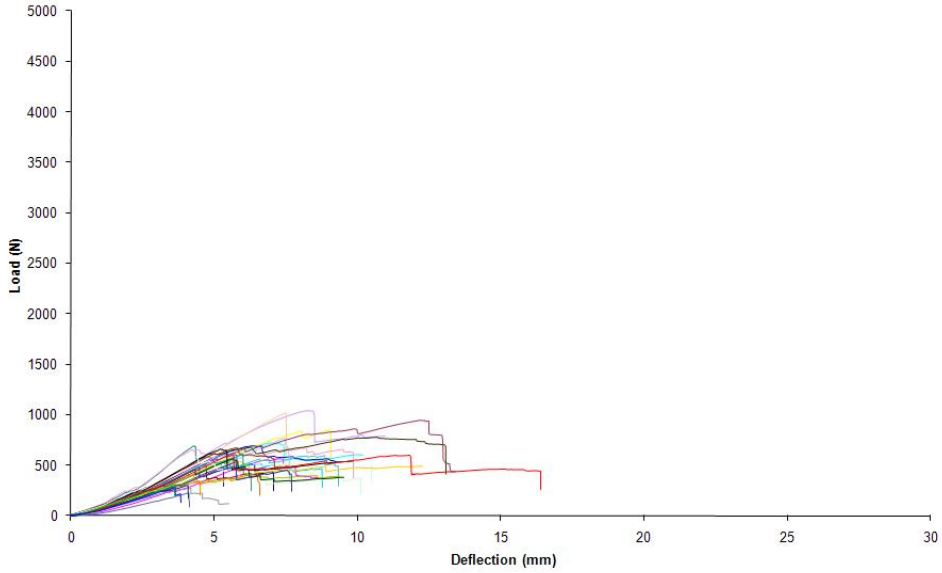

Fig. A10. Load Deflection curve in bending test for PWH 200^{o}C -2hr

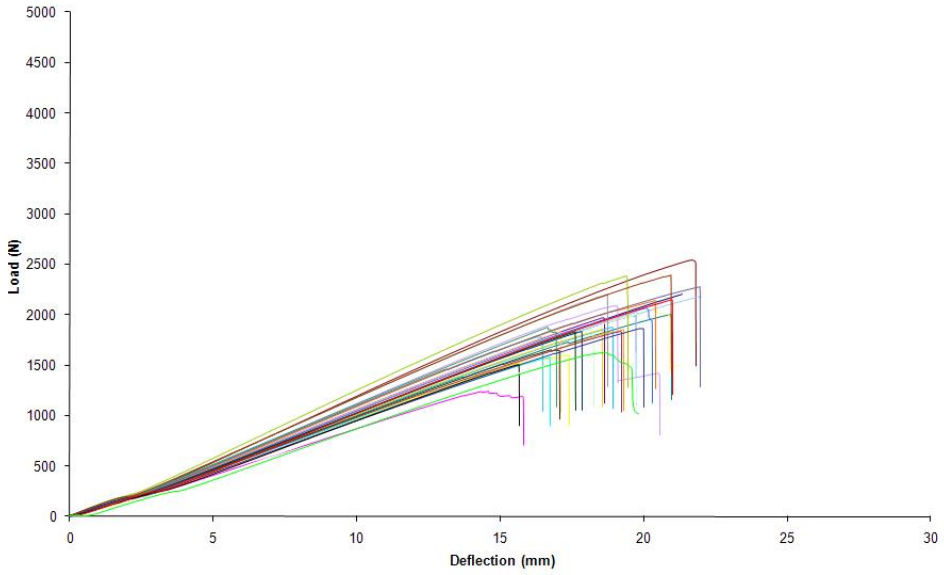

Fig. A11. Load Deflection curve in bending test for OSBO Control

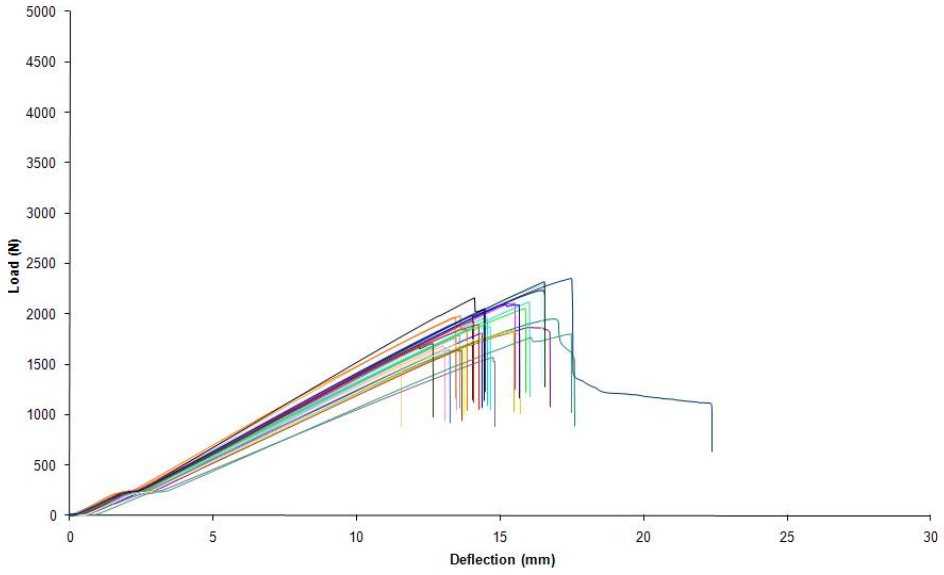

Fig. A12. Load Deflection curve in bending test for OSBO 100^{o}C -1hr

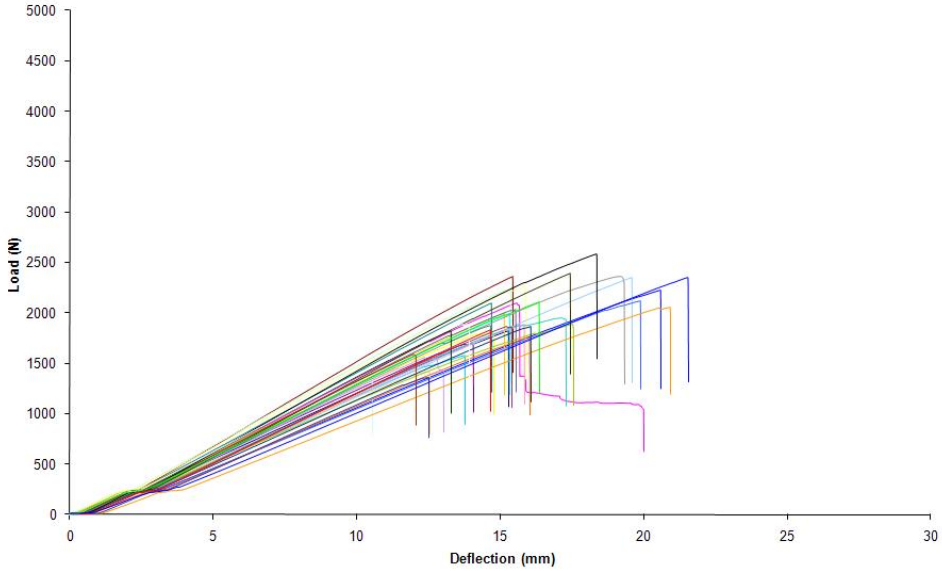

Fig. A13. Load Deflection curve in bending test for OSBO 100^{o}C -2hr

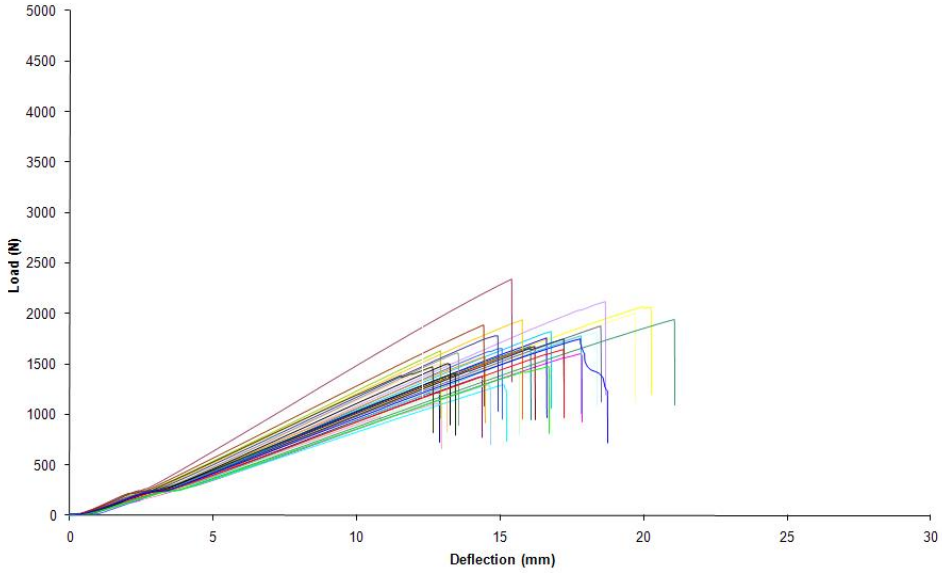

Fig. A14. Load Deflection curve in bending test for OSBO 200^{o}C -1hr

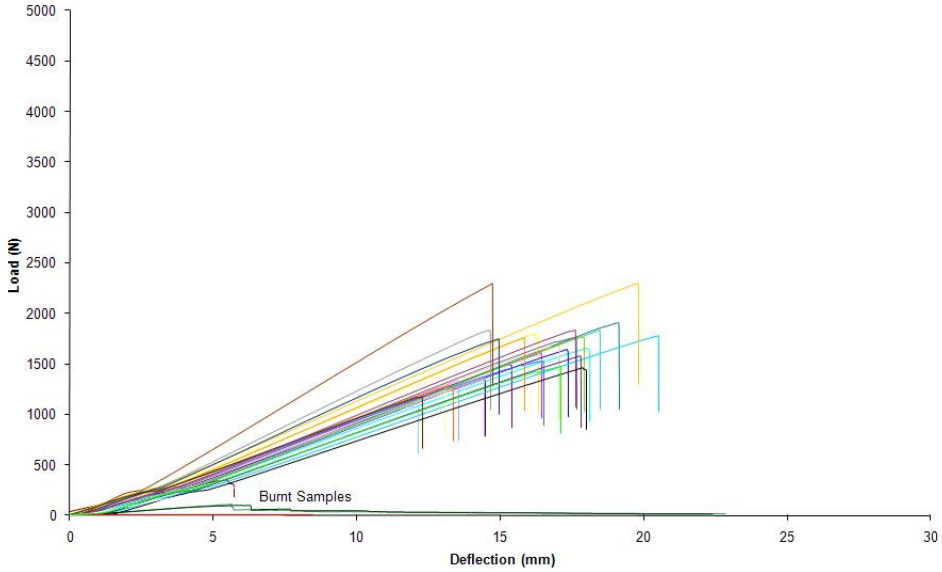

Fig. A15. Load Deflection curve in bending test for OSBO 200^{o}C -2hr

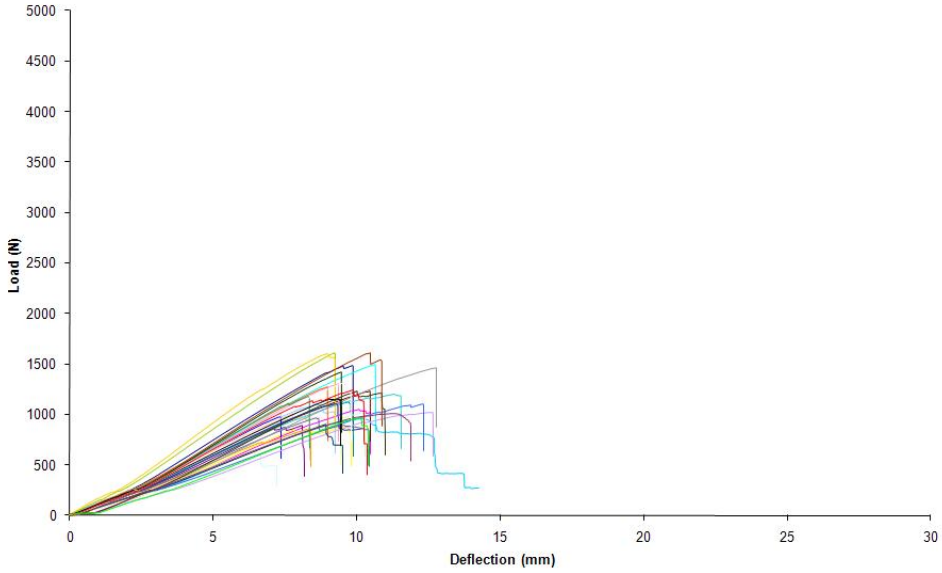

Fig. A16. Load Deflection curve in bending test for OSBH Control

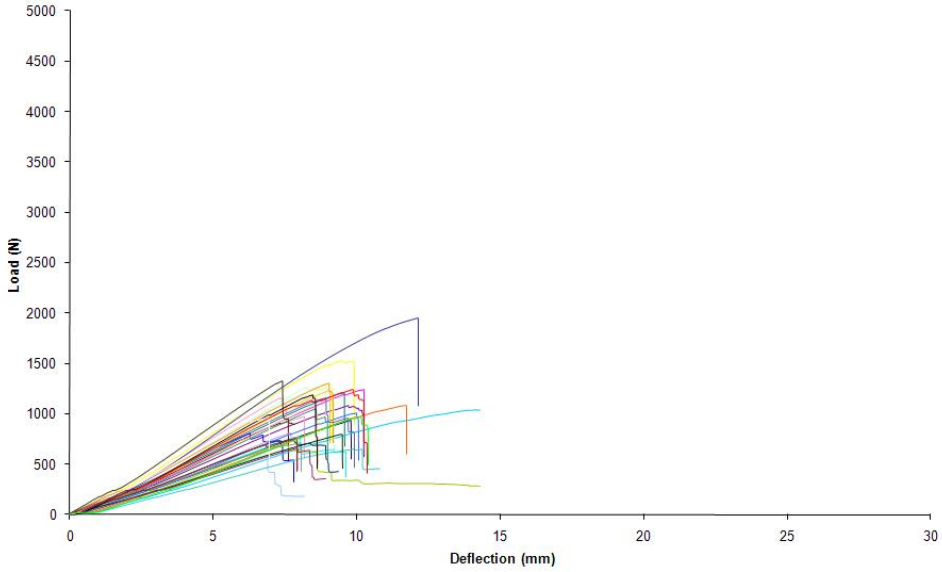

Fig. A17. Load Deflection curve in bending test for OSBH 100^{o}C -1hr

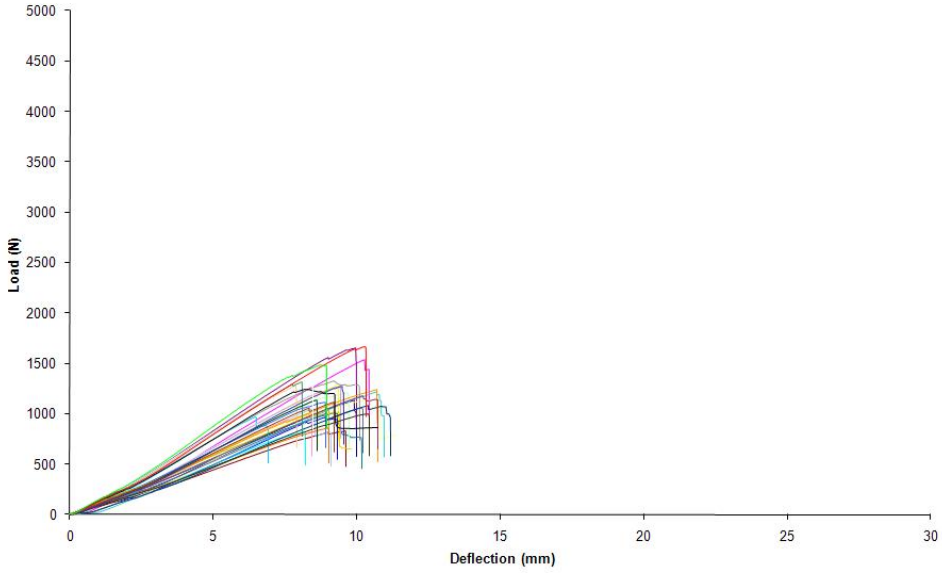

Fig. A18. Load Deflection curve in bending test for OSBH 100^{o}C -2hr

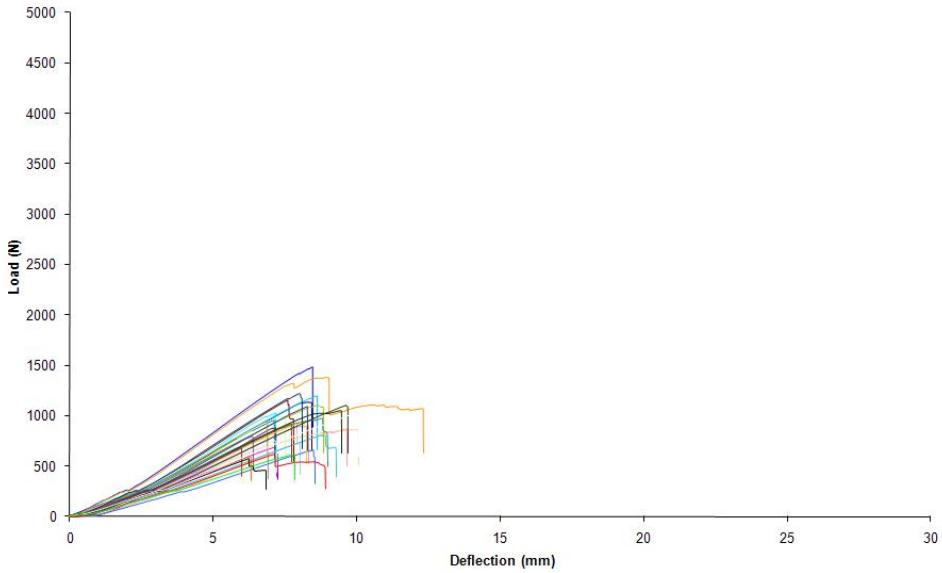

Fig. A19. Load Deflection curve in bending test for OSBH 200^{o}C -1hr

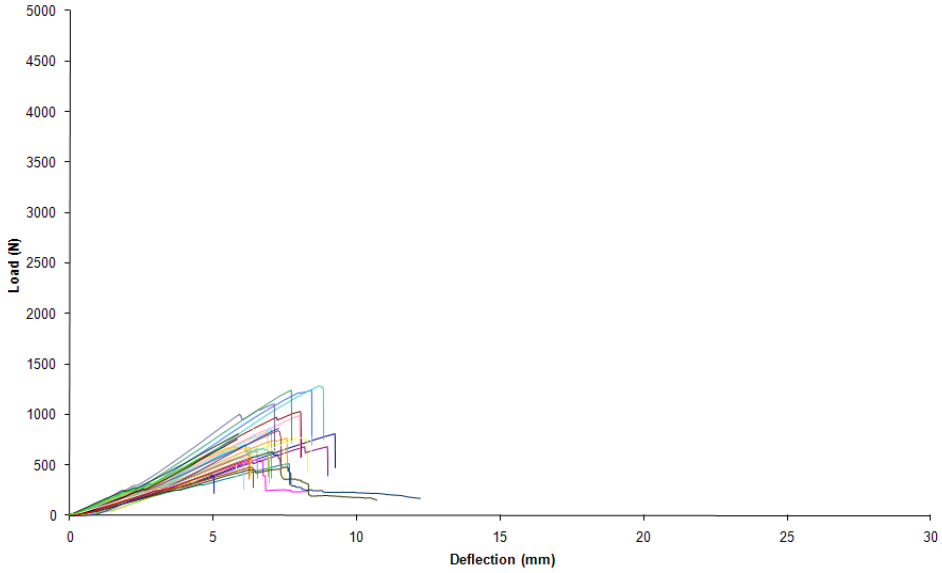

Fig. A20. Load Deflection curve in bending test for OSBO 200^{o}C -2hr

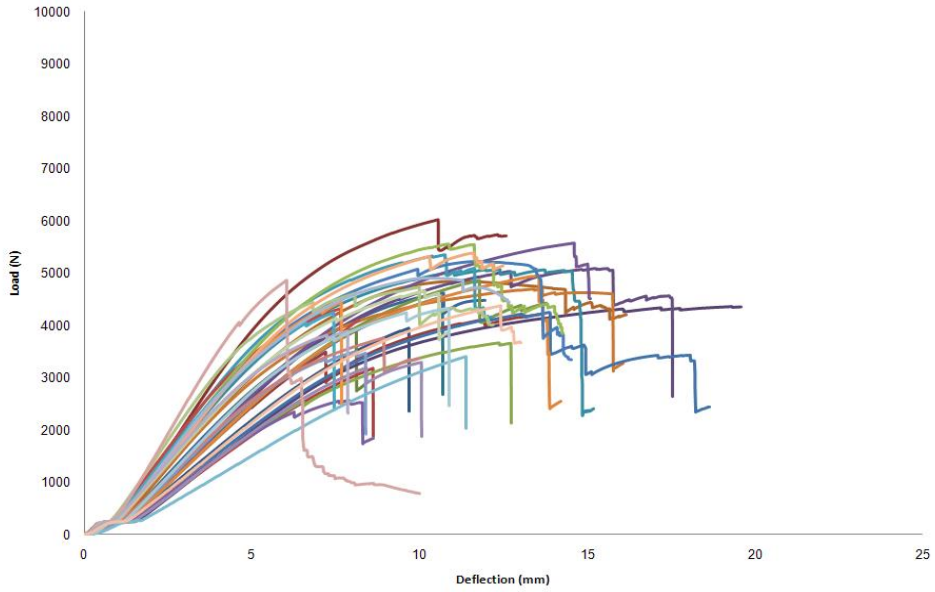

Fig. A21. Load Deflection curve in bending test for SSL Control

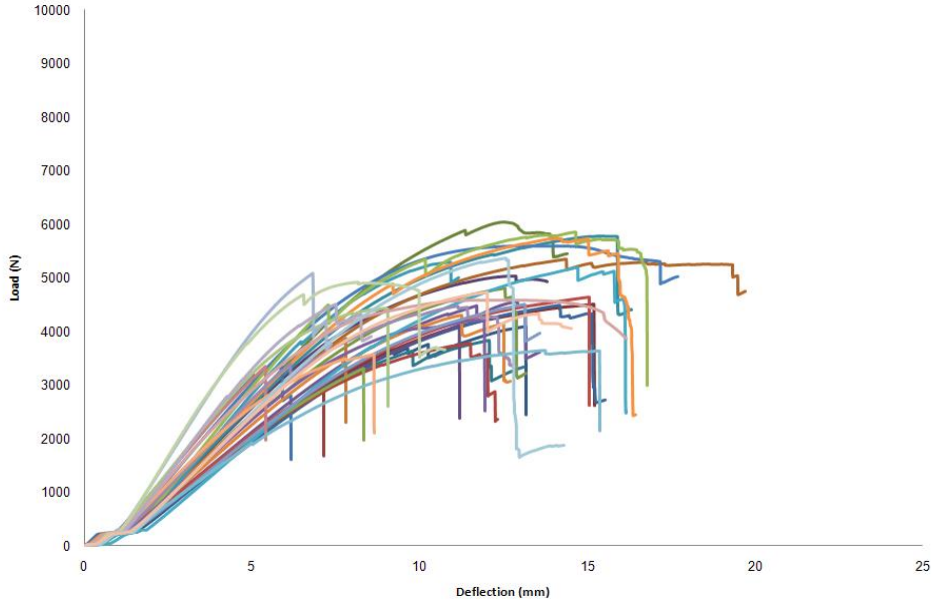

Fig. A22. Load Deflection curve in bending test for SSL 100^{o}C -1hr

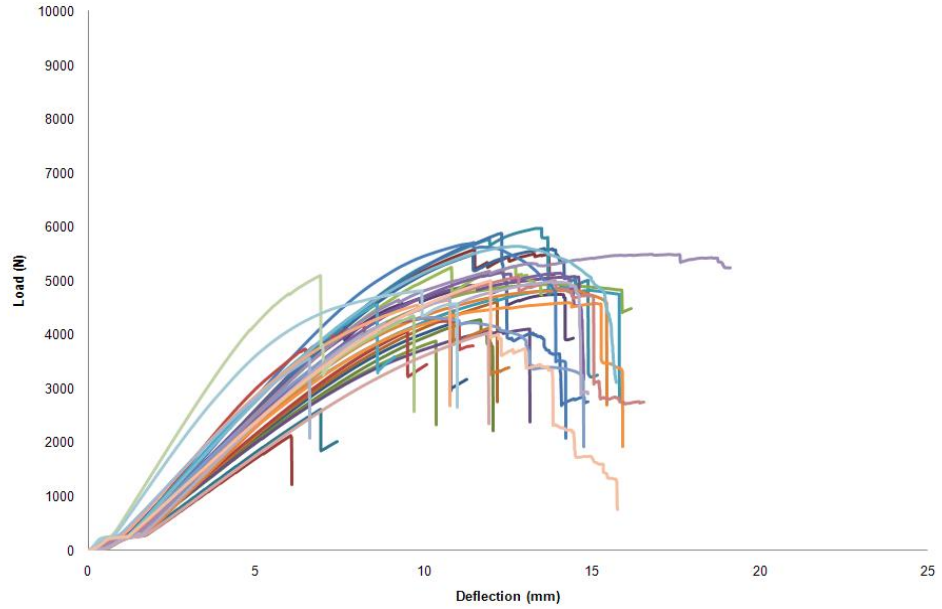

Fig. A23. Load Deflection curve in bending test for SSL 100^{o}C -2hr

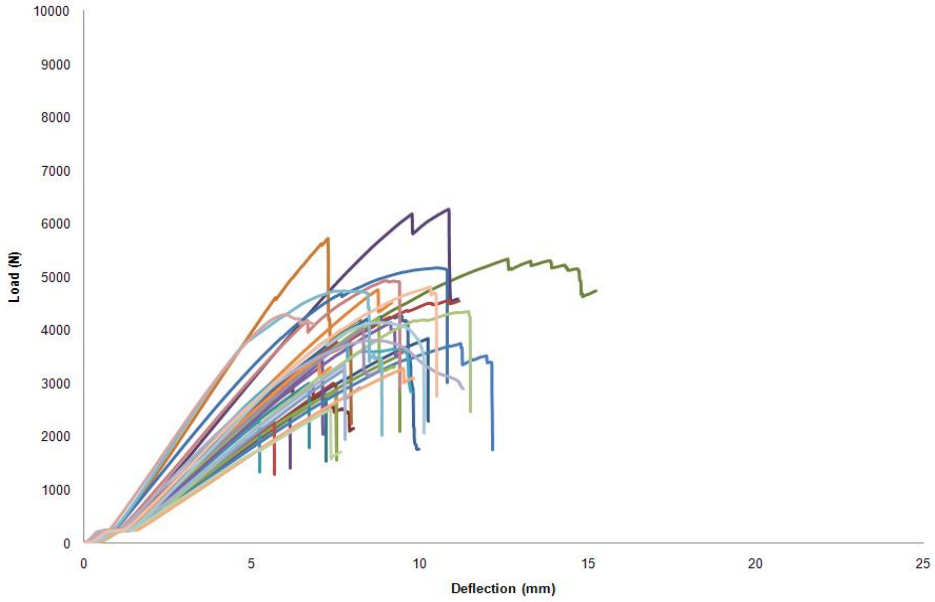

Fig. A24. Load Deflection curve in bending test for SSL 200^{o}C -1hr

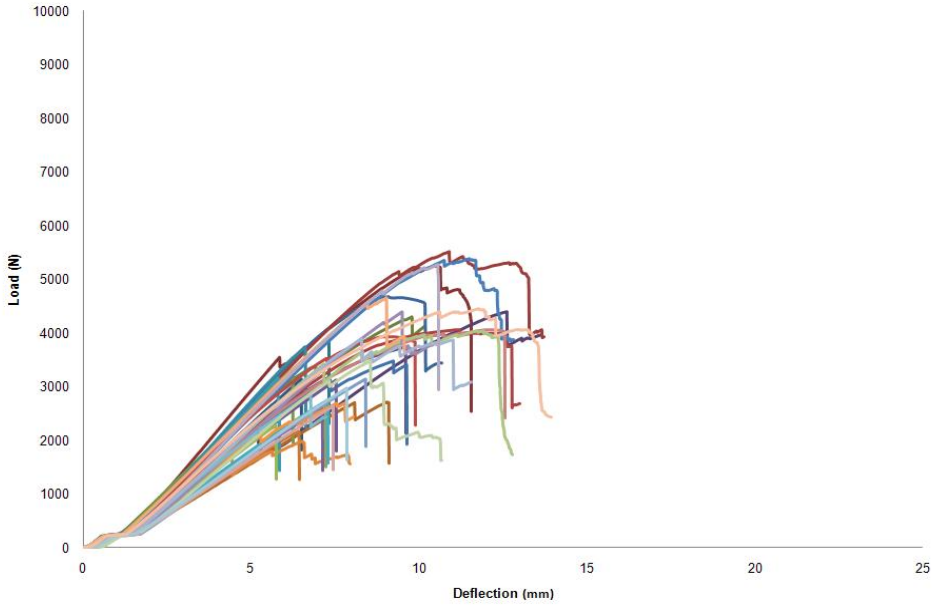

Fig. A25. Load Deflection curve in bending test for SSL 200^{o}C -2hr

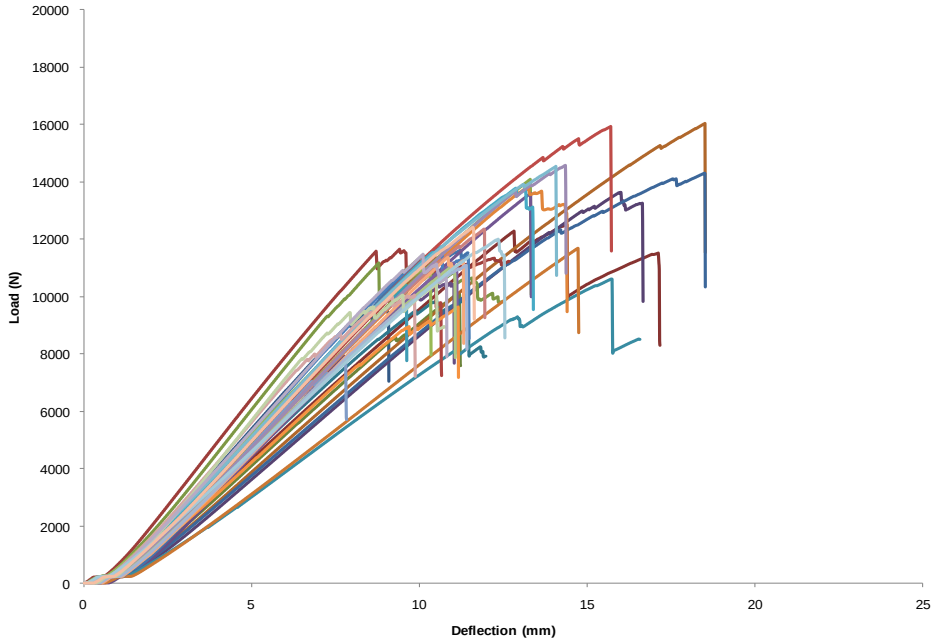

Fig. A26. Load Deflection curve in bending test for LVL Control

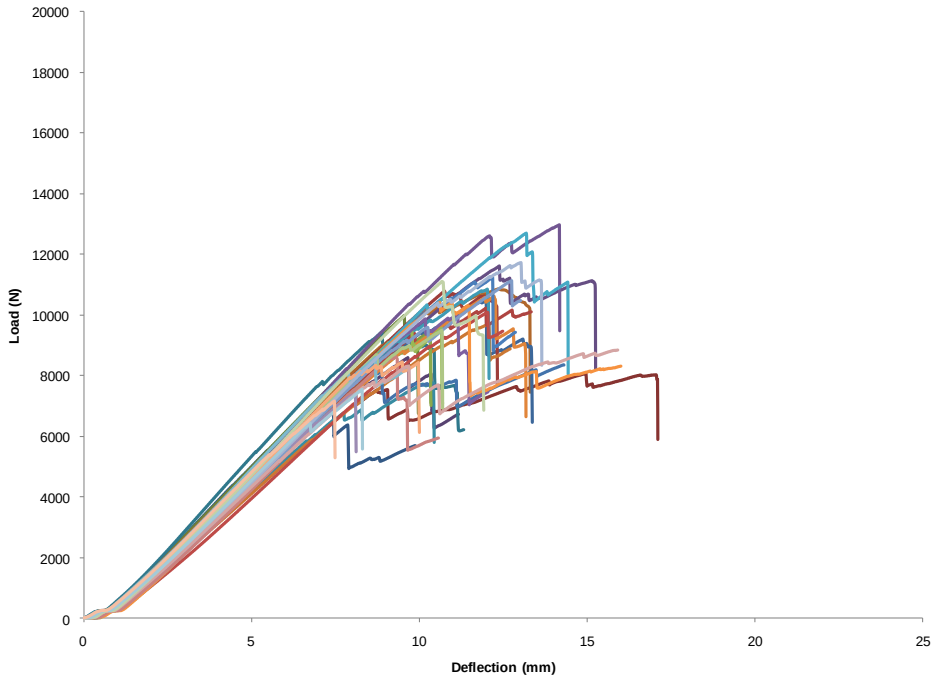

Fig. A27. Load Deflection curve in bending test for LVL 100^{o}C - 1hr

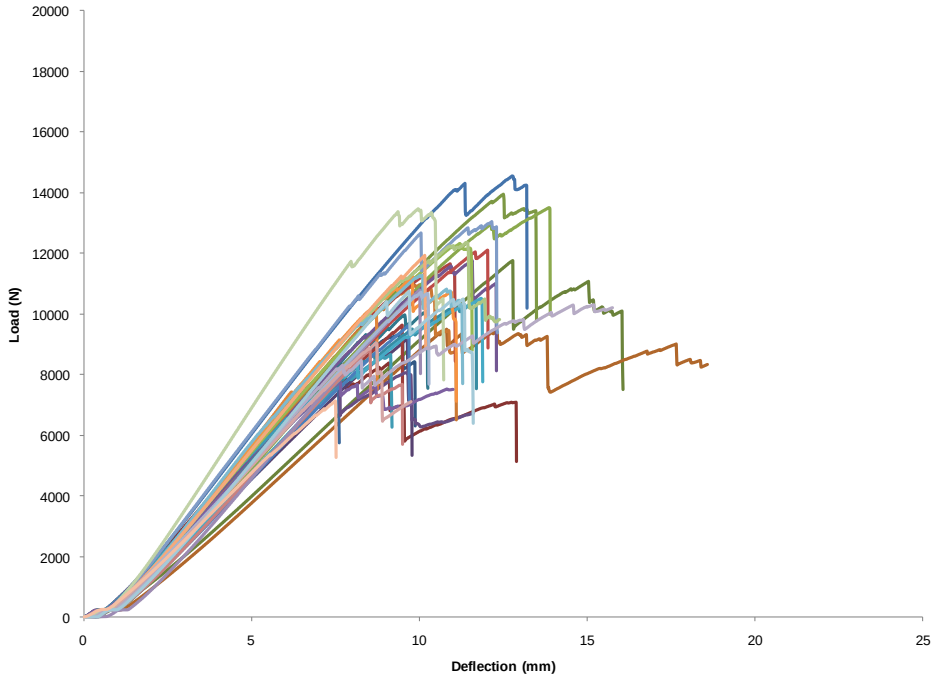

Fig. A28. Load Deflection curve in bending test for LVL 100^{o}C - 2hr

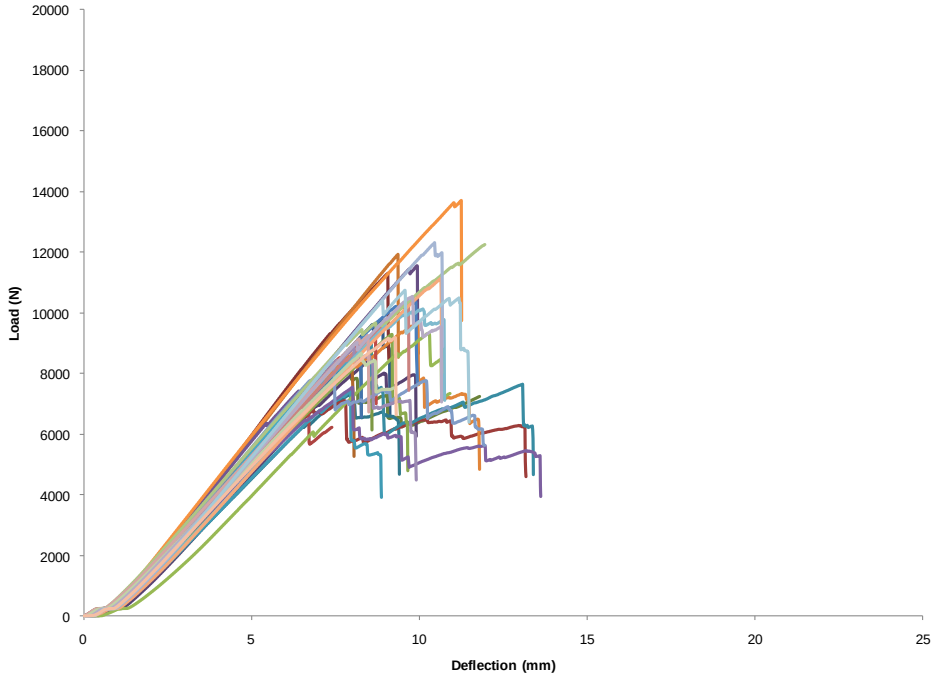

Fig. A29. Load Deflection curve in bending test for LVL 200^{o}C - 1hr

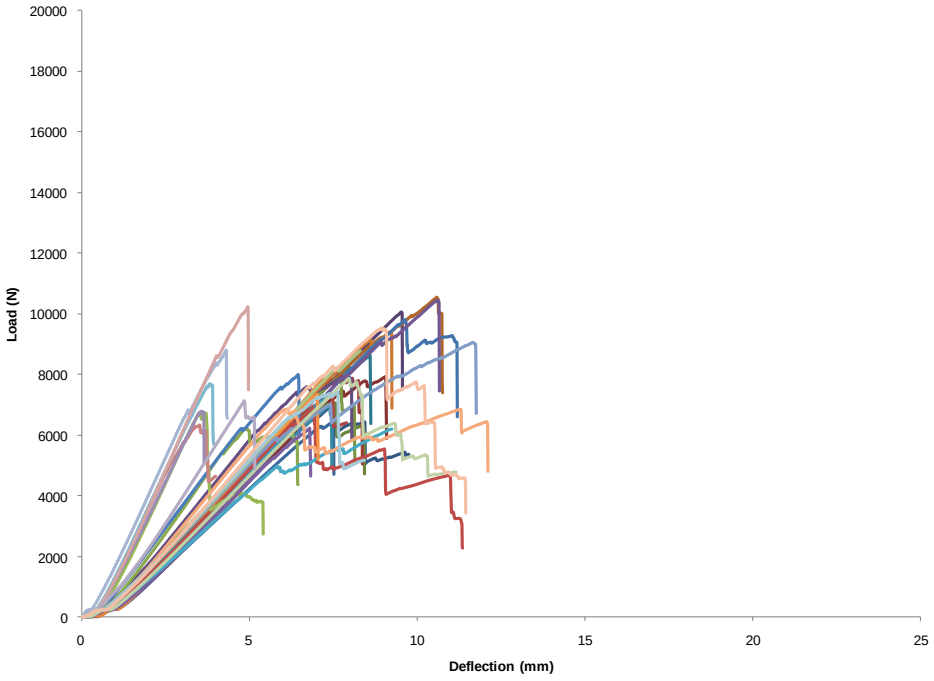

Fig. A30. Load Deflection curve in bending test for LVL 200^{o}C - 2hr

Table A2. Data for Bending Tests for Control (N = 36)

SSL		LVL		OSBH		OSBO		PWH		PWO	
MOR (MPa)	MOE (GPa)	MOR (MPa)	MOE (GPa)	MOR (MPa)	MOE (GPa)	MOR (MPa)	MOE (GPa)	MOR (MPa)	MOE (GPa)	MOR (MPa)	MOE (GPa)
105.5	13.7	50.9	13.4	42	7.9	37.6	8.1	52.7	11.3	34.4	7.1
91.4	12.8	66.6	14.1	29.7	5.7	20.2	6.7	54.7	11.4	22.3	5.7
100.5	12.3	53.8	15.4	24.9	6.2	26	7.8	47.2	11	40.4	6.2
105.1	14.4	72.5	13.6	42.2	7.1	25.8	8.7	29.3	7.7	30.1	5.2
98.6	13	53	10.9	25.3	6.2	32.2	8.5	70.6	14.9	31.5	6.1
95	11.4	85.3	13.3	34.9	6.7	41.5	9.2	42.9	9.3	49.8	9.6
85.8	11.6	76.1	14.1	31.8	6.9	32.5	8.5	45.2	9.6	37.8	6.8
130.6	16.9	61.9	16.3	27.6	8.2	32.4	8.6	55.9	10.6	40.4	7.1
85.4	11.4	60.8	14.9	26.9	5.7	30.6	8.1	36.4	8.1	22.8	5.1
110.5	14.1	55.7	12.1	18	4.9	30.2	7.6	51.4	9.6	37.7	6.3
110.1	13.4	56.4	11.1	28.7	6.2	33.2	9.2	36.2	8.4	44	8.2
102	11.8	62.1	11.8	25	5.7	36.4	8.8	41.1	8.1	34.4	5.8
92.3	11.1	61.7	13.1	31.3	7.9	36.4	8.8	49.6	9	31.3	8
69.1	10.4	60.4	13.1	36.8	6.9	33.9	9.1	63.6	12.1	37.9	8.1
79.4	9.7	74.9	11.6	28.9	5.4	29.9	9	27.5	7.4	35.8	7.4
121	14.2	72.2	11.9	28.4	7.4	33.7	8.3	53.6	11.3	35	7.1
116.1	14.5	55.3	13.4	31.1	4.8	29.1	8.3	30.2	8	38.3	6.7
107.6	13.9	73.4	12	33.8	5.8	38.8	9.8	41.3	9.6	55.1	7.7
113.1	14.6	62.4	13.7	45.5	9.4	30.2	8.1	45.4	9.1	30.2	6.6
93.8	12.2	84.6	12.5	45.2	9.8	30.2	7.9	46	9.5	28.1	6.3
120.4	14.5	58.7	12.4	24.3	5.6	34.9	9.4	45.2	8.1	33.4	6
55.9	8.2	59.5	11.6	36.1	8	37	8.8	50.7	11.7	29.5	6
92.3	11.9	73.3	12.5	27.5	6.4	35.9	9.5	66	11.9	46.2	8
96.7	12.1	51.2	11.3	41.2	6.5	29.9	8.7	24.7	7.3	36.6	7.6
75.7	10	40.9	12.9	25.5	6.3	30.5	9.3	53.6	14.4	36	7
81.6	10.6	65.7	12.6	33.4	8.3	27.3	8.4	40	10.5	47.4	7.8
102.7	14.1	58.9	12.5	40.2	8.8	29.9	7.7	52.6	11.9	34.7	5.8
71.5	10.7	77.4	11.6	34.7	7.6	27	8.2	48.3	8.1	40.2	7.2
74	8.8	77.2	11.9	45.6	8.8	38.9	9	59	14.3	30.5	6.1
117.1	14.6	60.5	12	28.6	5.2	29.8	7.6	41.9	7.8	29.9	8.5
106.4	12.5	58.9	12	31.3	6.3	30.3	7	50.1	10.1	39.1	7.5
105.7	16.6	53.5	14.2	32.8	7.5	24.6	7.6	34	10.3	37.8	6.8
100.9	11.9	55.5	14.6	37.5	7.6	24.6	8.3	32.2	7.5	38.8	8.8
84.5	11.2	60.9	12.6	35.2	7.3	35.1	9	64.8	11.6	41.4	8.1
94	11.8	63.7	11.8	27.3	5.3	26.4	1.7	17.3	7.1	25.7	6.7
94.8	11.9	65.9	13.8	26	6.6	29.9	5.6	65.7	11.7	25.8	6.3

Table A3. Data for bending tests 100^{o}C -1h

SSL		LVL		OSBH		OSBO		PWH		PWO	
MOR (MPa)	MOE (GPa)	MOR (MPa)	MOE (GPa)	MOR (MPa)	MOE (GPa)	MOR (MPa)	MOE (GPa)	MOR (MPa)	MOE (GPa)	MOR (MPa)	MOE (GPa)
88.7	11.5	40.1	12	26.5	4.7	36.5	8.4	37.9	7	26.8	5.6
97.9	10.7	42.9	11.1	34.9	6.2	34.4	8.8	50	11.4	20.2	7
131.2	15.8	53	12.1	43.1	9	27.9	8	43	7.3	27.4	5.8
109.1	13.8	45.7	11.6	21.8	4.9	30.5	8.3	6.8	10.3	29.4	7.1
83.4	10.6	50.1	13.5	30.5	6.6	30.5	8.1	48.5	11.1	24	5.8
116.2	13.4	57.7	11.1	26.1	6.1	32.4	9.6	49.3	10.8	29	6.2
97.5	10.9	55.6	10.9	34.1	7	31.7	8.3	34.3	9.3	37.4	8
64.2	11.1	57.3	11.1	22.9	6.7	29.5	7.8	41.2	9.3	32.6	6.8
104.3	12.1	50.3	11.1	29.4	5.3	32.2	8.3	47.5	8.8	24.4	5.4
89.2	10.5	61.7	11	36.7	7.8	35.7	8.7	20	6.9	33.1	6.8
125.5	14.2	41.2	10.7	35.8	8.6	31.5	8.5	41.9	7.8	28	6.7
83.9	12.6	51.6	9.6	36.4	7.4	28.5	8.3	47.8	9	47.8	7.7
72.8	15.6	44.4	11.2	16.5	4.9	37.4	8.9	37.3	8.6	34.3	6.9
82.1	10.5	54.3	10.8	32.8	7.8	27.5	8	30.3	7.5	22.8	5
71.7	10.1	53.6	9.4	22.8	5.8	28.7	8	37.8	7.1	27.7	6.8
99.2	11.1	49.7	11.5	30.7	7	25.8	9	43.1	9.3	33	8
114.8	16	68.9	12.4	28.5	5.8	26.8	7.9	42.8	9.1	32.2	6
93.3	11.9	57.7	10.9	18.3	4	34.5	8.2	44.1	8.9	27	6
121.2	15	56.5	10	19.5	5.2	29.9	8.2	40.4	7.9	19.1	5.7
100.8	10.7	59.6	11.6	34.9	7.1	29.7	8.2	31.7	10.1	31.6	6
126.9	17.4	50.9	11.9	37	7.3	32.1	9.5	66.7	10.2	33.3	7.8
91.8	10.6	53.1	12	30.5	4.7	32.3	8.8	50.7	12.7	30.2	8.7
112.8	13	67.4	12.1	32.8	7.1	25.5	7.2	48.5	8.3	33.6	8.4
124.4	15.3	55.4	12	32.3	6.9	29.2	7.6	57.4	14.2	18.2	6.3
98	11.7	59.2	11.7	26.7	6.2	38.3	9.2	50	13.3	20.9	5.8
72.8	10.9	45.9	10.6	20.2	5	29.4	7.4	47.3	13.4	28.5	6.9
96.3	11.7	50.4	10.7	21.1	5.7	37.8	9.6	47	8.2	31.5	7.6
97.1	12.5	39.3	10.7	29.6	6.2	27.8	8.5	31.2	7.9	22.3	8.3
79.2	9.7	45.7	12.4	22.5	5.5	26.7	7.5	36.5	4.5	29.5	6.2
77.6	9.3	44.9	11	37.3	9.5	31.5	8.4	56.8	11.2	19.1	4.7
110.2	14.9	62.3	10.6	21.3	5.5	33.4	8.9	54.8	10.7	23.1	6.6
99.4	14.5	47	11.4	18.7	5.3	35.2	9.6	60.1	10.8	32.9	6.8
106.9	14.5	38	12	55.1	9.6	28.7	8.1	57.1	10.8	42.4	8.4
98	13.3	59	11.5	33.4	7.7	30.9	8.9	63.5	11	29.2	7.3
116.7	14.1	69.5	11.8	26.9	6.5	33.5	8.7	65.6	12.6	39	7
102.8	13.7	40.1	11.6	25.1	5.3	34.1	8.5	46.4	8.7	18.8	5.3

Table A4. Data for bending tests 100^{o}C -2h

SSL		LVL		OSBH		OSBO		PWH		PWO	
MOR (MPa)	MOE (GPa)	MOR (MPa)	MOE (GPa)	MOR (MPa)	MOE (GPa)	MOR (MPa)	MOE (GPa)	MOR (MPa)	MOE (GPa)	MOR (MPa)	MOE (GPa)
91.2	11.3	53.6	12.5	31.9	5.6	29.7	7.5	42	8.7	22	5.9
121.2	15.5	49.6	13.6	43.3	8.3	34.1	9	51.5	8.8	21.6	7.9
92.8	10.5	44.5	14.4	36.3	7.3	29.4	7.6	33.6	10.2	30.2	5.9
107.6	14	62.4	14.2	23.1	4.7	32.5	8.2	27	7.8	33	7.3
57	10.4	48.7	11.4	46.8	8.8	27.7	7.6	43.6	8.5	22.3	5.8
100.1	12	50.5	14.7	23.4	5.3	38.5	9.9	28.5	8.1	33.3	6.5
121.7	14.9	43.2	13.5	28.5	5.6	34.1	9	46.8	10	34.5	9.1
46.1	9.7	51.2	14.3	27.2	6.4	36.2	8.3	58.4	10.4	25.2	7.8
84.2	11.1	74.1	13.4	27.4	8.6	25.7	7	40.2	9.5	40.3	7
89.1	10.5	43.6	13.3	30.9	7.5	21.4	7.3	50.1	10	44.1	7.6
129.6	15.4	55.6	12.6	34.3	7	36.5	9.4	51.7	14.6	26.3	6
96.4	12.7	58.3	13.1	32.2	7.1	36.9	9.1	27.1	7.4	32.9	6.3
127.5	14.8	77.3	14.2	29.6	6.3	38.4	9.9	27.8	7.8	25.3	6.7
87.8	12.4	57.9	13.1	28.2	6.4	30.8	8.2	43.4	9.8	40.5	7.8
106.9	13.1	61.9	14.5	36.1	8	25.4	8.2	43	8.8	39	8.1
110.2	13.8	71.7	13.3	36.4	9.3	23.1	7.6	57.1	13.4	29.6	7.1
105.9	13.2	62.5	13.4	31.6	6.5	34.5	8.7	33.1	8.5	46.9	7.1
104.5	13	46	13.4	34.4	7.4	31.8	8	19.9	7	29.3	7.6
123.4	16.4	54.6	15.3	29.5	6.1	30.7	6.9	39.2	7.3	35.1	6.7
93.8	13.7	51.2	12.3	28.8	6.5	32.5	8.2	14.6	5.5	18.2	5.4
114.2	14.3	64.3	12.7	35.1	6.1	33.5	9.1	54.8	12.5	15.5	4.5
111.9	12.6	65.5	14.2	24.3	5.5	28.6	7.3	47	11	35.3	6.3
98.7	13.4	41.3	12.8	30	5.7	33.1	8.3	19.7	9	46.2	8.1
99.7	11.7	55.8	12	37.4	7.4	38.5	7.9	42.5	8.7	33.1	6.1
93.5	12.1	59.7	15.1	30.5	5.6	30.4	7.1	28.7	7	33.4	6.7
110	12.3	69.4	14.9	37.3	8.6	30.5	8.2	38	10.8	33.4	8.3
94.4	12	46.8	13.2	32.2	7.1	29.7	9.1	40.7	12.3	26.7	5.6
119.1	14.3	65.7	14.4	28.3	4.8	38.9	9	49.8	10.8	36.6	4.9
122.5	14.1	57.4	13.8	31.5	6.1	25.9	8.3	45.8	9.9	31.3	5.8
100.7	11.4	59.9	14.6	33.2	5.6	30.4	7.9	50	11.2	36.6	7.7
77.4	10.3	63.5	14.5	35.9	6.9	22.1	7.5	54.9	9.5	30.2	7.9
87.4	9.7	57	12.5	35	7.8	42.2	9.3	33.9	10.2	27.8	6.6
110.5	14.5	48.1	12.6	39.9	9.4	30.7	8.8	60.4	10.1	41	7.6
108.1	13.3	71.5	14.4	47.2	9.2	29.9	8.2	56.8	12.1	22.1	4.6
104.4	11.7	54.8	13.7	42	7.8	34.3	7.6	30	10.3	18.6	5.6
108.4	12.7	57	13.4	31.3	5.5	38.3	8.6	49	13.4	27.7	5.8

Table A5. Data for bending tests 200^{o}C -1h

SSL		LVL		OSBH		OSBO		PWH		PWO	
MOR (MPa)	MOE (GPa)	MOR (MPa)	MOE (GPa)	MOR (MPa)	MOE (GPa)	MOR (MPa)	MOE (GPa)	MOR (MPa)	MOE (GPa)	MOR (MPa)	MOE (GPa)
83.4	10.4	51.9	12.6	32.2	7.9	19.9	8.4	32.7	7.7	10.4	4.9
64.2	9.7	60.2	15.8	19.6	5.2	26.1	7.6	22.9	7.5	8.5	4.7
116.1	13.7	43.9	13.8	26.1	8.4	33.7	7.5	40.3	15.2	16.8	4.7
136.1	17.4	44.8	13.3	29.1	8.2	21	7	15.8	9.3	18.9	5.8
60.6	10.3	38.9	12	24.8	7.6	22.5	9	30	8.3	17.7	5.9
81.5	14.2	43.3	12.3	32.5	8.2	27.3	8	21.8	7.4	19.9	6.7
92.7	13.1	46.7	12.7	27.2	7.7	28.7	8.7	22.7	6.9	28.6	7.6
65.2	11.1	37.8	13.2	42	9.8	20	7.4	25.4	8.7	26.2	6.6
76.5	9.7	47.7	13.4	33.7	8	29.7	9	35	9	18.1	4.3
51.5	10.5	61.4	14.4	21.3	6.7	29.6	8	39.1	11.2	22.1	6.6
65.4	11.6	49.2	12.7	28.1	7.1	23.5	8	42.5	11.5	25.1	5.9
124.2	17.9	63.4	16.5	18	6.5	32.6	8.3	45.1	9.9	19.6	6.5
112.1	13.6	46.6	12.3	26.2	6.3	21.1	7.7	37.1	10.4	15.4	5.1
99.1	13.5	36.8	13.1	24.6	4.8	18.2	6	28.2	9	22.1	5.9
61.8	10.4	51.2	13.1	25.6	6.8	34.5	9.1	40.8	11.6	14.8	5.4
74.5	12.2	49.4	12.5	24.5	4.7	24.6	7.8	30.5	7.9	22.1	7.4
49.9	11.4	41.8	14	18.7	4.7	26.9	6.6	33.4	7.3	14.9	4.2
103.4	13.8	39.5	11.9	22.8	5.5	29	7.3	25.5	6.6	20.4	7.2
81.4	10	55.3	13	31.2	6.7	31.6	7	17.1	6.7	14	4.9
49.4	10.6	49.8	13.6	26.6	6.3	25.6	7.2	24.9	8.9	34.9	7
91.8	12.9	49.6	10.6	39.1	9.8	26.6	6.9	14.6	5.9	16.5	6.1
90	12.9	40.1	12.5	16.8	5	30.5	8.5	15.4	8.6	21.5	6.8
81.7	13.5	46.8	13.8	22.6	7.8	26.2	7	14.1	5.4	18.9	5.1
76.2	11.3	72.8	14.6	27.1	7.3	28.5	9	33.8	11.3	20.6	7.9
70.9	11.2	60.7	13.1	34.5	8.6	31.6	7.6	57.9	12.3	23.3	7
106.8	14	44.4	13.9	27.6	7.2	23.1	6.8	35.5	6.2	21.9	7.4
94.6	12.4	55.1	13	29.8	7.4	24	7.3	37	8.9	20.6	5.8
87.6	12.6	65	14.2	31.3	6.9	26.6	8	30.7	10.9	17.4	6.5
102.9	14.2	47.2	13.4	26.2	6.5	30.8	7.9	43.8	12.4	27.5	6.1
71.4	9.6	53.8	12.3	19.3	6.3	38.1	10.4	33.1	9	21.1	7.1
73	11.6	59.2	12.8	30.9	6.9	29	7.1	29.6	9.6	30.1	7.7
93.4	13.7	65.4	13.5	16.3	5.6	24.6	7.2	44.6	10.1	30	7
54.9	7.7	49.2	12.3	29.2	5.7	31.7	7.4	22.9	7.3	22.2	6.6
82.9	11.7	46.1	12.6	17.6	5.3	26.7	7.3	39.8	13.9	25.4	7.7
90.1	15.1	55.9	13.8	17.4	4.9	24.1	7.1	27.5	7.7	17.1	5.3
104.4	14	48.8	11.8	32.9	9	28.4	8.6	39.2	9.6	26.2	7.6

Table A6. Data for bending tests 200^{o}C -2h

SSL		LVL		OSBH		OSBO		PWH		PWO	
MOR (MPa)	MOE (GPa)	MOR (MPa)	MOE (GPa)	MOR (MPa)	MOE (GPa)	MOR (MPa)	MOE (GPa)	MOR (MPa)	MOE (GPa)	MOR (MPa)	MOE (GPa)
68.1	14.1	37	11.8	22.9	5.3	22	7.6	16.2	5.3	17	6.9
114	16.6	42.2	12.2	15.6	2.8	26.2	7.7	17.8	5.9	22.7	5.5
93.5	11.7	37.6	12.3	21.5	5.6	29.4	10.1	26.7	8.3	17.8	5.8
95.4	11	53.5	11.7	24.1	7	27	7.8	22.6	6.7	16.8	5.3
84.9	14	45.8	11.8	19.1	4.8	24.3	7.8	15.3	6.3	25.8	8.4
59	8.5	56	11.8	29.2	8.2	5.8	6.9	15.7	2.6	15.6	5
102	15.4	34.1	10.9	14.6	3.5	31.1	8.6	21.7	6.3	24.2	8.1
120	14.9	42.2	11.9	11.6	6.8	26.8	8.2	21.8	8.2	18.4	6.8
72.4	14.3	41.8	12	19.8	7.3	29	7	17.6	5.6	20.6	6.4
81.2	11	42.1	14.6	27.3	9.2	20.6	7.6	19.3	7.9	26.2	6
81.1	16	37.1	11.8	19.2	6.4	25.8	6.9	12.4	5	27.6	5.7
47	9.7	50.1	12.9	18.6	5.9	22.6	7.9	16.3	6.8	14.3	5.6
75.4	11.1	52.2	12.6	16.4	5.6	25.5	8.4	23.9	7.8	14.9	4.5
88.2	12	39.1	12.5	27.9	7.3	17.6	7.2	21	7	16.5	6.4
57.9	9.9	33	12.8	16.3	4.8	22.1	7.5	32.7	9	18.2	4.8
96.7	12.5	55.5	11.7	23.3	6.5	21.8	7.8	31.8	8.6	17.5	5.3
64.4	10.7	38.7	12.1	35	8.8	27.5	8.3	19.2	7	28.8	7
67.6	11	41.9	13.9	36.3	8.6	25	7.3	18.7	9.6	18.9	6.9
68.8	15.8	42.6	12.3	18.3	6.5	29.8	7.5	12.5	2.7	15.5	6
43.2	8.9	36.7	12.1	19.1	6.8	28.8	7.9	17.1	4.9	17.4	5
117	14.2	35.9	11.9	21.7	5.7	37.4	9	13.4		16.9	5.9
85.5	12.9	33	12.4	17.1	5.9	28.6	9.1	13.1	3.8	14	5.3
49.7	10.8	32.9	11.5	31.2	9.8	20.9	7.7	7		19.8	5.8
56.6	9.7	39	12.2	18.1	5.4	28.6	7.7	8.9	0.6	18.4	5.4
59.8	10	48.2	12.8	17.6	5.5	29.9	7.4	9.4		15.2	6.8
58.4	11	33.7	12.6	35	9.5	28.4	7.9	19	6.6	13.6	6.4
68.3	10.3	46.7	12.2	23	6.5	1.8	0.1	17.6	6.4	13.4	6.6
88.1	11.2	36.1	11.4	13	3.7	1.7	2.2	24.2		13.3	7
87.7	13.2	40.9	13.1	13.5	3.5	19.1	7	21	3.6	12.2	6.6
95.4	13.2	36.4	13	23.7	6.5	37.4	10.2	29.8	7.7	11.7	5.2
62.1	10.5	46.7	12.5	24.4	7.3	29.9	8.6	16.8	8.1	8.2	4.6
101	14.4	54.4	13	21.5	7.9	25.8	7.3	20.7	7.7	15.4	6.1
84.5	12.5	41.8	11.8	22.4	5	23.9	6.4	18.4		22.5	6.4
57.2	9.5	37.9	12.1	16.1	5.1	Burnt	Burnt	19	7.8	19	7.5
75.6	12.4	39.4	12.3	15.9	5.9	Burnt	Burnt	9.8		23.6	6
115	14.8	50.7	13.4	16.7	5.9			8.8		23.6	7.4

Appendix B

This appendix is a compilation of load deflection diagram and tables representing MOE and MOR for OSBH and PWH for manuscript 2 (chapter 3).

Table B1. Test Matrix for Chapter 3 (manuscript 2)

Temperature (^{o}C) / Time (hours)	50	75	100	125	150	175	183	191	200	TOTAL
1	8	8	8	8	8	8	8	8	8	72
2	8	8	8	8	8	8	8	8	8	72
3	8	8	8	8	8	8	8	8	8	72
4	8	8	8	8	8	8	8	8	8	72
5	8	8	8	8	8	8	8	8	8	72
6	8	8	8	8	8	8	8	8	8	72
7	8	8	8	8	8	8	8	8	8	72
8	8	8	8	8	8	8	8	8	8	72
Total	64	64	64	64	64	64	64	64	64	**576**

Load Deflection Diagrams

Each of te following figure is a compilation of 8 different graphs from ‘a’ to ‘h’ representing 1hr through 8 hr exposure time at a temperature. For 200oC figures some off the graphs are missing because the sample caught on fire and hence the strength could not be determined. The ranges in the axes are slightly different for both the materials. Each graph has 8 load deflection diagrams representing one cell of the above matrix (Table B1).

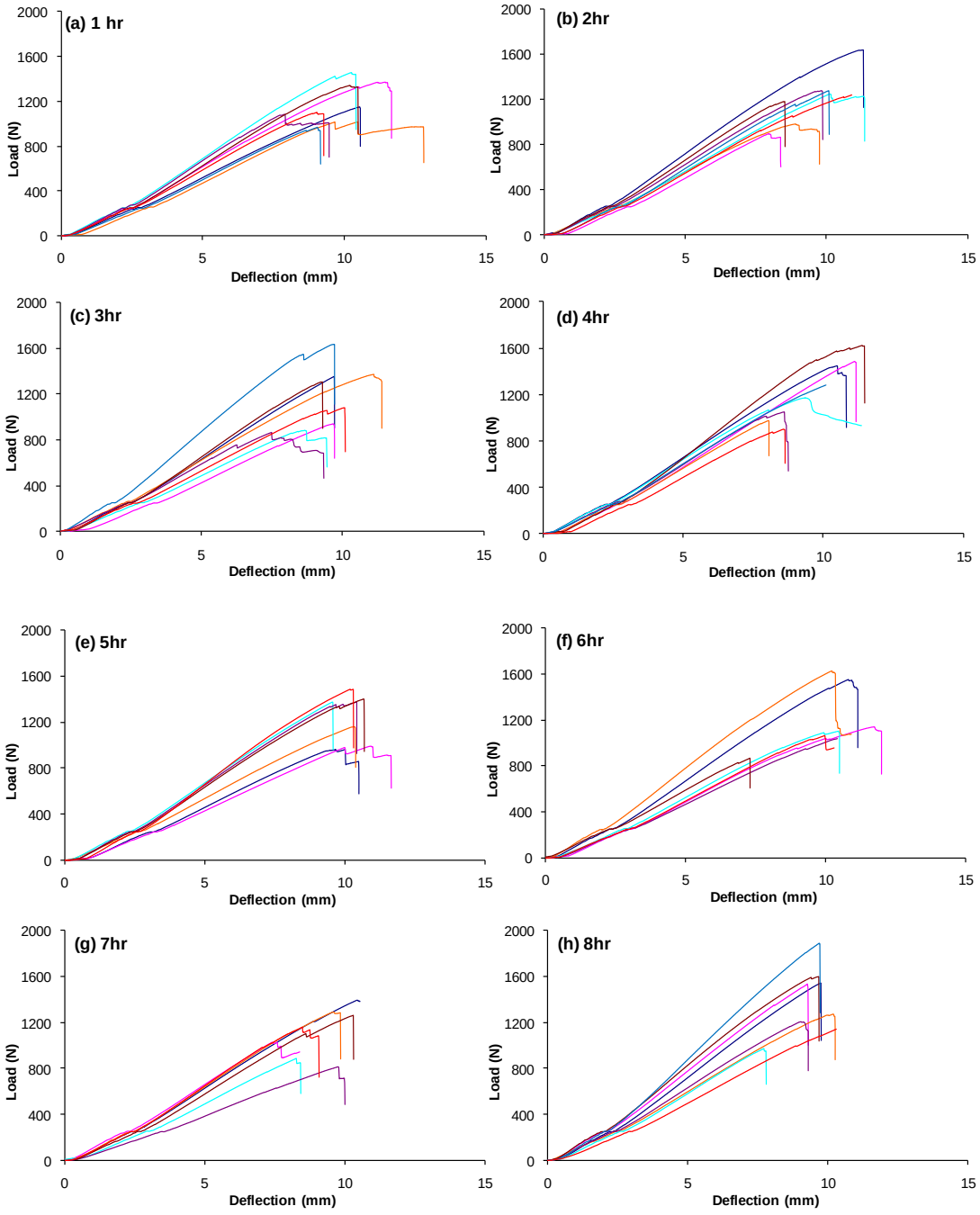

Fig. B1. Load deflection curves for OSBH at 50^{o}C

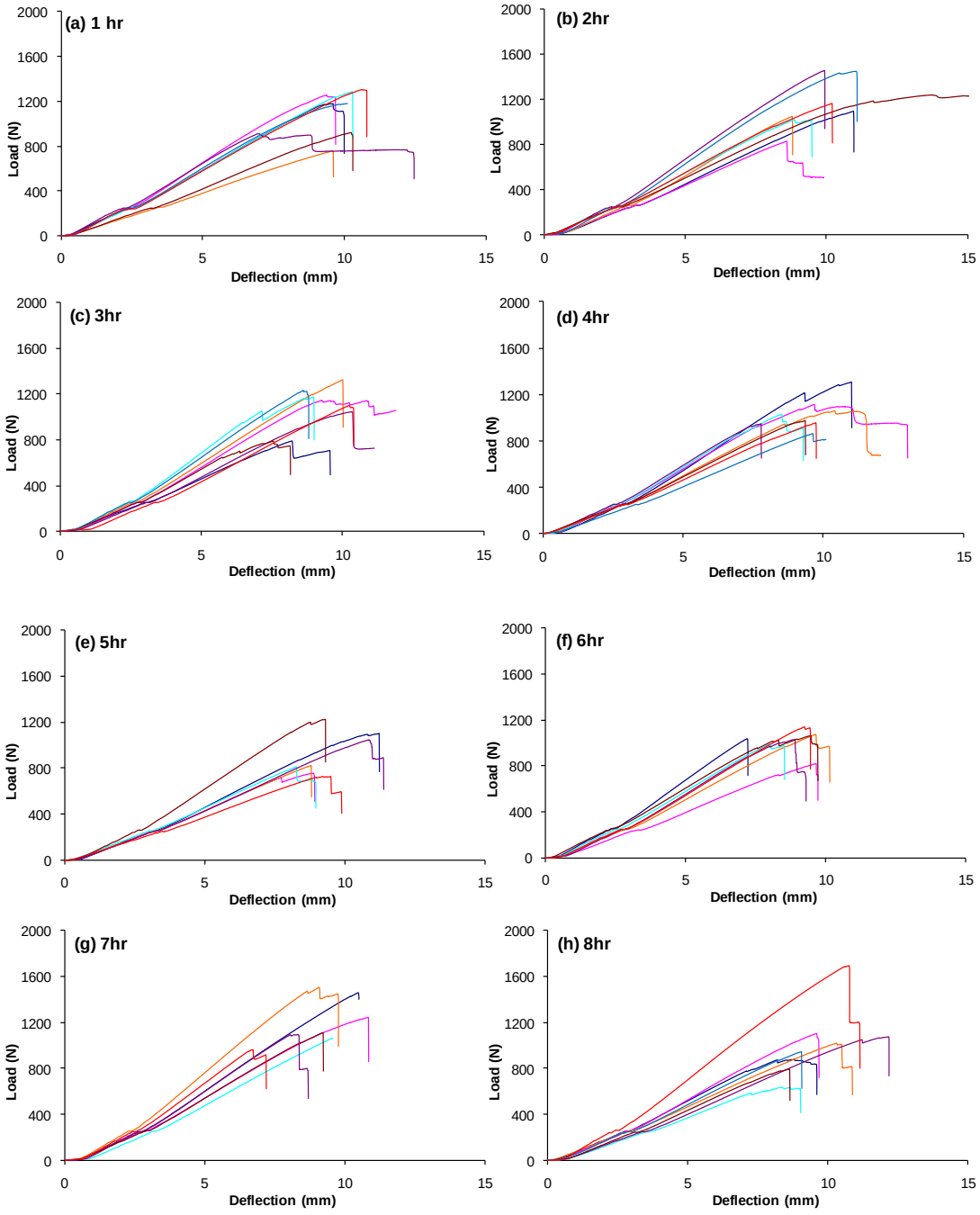

Fig. B2. Load deflection curves for OSBH at 75^{o}C

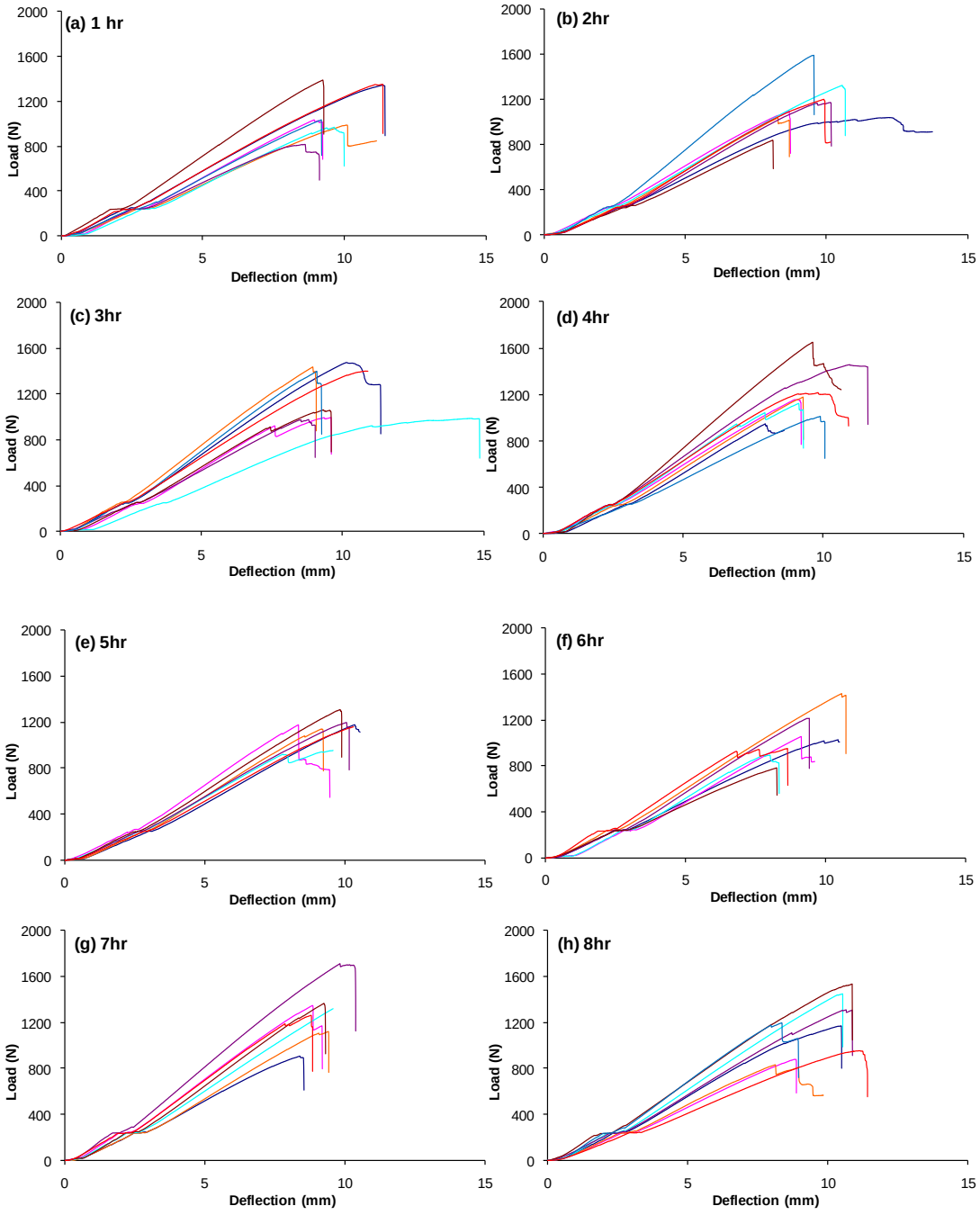

Fig. B3. Load deflection curves for OSBH at 100^{o}C

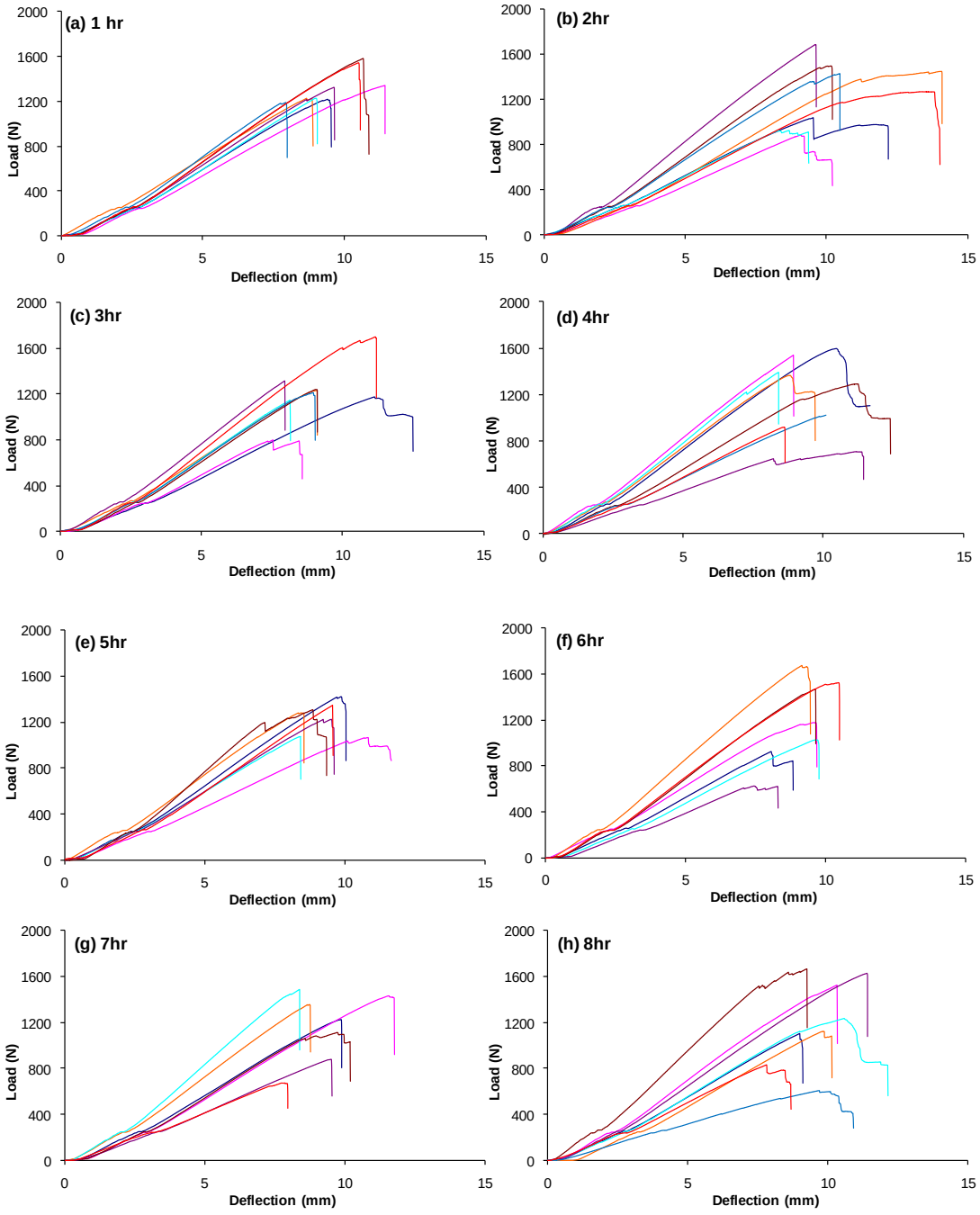

Fig. B4. Load deflection curves for OSBH at 125^{o}C

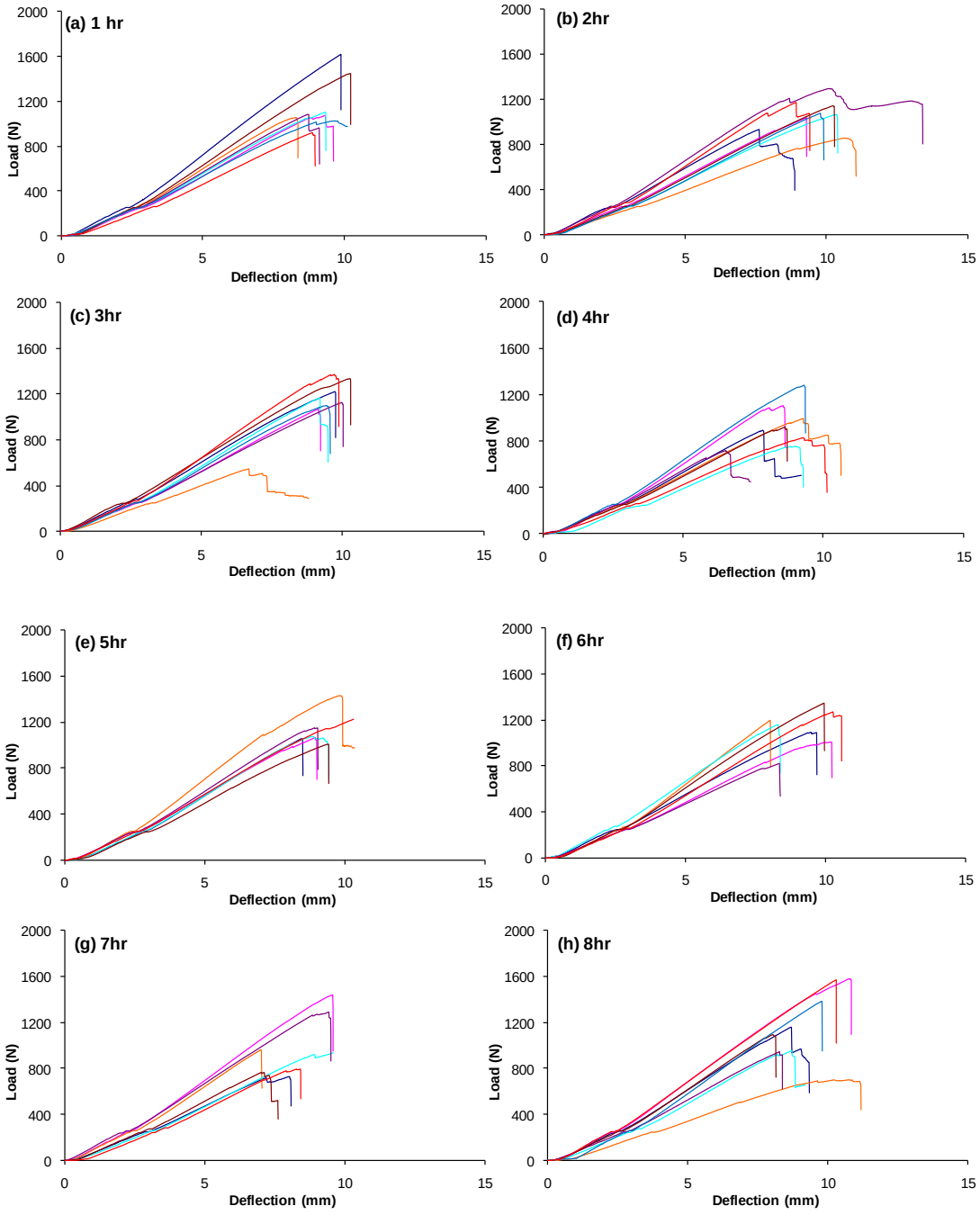

Fig. B5. Load deflection curves for OSBH at 150^{o}C

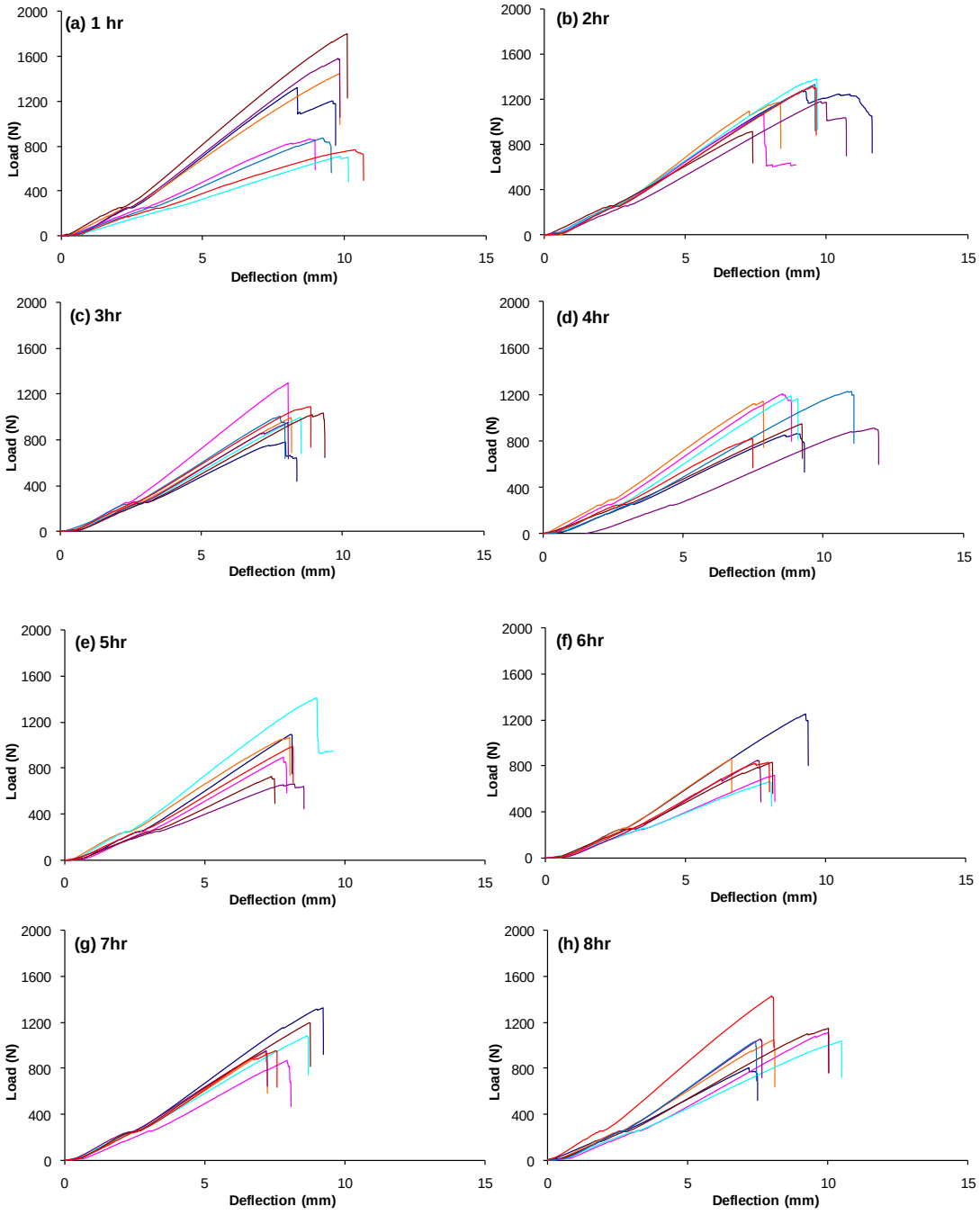

Fig. B6. Load deflection curves for OSBH at 175^{o}C

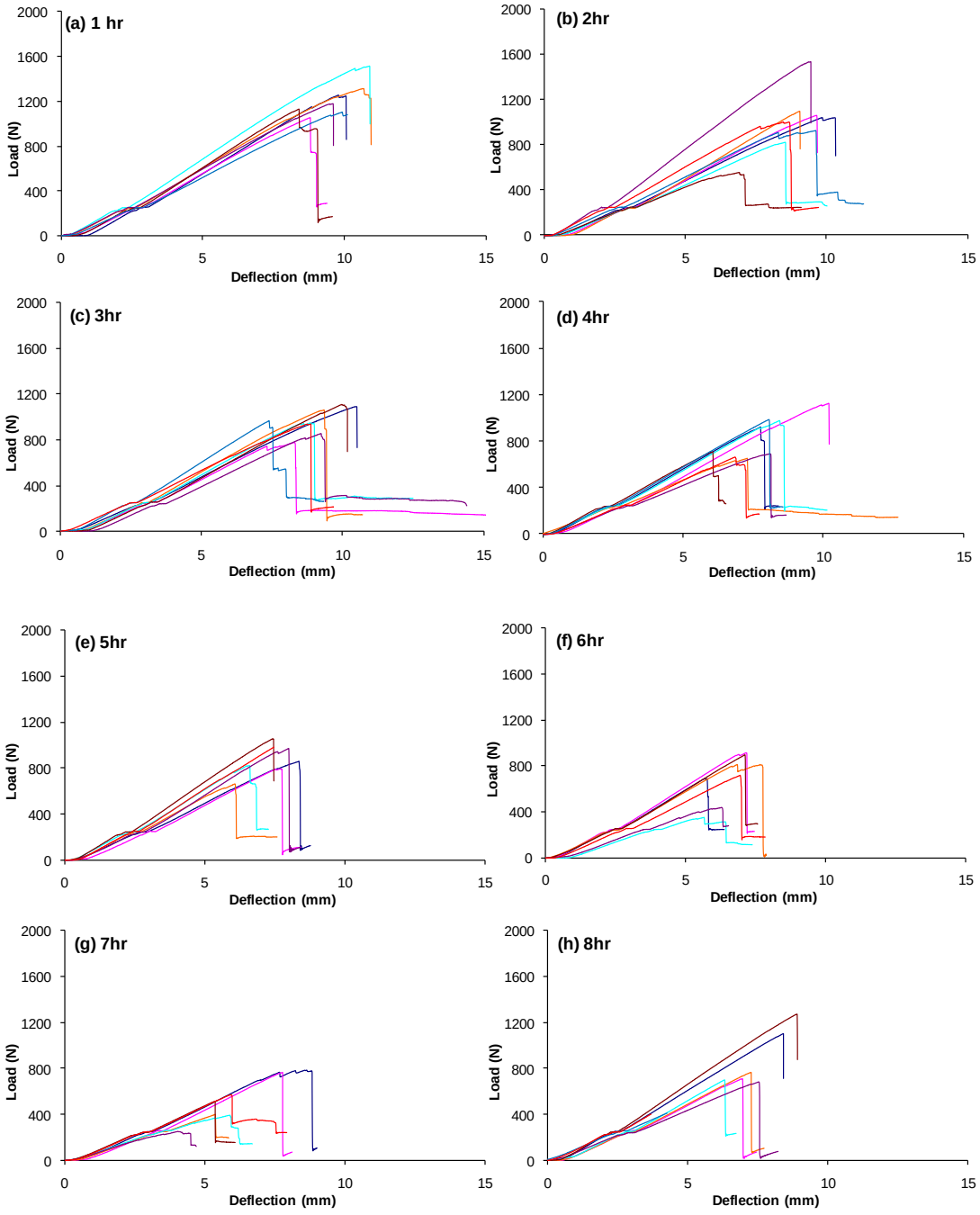

Fig. B7. Load deflection curves for OSBH at 183^{o}C

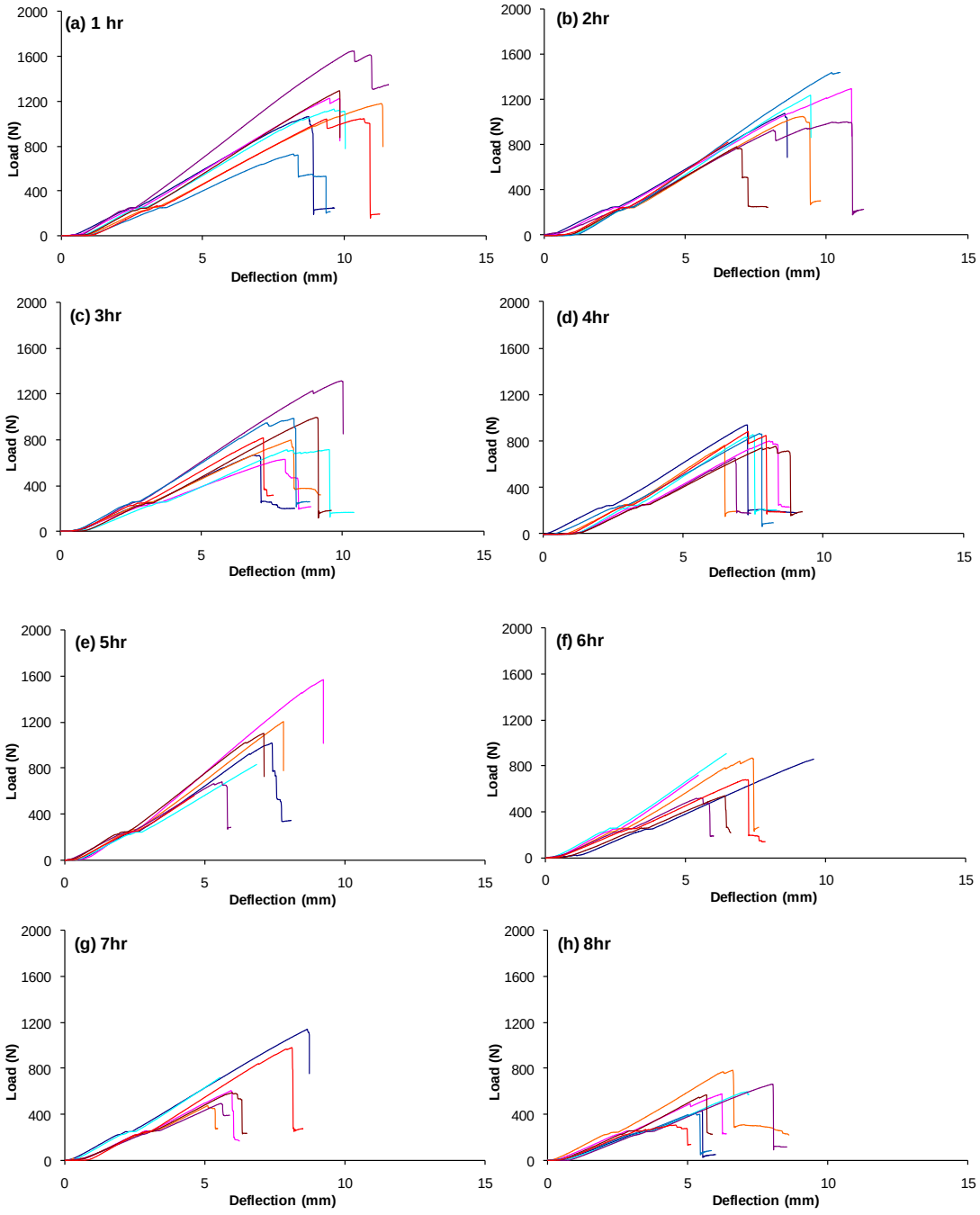

Fig. B8. Load deflection curves for OSBH at 191^{o}C

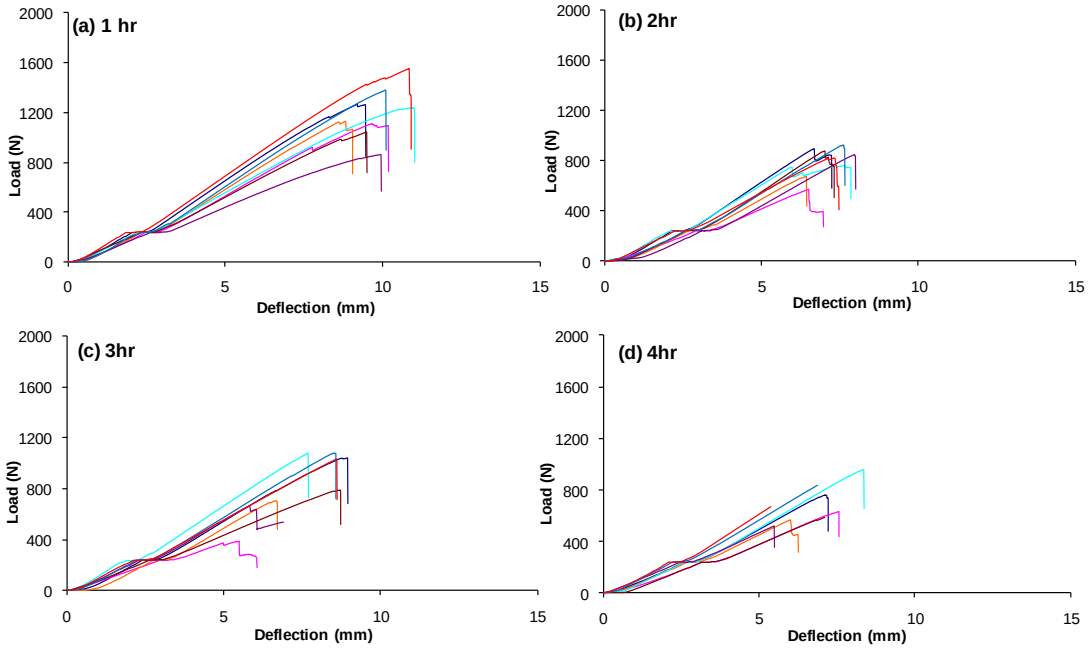

Fig. B9. Load deflection curves for OSBH at 200^{o}C

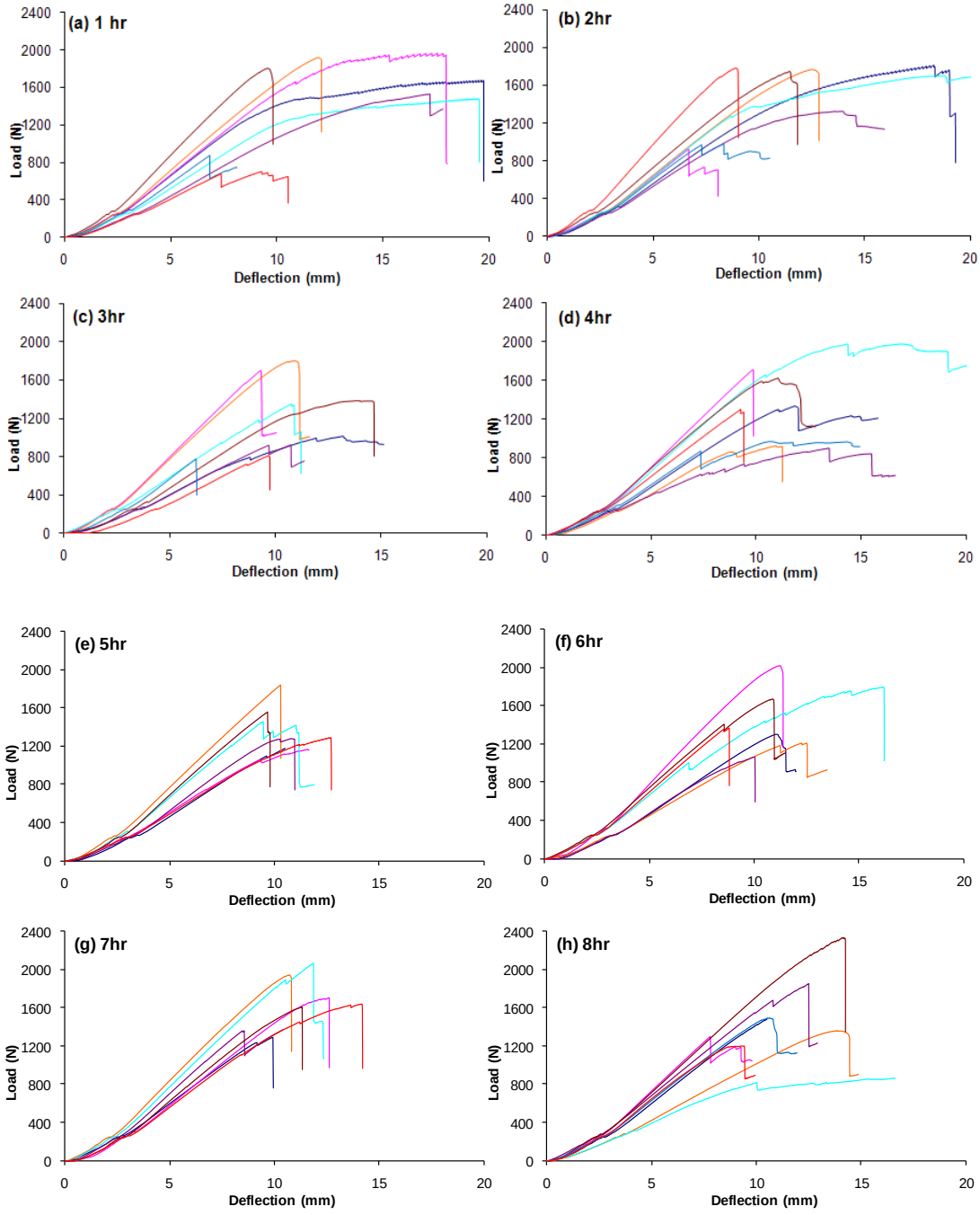

Fig. B10. Load deflection curves for PWH at 50^{o}C

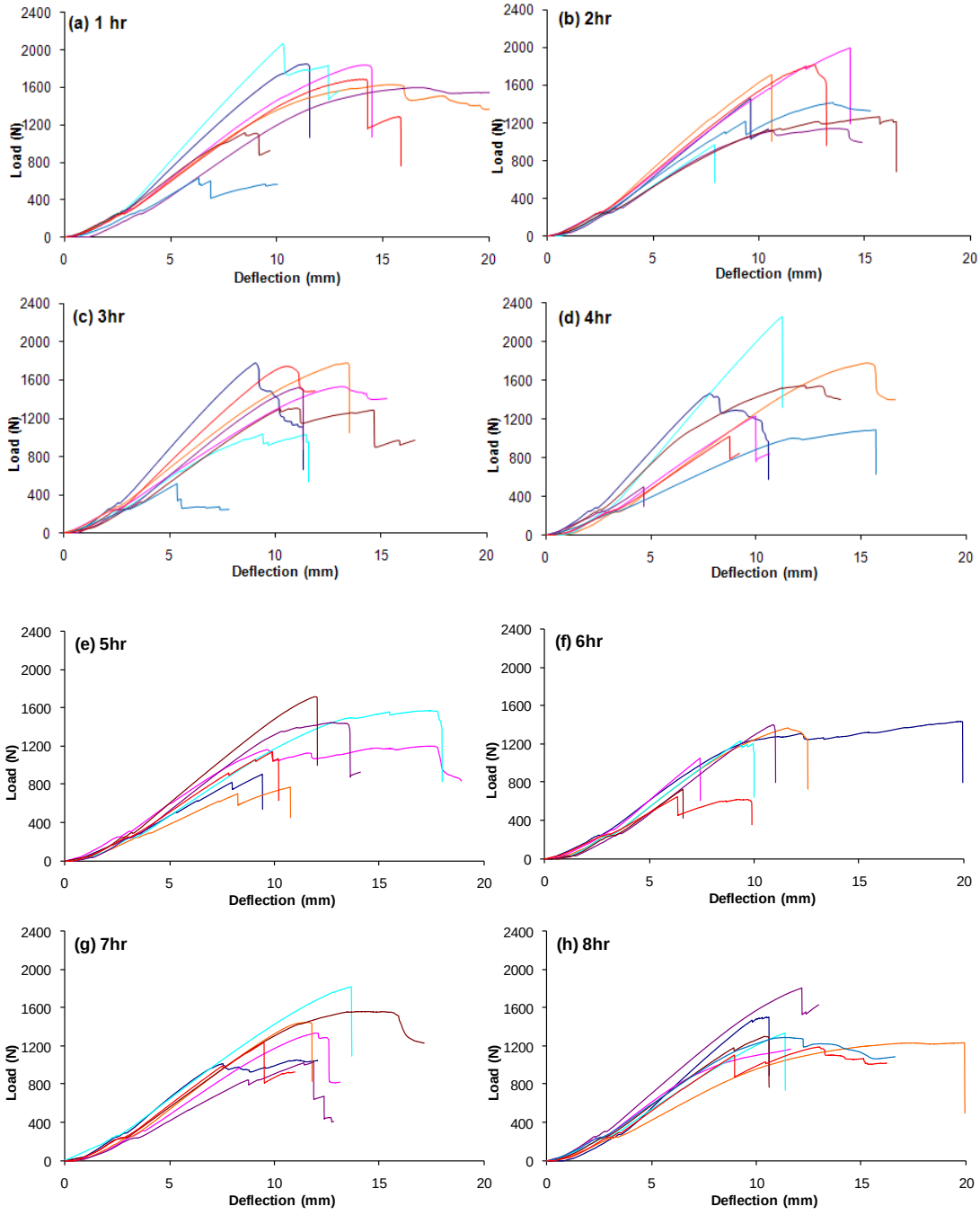

Fig. B11. Load deflection curves for PWH at 75^{o}C

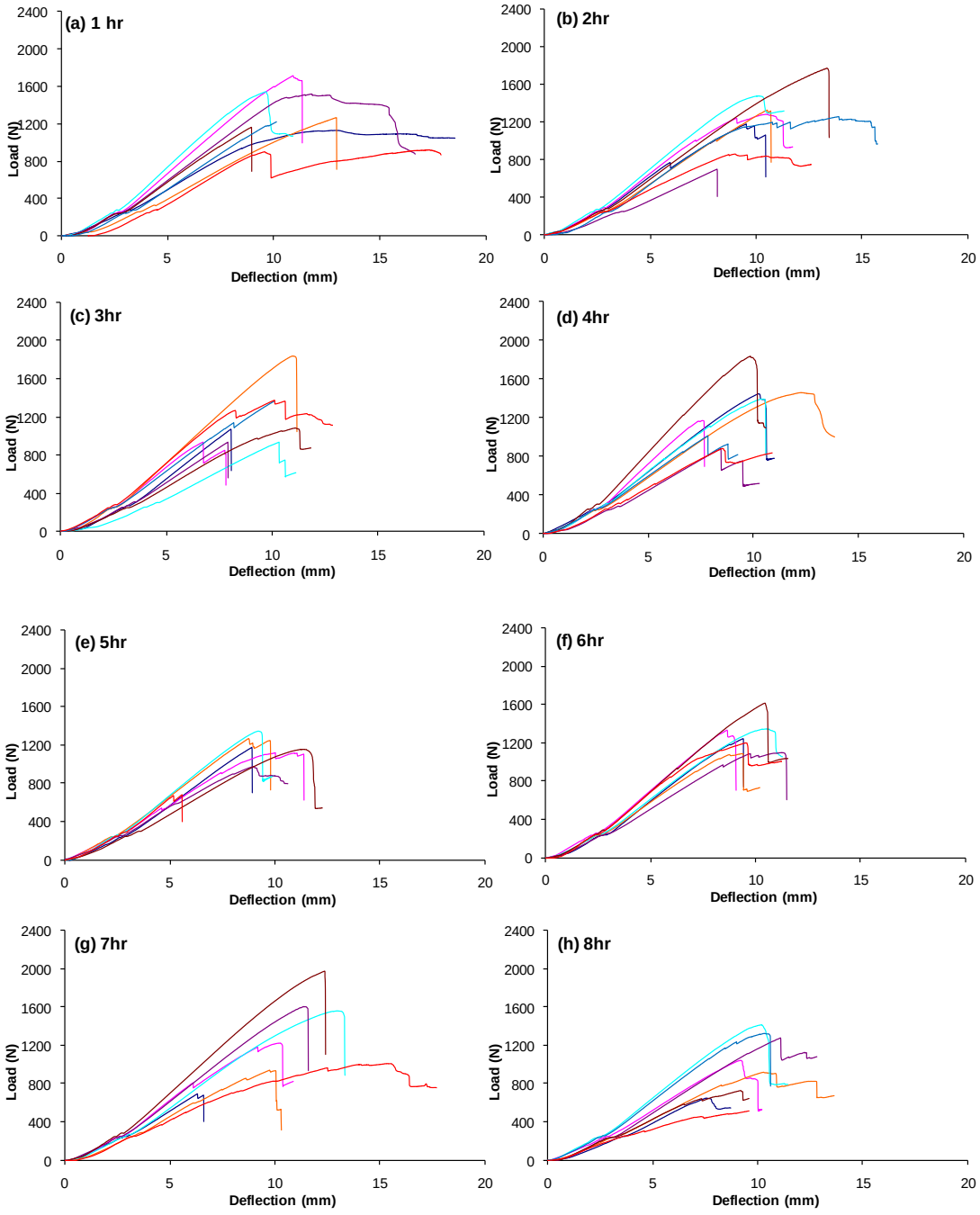

Fig. B12. Load deflection curves for PWH at 100^{o}C

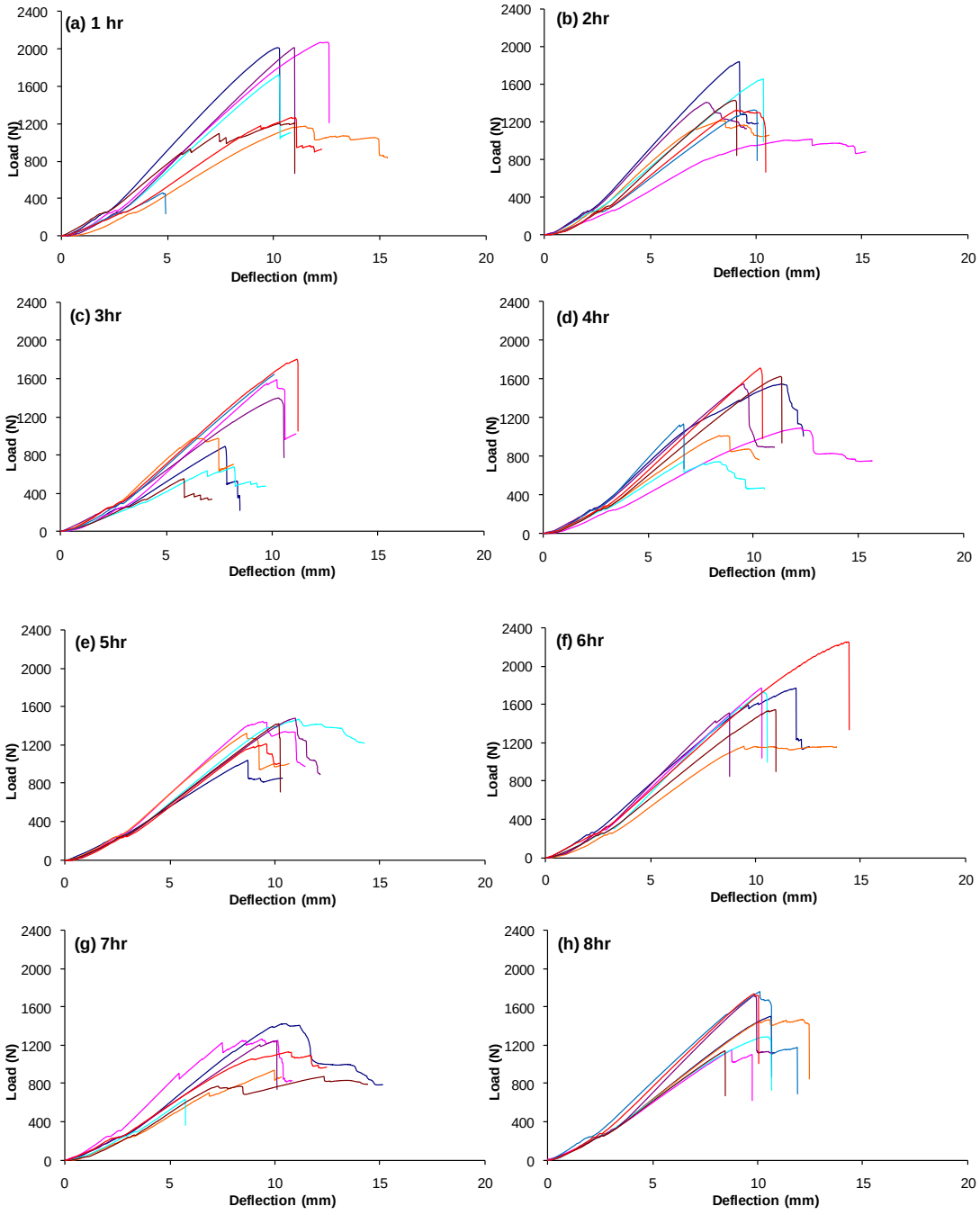

Fig. B13. Load deflection curves for PWH at 125^{o}C

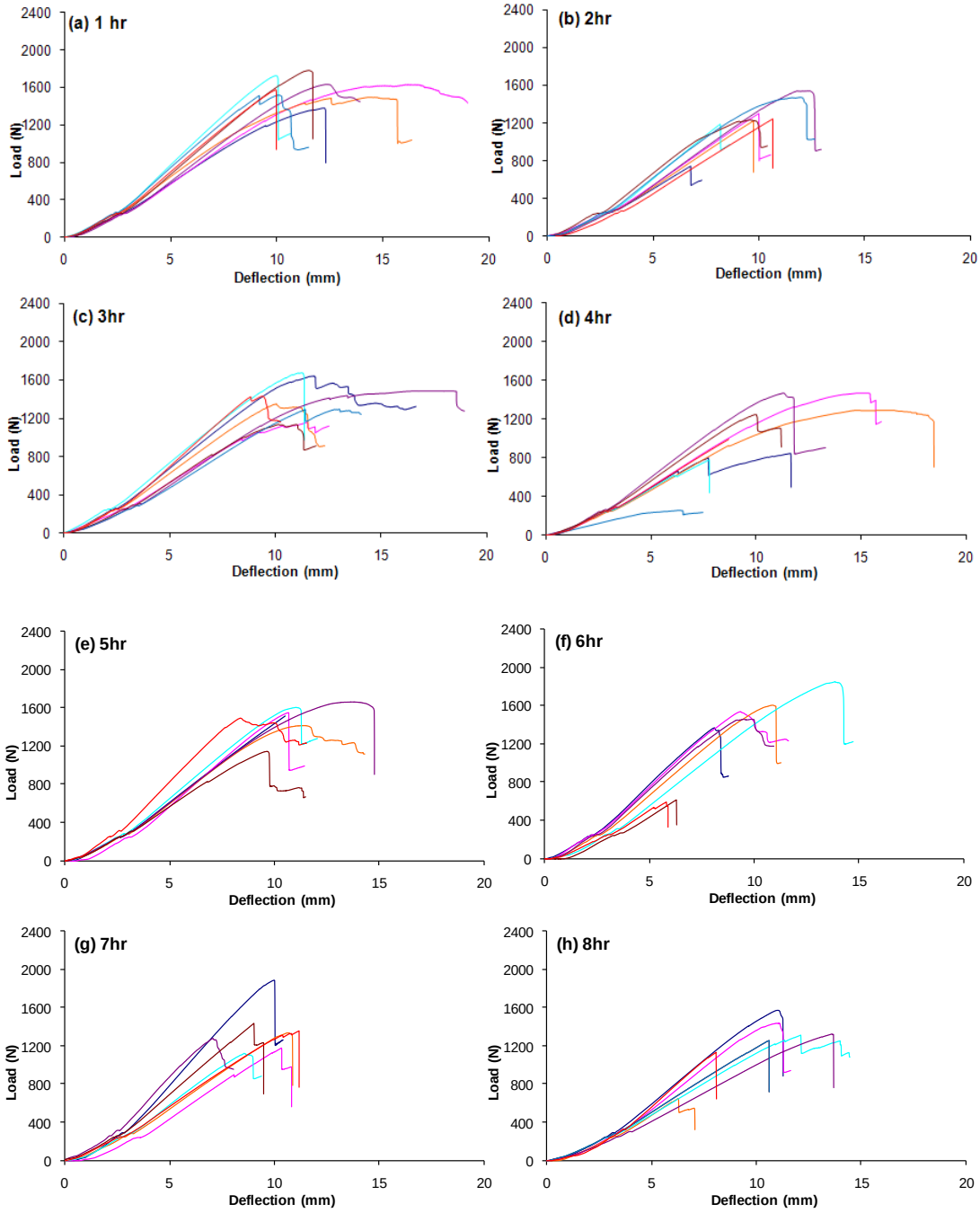

Fig. B14. Load deflection curves for PWH at 150^{o}C

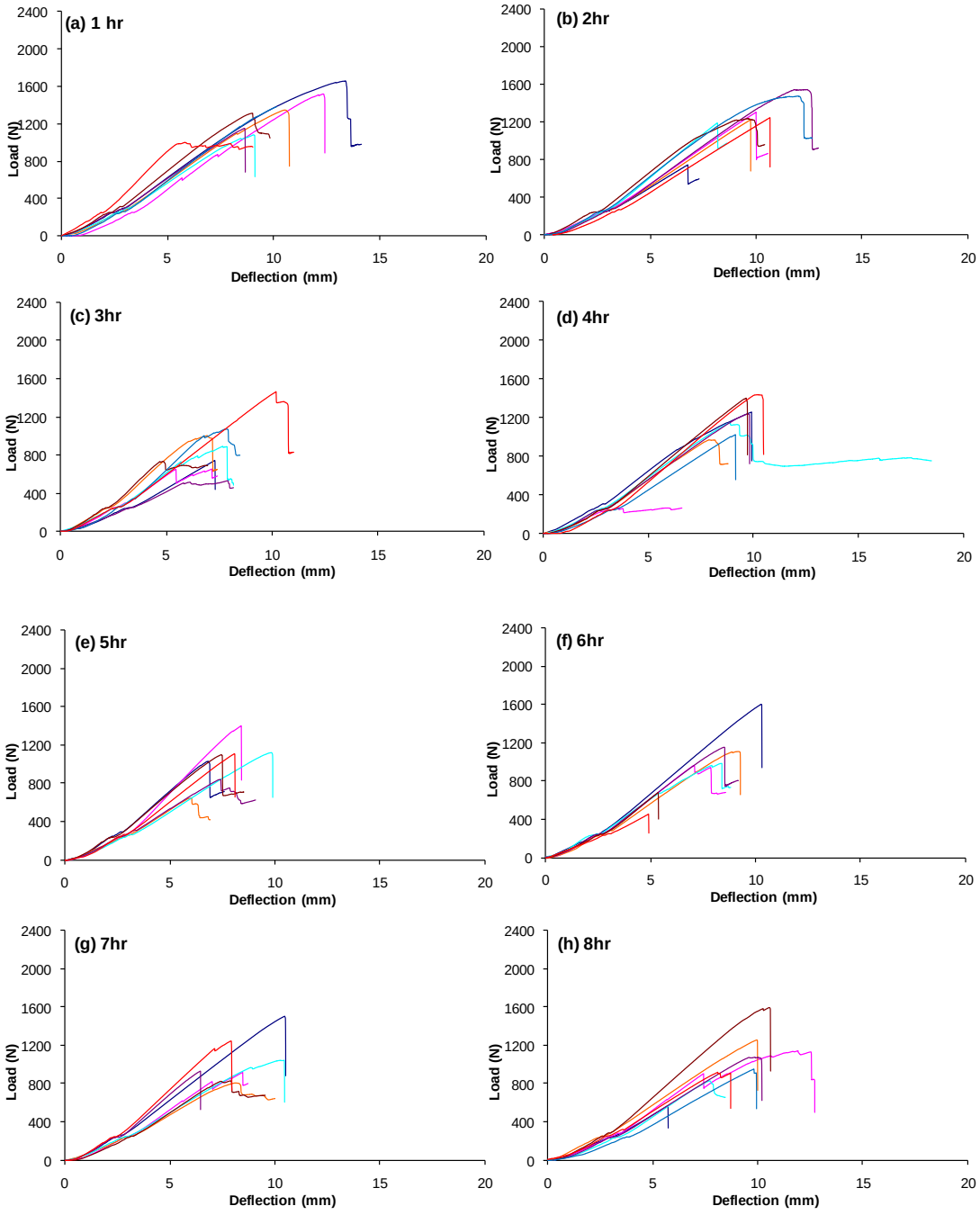

Fig. B15. Load deflection curves for PWH at 175^{o}C

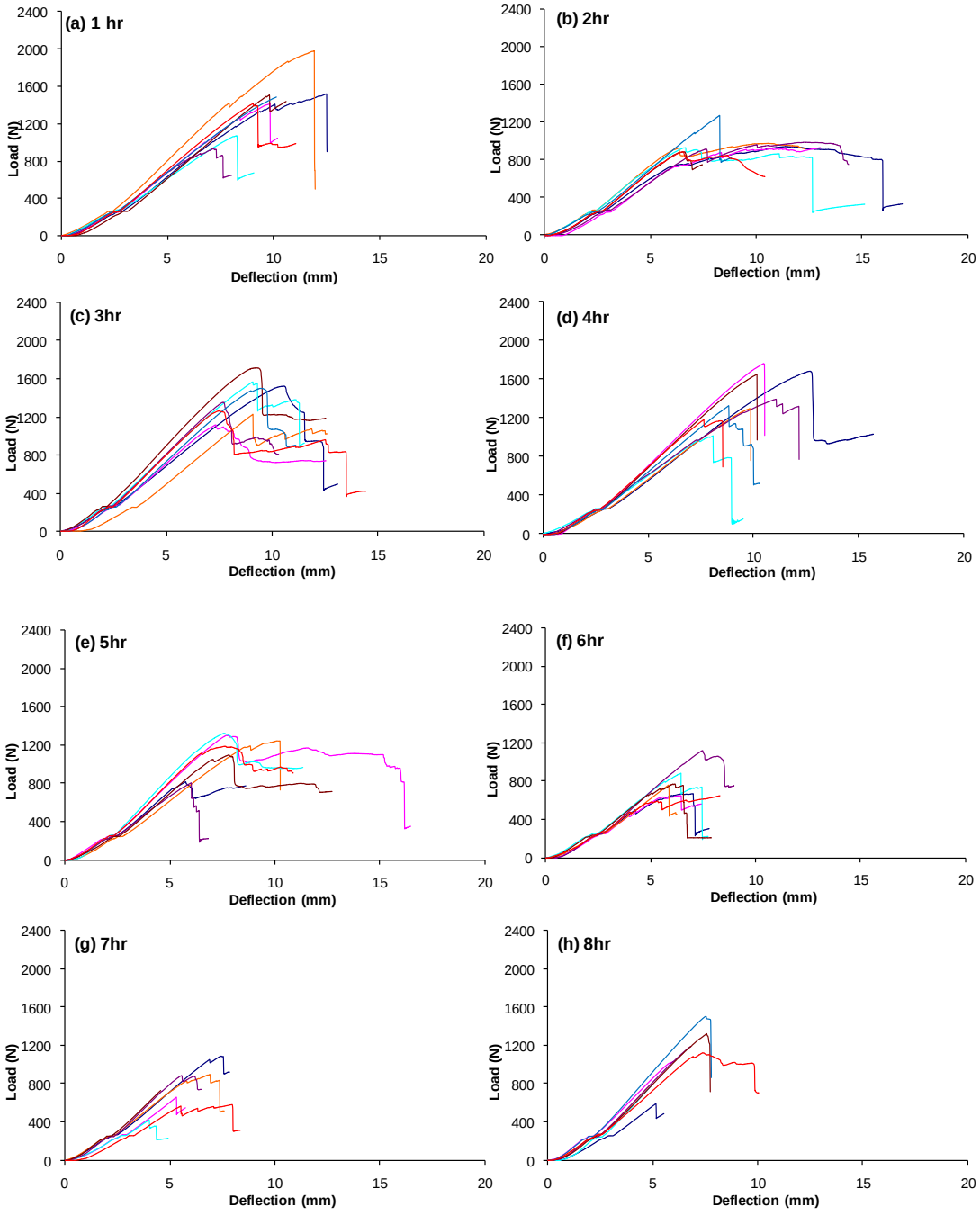

Fig. B16. Load deflection curves for PWH at 183^{o}C

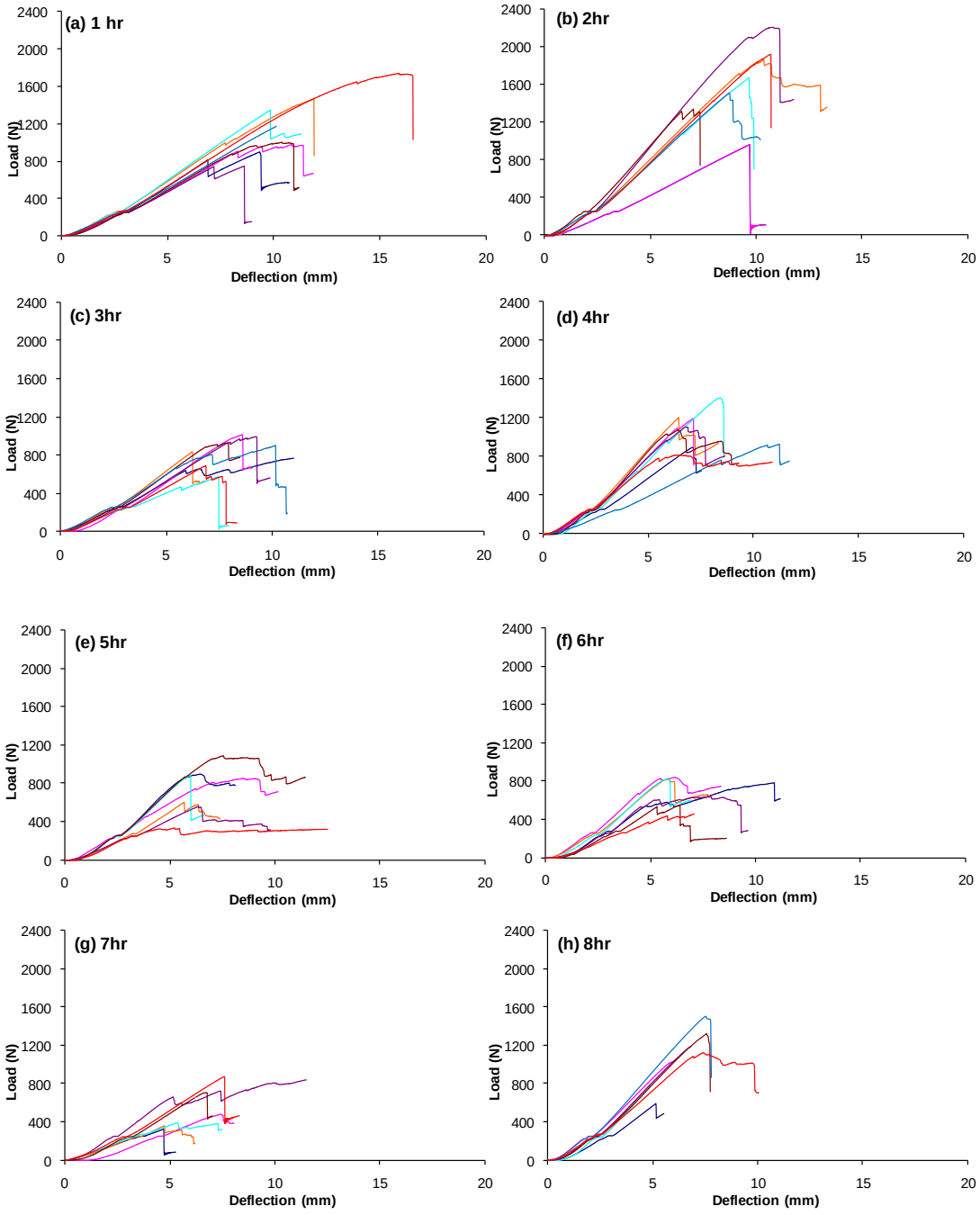

Fig. B17. Load deflection curves for PWH at 191^{o}C

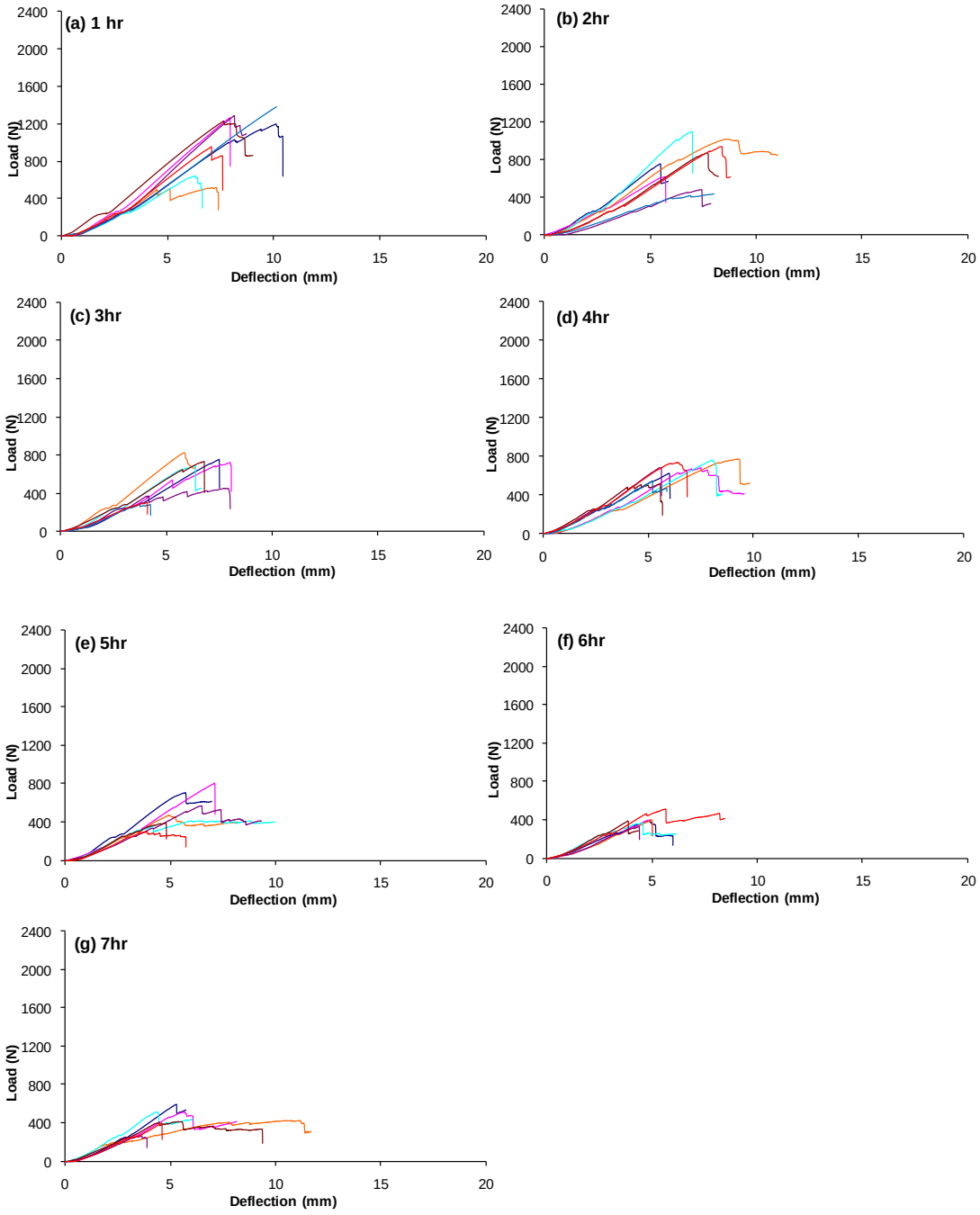

Fig. B18. Load deflection curves for PWH at 200^{o}C

Table B2. 50°C Bending Data

	Plywood		OSB			Plywood		OSB	
t	MOR	MOE	MOR	MOE	t	MOR	MOE	MOR	MOE
(hr)	(MPa)	(GPa)	(MPa)	(GPa)	(hr)	(MPa)	(GPa)	(MPa)	(GPa)
1	52.9	10.1	32.6	5.8	5	39.9	7.8	27.3	6.0
	61.7	10.1	38.6	7.3		37.0	8.0	28.0	5.2
	60.1	10.0	28.7	5.8		57.8	11.7	32.7	5.7
	46.4	7.7	41.3	8.5		45.5	10.4	38.8	7.2
	48.1	7.7	30.5	7.7		40.1	9.6	38.9	8.0
	56.5	13.0	37.9	7.5		48.6	10.8	39.6	8.3
	27.4	8.2	27.3	5.9		41.6	8.5	47.0	9.7
	21.9	6.6	31.2	6.5		40.3	7.6	42.0	8.4
2	57	8.7	46.3	8.6	6	40.8	8.0	43.9	8.4
	29.1	9.2	25.4	7.0		63.1	13.1	32.1	6.5
	55.3	10.2	27.7	6.4		38.1	7.0	46.1	9.4
	53.2	10.3	35.2	6.9		56.2	10.1	31.1	6.3
	41.6	7.6	36.1	7.6		33.3	8.4	31.0	5.4
	54.7	10.3	33.4	7.6		52.4	10.9	24.5	6.5
	30.9	9.4	36.1	7.8		19.0	8.1	24.8	6.5
	55.8	14.5	35.1	7.2		42.7	9.9	30.1	5.9
3	31.7	6.4	38.2	8.3	7	40.3	9.2	39.3	8.0
	53.4	11.8	26.4	5.5		53.3	10.4	29.0	7.3
	56.3	11.4	38.6	7.0		60.6	12.3	36.3	7.8
	42.5	8.2	25.0	6.1		64.7	11.7	25.0	6.2
	28.9	6.8	24.3	6.4		50.0	11.1	23.0	4.6
	43.5	8.4	36.8	8.5		50.3	10.1	35.6	7.0
	24.5	10.0	46.0	9.6		85.4	14.4	34.2	7.5
	25.4	5.4	30.5	6.6		51.3	9.4	32.6	8.3
4	41.8	8.1	40.9	7.8	8	46.8	9.2	43.6	9.7
	53.8	11.6	42.1	7.4		40.7	12.0	43.3	8.8
	28.9	7.4	27.5	6.8		42.4	6.4	35.8	6.6
	61.9	10.9	33.0	6.8		31.3	6.1	27.4	7.4
	28.2	6.1	29.7	7.4		57.9	9.6	33.9	7.3
	51.1	10.8	45.8	9.3		73.0	10.8	45.1	9.4
	30.3	8.2	38.3	7.3		46.7	10.2	53.3	11.3
	40.9	9.9	25.5	6.6		37.6	9.7	33.9	6.0

Table B3. 75°C Bending Data

	Plywood		OSB			Plywood		OSB	
t (hr)	MOR (MPa)	MOE (GPa)	MOR (MPa)	MOE (GPa)	t (hr)	MOR (MPa)	MOE (GPa)	MOR (MPa)	MOE (GPa)
1	57.9	12.4	33.3	6.8	5	28.5	7.8	31.2	5.9
	57.7	9.8	35.4	8		37.5	6	21.3	4.9
	51.3	9.6	21.3	3.6		24.3	5.1	23.3	4.7
	64.8	14.3	36.2	7.3		49.3	7.7	23	5.6
	50.2	8.3	25.6	7.5		45.3	9.4	29.4	5.1
	35.1	10	26.1	4.8		53.8	9.8	34.5	7.1
	19.7	7.3	33.5	7.3		42.5	8.9	27.8	6.3
	52.8	9.6	36.9	7		35.7	7.7	20.6	4.3
2	45.9	11.1	31	5.8	6	45.3	8.4	29.3	7.4
	62.5	10.2	23.5	5.5		32.9	10.7	23.2	4.9
	53.6	11.1	29.6	6.6		43	9.9	30.2	6.5
	35.8	8.2	28.8	5.9		38.5	9.3	27.9	6.8
	30.6	8.5	41.2	8.4		43.8	10.3	29.1	7.1
	39.8	7.5	34.9	5.9		22.6	9.1	30.1	6.7
	44.3	9.2	40.8	7.8		25.3	9	35.2	6.9
	56.8	10.5	32.9	6.6		20.3	7.3	32.2	7.4
3	55.8	13.5	22.3	5.3	7	32.8	10.1	41.1	8
	48.2	8.2	32.2	7.3		41.8	8.1	35.1	6.9
	55.8	9.6	37.3	7.6		45.2	9.5	42.6	9.9
	32.4	7.9	33.1	8.6		57	8.9	32.1	6.7
	47.6	9.5	29.4	6.3		32.3	7.1	30.9	8.2
	40.8	9.5	22.4	6.8		48.9	8.3	31.3	6.2
	16.2	6.7	34.6	8.5		47.3	8.9	38	7.5
	54.8	12.1	30.9	6.2		38.7	9.4	27.2	8.6
4	45.9	13	37.1	7.2	8	46.9	11.3	24.7	6.2
	38.6	8.4	31.5	6.7		41.4	8.5	31	7
	55.9	8.7	29.8	5.6		39.2	6.3	28.8	5.2
	70.7	13.4	29	7.1		41.9	7.9	17.9	5
	48.5	11.5	26.8	7.1		56.5	10.1	30.4	4.9
	15.8	9.7	27.5	6.7		40.7	9.4	22.4	5.4
	34.2	5	26.2	4.8		40.2	8.5	26.6	5.7
	32.1	7.8	27.1	5.5		37.1	9.1	47.7	9.2

Table B4. 100°C Bending Data

	Plywood		OSB			Plywood		OSB	
t (hr)	MOR (MPa)	MOE (GPa)	MOR (MPa)	MOE (GPa)	t (hr)	MOR (MPa)	MOE (GPa)	MOR (MPa)	MOE (GPa)
1	35.4	7.5	37.9	6.4	5	36.8	9	33.3	6.1
	53.7	10.8	29.3	6.5		35.2	8.1	33.3	7.9
	39.5	7.3	27.9	5.8		39.6	9	32.2	7.3
	48.4	12.2	27.3	6.1		42	10	28.2	6
	47.5	8.9	23	5.9		30.6	6.6	33.6	7.1
	36.3	9.2	39.4	8		36.2	6.6	36.9	7.4
	41.8	8.6	29.3	6		49.9	11.1	26.4	7.1
	28.9	7	38.2	6.6		21.3	9.8	33.5	5.8
2	37	9.3	29.5	6.3	6	38.9	9.5	29.1	5.9
	40.3	9.2	30.9	6.9		41.7	10.2	29.7	7.1
	41.6	8.7	29.4	7		34	9.6	40.4	7.3
	46.2	10.6	37.3	6.9		42	9	25.2	7
	22	5.9	33.2	7		34.5	7.3	34.2	7.3
	55.4	8.7	23.8	5.9		50.6	10.8	22	5.5
	39.3	9.7	45	9.7		41.4	10.2	39.7	7.3
	26.9	6.3	33.9	7.4		37.5	9.2	26.9	6.9
3	33.5	9.7	41.6	8.6	7	21.8	7.3	25.7	6.3
	29.3	9.6	28.1	7		38.3	9.3	38	9.4
	57.6	11.1	40.5	8.4		29.4	7.1	31.7	7.9
	29.2	6.4	27.9	5.1		48.8	9.3	43.3	7.7
	29.4	8.7	27.6	6.7		50.3	9.9	48.4	9.5
	34	6.9	29.9	7.2		61.7	11.3	38.4	8.8
	45.9	9.5	39.4	8.6		50.8	11.4	20.5	4.9
	43	11.3	39.6	7.5		31.5	6.7	35.7	8.2
4	45.3	9.1	26.8	7.2	8	20.3	7	33	6.5
	36.7	11.9	32.7	7.2		32.8	7.9	24.7	5.2
	45.6	7.9	33.2	7.4		28.8	6.6	23.3	6
	43.7	10	34.4	7.3		44.2	10.3	40.9	8.1
	27.7	7.1	31.6	7.9		40.1	8.8	37	6.8
	57.6	12.5	41.1	8.6		22.7	6.3	43.3	8.1
	31.7	8.4	46.7	10.2		41.4	9.3	33.9	8.9
	28	7.7	28.7	5.6		16.1	4.4	26.9	5.3

Table B5. 125°C Bending Data

	Plywood		OSB			Plywood		OSB	
t (hr)	MOR (MPa)	MOE (GPa)	MOR (MPa)	MOE (GPa)	t (hr)	MOR (MPa)	MOE (GPa)	MOR (MPa)	MOE (GPa)
1	63.2	13.2	34.5	7.4	5	32.5	8.2	40.2	8.8
	64.9	11.7	37.9	6.6		45.4	11.2	30.1	5.6
	36.6	8.7	34.7	7.6		41.4	10.9	36	8.6
	54	12	34.5	8.6		46.2	9.9	30.2	7.1
	63	12.5	37.4	7.2		46.4	9.3	34.7	7.4
	37.8	10	44.6	7.6		44.7	10	37.1	9.8
	14.6	11	33.5	8.5		33.8	9.6	38.2	8.8
	39.8	8.7	43.5	8.4		37.9	9.6	38	8.1
2	57.7	14	29.2	6.3	6	55.4	11.2	26.1	6.7
	32	7.6	40.3	8		55.4	11.9	33.3	7
	38	11.2	42.1	9.2		36.6	9.8	47.3	9.9
	52	11.1	47.6	9.9		54.2	12.2	29	6.7
	44.2	12.6	26	5.9		47.5	12	17.6	4.9
	44.6	11.5	40.8	6.7		48.6	9.4	41.3	9
	41.5	9.4	25.1	5.7		11.7	2.3	28.8	6
	41.7	10.1	35.7	6.5		70.8	10.1	43.2	9.3
3	27.9	8.1	34.8	8.2	7	35.6	8.6	34.5	6.2
	49.6	11.3	22.5	6.4		39.6	12.4	40.5	6.7
	30.6	10.7	32.2	8.3		29.4	7.3	38.2	8.8
	21.1	6.7	37	9.3		19.9	8.2	42	10.3
	43.6	9.6	34.9	7.6		39.1	8.3	24.7	5.4
	17.1	6.9	34.1	8		27.3	8.3	31.4	7.3
	54	11	47.9	9.4		17.5	6.1	23.6	5
	56.5	10.8	33	6.1		44.7	10.2	18.9	5
4	48.4	10.9	45.2	8.7	8	46.9	9.7	31.2	6.6
	34.2	6.8	43.6	9.3		36.3	8.7	43.1	8.4
	31.9	8.3	38.6	8.9		45.9	9.6	31.5	7.2
	23.6	8.3	39.2	9.5		40.3	9.5	34.9	7.4
	48.4	11.2	20.1	4		53.7	12.2	45.9	8.4
	51.1	10.7	36.4	6.8		35.6	9.1	47	11.1
	35.5	13.1	30.5	5.3		55.3	11.7	17.1	3.4
	53.8	10.4	26	5.8		54.4	11.9	23.5	6.3

Table B6. 150°C Bending Data

	Plywood		OSB			Plywood		OSB	
t (hr)	MOR (MPa)	MOE (GPa)	MOR (MPa)	MOE (GPa)	t (hr)	MOR (MPa)	MOE (GPa)	MOR (MPa)	MOE (GPa)
1	43.1	8.3	45.8	9.5	5	51.1	9.2	31.3	7
	51.1	8.8	30.2	6.7		48.5	10.5	28.4	7.4
	46.7	9.1	29.8	7.8		44.3	9.4	32.4	7.3
	54	12.6	31.2	7		50.2	10.6	30.4	6.9
	51.2	9.3	30.6	7		52.1	8.9	40.3	8.3
	55.8	10.7	40.9	8.5		35.7	8.9	30	6.6
	47.5	11.4	28.9	6.7		42.3	11.8	29.9	6.8
	49.3	10.4	25.9	5.8		46.6	12.6	34.9	7
2	23.2	7.3	26.4	6.6	6	42.9	12	30.7	6.3
	40.7	8.9	29.3	6.3		48.1	11.9	28.5	6.2
	38.5	7.7	24.4	4.1		50.2	10.1	33.8	8.7
	37.4	10.8	30.1	6		58.1	9.9	32.7	7.6
	48.5	9.3	32.2	5.7		45.7	11	23.2	5.4
	38.7	10.7	36.5	7.3		19.3	8.2	37.9	8
	46.1	10.5	30.3	6.6		18.4	8.4	34.3	9.6
	39	8.3	33	8.3		44.3	8	35.8	7
3	51.4	10.1	34.4	7.6	7	58.9	13.6	20.7	5.3
	36.4	7.2	30.3	6		36.7	8.5	40.7	8.6
	42.5	9.3	15.4	4.5		41.8	8.5	27.1	7.5
	52.4	10.9	32.9	6.8		35.1	9.7	26.5	5.9
	46.5	8.1	31.8	6.6		39.8	12.6	36.4	7.8
	35.6	8.4	37.8	7.5		44.8	10.3	21.6	5.7
	40.6	7.6	31.1	7.2		34.1	9.5	17.5	4
	44.7	11.2	38.6	8.5		42.3	8.2	22.4	6.4
4	26.6	6.8	25.3	7	8	49.2	10.3	32.7	7.1
	46.1	8.1	31.2	7.8		45.1	9.3	44.7	8.6
	40.6	6.5	28	6.6		20.2	8	19.6	4.3
	24.4	7	21.3	5.5		41.1	7.4	26.9	7.5
	46.2	9.4	20.3	6.5		41.6	6.9	26.7	6.4
	39.2	8.6	25.9	6.2		39.4	7.2	30.7	7.9
	8	2.3	36.2	8.4		34	9.5	39.1	8
	36.4	7.2	23.4	5.1		35.6	10.8	44.3	8.5

Table B7. 175°C Bending Data

	Plywood		OSB			Plywood		OSB	
t (hr)	MOR (MPa)	MOE (GPa)	MOR (MPa)	MOE (GPa)	t (hr)	MOR (MPa)	MOE (GPa)	MOR (MPa)	MOE (GPa)
1	52.1	9.6	21.7	4.3	5	28.1	8.9	31	7
	47.5	10	24.4	5.7		32.1	10.8	25.4	6.5
	42.1	9	40.9	8.3		43.7	12.7	30	7.3
	33.7	8.3	20.1	4.1		20.2	8	39.8	9.4
	36.1	8.1	44.6	9.4		35.2	6.8	18.6	4.6
	41.1	10	50.9	10.5		26.2	7.9	20.6	5.5
	46.5	9.1	24.7	5.3		34.5	10.4	38.5	8.2
	31.5	10.5	37.3	9.7		34.7	9.3	28	6.6
2	45.3	9.5	36	8	6	50.3	10	35.3	7.8
	44.8	10.6	30.1	6.3		30	9	27.8	7.7
	25.5	7.7	33.1	9.5		34.7	8.1	20.3	5.1
	47.3	10.8	39	7.6		30.9	8.2	24.2	7.2
	24.9	7	33.2	6.3		36.3	9.6	18.6	4.6
	50.4	13.5	25.9	6.9		21.3	9.3	24	7.1
	37.7	10.7	37.6	7.4		43.5	10.3	23.5	6
	24.1	5.6	37.1	7.7		14.3	9.2	23.4	6.8
3	23.1	6.9	22	6.4	7	47.1	9.5	37.4	8.1
	20.5	8.9	36.6	9.2		28.7	8.8	24.5	6.3
	31.5	10.5	28.2	6.6		25.2	7.2	26.7	7.5
	27.8	9.1	28	6.9		32.6	7	30.5	6.8
	16.7	6.8	26.9	7.2		29	10	26.8	6.8
	23	5.5	29.2	5.9		25.9	8.4	33.9	7.4
	33.5	11.3	28.4	7		30.5	8.4	32.7	8
	45.8	9.7	30.7	7.2		38.8	11.3	26.8	8.2
4	39.5	8.7	24.4	6	8	17.7	7.3	22.8	5.7
	8.6	1	34	7.7		35.7	8.4	31.4	6.9
	30.5	9.6	32.4	8.5		39.3	8.2	29.4	7
	35.8	9.1	33.6	8.1		25.9	8.1	29.3	5.5
	39	8.6	25.9	4.6		33.8	7.6	29.9	8.2
	44.1	10.2	26.7	6		49.9	10.5	32.4	7.1
	32	7.7	34.6	6.5		29.8	7.3	29.2	7.8
	45.1	10.6	23.2	6.4		28.8	7.8	40.3	9.9

Table B8. 183°C Bending Data

	Plywood		OSB			Plywood		OSB	
t (hr)	MOR (MPa)	MOE (GPa)	MOR (MPa)	MOE (GPa)	t (hr)	MOR (MPa)	MOE (GPa)	MOR (MPa)	MOE (GPa)
1	52.4	12.5	35.5	7.4	5	30.5	13.9	24.1	5.99
	47.4	10.8	29.9	7.0		34.3	9.9	22.5	6.19
	29.2	10.7	37.1	7.2		37.1	15	18.8	6.42
	33.4	8.9	42.8	7.9		40.8	12.4	23.2	7.31
	62.1	9	33.2	6.8		25.5	12.4	27.4	7.41
	44.5	10.5	32	7.8		38.8	5.8	29.8	7.97
	47.6	9.7	31.5	6.2		41.4	11.8	23.9	6.70
	44.4	11.5	34.6	7.2		25.1	7.7	27.8	7.59
2	29.3	12.5	29.2	7.1	6	21.5	9.28	19.5	7.01
	29.2	4.7	29.8	5.1		24.2	9.81	25.7	7.28
	29	11	30.8	10.8		20.4	9.83	22.9	6.67
	30.4	9.8	23	7.7		20.4	9.20	9.8	4.02
	30.9	8.7	43.3	8.3		21	9.30	12.3	4.43
	27.5	9	15.6	5.7		23.7	9.30	25.3	7.14
	39.6	11.4	26	3.1		27.6	9.73	18.1	5.64
	27.6	11	28.2	6.5		35.2	10.90	20.2	5.86
3	47.6	9.9	30.7	6.0	7	33.9	10.4	22.1	5.72
	38.3	7.7	21.9	6.0		20.5	9.5	21.7	5.84
	48.9	15.6	30	6.8		28	9.7	11.2	4.17
	46.8	11.3	26.6	6.4		13	8.2	11.1	4.00
	53.8	11.6	24.3	5.8		27.6	11.8	7	3.68
	42.3	12.7	31.2	6.6		33.9	10.9	14.5	5.50
	39.6	12.1	27.2	7.4		22.9	11.9	18.9	6.57
	34.8	8.8	26.6	5.9		18	8.0	16	5.48
4	51.5	13.3	26.1	6.5	8	18.4	9.1	31.1	7.15
	43.5	8.2	31.6	6.4		32.2	12.3	20	6.12
	41.5	6.2	19.4	4.7		24.6	12.8	21.6	6.06
	37.1	11.4	18.3	4.9		24.2	13.1	19.8	6.65
	55	9.8	27.5	6.5		37.1	12.5	19.2	4.92
	52.7	10.8	20	6.5		41.4	12.6	35.8	7.85
	31.7	10.8	27.8	6.5		47.2	13.9	11.6	5.15
	40.7	6.1	18.7	5.6		35.2	10.9	11.2	6.65

Table B9. 191°C Bending Data

	Plywood		OSB			Plywood		OSB	
t (hr)	MOR (MPa)	MOE (GPa)	MOR (MPa)	MOE (GPa)	t (hr)	MOR (MPa)	MOE (GPa)	MOR (MPa)	MOE (GPa)
1	23.6	7.0	30.1	6.9	5	17.5	6.4	28.8	8.36
	47.2	7.3	34.7	7.3		14.4	10	44.3	9.96
	54.3	7.9	33.3	6.5		10.5	3.5	34	8.87
	45.6	8.4	31.9	7.1		18.9	10.1	23.6	6.93
	30.7	7.3	46.5	9.3		26.6	7.8	19.3	7.00
	28.1	8.3	36.5	7.7		28	13.9	31.1	9.04
	42	8.8	20.7	5.7		27.7	13.5	17.9	8.15
	31.5	7.3	29.4	6.6		34	6.4	15.8	7.47
2	30.1	6.4	32.9	7.1	6	24.4	9.3	24.3	5.22
	31.6	7.7	30.5	6.9		29.5	12.3	20.4	8.22
	58.3	12.1	36.6	6.7		17	8.0	24.4	7.33
	52.2	11.4	29.5	7.0		19.9	11.2	25.5	8.06
	69	15.2	34.8	7.9		26	10.5	14.8	5.55
	41.9	14.0	28.2	6.5		26.1	11.2	15.2	5.01
	47.2	11.6	22.1	7.0		25.7	11.3	21.5	6.75
	59.9	12.2	40.7	8.4		14.2	5.2	19.2	5.34
3	28.3	7.2	23.2	7.9	7	10.8	2.5	32.1	6.95
	29.1	10.3	18.9	5.8		17.6	4.6741	17	6.04
	30.9	9.3	17.8	4.5		7.6	5.2	13.3	5.74
	21.4	14.4	22.5	5.6		8.4	3.8	20.2	7.53
	31.8	11.3	20.3	5.3		12.9	4.9	14	5.21
	24.1	9.1	37	7.8		12.4	2.8	16.6	6.00
	26.1	10.5	28.1	6.5		10.3	5.84	19.2	8.29
	18.1	5.2	27.7	7.5		17.7	9.1	27.7	7.35
4	28	11.6	23	6.7	8	10	7.8	12	4.60
	29.1	9.9	26.5	7.2		15.1	4.5	16.2	5.49
	33.4	15.4	22.6	6.2		11.3	5.8	22.1	7.02
	34.8	9.8	21.4	7.5		12.1	2.1	16.8	5.12
	44.1	16.1	24.2	7.5		26.4	8.9	18.8	4.93
	37.7	11.4	18.3	6.3		21.9	13.2	16	6.24
	37.3	11.2	21.4	6.0		24.1	12.2	11.4	4.54
	26.8	10.6	24.4	6.4		27.4	6.9	8.7	4.92

Table B10. 200°C Bending Data

	Plywood		OSB			Plywood		OSB	
t (hr)	MOR (MPa)	MOE (GPa)	MOR (MPa)	MOE (GPa)	t (hr)	MOR (MPa)	MOE (GPa)	MOR (MPa)	MOE (GPa)
1	37.5	9.1	35.7	7.8	5	22	6.4	7.2	2
	39.7	10.9	31.9	7.4		14.7	5.9	18.1	6.9
	16.4	7.5	35	5.9		13	5.7		
	20.2	8.3	24.4	5.1		12.1	6.2		
	40.4	12.1	29.5	6.3		17.7	7.7		
	38.6	9.9	38.9	7.3		18.9	1.5		
	49.8	9.6	44	8.2		9.5	1.1		
	30	9.8	31.3	6.5		25.4	5.1		
2	32	9.5	25.3	7.9	6	16	3.1		
	19.5	8	16.1	5.5		12.4	2.02		
	34.4	12.3	19.1	6.8		12.7	1.46		
	23.8	9.1	21.7	7.3		11.4	3.2		
	15.2	7.5	24.7	8		10.4	4.1		
	29.3	8.4	24	6.7		12	2.6		
	13.8	5.4	26.1	7.8		19.2	4.4		
	27.5	9	23.2	6.2		12.1	3.9		
3	23.6	7.7	29.4	7.1	7	18.6	7.9		
	22.6	8.8	11	4.4		16	2.3		
	25.7	8.9	19.8	7		13.4	4.3		
	21.4	7.8	30.6	7.8		15.9	3.02	Fire	
	14.1	5	18.8	7		8.2	4.71		
	22.8	8	22.3	4.8		12.7	4.79		
	8.7	7.9	30.6	7.9		9.1	4.87		
	9.6	7.5	29.1	6.7		12.6	4.95		
4	19.7	6.7	21.5	6.6	8				
	21.3	7.9	18	5.1					
	24.2	6	16	5.3					
	23.7	7.2	27.1	6.9		Fire			
	21.4	7.2	14.8	5.3					
	16.1	6.5	16.5	5.5					
	17.3	8.2	23.6	6.7					
	23.1	7.3	18.9	6.9					

Appendix C

Load deflection diagrams of lateral nail tests.

ESPH ESOH ESOO ESPO

ELPH ELOH ELOO ELPO

PSPH PSOH PSOO PSPO

PLPH PLOH PLOO PLPO

1st Letter – Geometry; Edge (E) or Plate (P)
2nd Letter – Framing Member; SSL (S) or LVL (L)
3rd Letter – Sheathing Member; plywood (P) or OSB (O)
4th Letter – Sheathing thickness; half inch (H) or One inch (O)

Fig. C1. Various connection configurations.

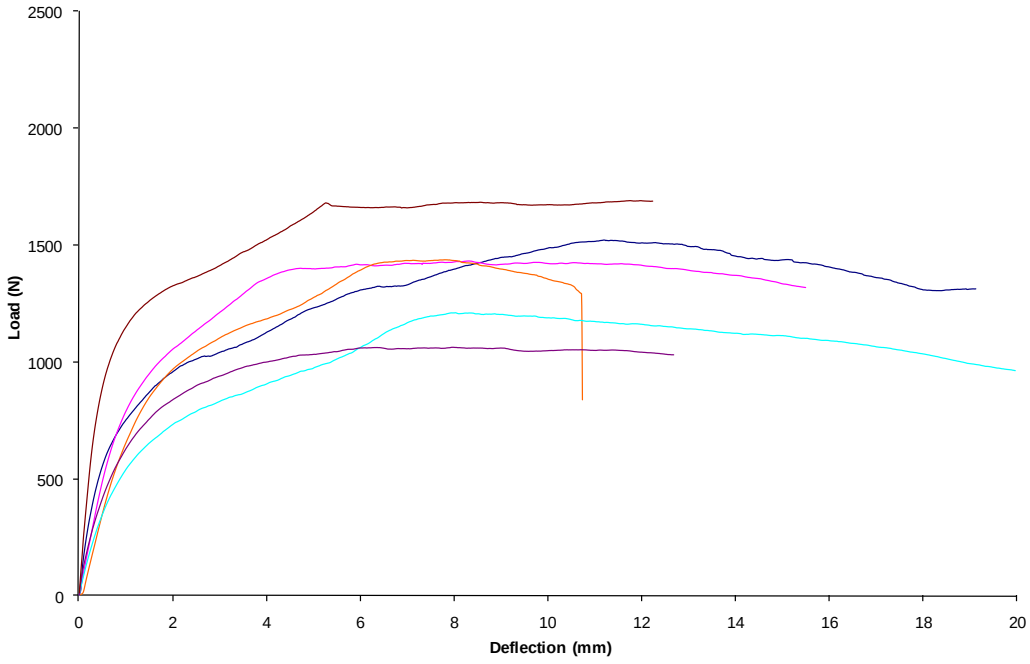

Fig. C2. Load displacement diagram Edge SSL-OSBO control

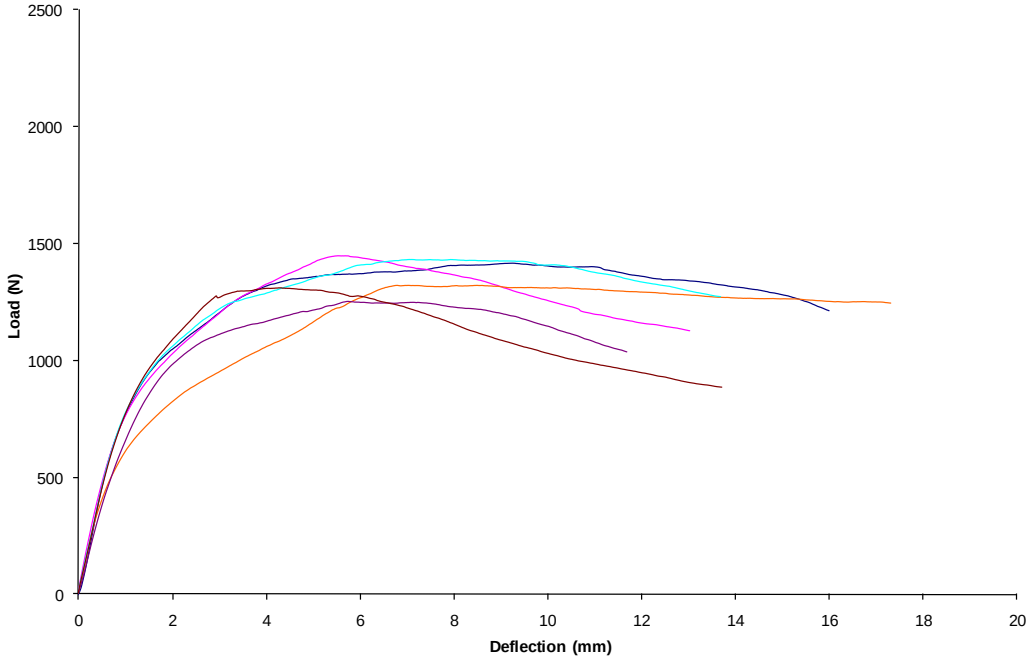

Fig. C3. Load displacement diagram Edge SSL-OSBO 100^{o}C -1hr

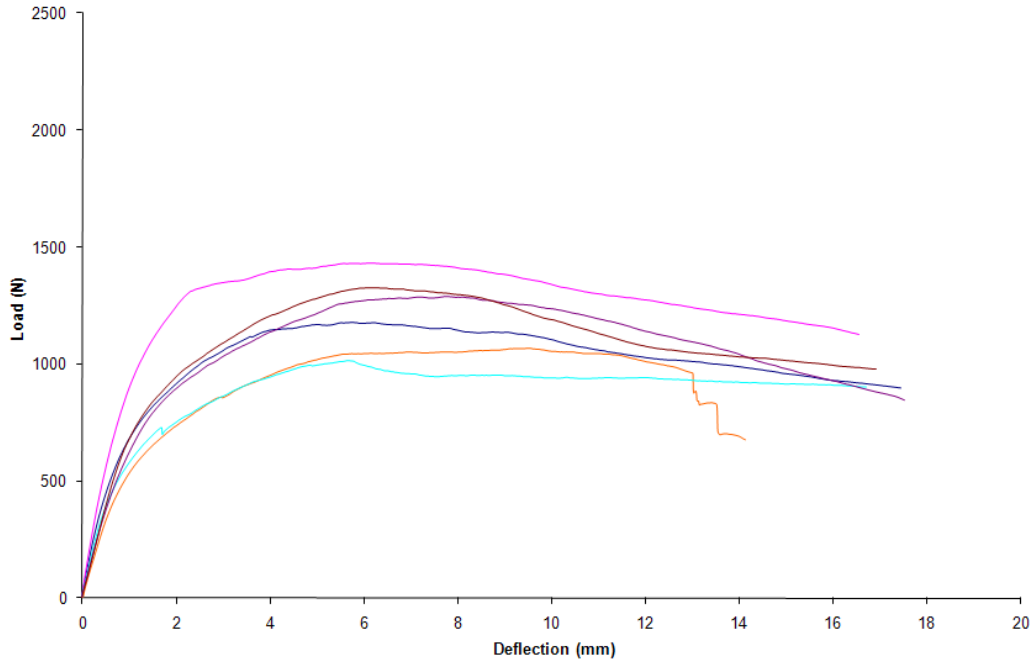

Fig. C4. Load displacement diagram Edge SSL-OSBO 100^{o}C -2hr

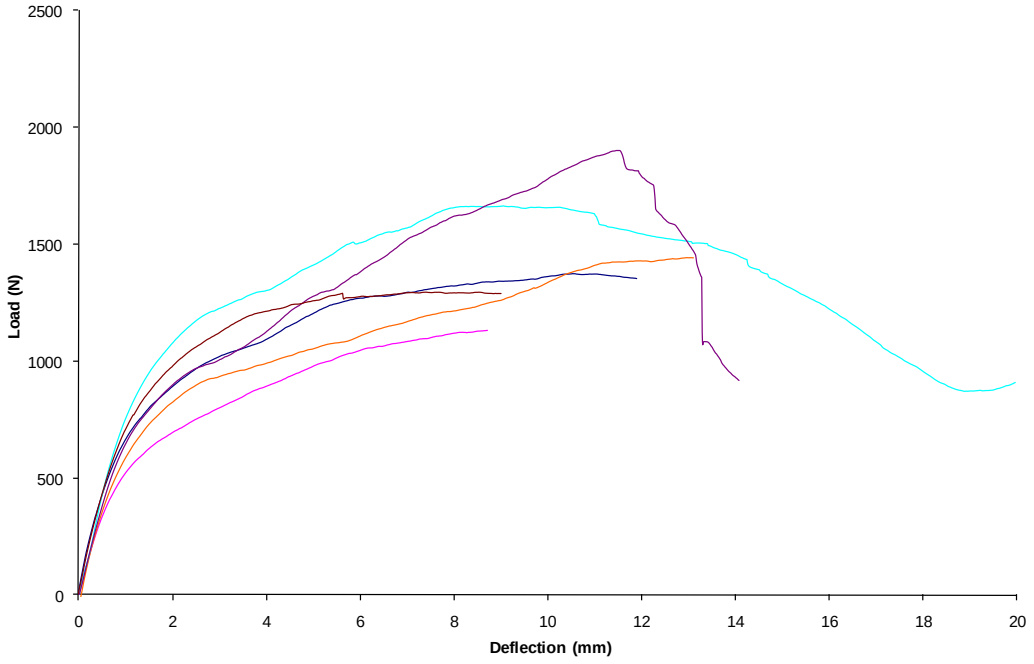

Fig. C5. Load displacement diagram Edge SSL-OSBO 200^{o}C -1hr

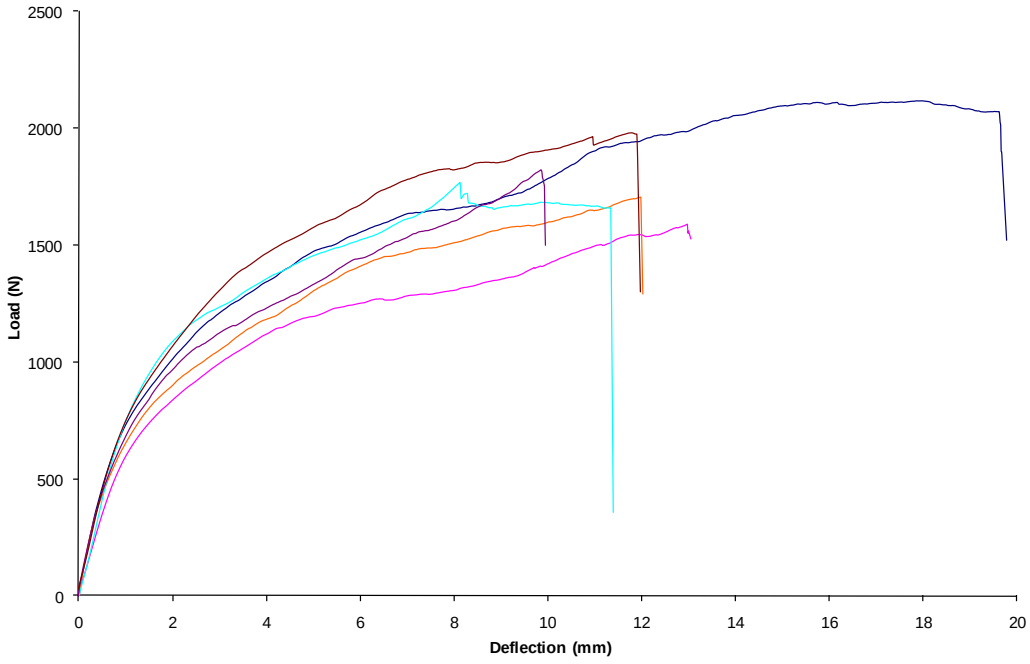

Fig. C6. Load displacement diagram Edge SSL-OSBO 200^{o}C -2hr

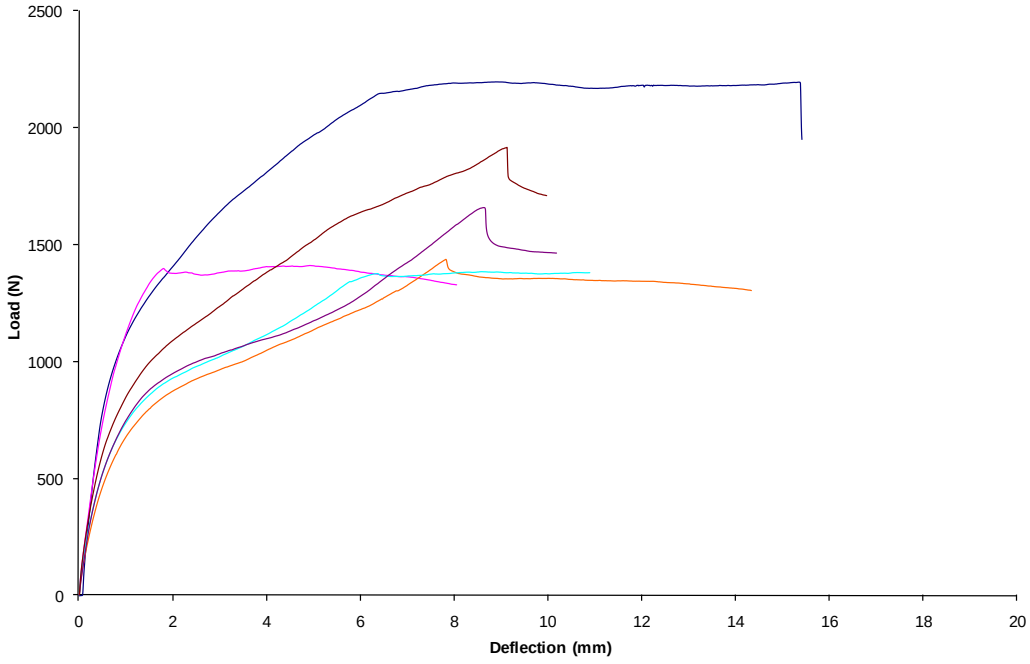

Fig. C7. Load displacement diagram Edge SSL-PWO Control

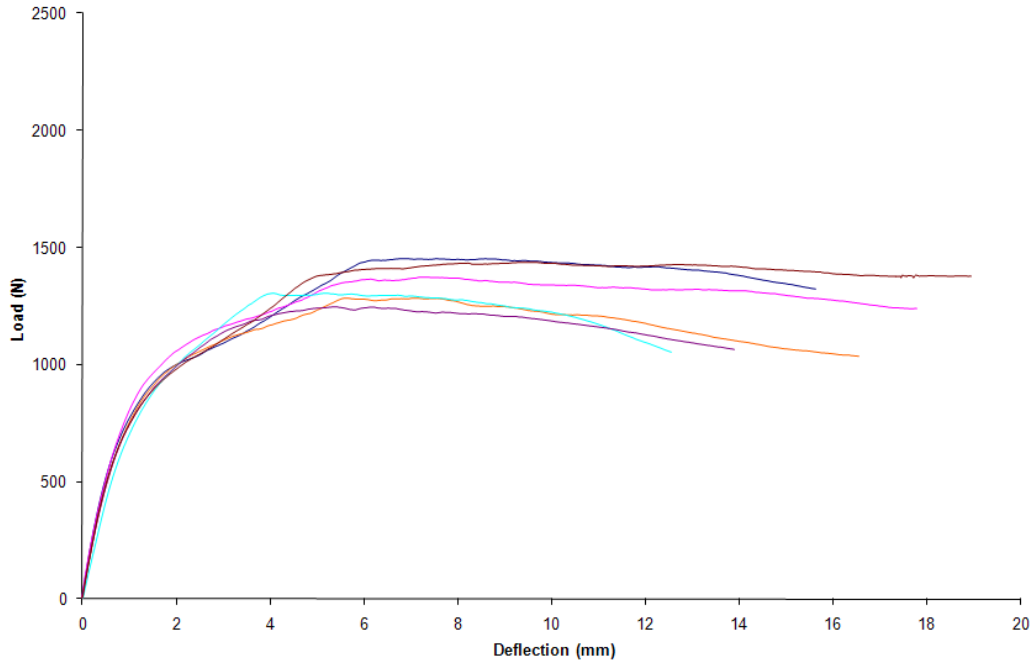

Fig. 8 Load displacement diagram Edge SSL-PWO 100^{o}C -1hr

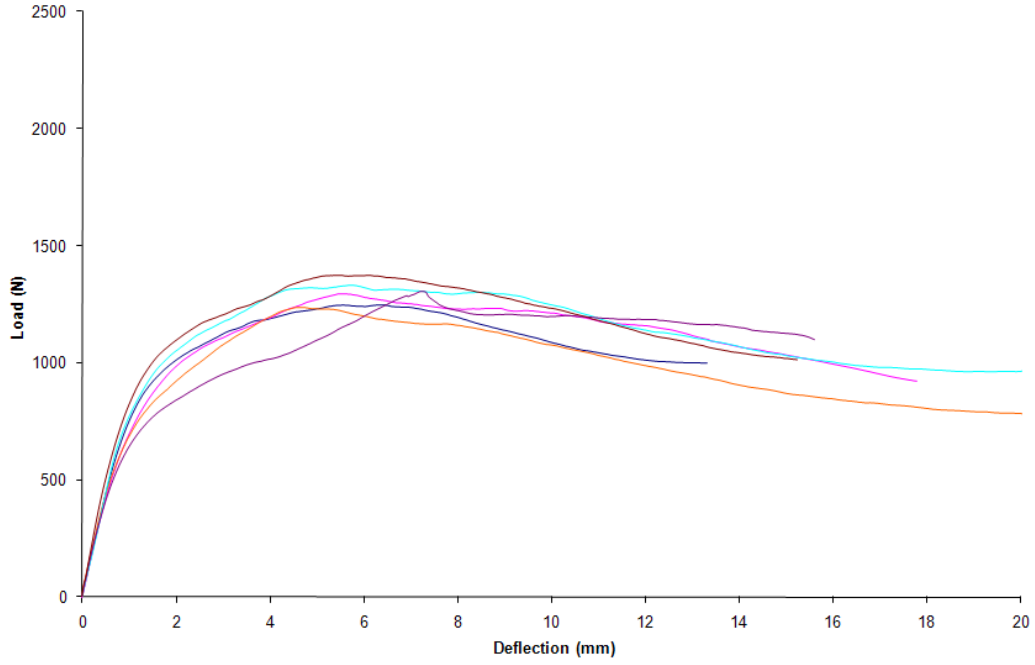

Fig. C9. Load displacement diagram Edge SSL-PWO 100^{o}C -2hr

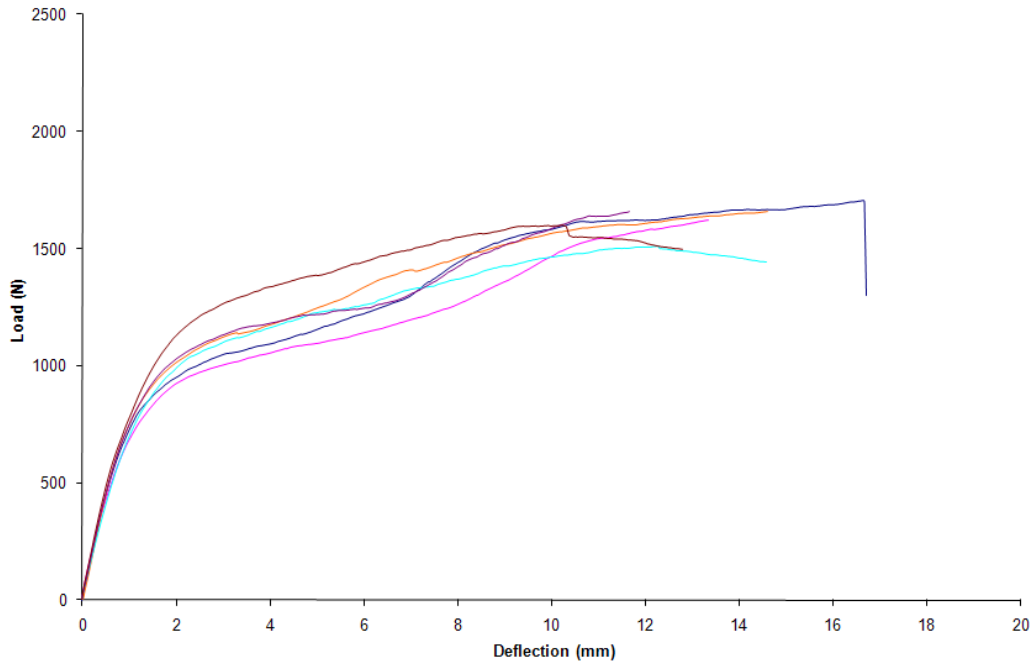

Fig. C10. Load displacement diagram Edge SSL-PWO 200^{o}C -1hr

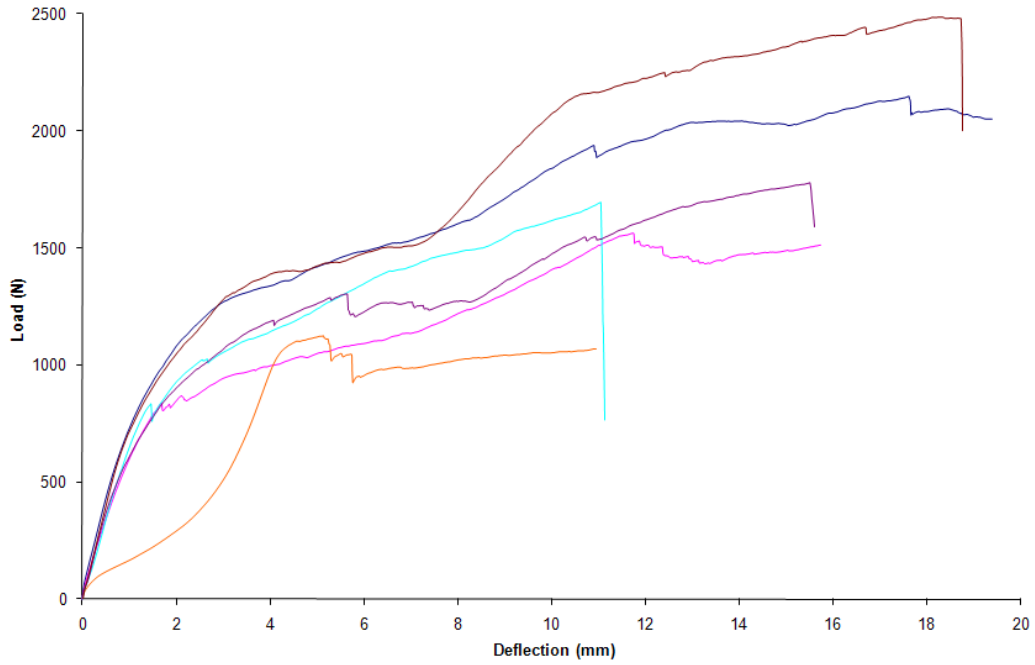

Fig. C11. Load displacement diagram Edge SSL-PWO 200^{o}C -2hr

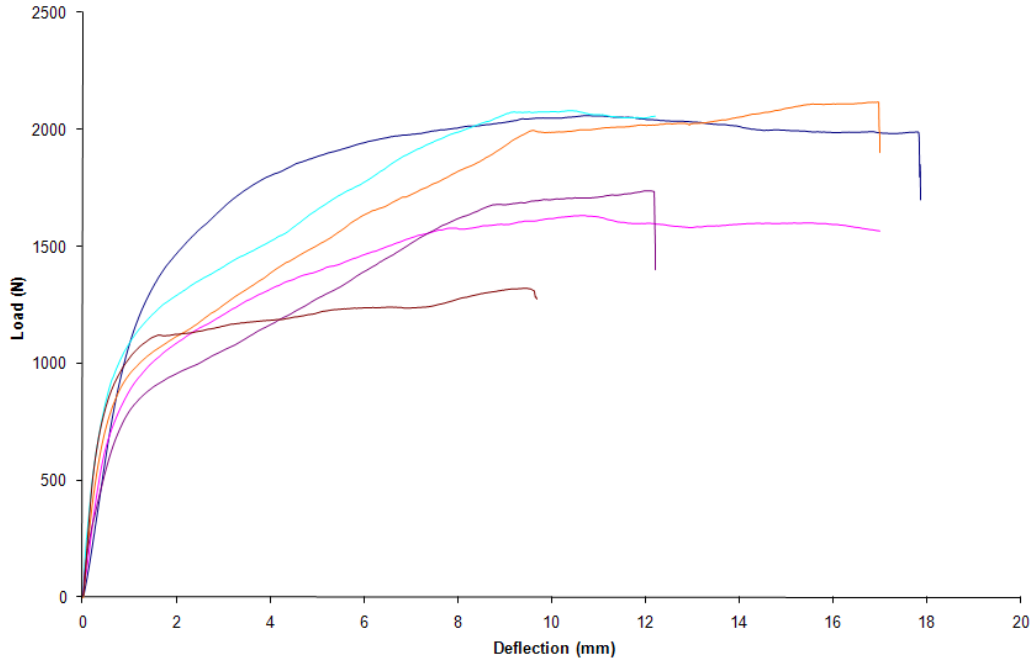

Fig. C12. Load displacement diagram Edge SSL-OSBH Control

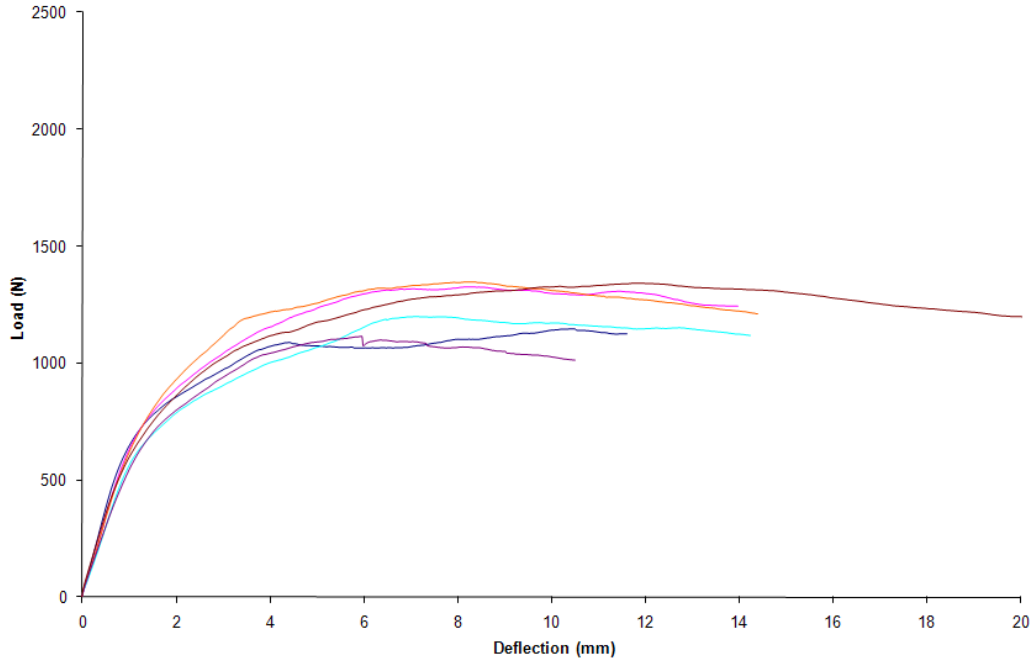

Fig. C13. Load displacement diagram Edge SSL-OSBH 100^{o}C -1hr

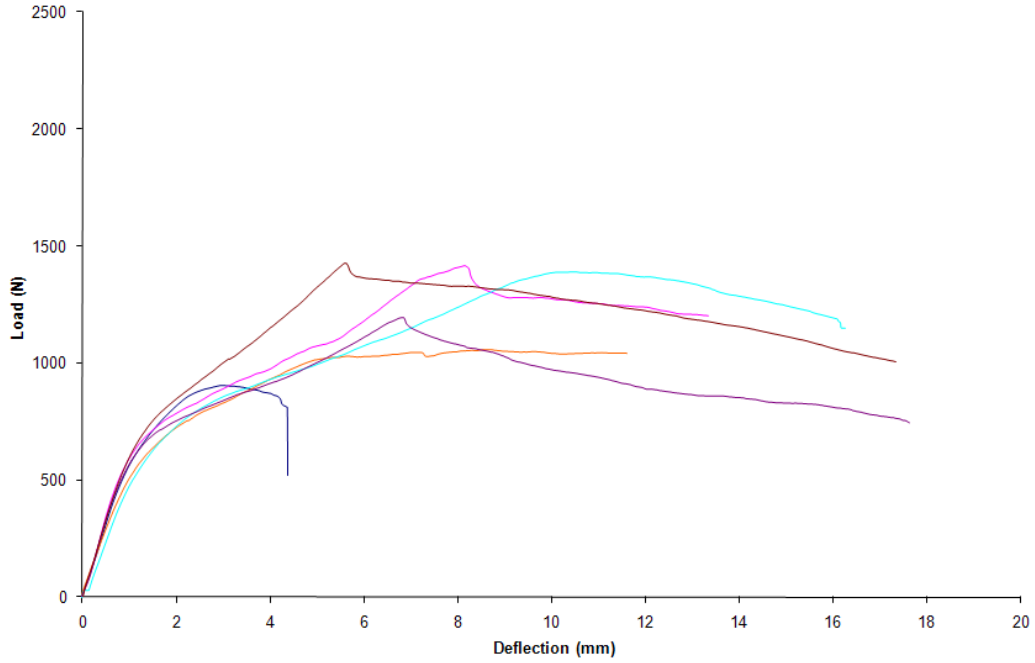

Fig. C14. Load displacement diagram Edge SSL-OSBH 100^{o}C -2hr

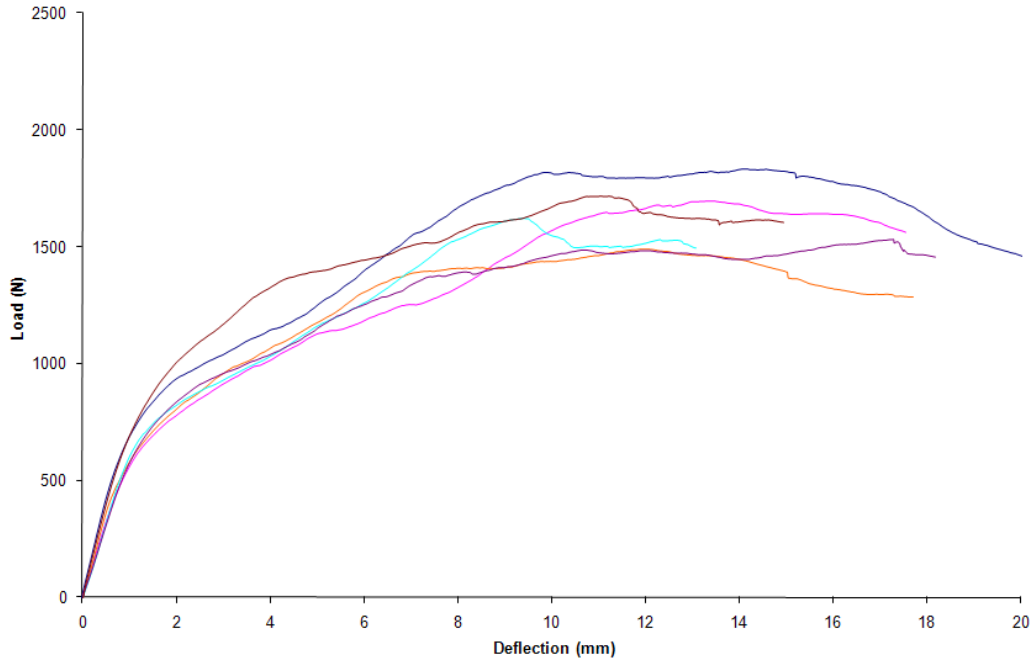

Fig. C15. Load displacement diagram Edge SSL-OSBH 200^{o}C -1hr

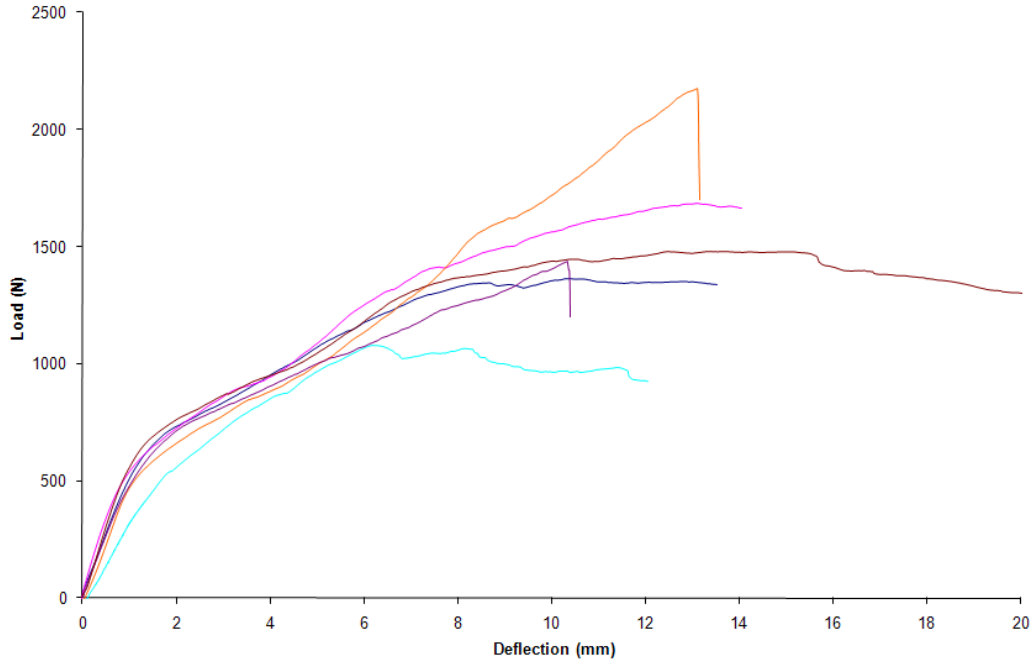

Fig. C16. Load displacement diagram Edge SSL-OSBO 200^{o}C -2hr

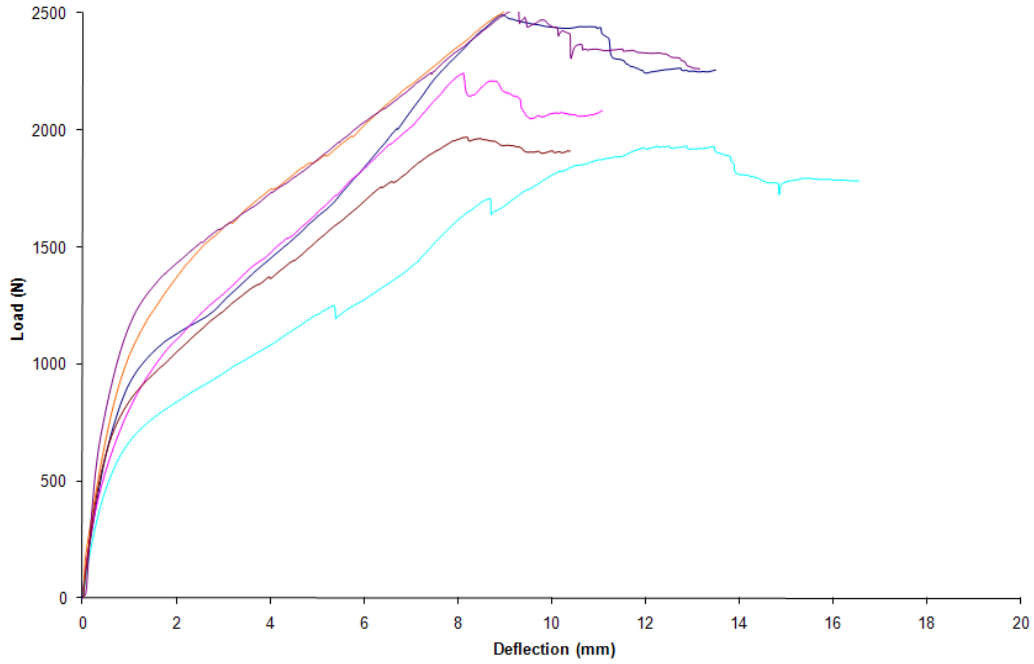

Fig. C17. Load displacement diagram Edge SSL-PWH Contol

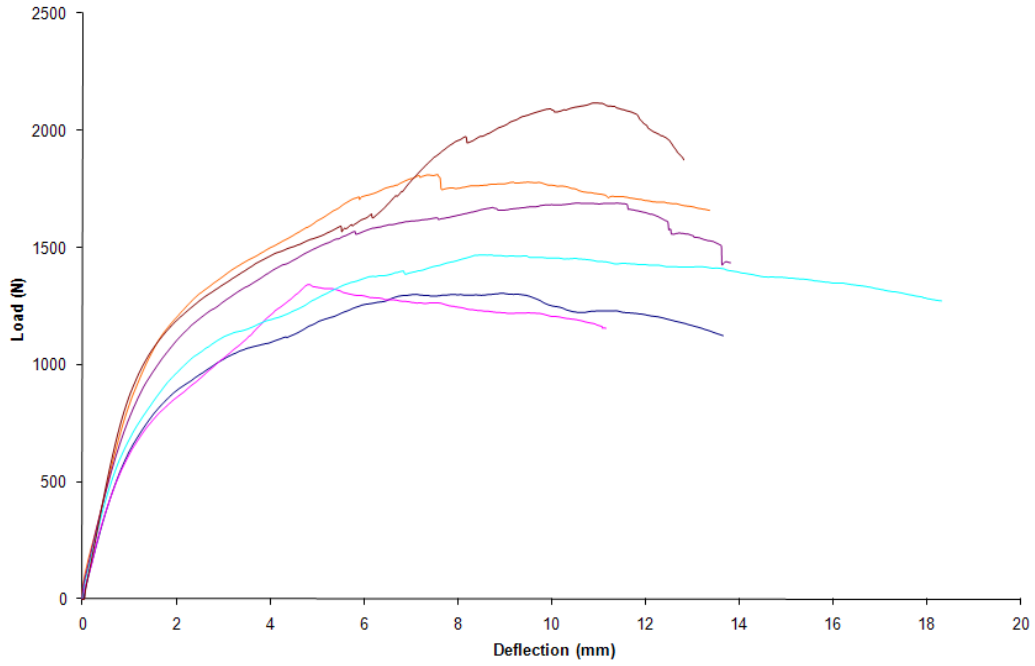

Fig. C18. Load displacement diagram Edge SSL-PWH 100^{o}C -1hr

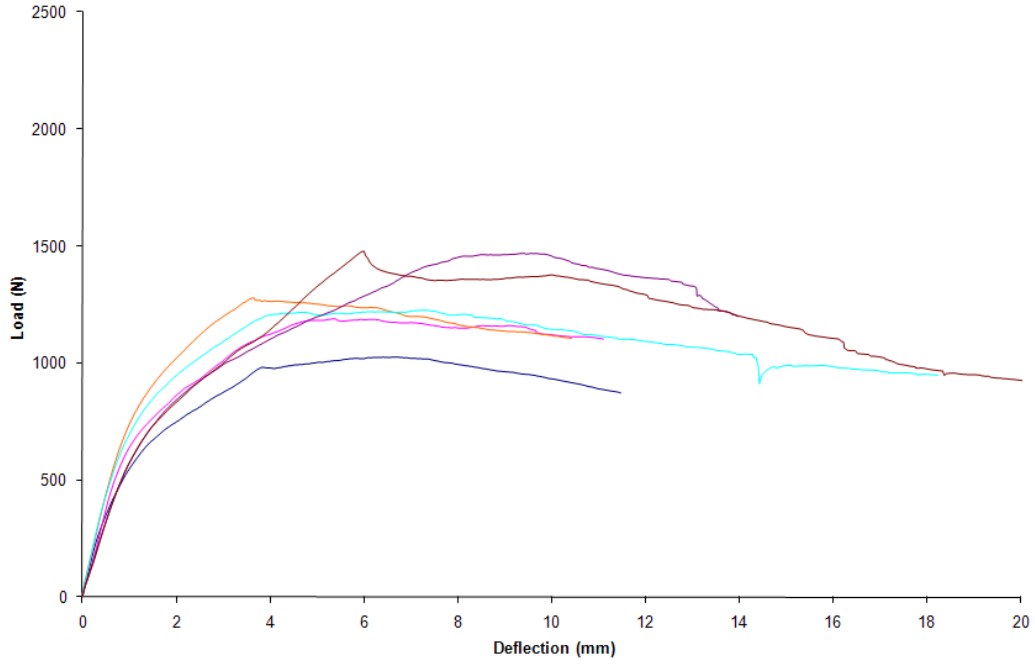

Fig. C19. Load displacement diagram Edge SSL-PWH 100^{o}C -2hr

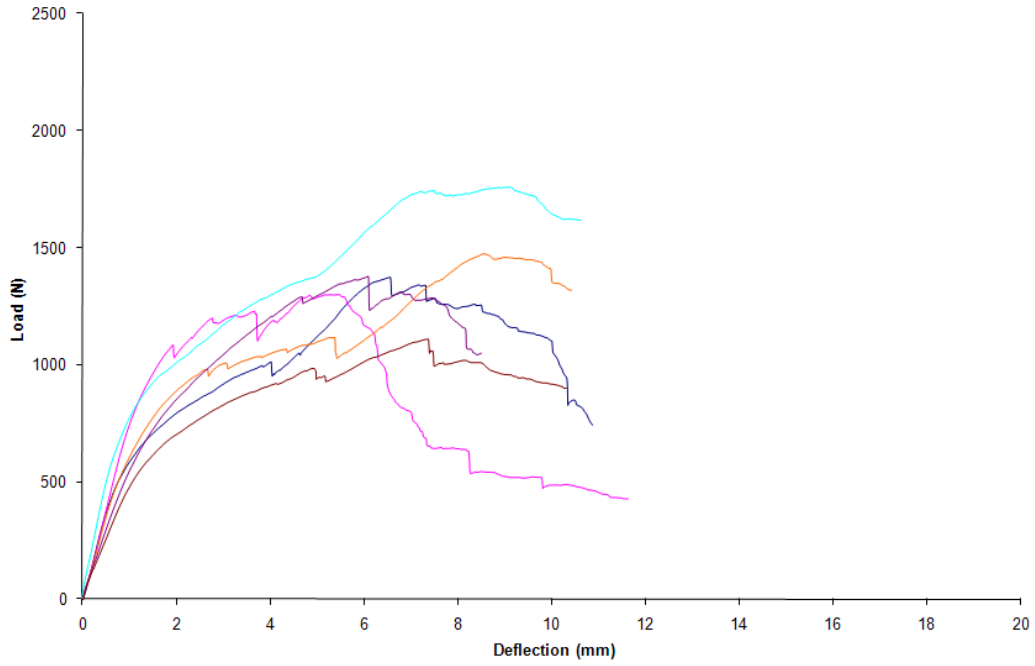

Fig. C20. Load displacement diagram Edge SSL-PWH 200^{o}C -1hr

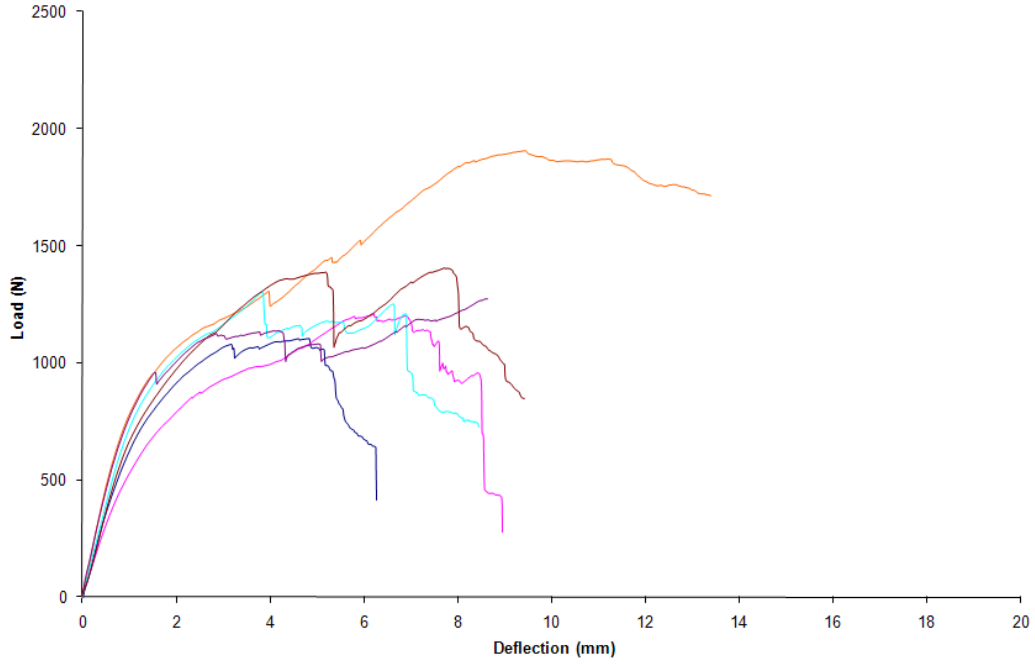

Fig. C21. Load displacement diagram for Edge SSL-PWH 200^{o}C -2hr

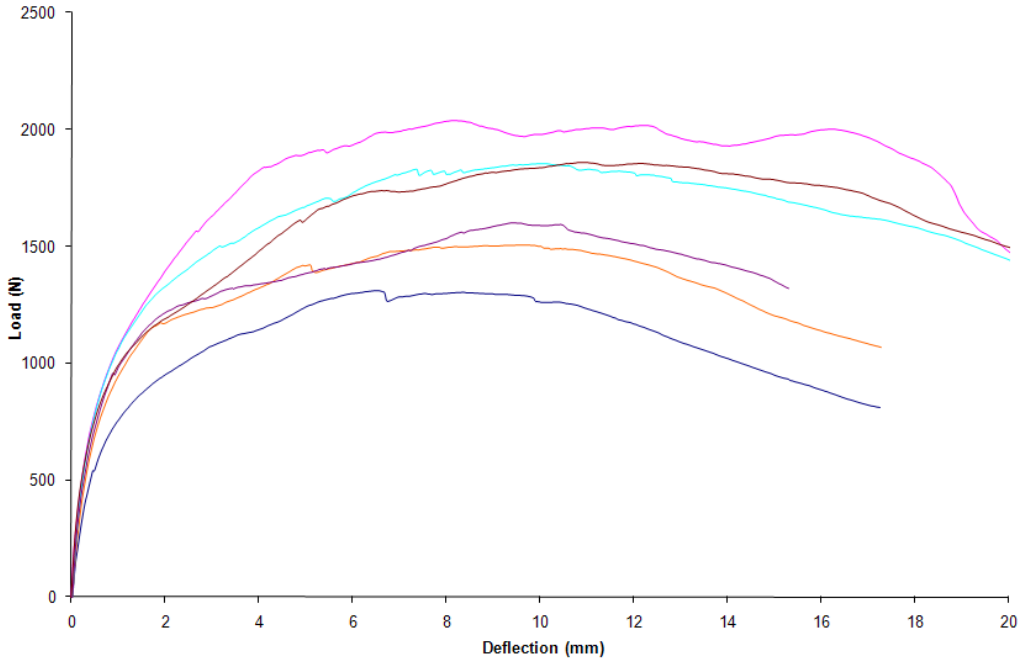

Fig. C22. Load displacement diagram for Plate SSL-OSBO Control

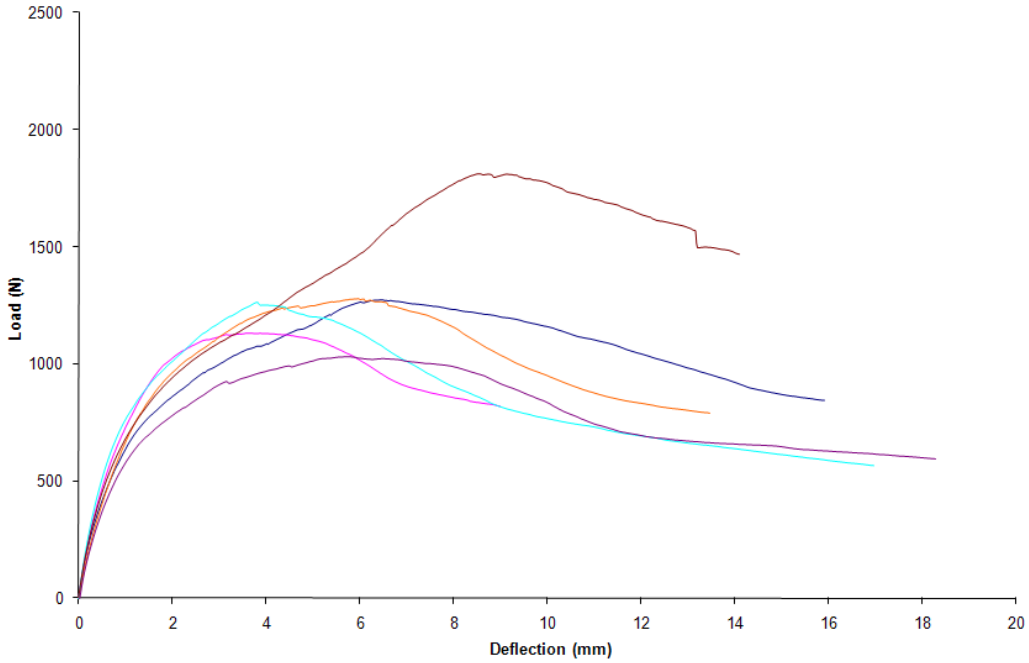

Fig. C23. Load displacement diagram for Plate SSL-OSBO 100^{o}C-1hr

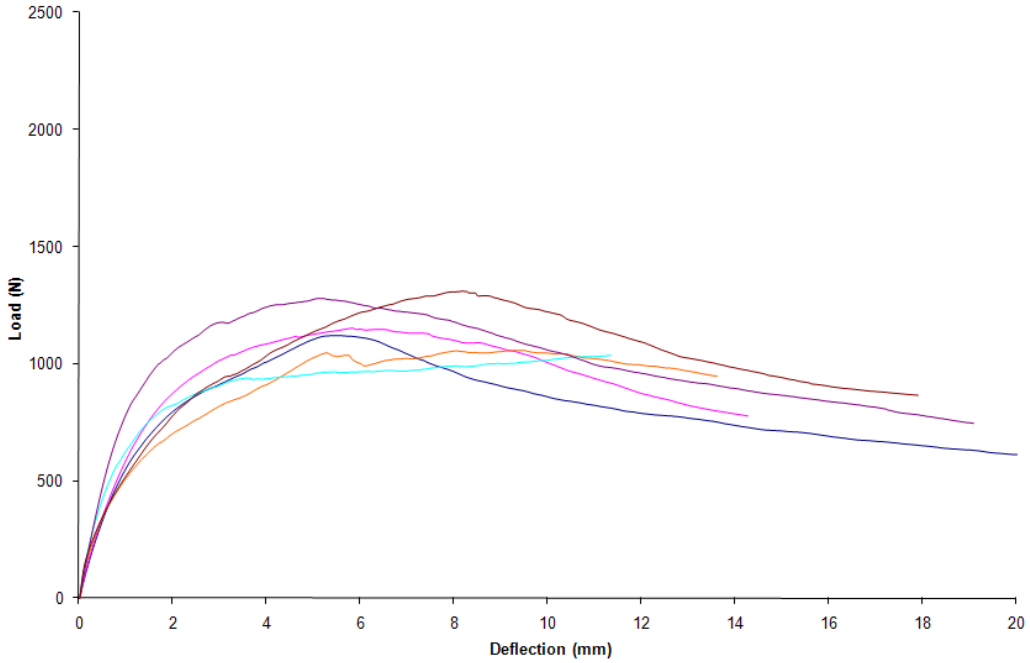

Fig. C24. Load displacement diagram for Plate SSL-OSBO 100^{o}C-2hr

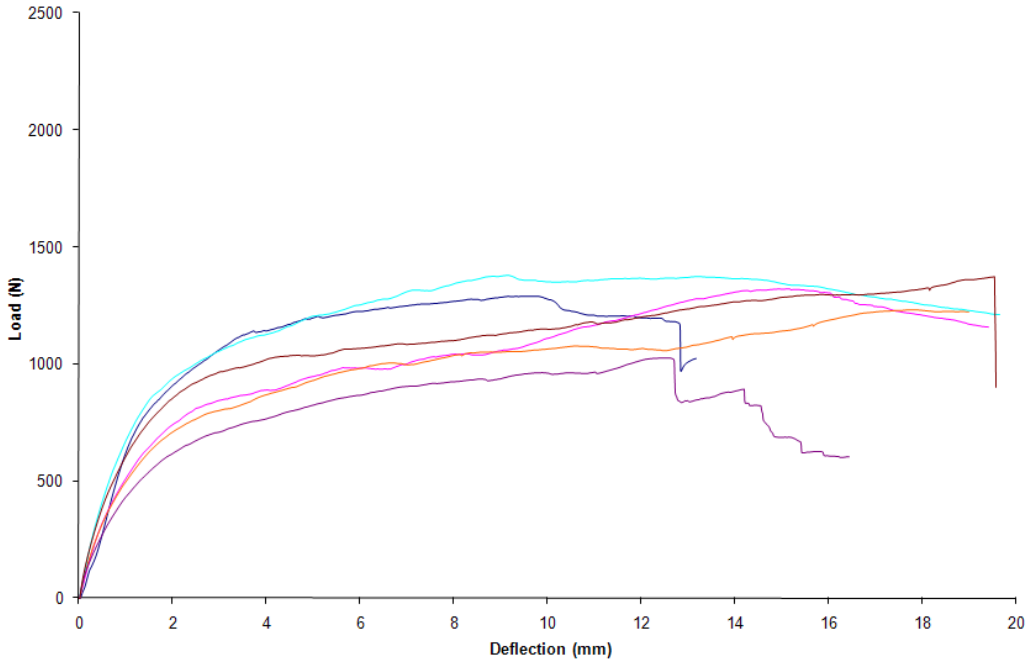

Fig. C25. Load displacement diagram for Plate SSL-OSBO 200^{o}C-1hr

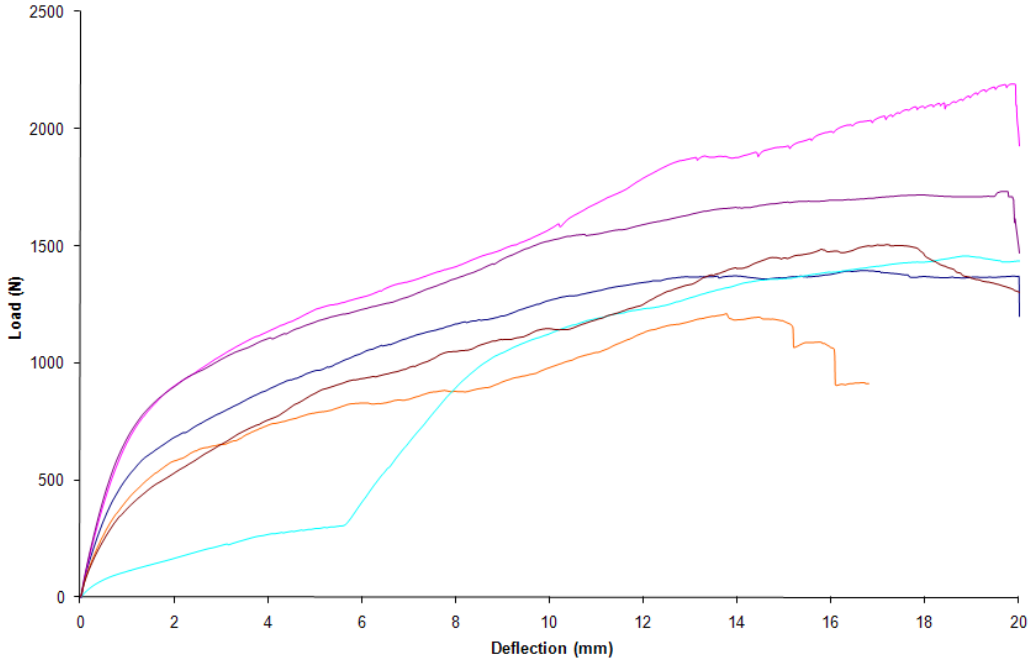

Fig. C26. Load displacement diagram for Plate SSL-OSBO 200^{o}C-2hr

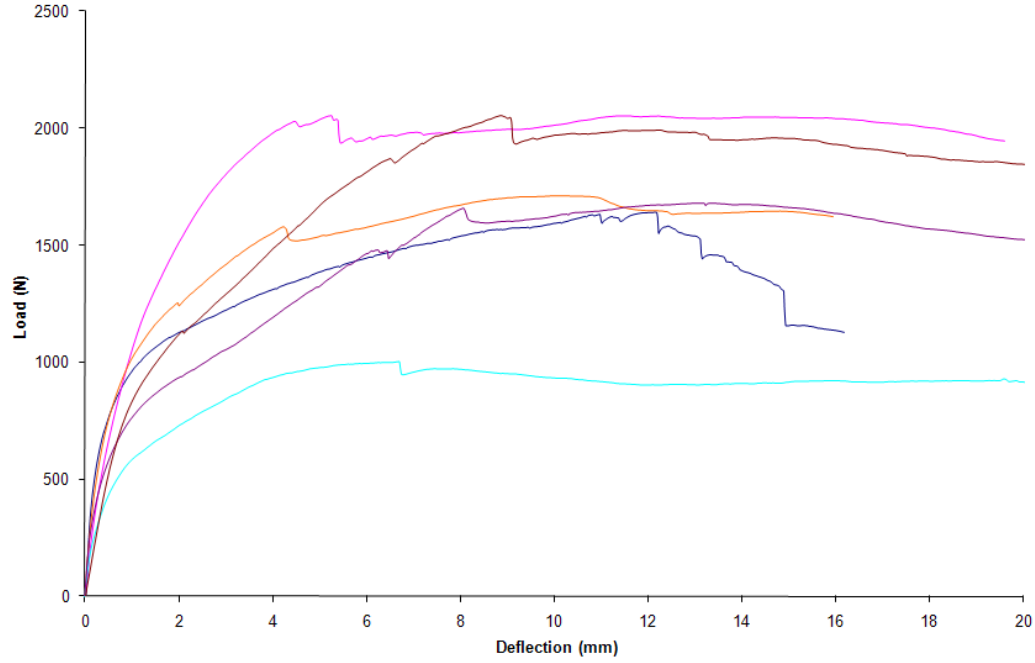

Fig. C27. Load displacement diagram for Plate SSL-PWO Control

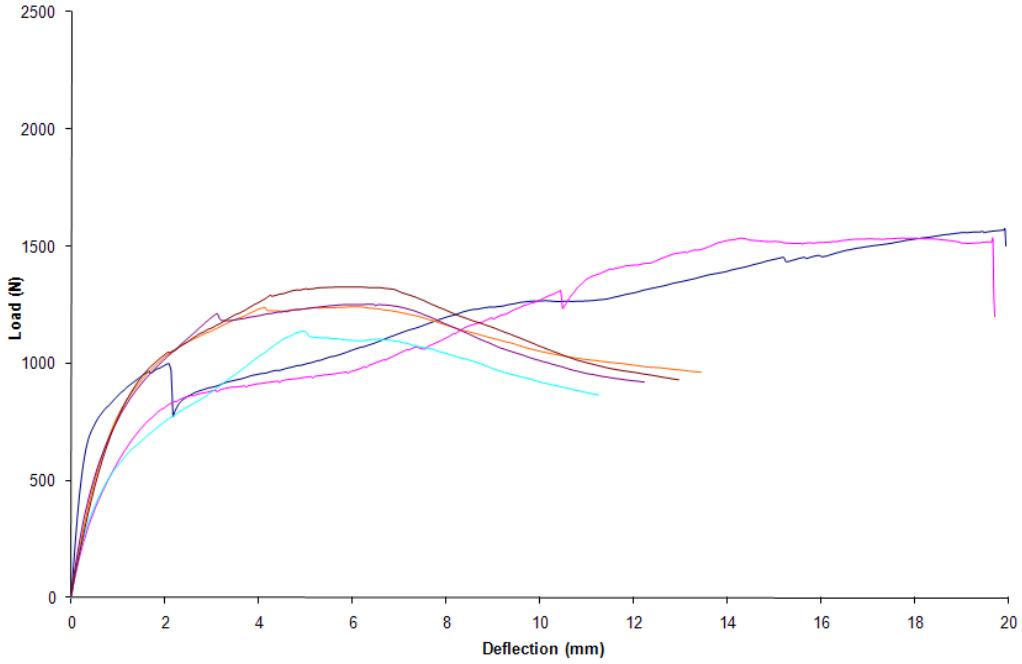

Fig. C28. Load displacement diagram for Plate SSL-PWO 100^{o}C-1hr

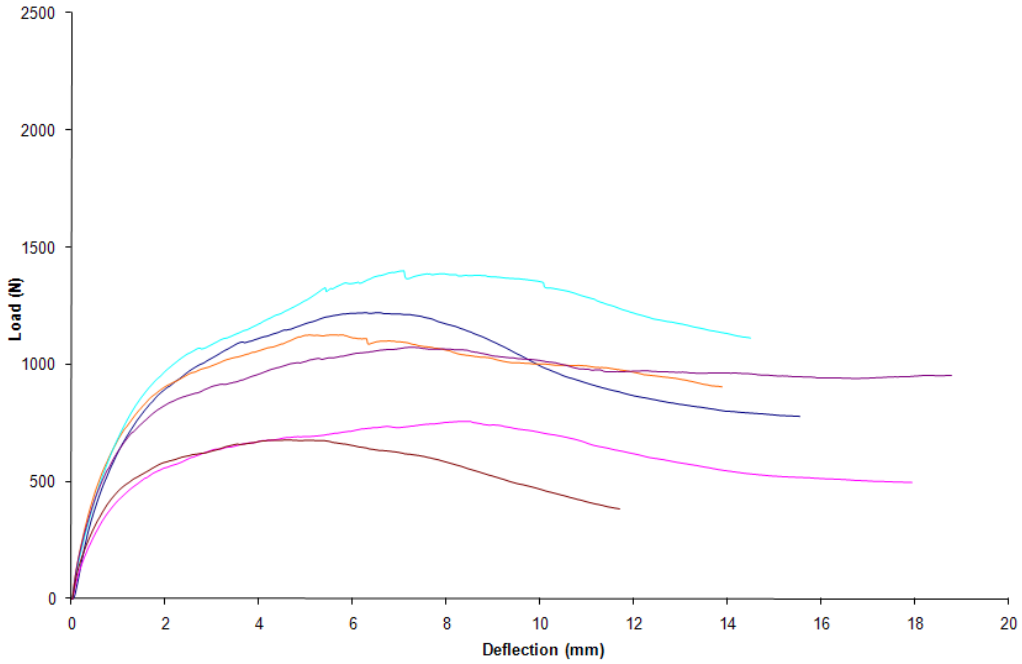

Fig. C29. Load displacement diagram for Plate SSL-PWO 100^{o}C-2hr

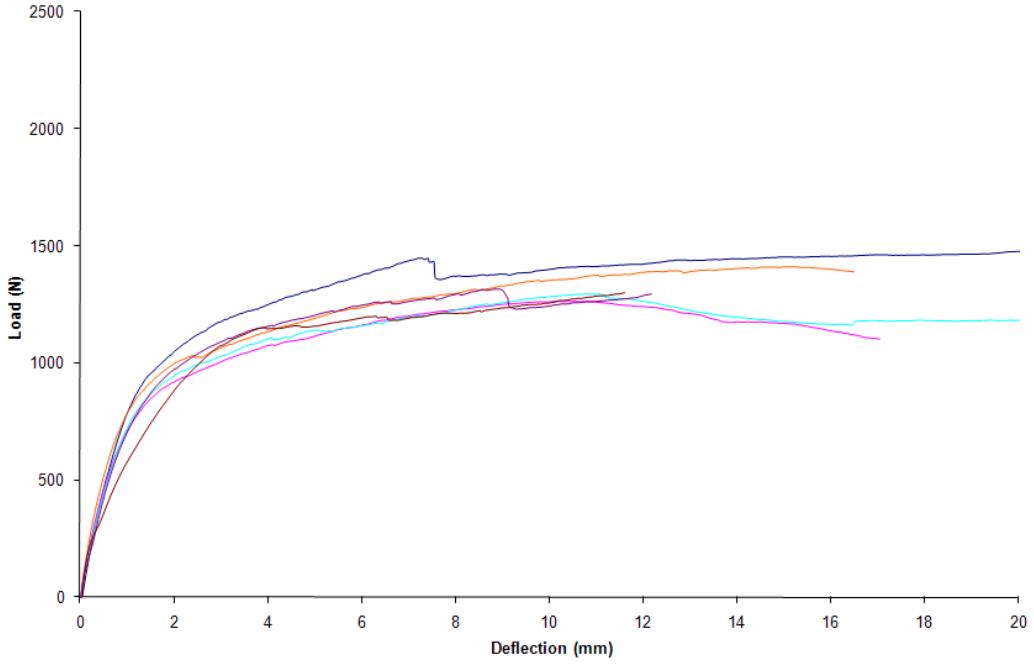

Fig. C30. Load displacement diagram for Plate SSL-PWO 200^{o}C-1hr

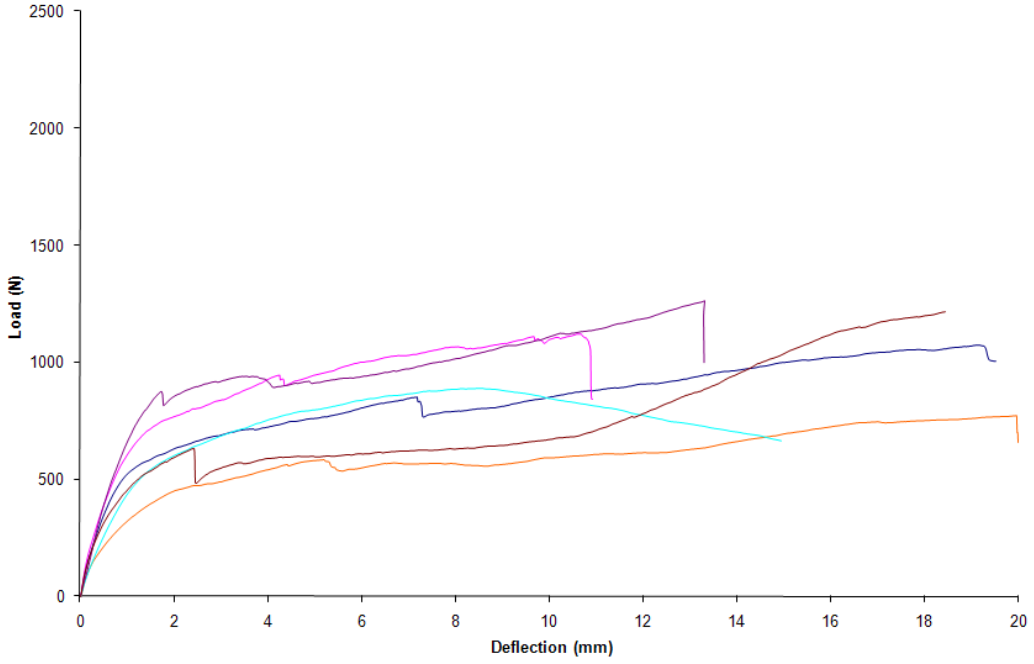

Fig. C31. Load displacement diagram for Plate SSL-PWO 200^{o}C-2hr

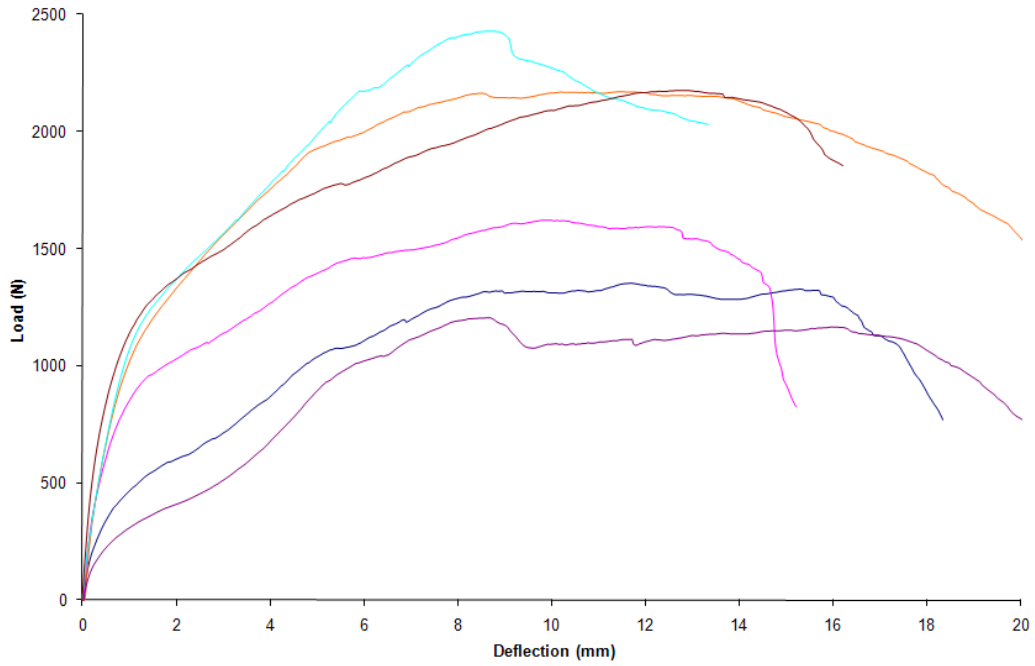

Fig. C32. Load displacement diagram Plate SSL-OSBH Control

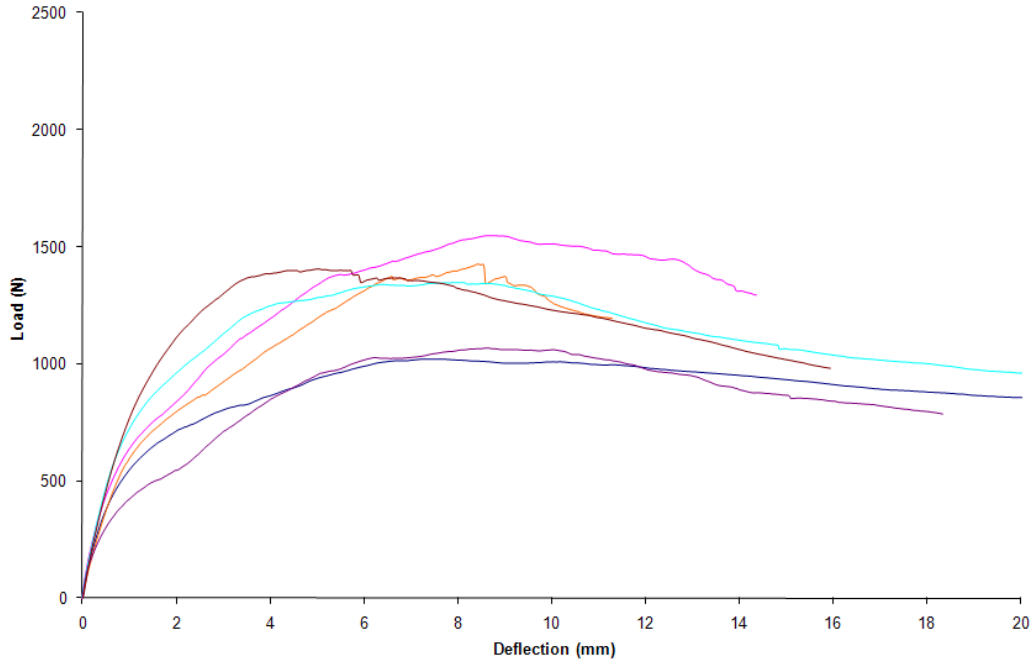

Fig. C33. Load displacement diagram for Plate SSL-OSBH 100^{o}C-1hr

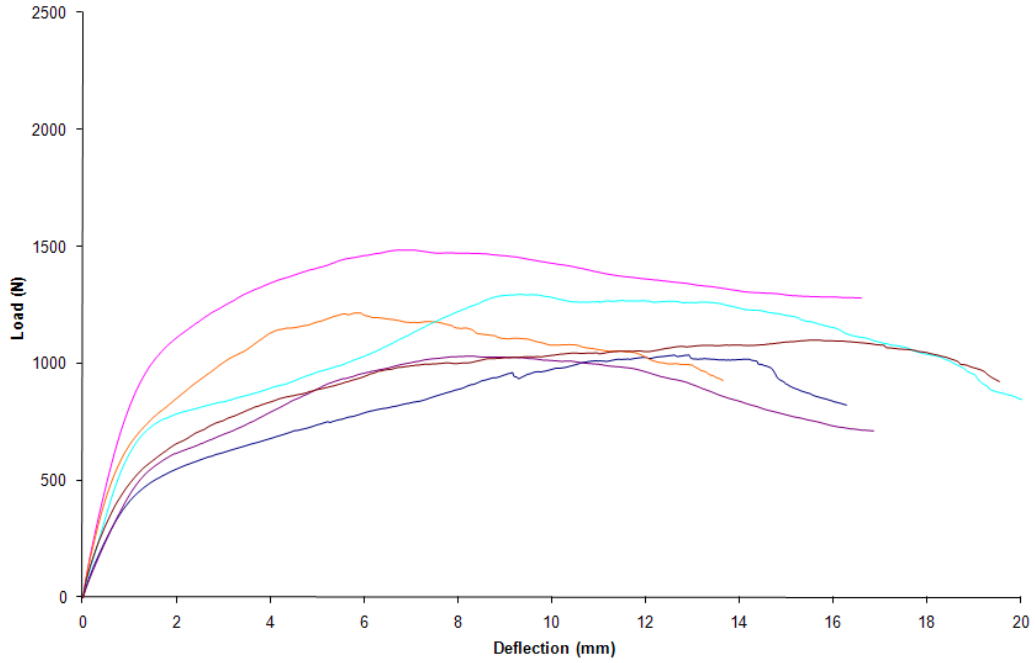

Fig. C34. Load displacement diagram for Plate SSL-OSBH 100^{o}C-2hr

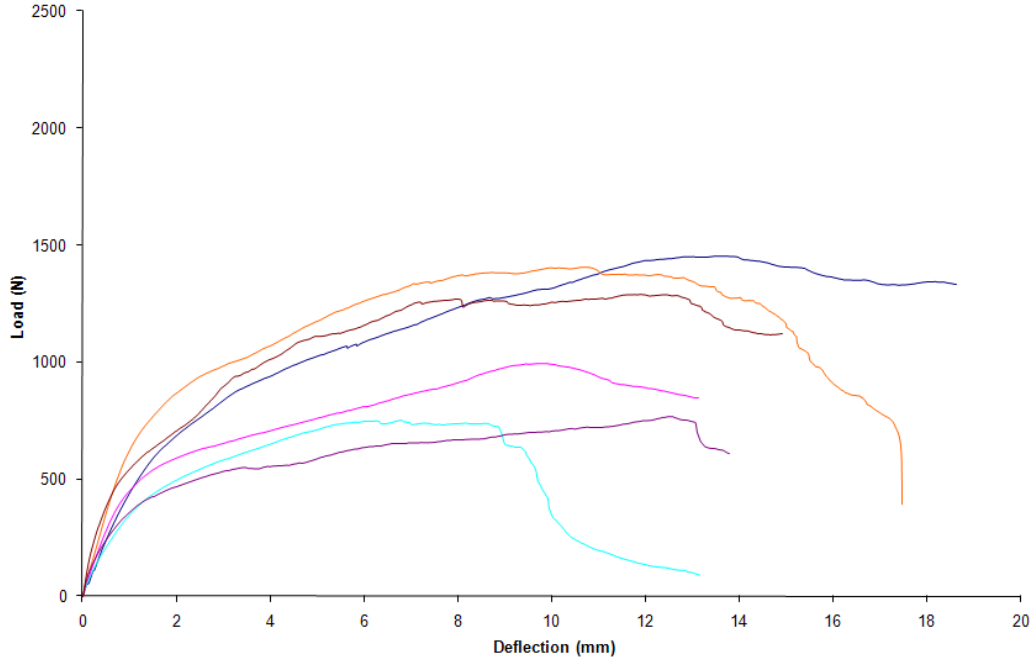

Fig. C35. Load displacement diagram for Plate SSL-OSBH 200^{o}C-1hr

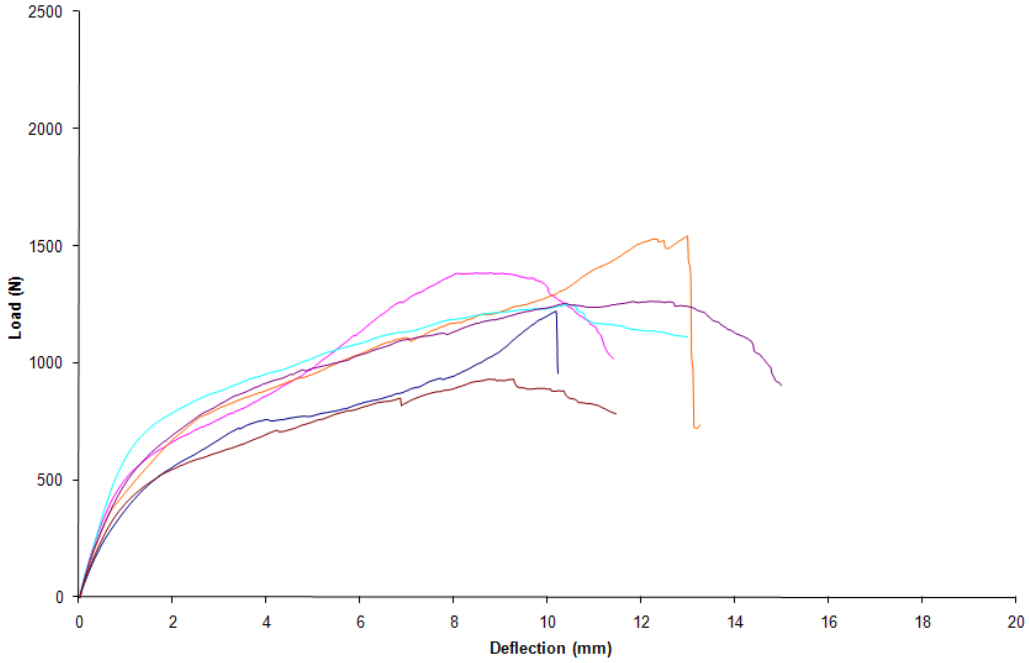

Fig. C36. Load displacement diagram for Plate SSL-OSBH 200^{o}C-2hr

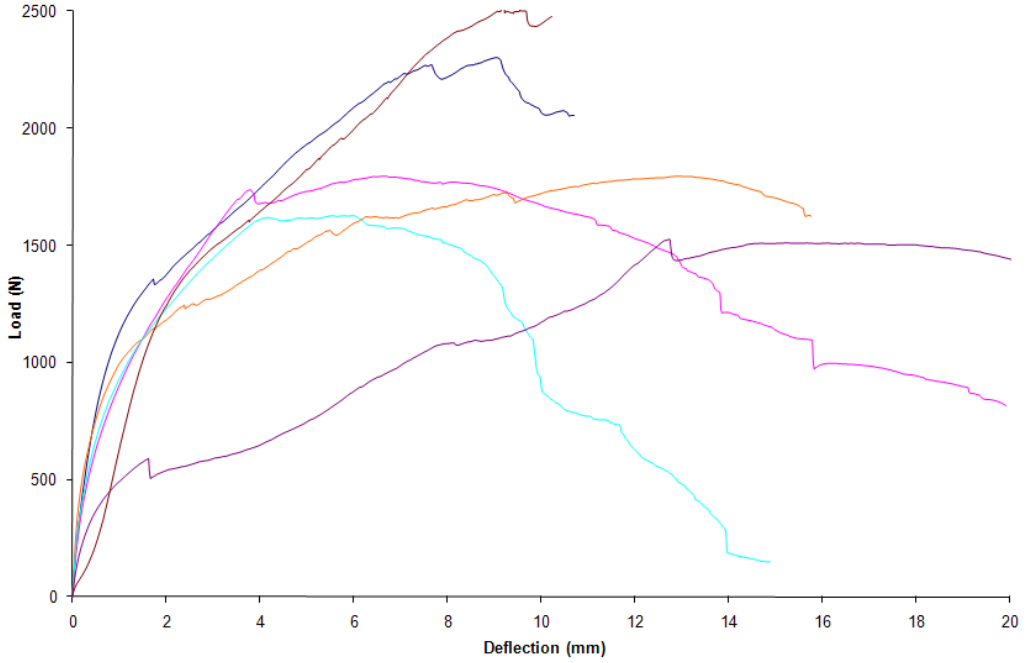

Fig. C37. Load displacement diagram for Plate SSL-PWH Control

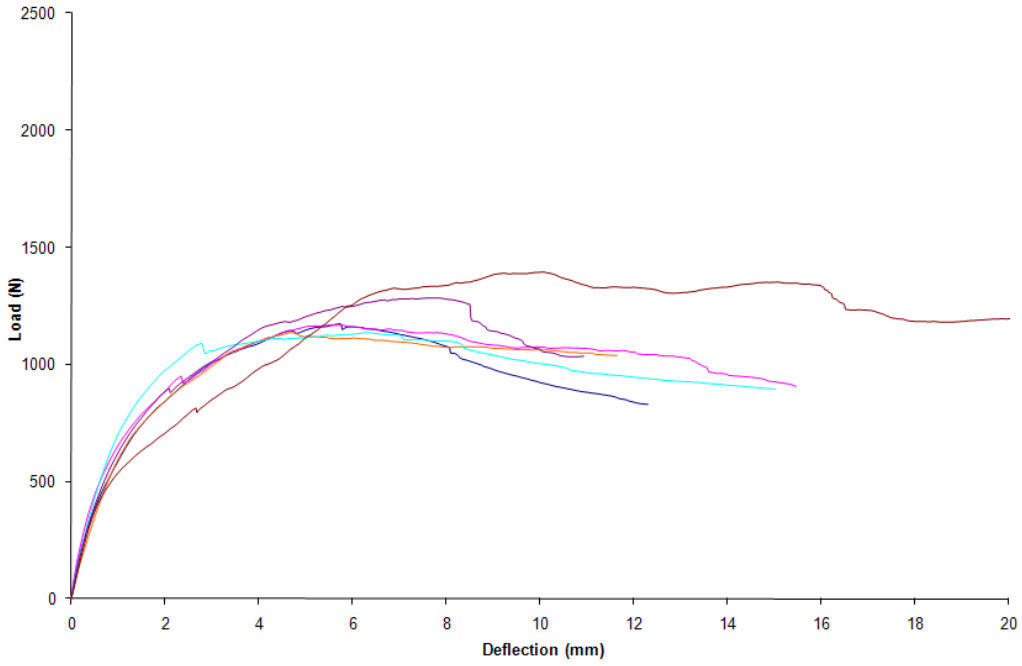

Fig. C38. Load displacement diagram for Plate SSL-PWH 100^{o}C-1hr

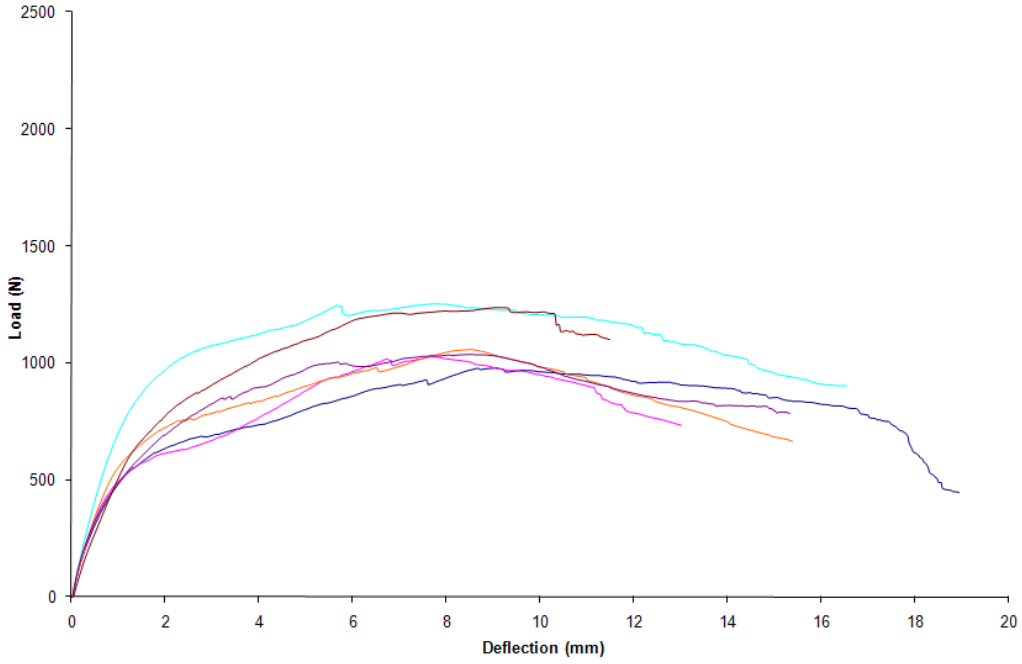

Fig. C39. Load displacement diagram for Plate SSL-PWH 100^{o}C-2hr

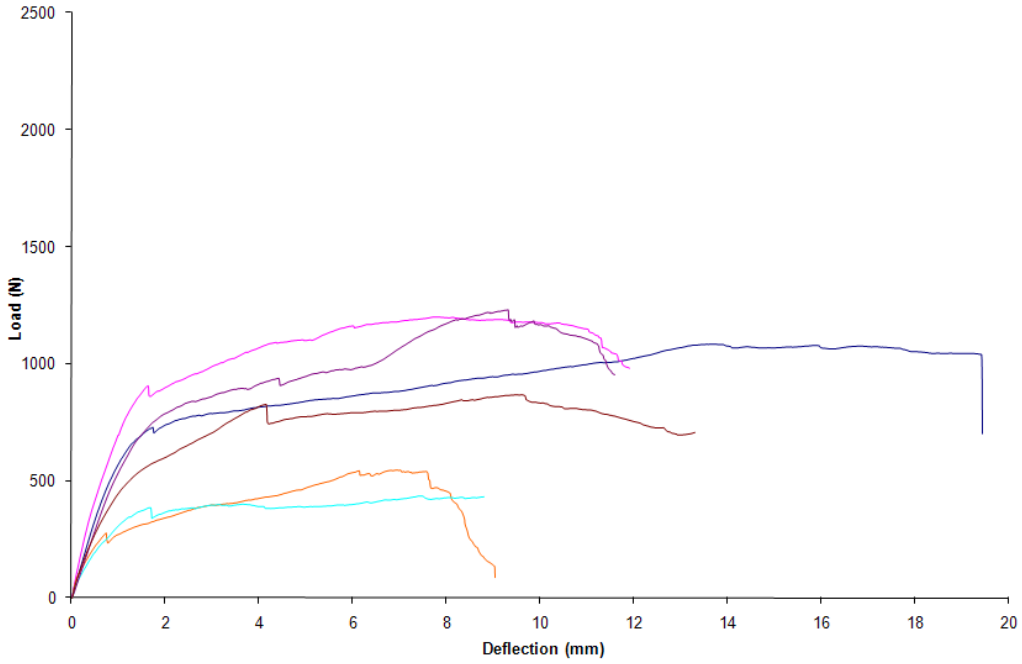

Fig. C40. Load displacement diagram for Plate SSL-PWH 200^{o}C-1hr

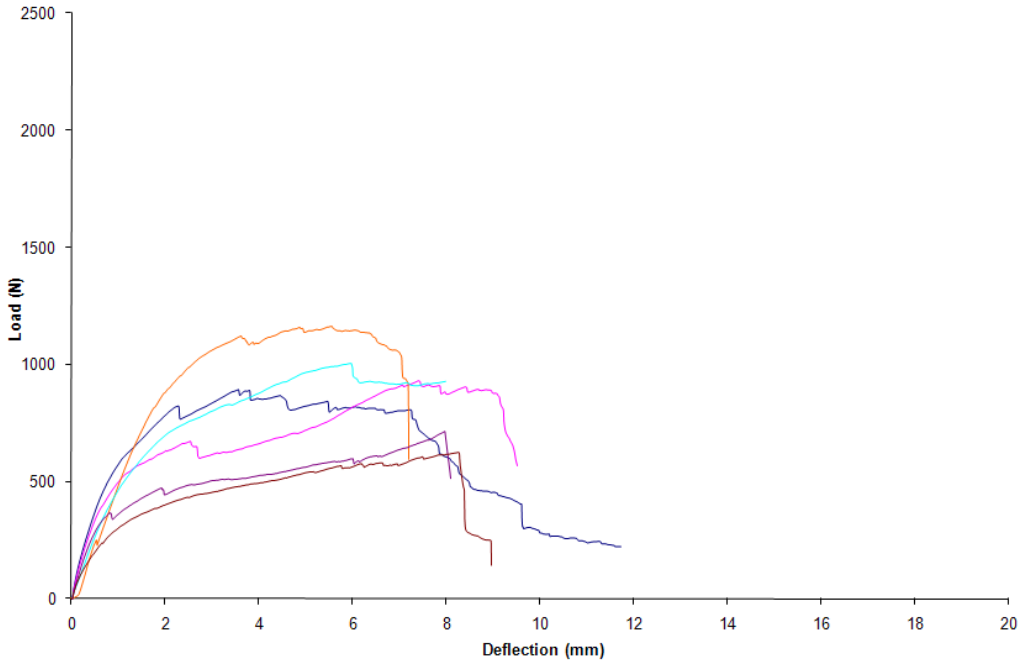

Fig. C41. Load displacement diagram for Plate SSL-PWH 200^{o}C-2hr

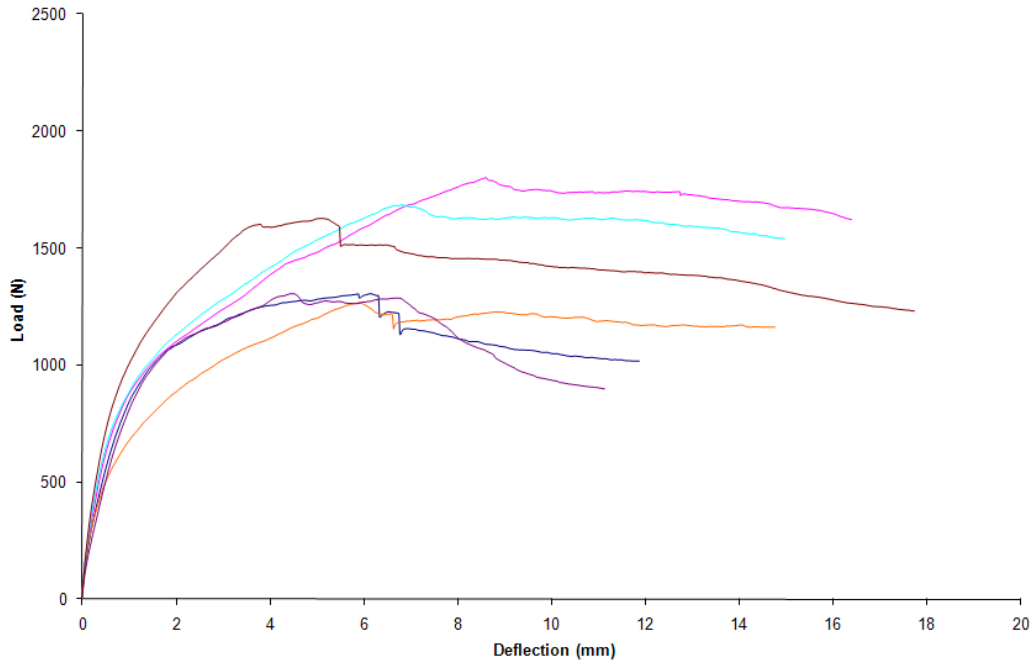

Fig. C42. Load displacement diagram for Edge LVL-OSBO Control

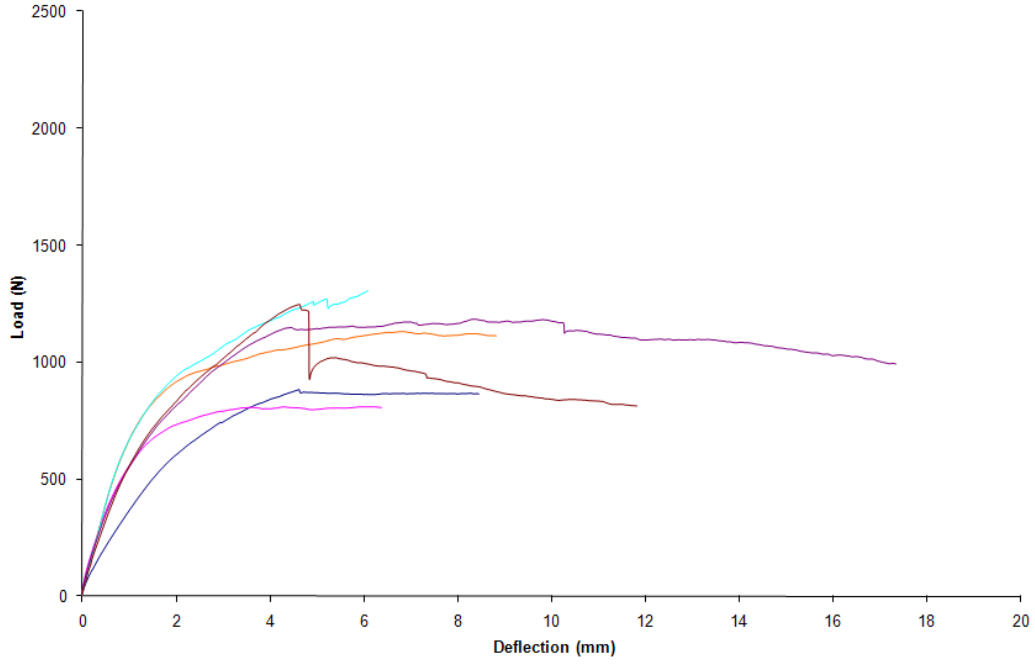

Fig. C43. Load displacement diagram for Edge LVL-OSBO 100^{o}C-1hr

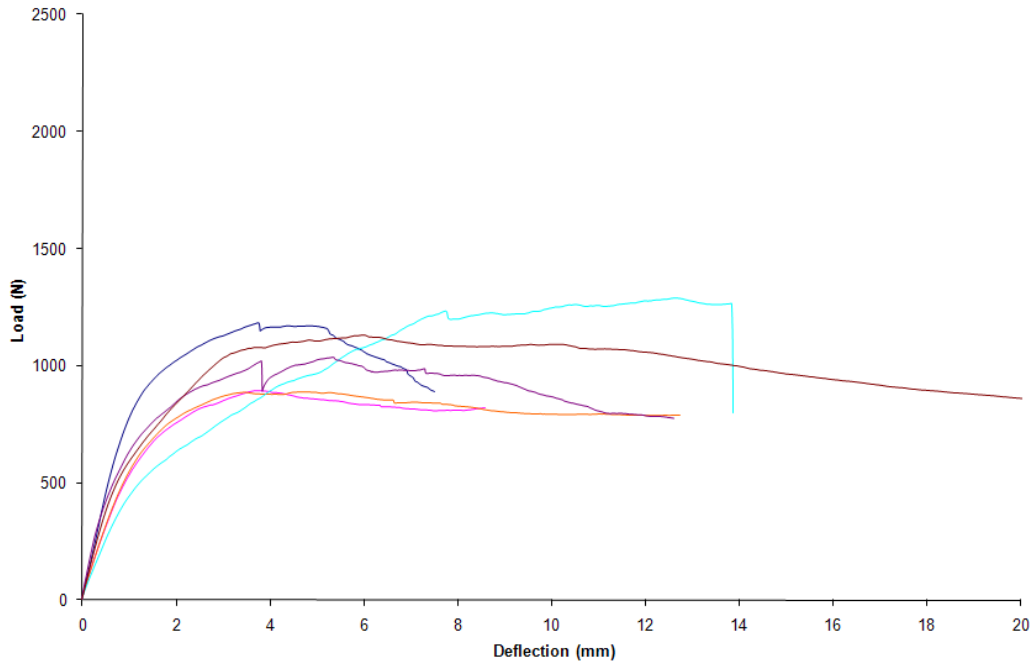

Fig. C44. Load displacement diagram for Edge LVL-OSBO 100^{o}C-2hr

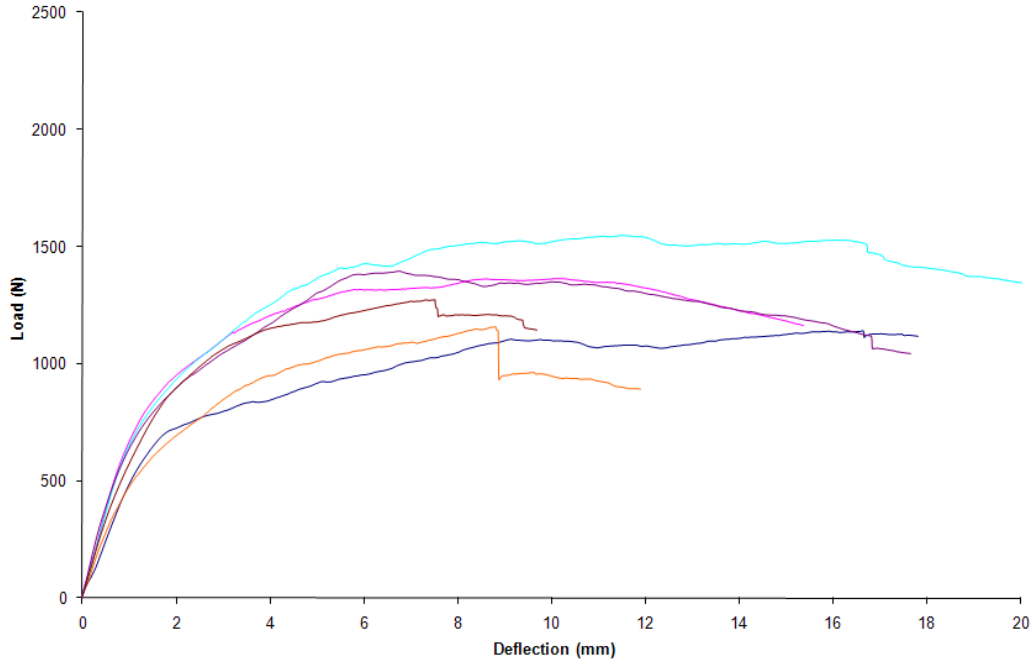

Fig. C45. Load displacement diagram for Edge LVL-OSBO 200^{o}C-1hr

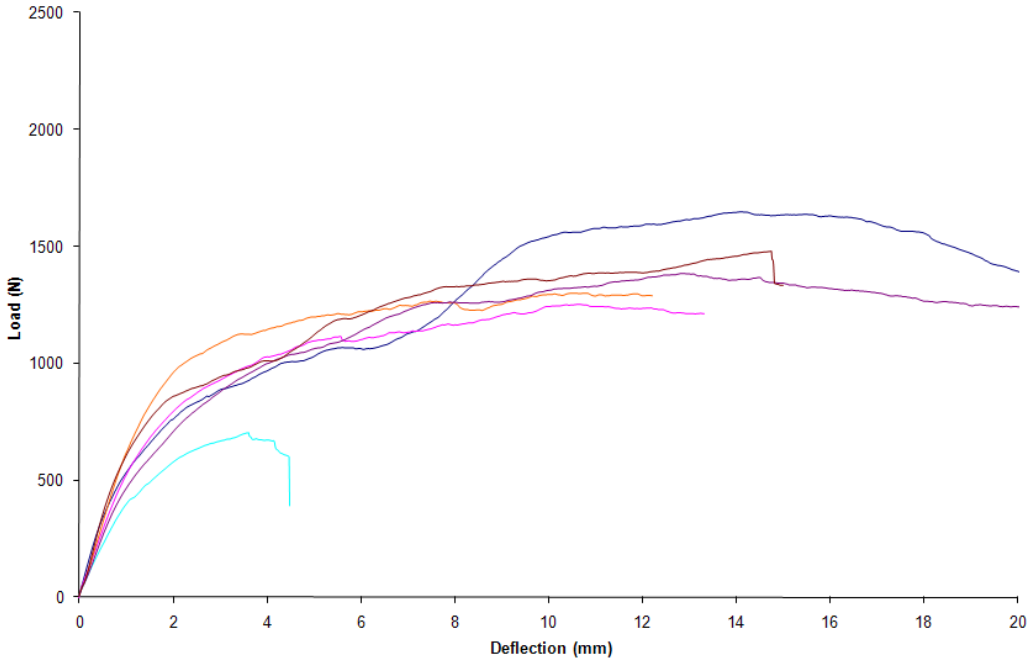

Fig. C46. Load displacement diagram for Edge LVL-OSBO 200^{o}C-2hr

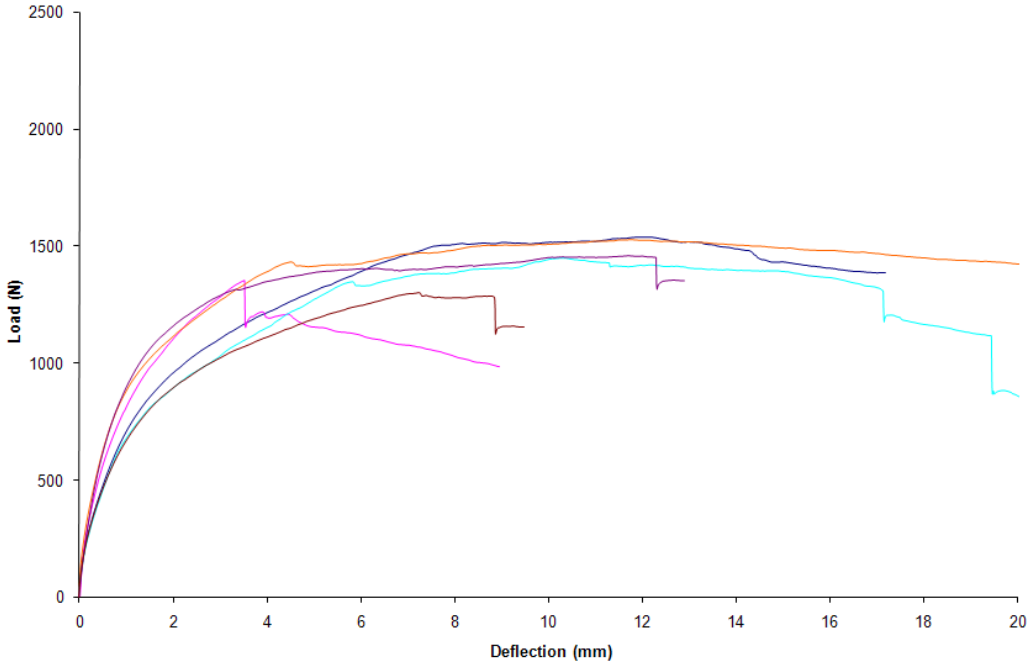

Fig. C47. Load displacement diagram for Edge LVL-PWO Control

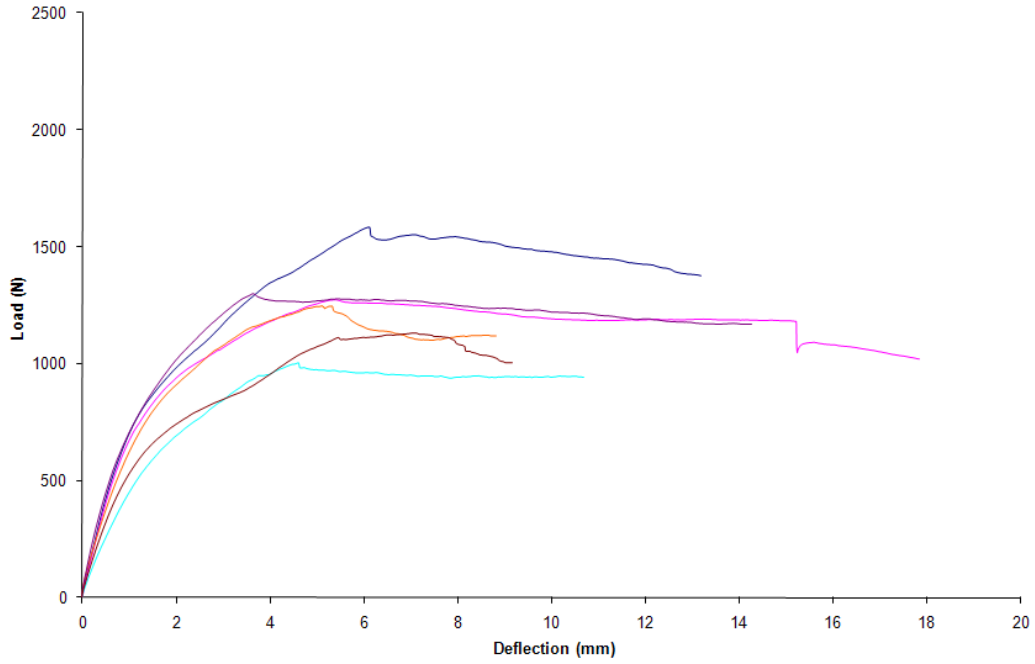

Fig. C48. Load displacement diagram for Edge LVL-PWO 100^{o}C-1hr

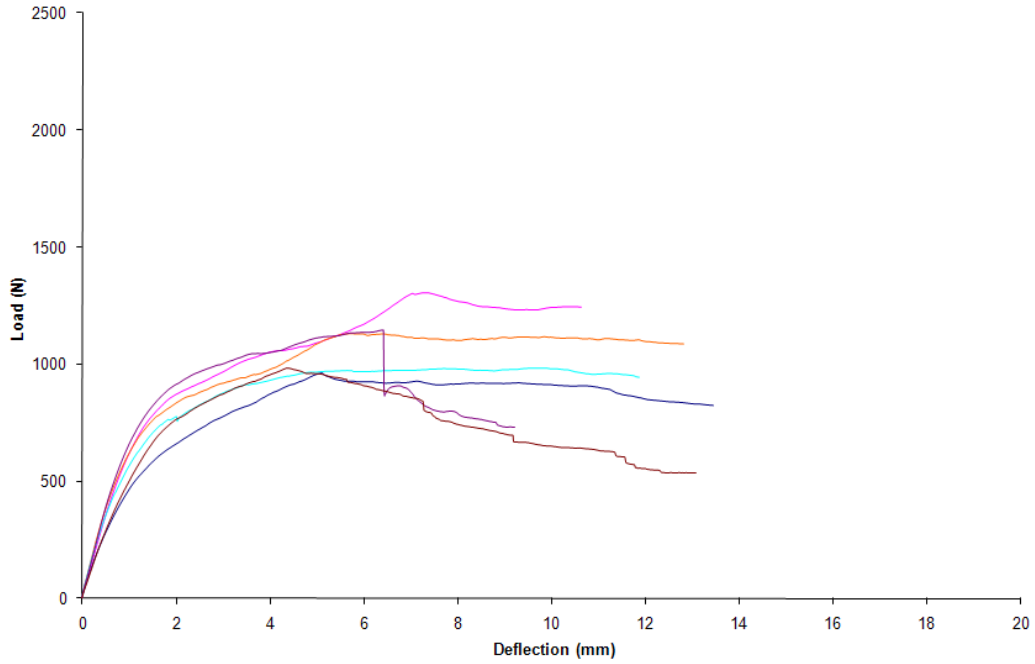

Fig. C49. Load displacement diagram for Edge LVL-PWO 100^{o}C-2hr

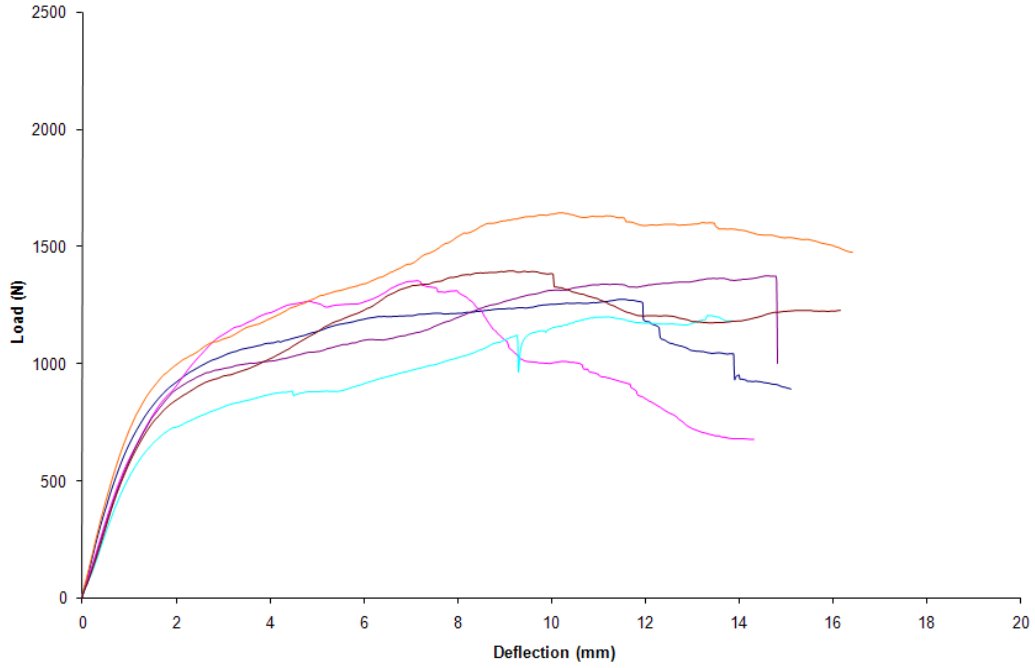

Fig. C50. Load displacement diagram for Edge LVL-PWO 200^{o}C-1hr

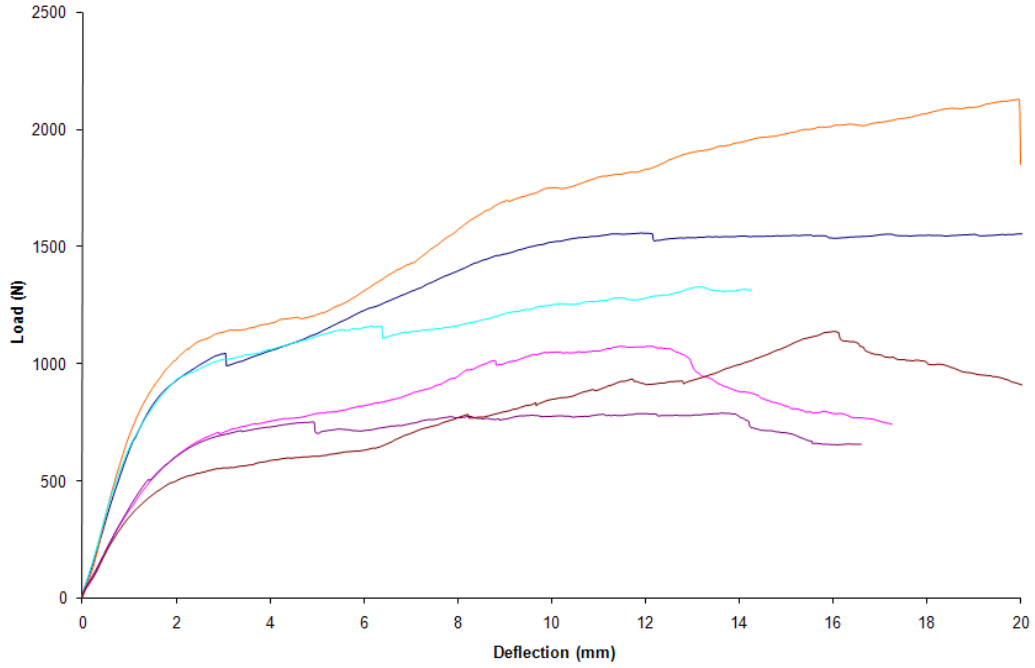

Fig. C51. Load displacement diagram for Edge LVL-PWO 200^{o}C-2hr

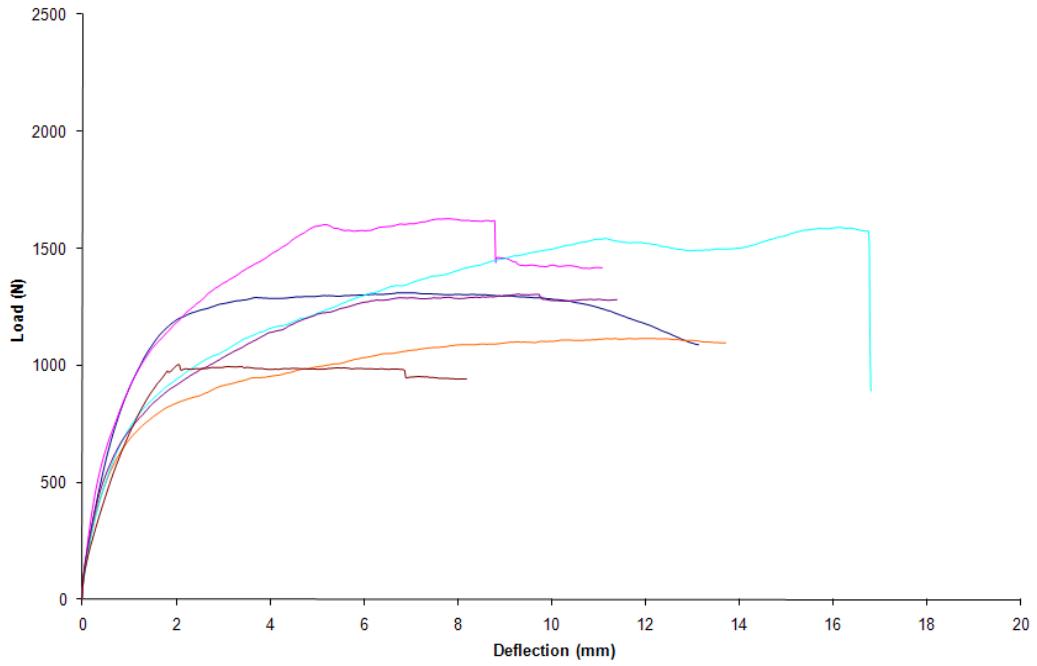

Fig. C52. Load displacement diagram for Edge LVL-OSBH Control

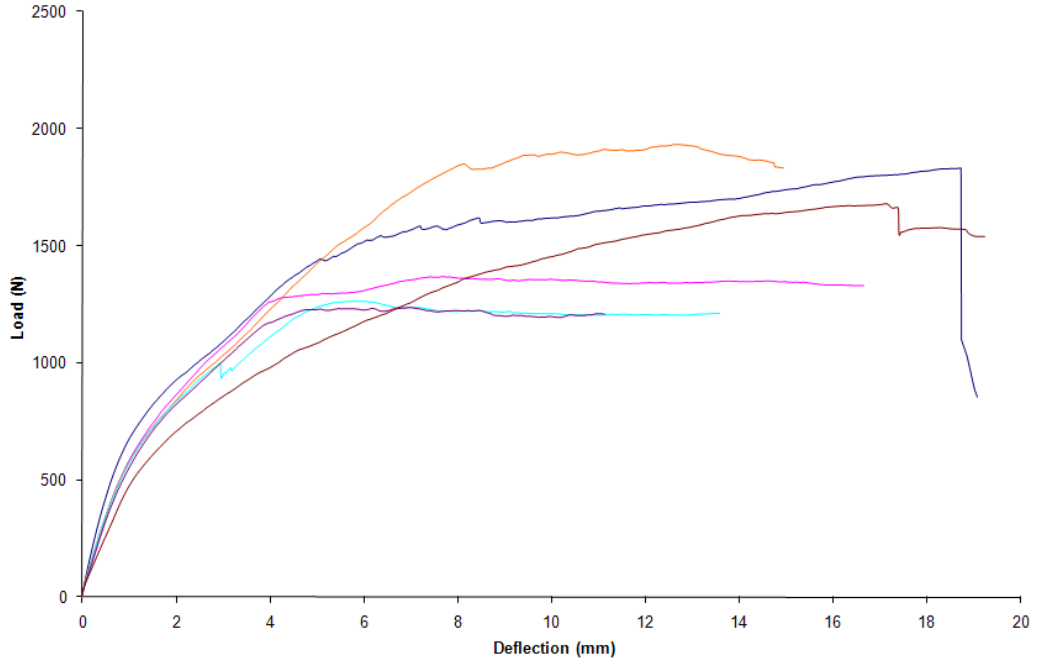

Fig. C53. Load displacement diagram for Edge LVL-OSBH 100^{o}C-1hr

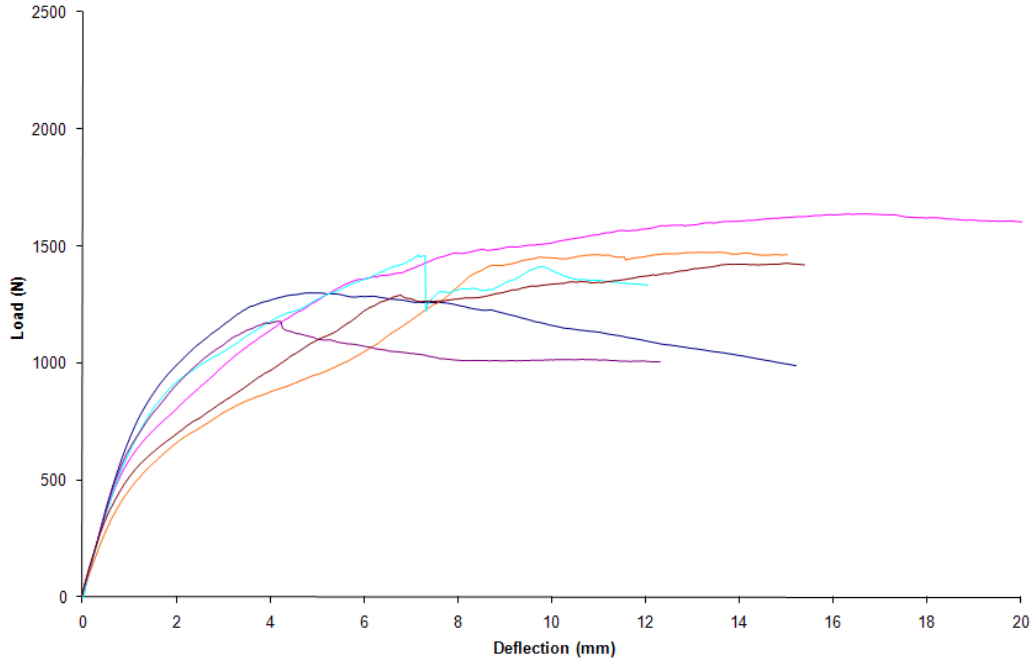

Fig. C54. Load displacement diagram for Edge LVL-OSBH 100^{o}C-2hr

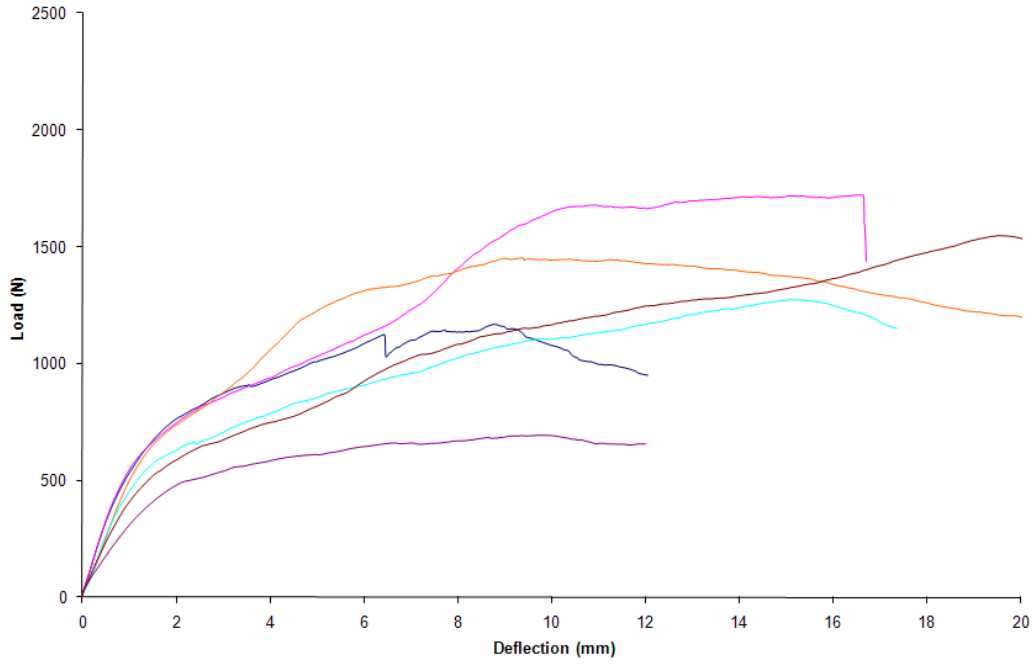

Fig. C55. Load displacement diagram for Edge LVL-OSBH 200^{o}C-1hr

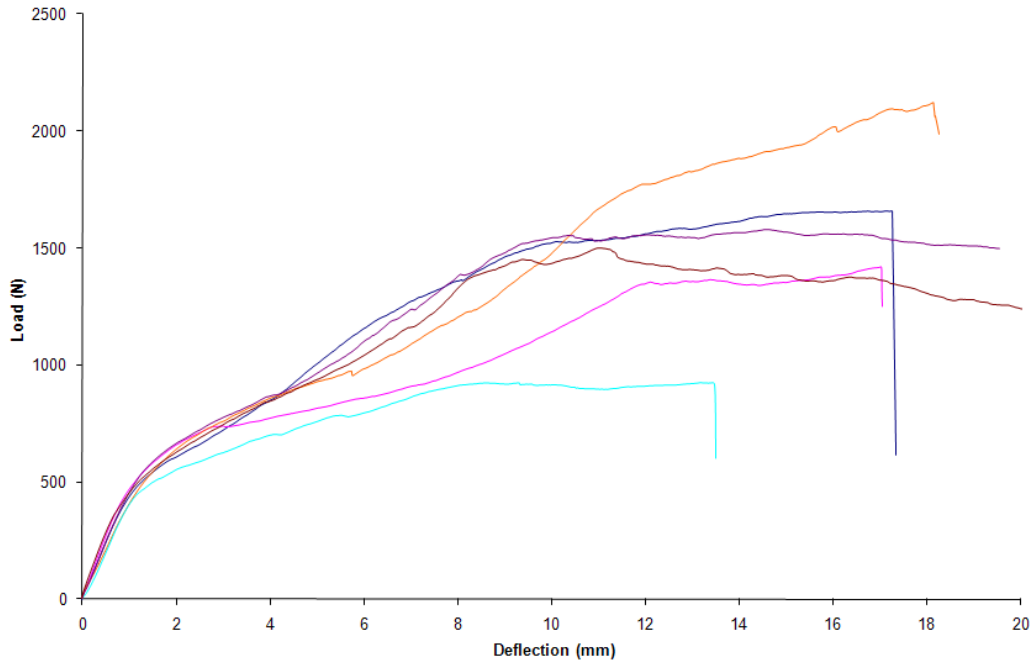

Fig. C56. Load displacement diagram for Edge LVL-OSBH 200^{o}C-2hr

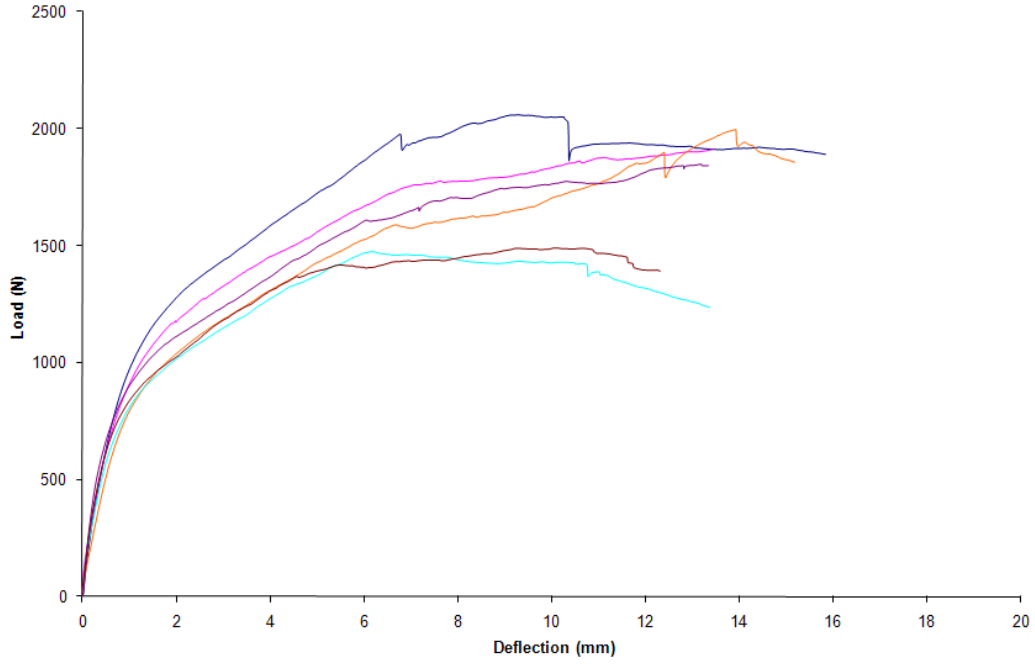

Fig. C57. Load displacement diagram for Edge LVL-PWH Control

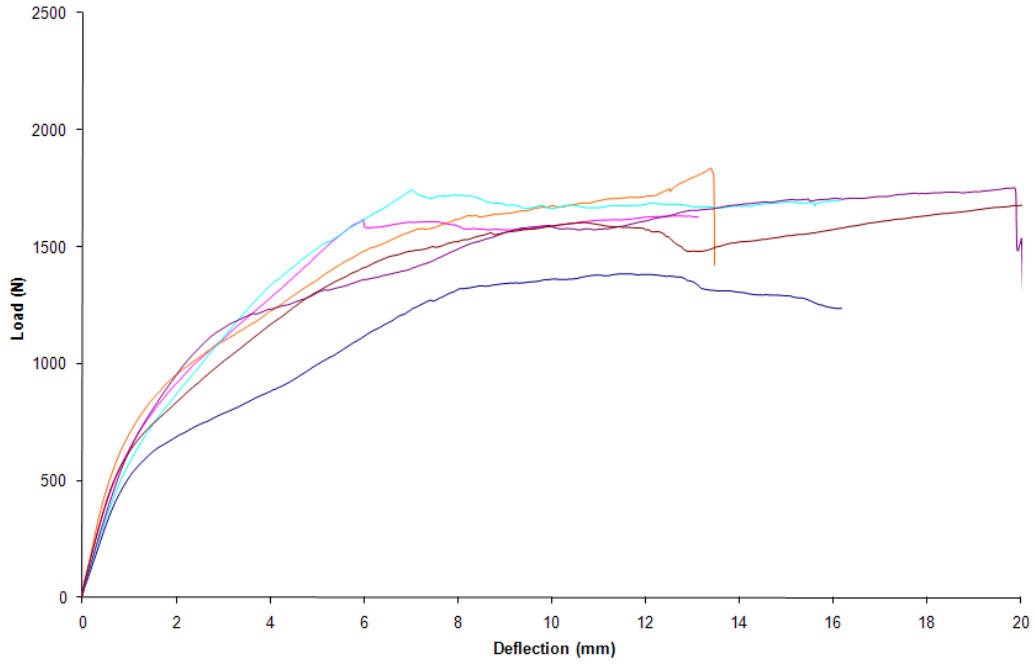

Fig. C58. Load displacement diagram for Edge LVL-PWH 100^{o}C-1hr

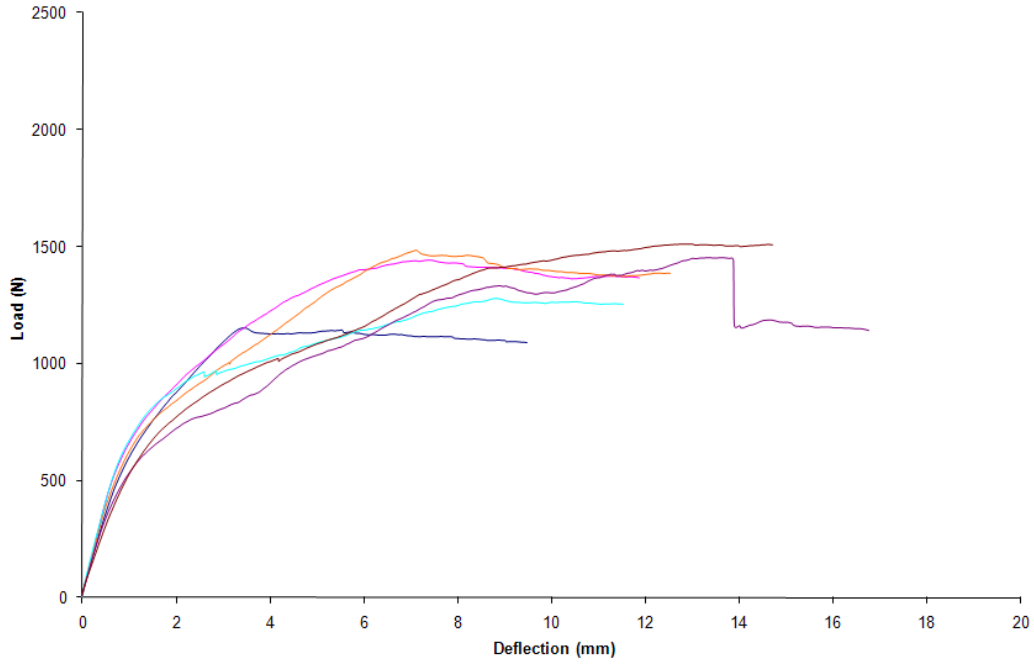

Fig. C59. Load displacement diagram for Edge LVL-PWH 100^{o}C-2hr

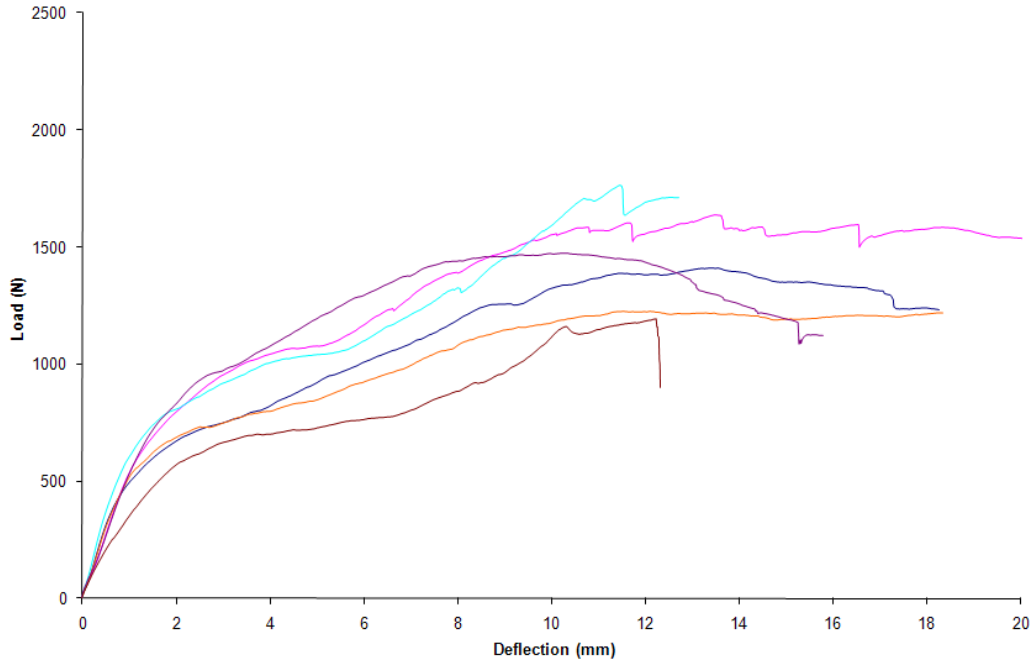

Fig. C60. Load displacement diagram for Edge LVL-PWH 200^{o}C-1hr

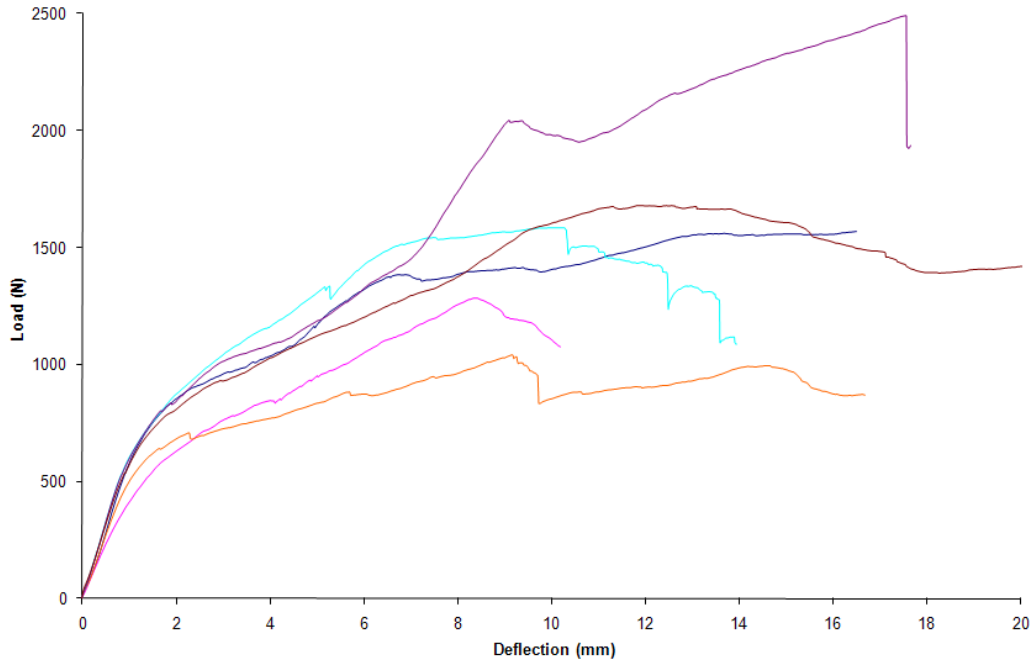

Fig. C61. Load displacement diagram for Edge LVL-PWH 200^{o}C-2hr

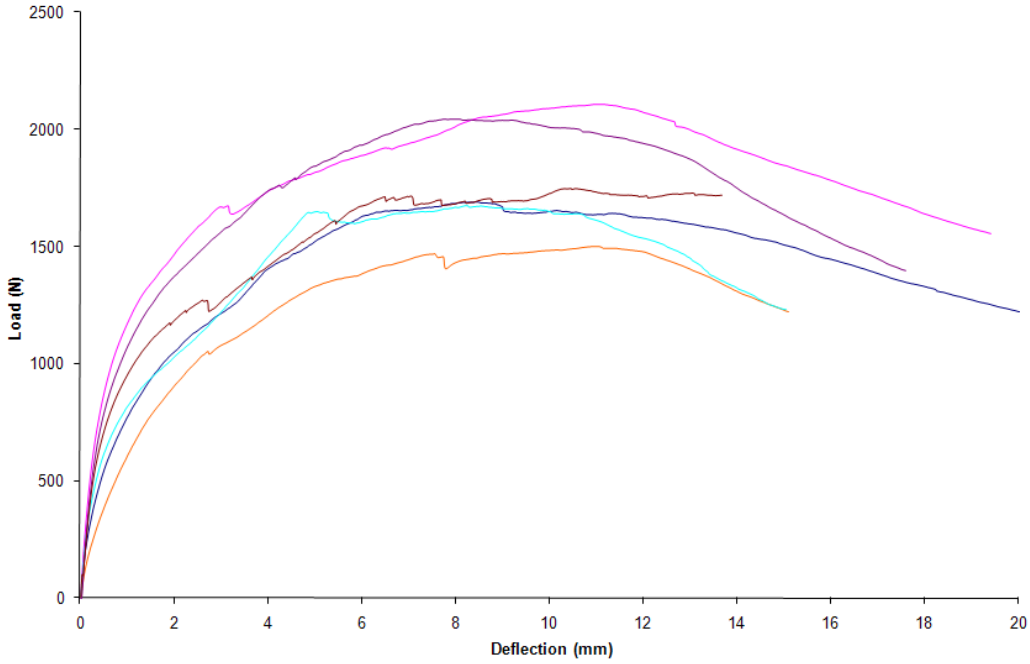

Fig. C62. Load displacement diagram for Plate LVL-OSBO Control

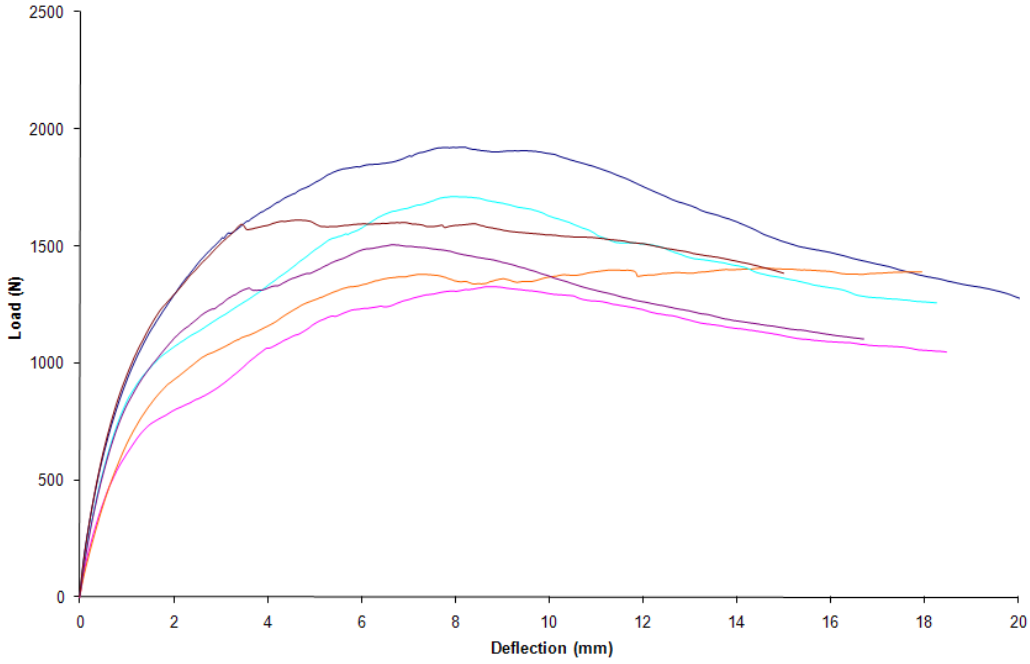

Fig. C63. Load displacement diagram for Plate LVL-OSBO 100^{o}C-1hr

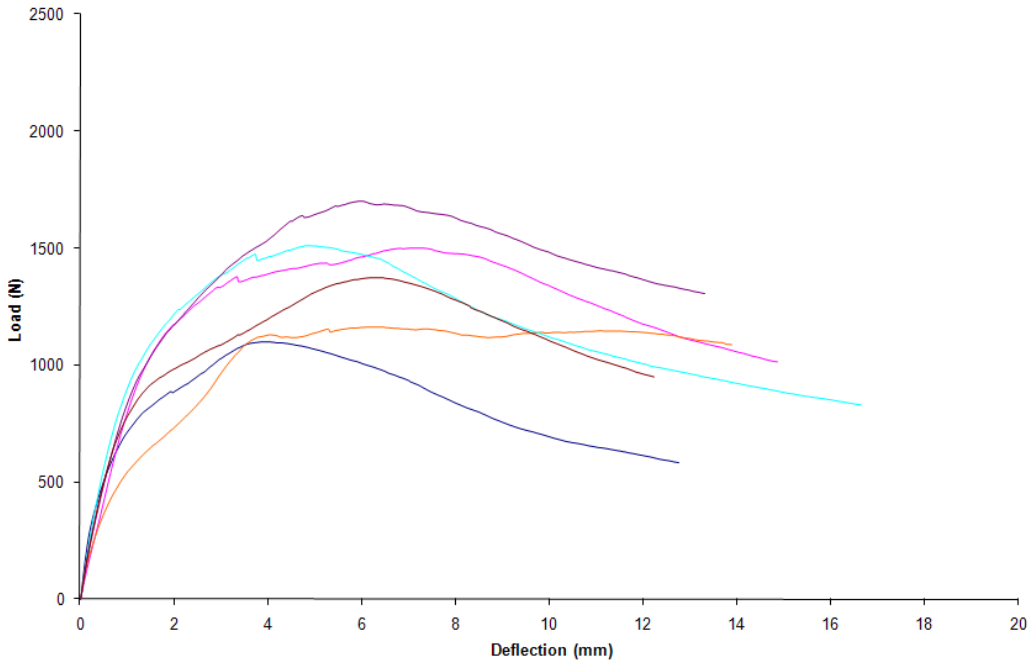

Fig. C64. Load displacement diagram for Plate LVL-OSBO 100^{o}C-2hr

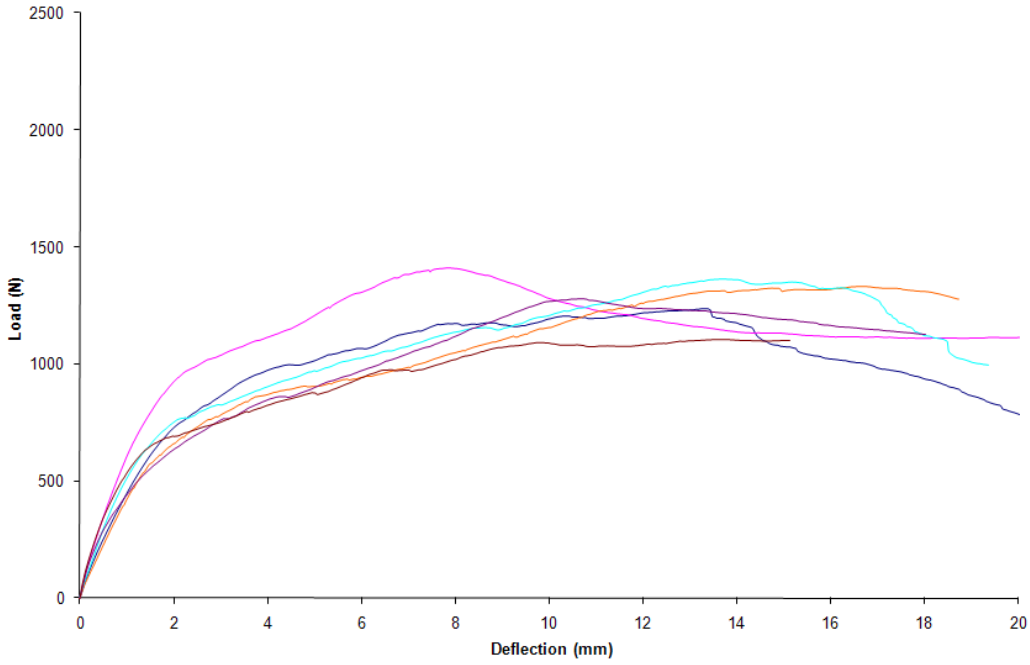

Fig. C65. Load displacement diagram for Plate LVL-OSBO 200^{o}C-1hr

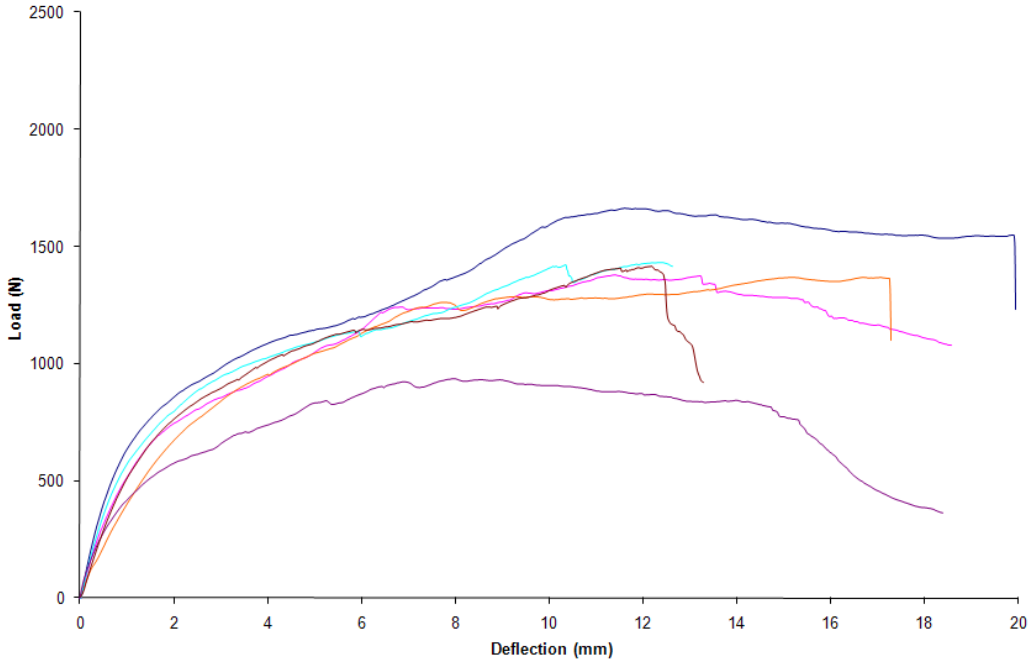

Fig. C66. Load displacement diagram for Plate LVL-OSBO 200^{o}C-2hr

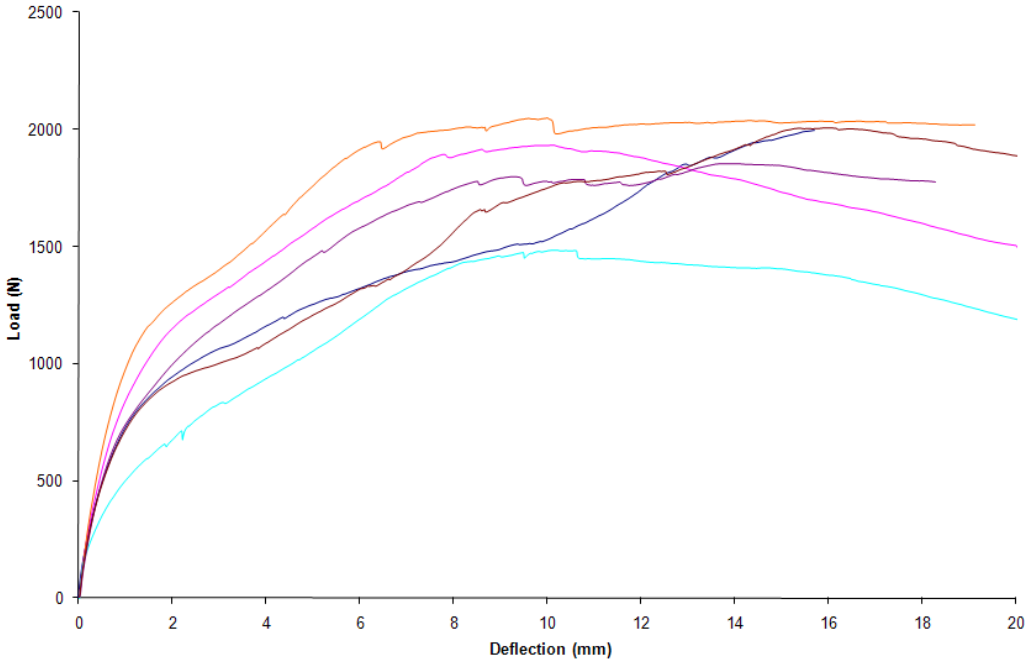

Fig. C67. Load displacement diagram for Plate LVL-PWO Control

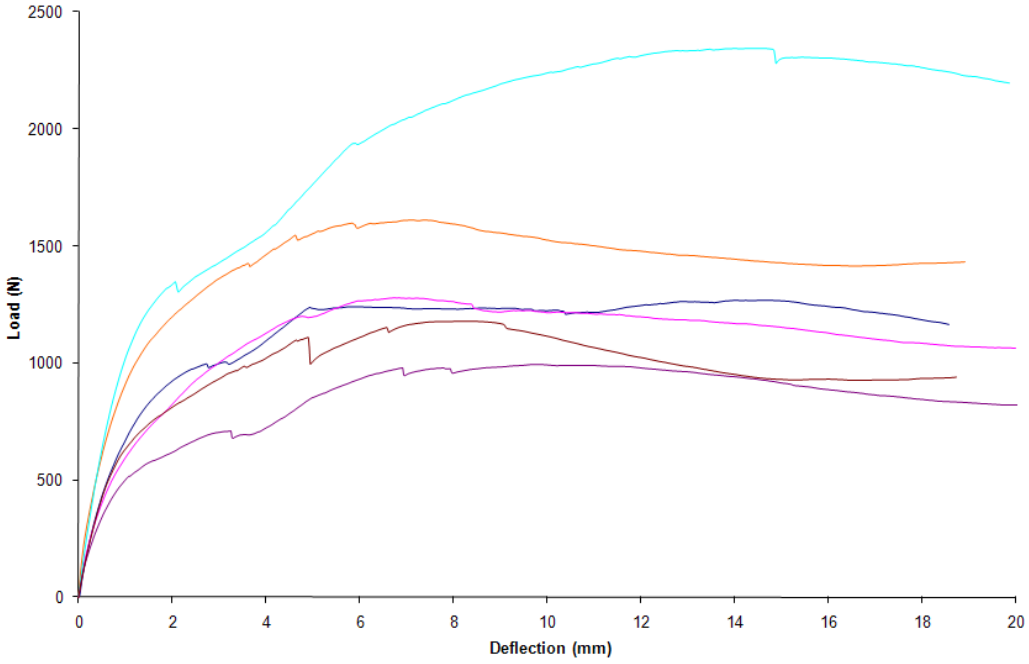

Fig. C68. Load displacement diagram for Plate LVL-PWO 100^{o}C-1hr

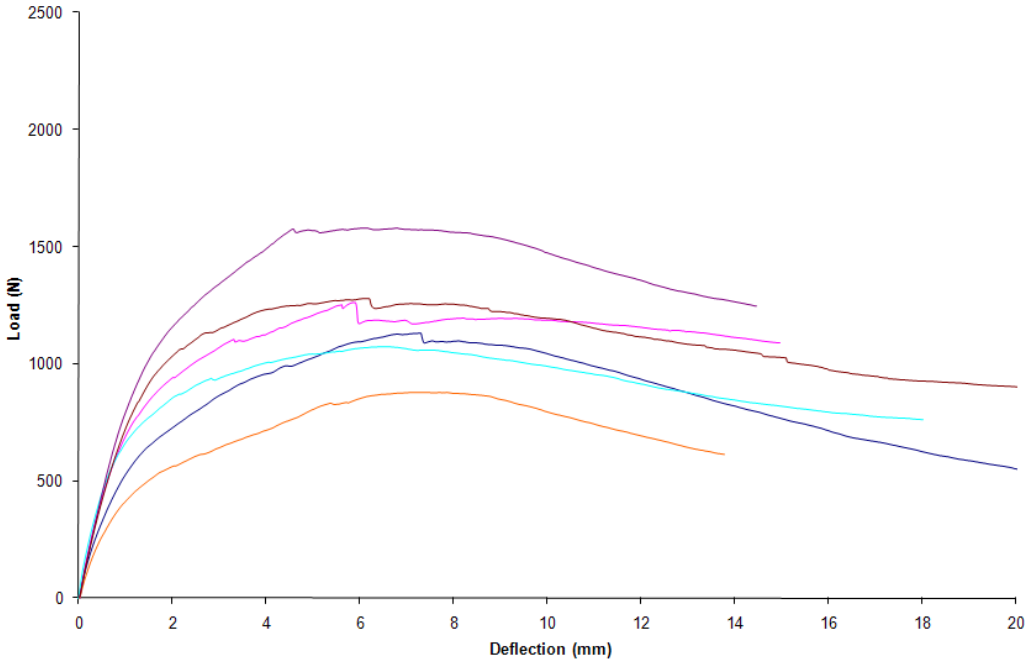

Fig. C69. Load displacement diagram for Plate LVL-PWO 100^{o}C-2hr

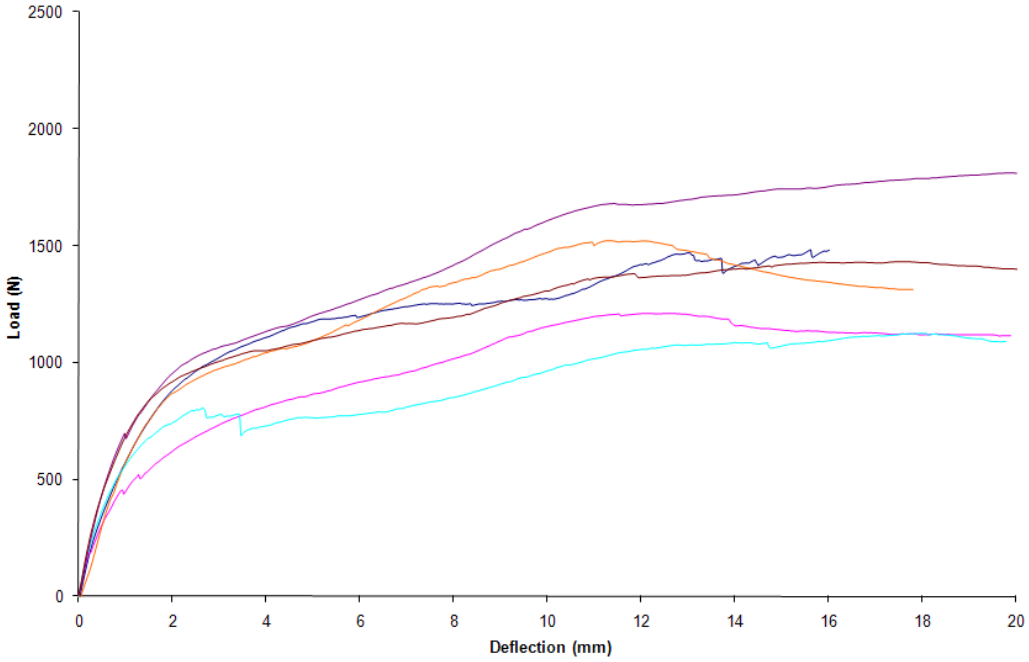

Fig. C70. Load displacement diagram for Plate LVL-PWO 200^{o}C-1hr

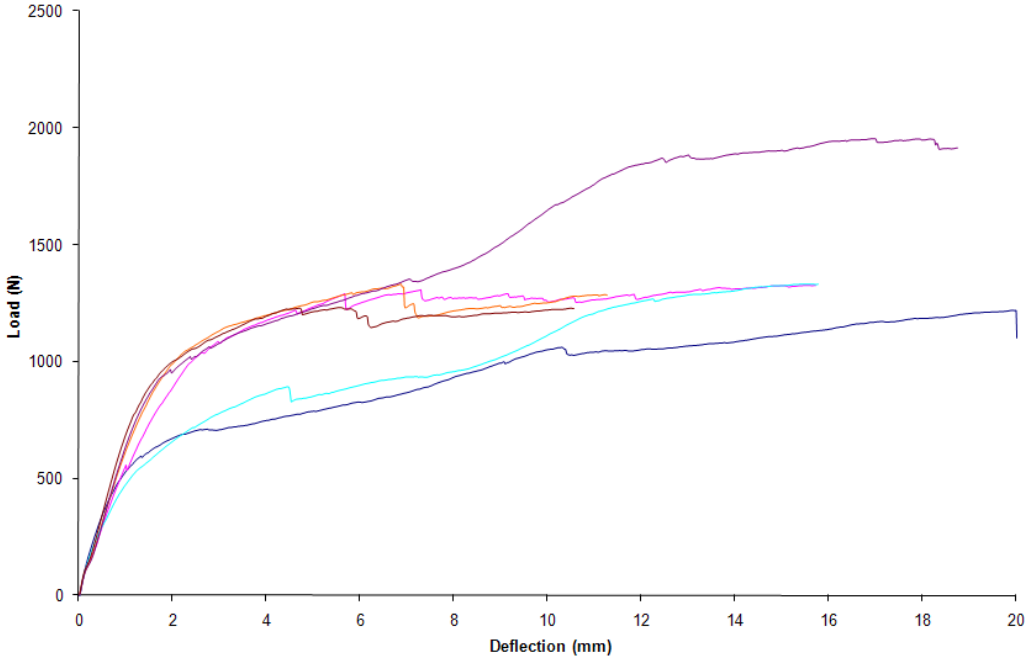

Fig. C71. Load displacement diagram for Plate LVL-PWO 200^{o}C-2hr

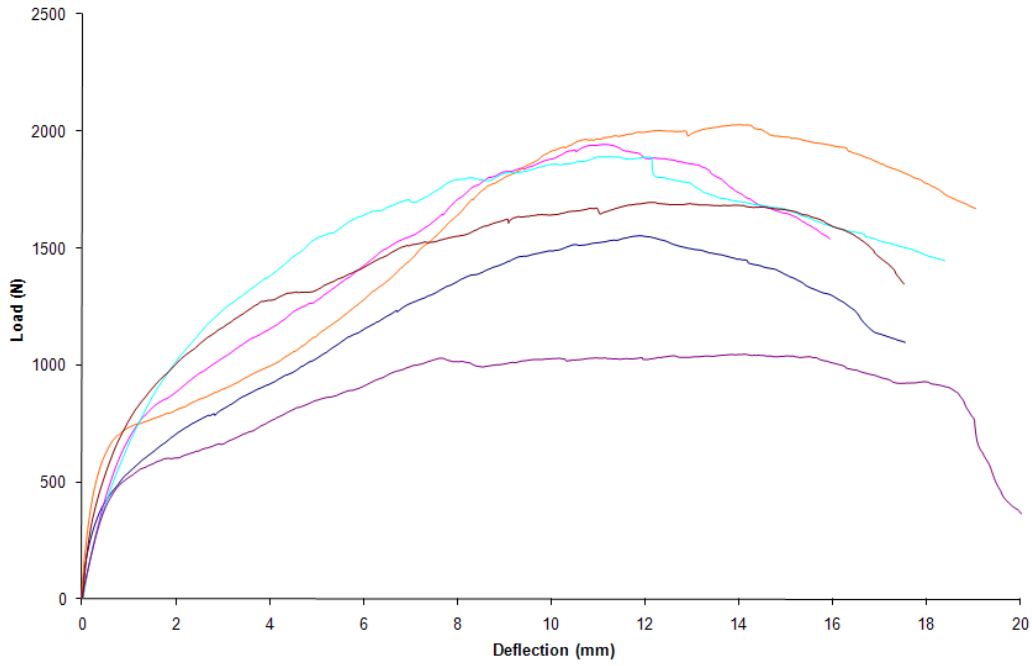

Fig. C72. Load displacement diagram for Plate LVL-OSBH Control

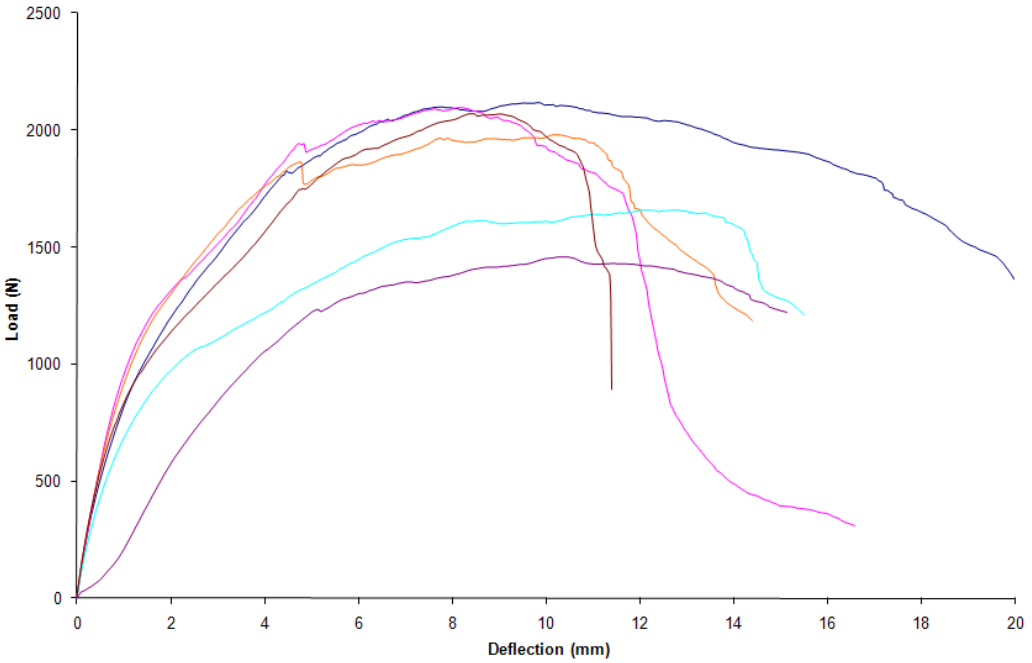

Fig. C73. Load displacement diagram for Plate LVL-OSBH 100^{o}C-1hr

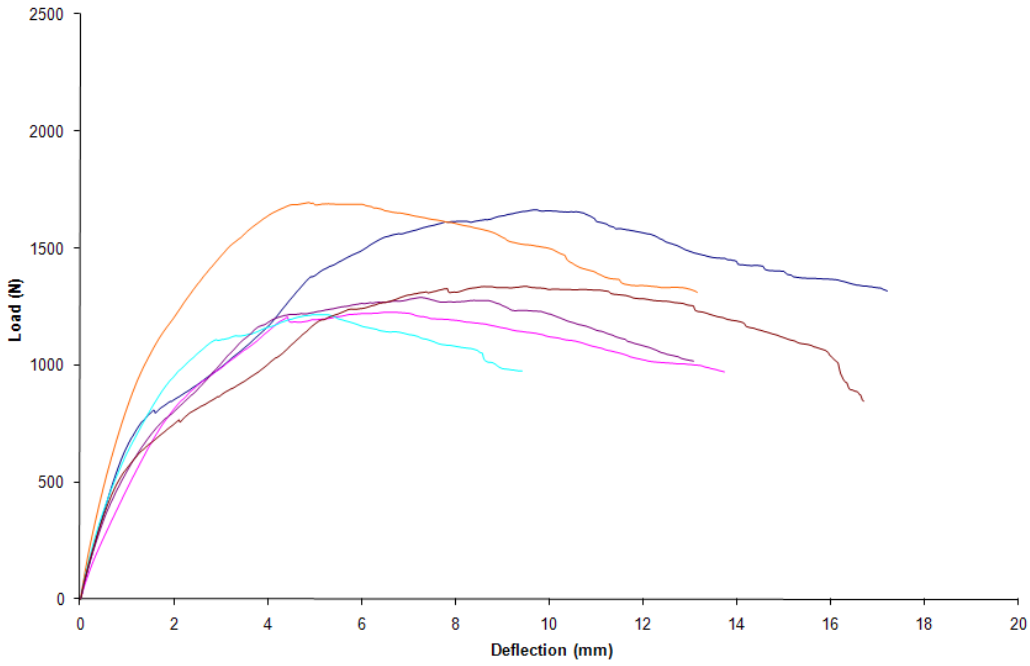

Fig. C74. Load displacement diagram for Plate LVL-OSBH 100^{o}C-2hr

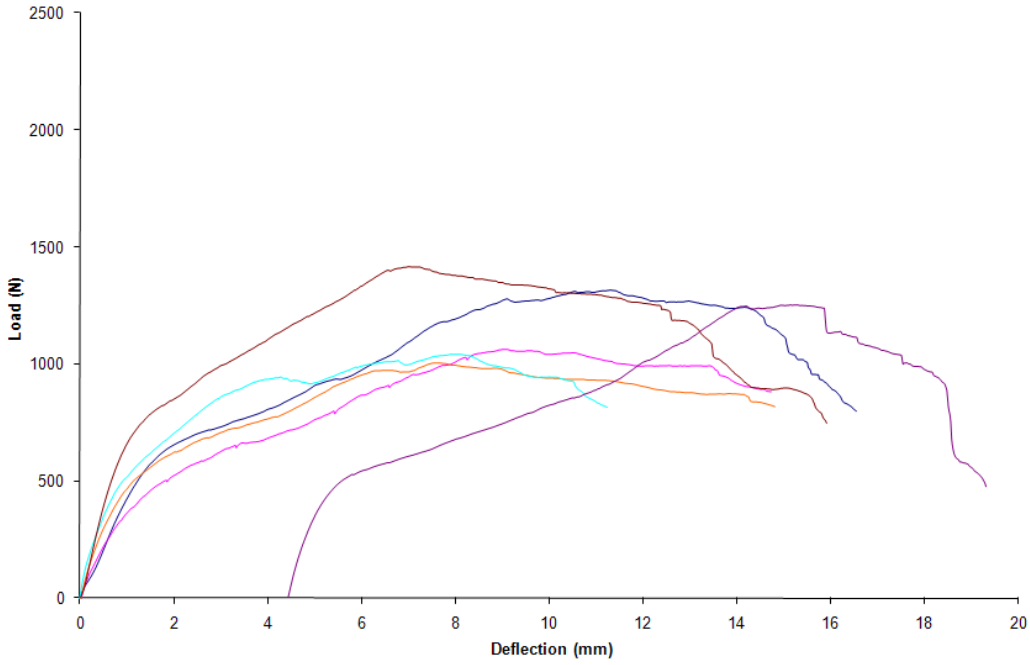

Fig. C75. Load displacement diagram for Plate LVL-OSBH 200^{o}C-1hr

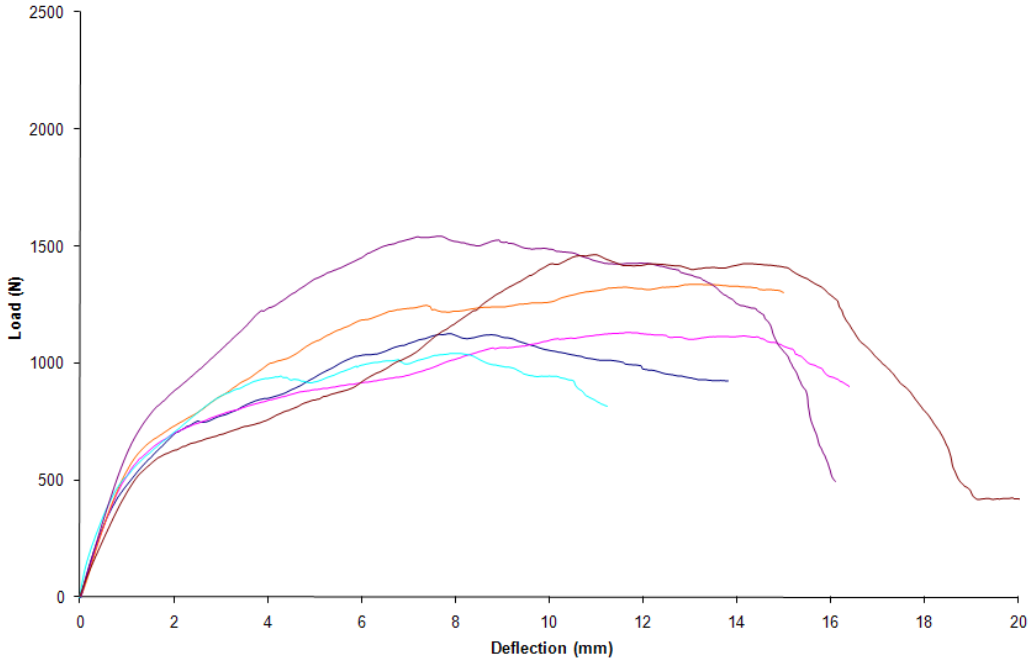

Fig. C76. Load displacement diagram for Plate LVL-OSBH 200^{o}C-2hr

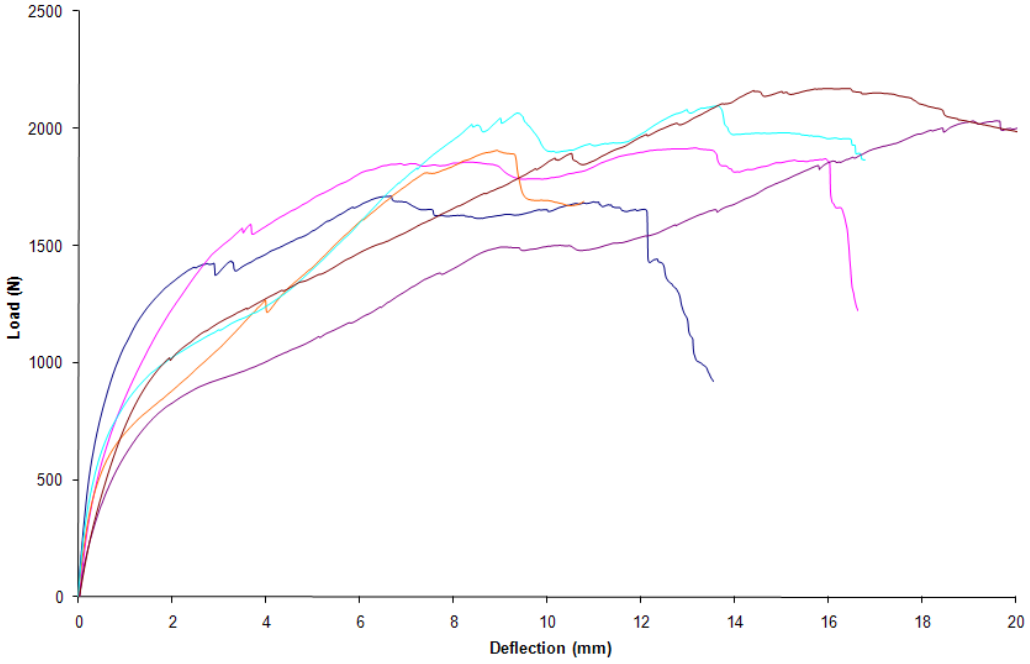

Fig. C78. Load displacement diagram for Plate LVL-PWH Control

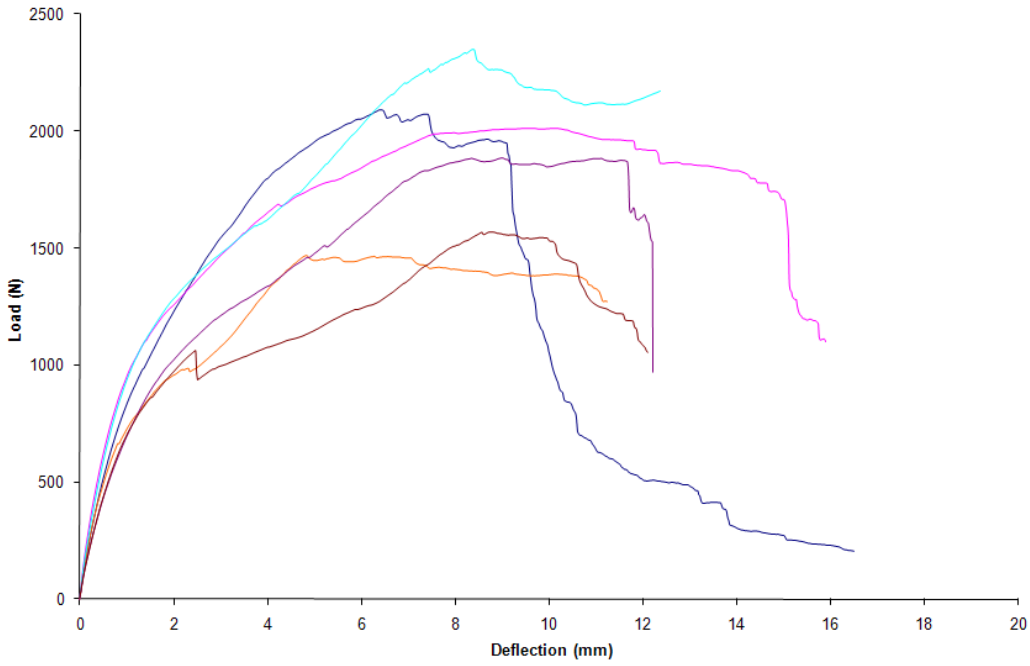

Fig. C78. Load displacement diagram for Plate LVL-PWH 100^{o}C-1hr

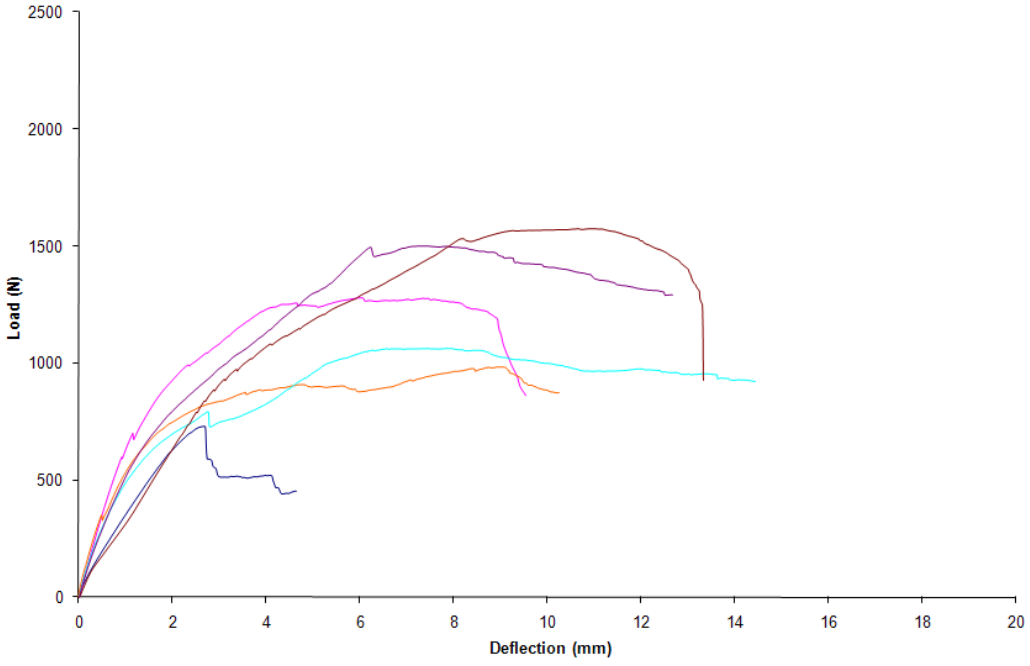

Fig. C79. Load displacement diagram for Plate LVL-PWH 100^{o}C-2hr

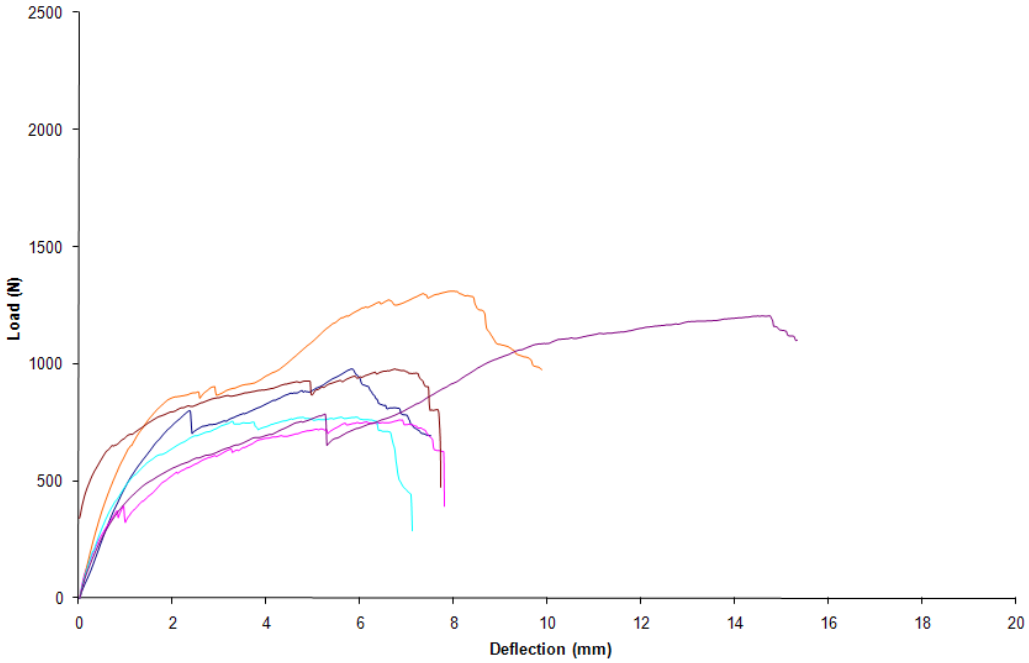

Fig. C80. Load displacement diagram for Plate LVL-PWH 200^{o}C-1hr

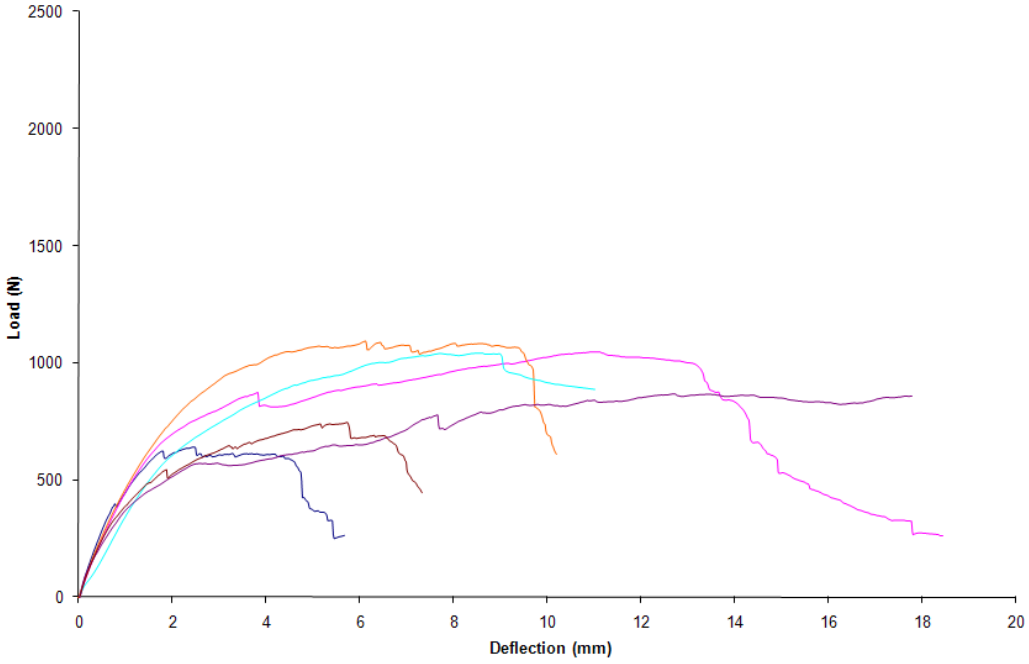

Fig. C81. Load displacement diagram for Plate LVL-PWH 200^{o}C-2hr

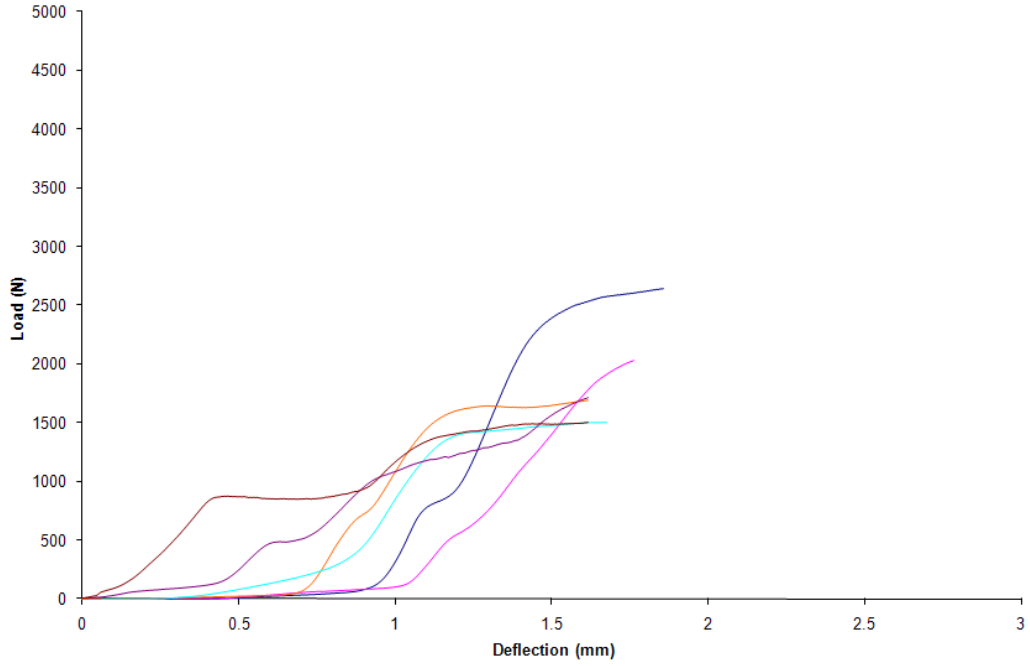

Fig. C82. Dowel Bearing load deflection diagram for OSBH Control

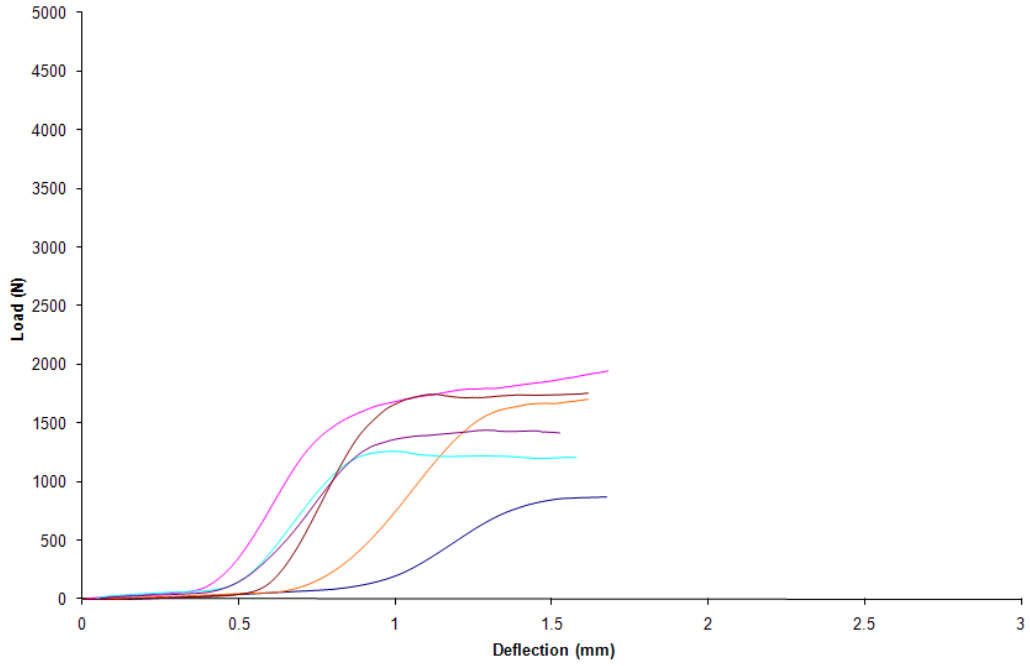

Fig. C83. Dowel Bearing load deflection diagram for OSBH 100^{o}C – 1hr

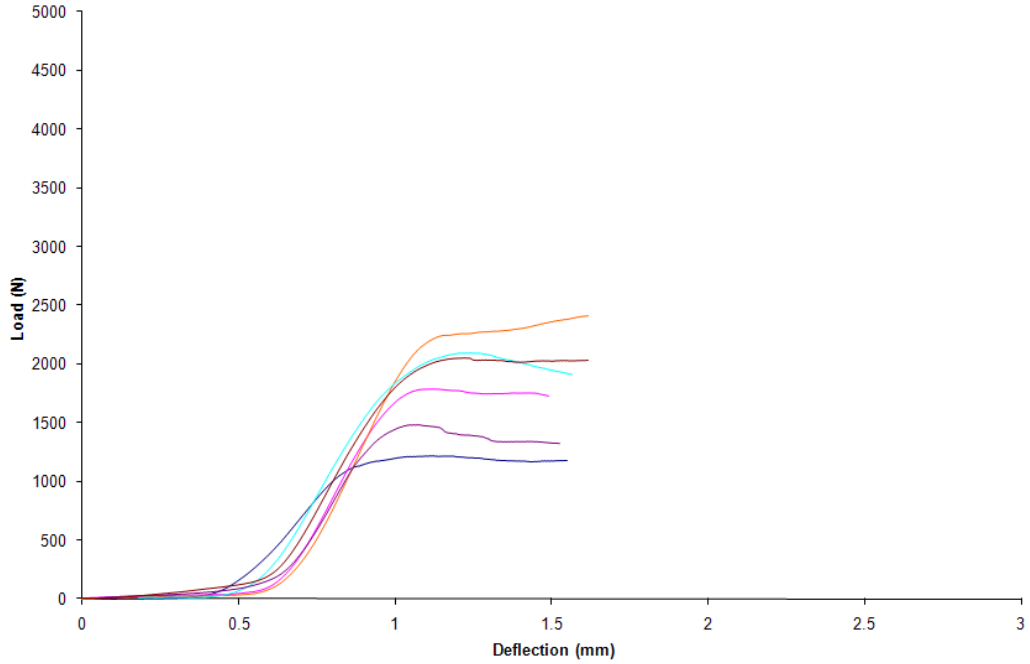

Fig. C84. Dowel Bearing load deflection diagram for OSBH 100°C – 2hr

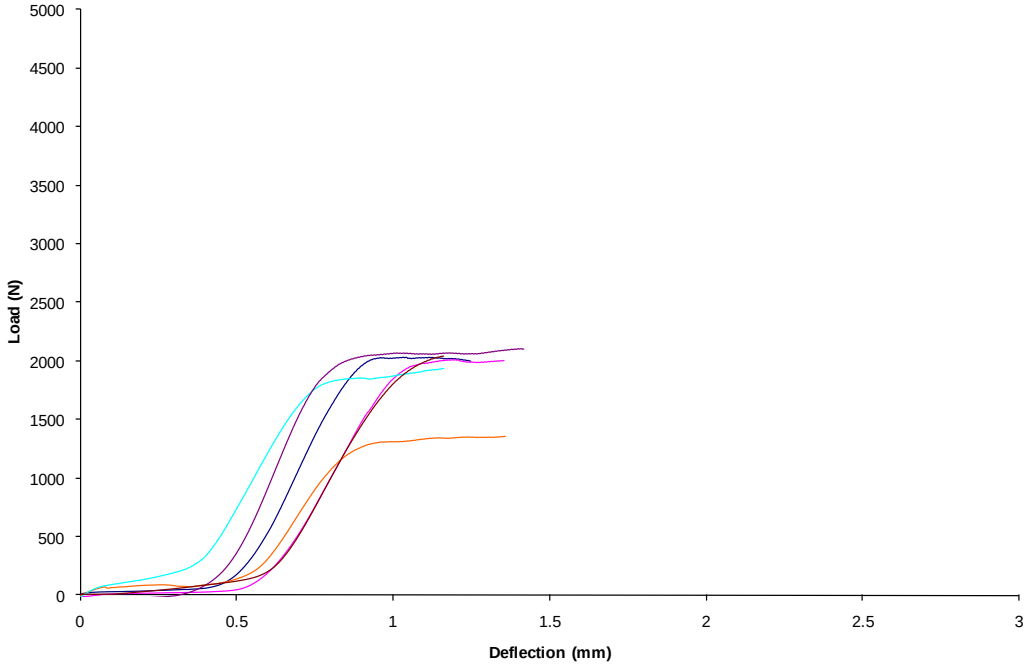

Fig. C85. Dowel Bearing load deflection diagram for OSBH 200°C – 1hr

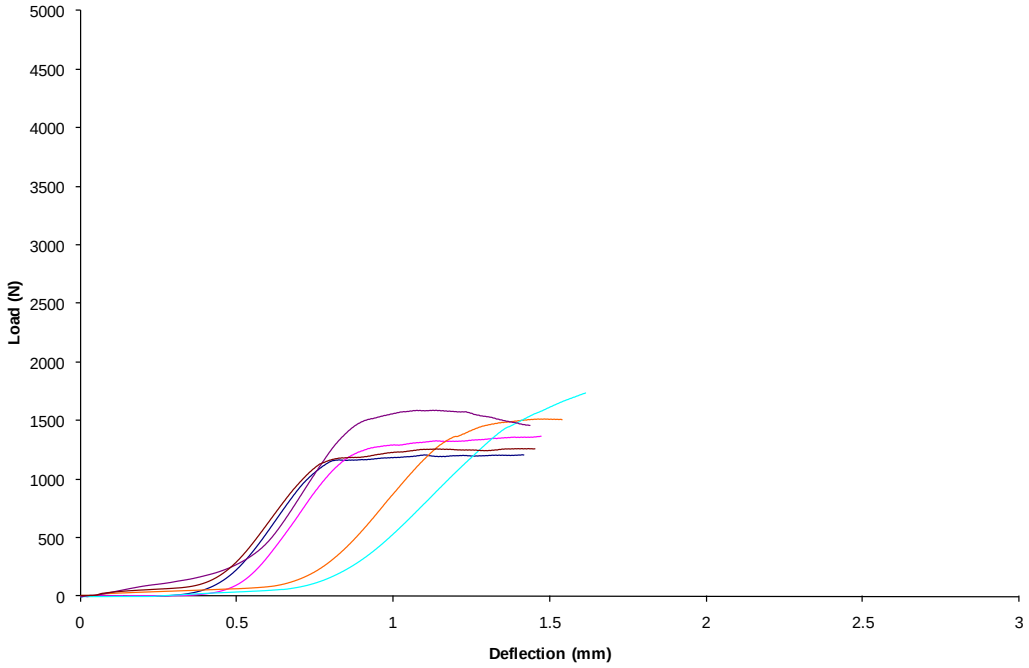

Fig. C86. Dowel Bearing load deflection diagram for OSBH 200^{o}C – 2hr

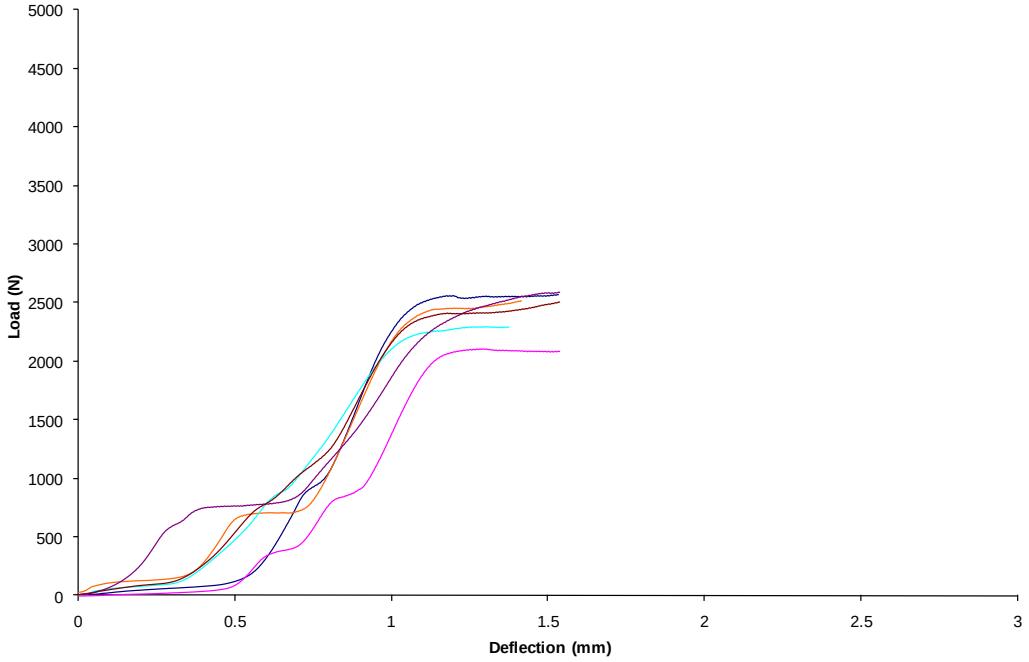

Fig. C87. Dowel Bearing load deflection diagram for OSBO Control

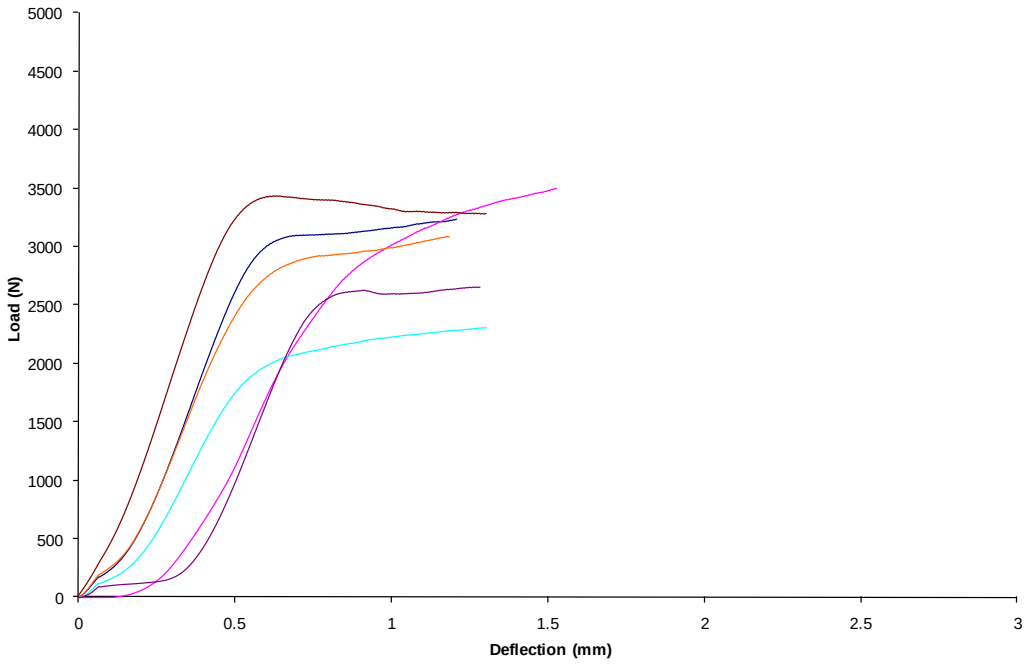

Fig. C88. Dowel Bearing load deflection diagram for OSBO 100^{o}C – 1hr

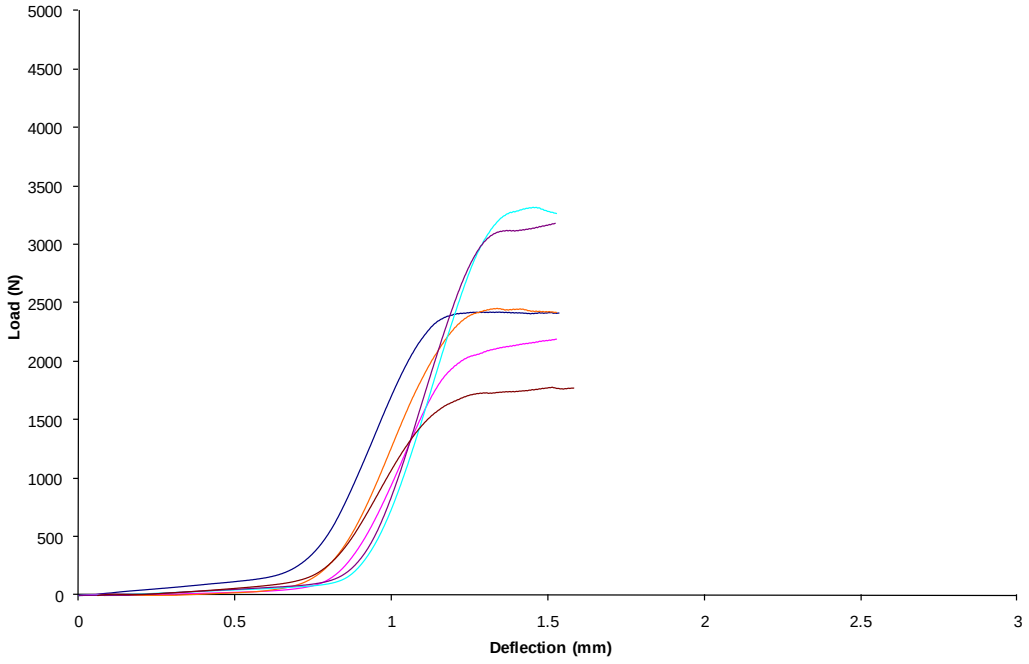

Fig. C89. Dowel Bearing load deflection diagram for OSBO 100^{o}C – 2hr

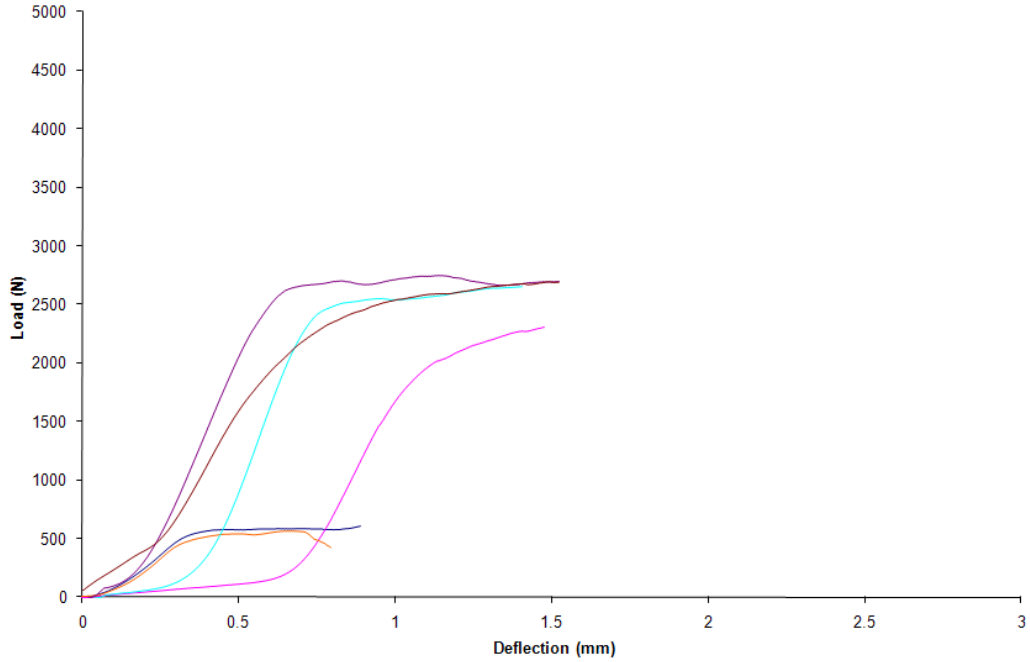

Fig. C90. Dowel Bearing load deflection diagram for OSBO 200^{o}C – 1hr

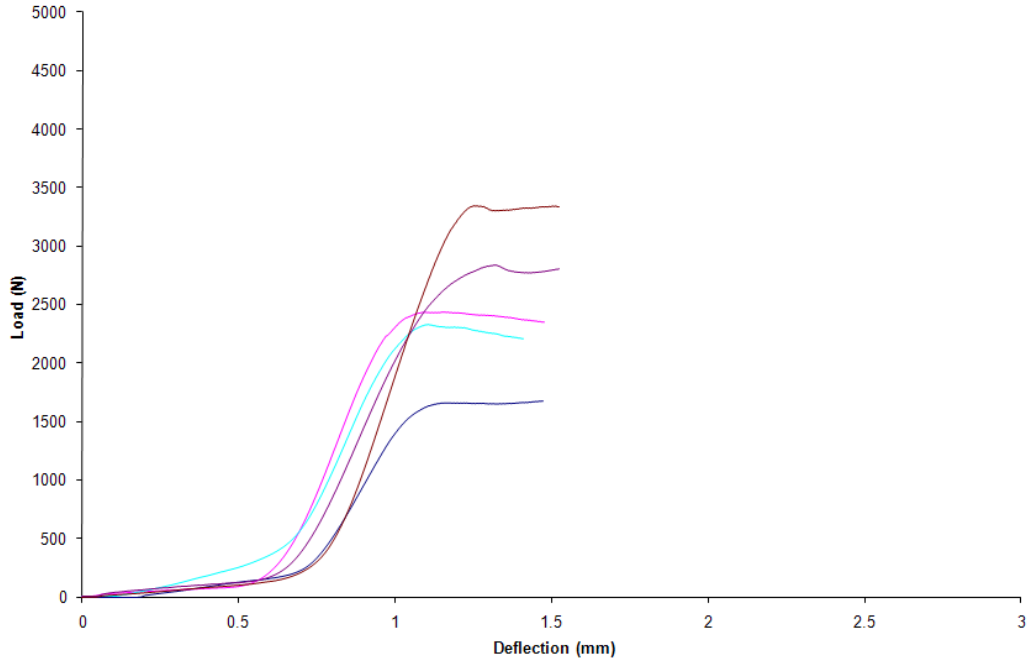

Fig. C91. Dowel Bearing load deflection diagram for OSBO 200^{o}C – 2hr

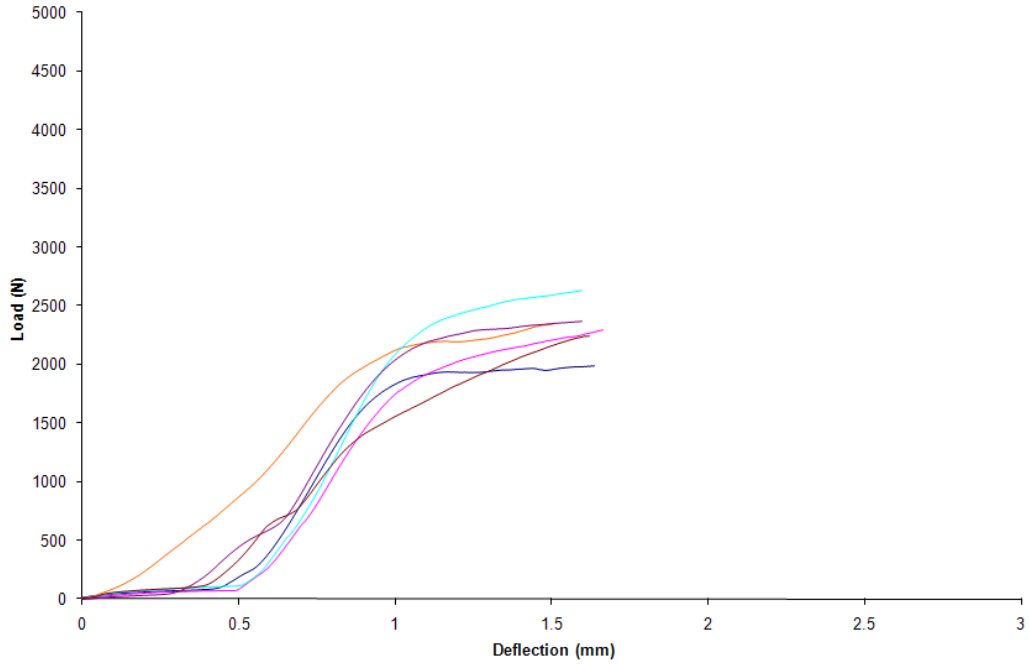

Fig. C92. Dowel Bearing load deflection diagram for PWH Control

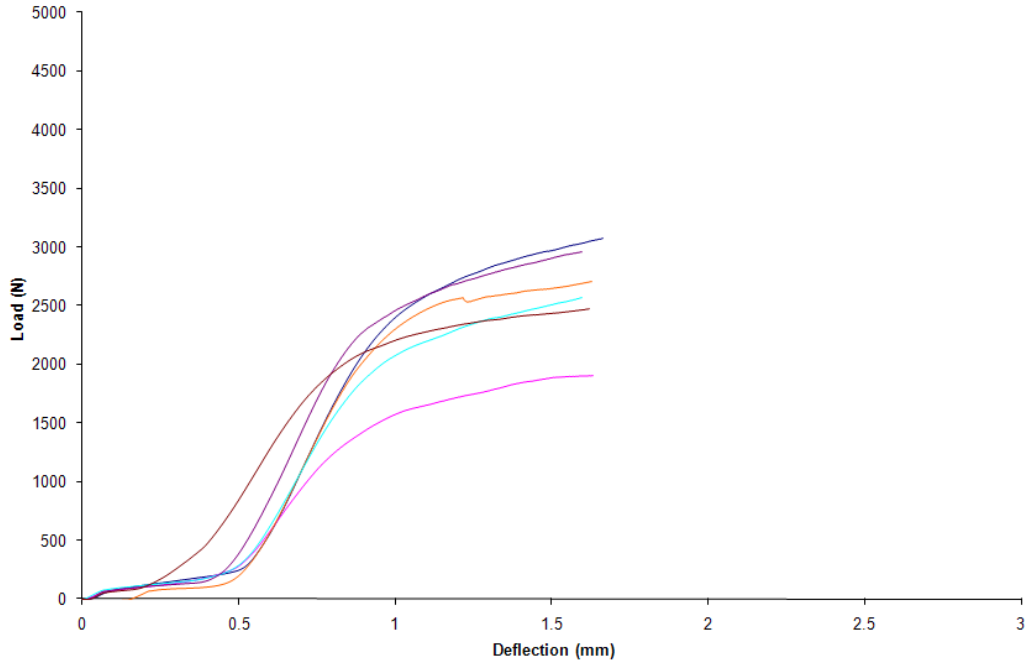

Fig. C93. Dowel Bearing load deflection diagram for PWH 100^{o}C – 1hr

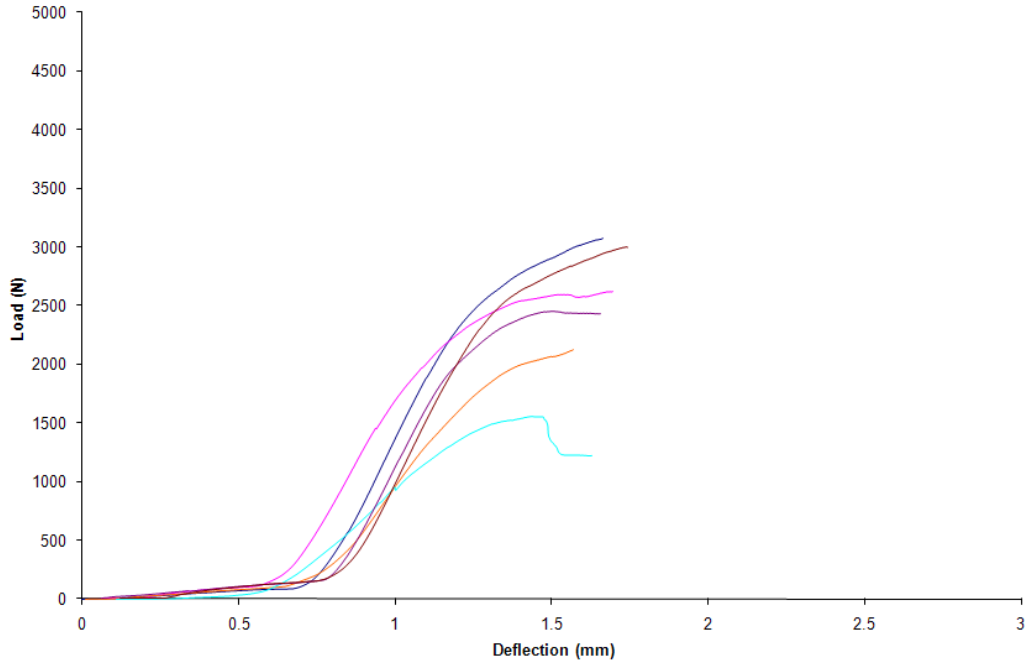

Fig. C94. Dowel Bearing load deflection diagram for PWH 100^{o}C – 2hr

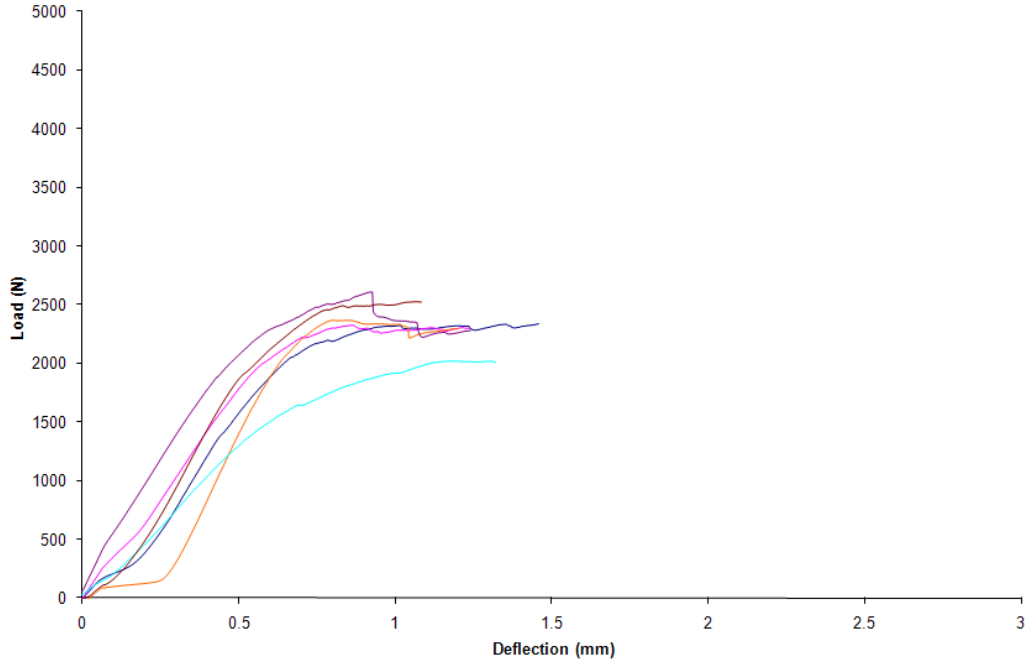

Fig. C95. Dowel Bearing load deflection diagram for PWH 200^{o}C – 1hr

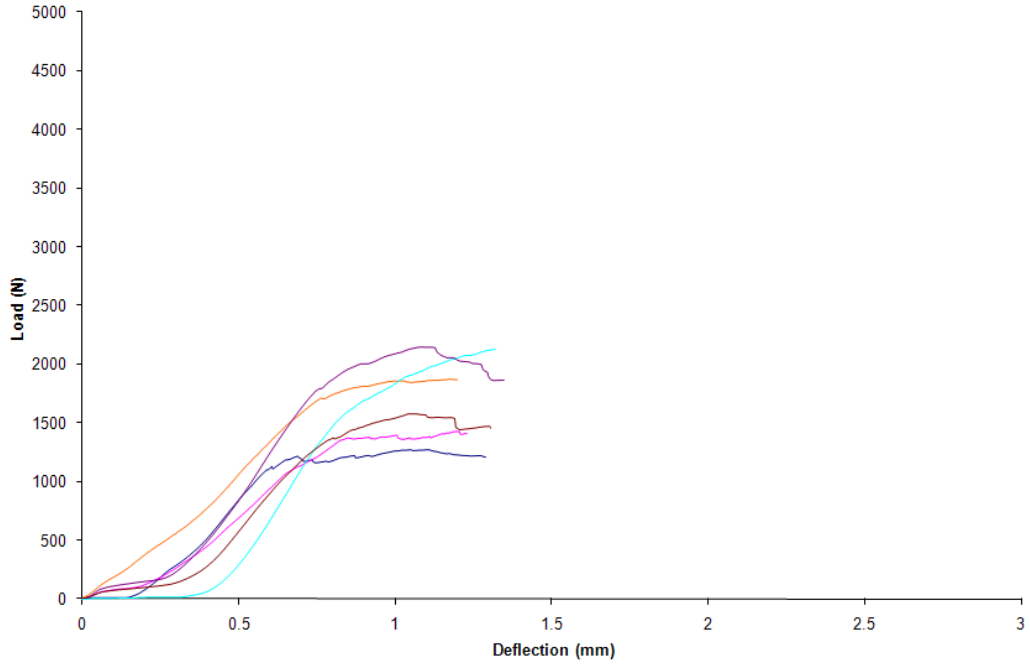

Fig. C96. Dowel Bearing load deflection diagram for PWH 200^{o}C – 2hr

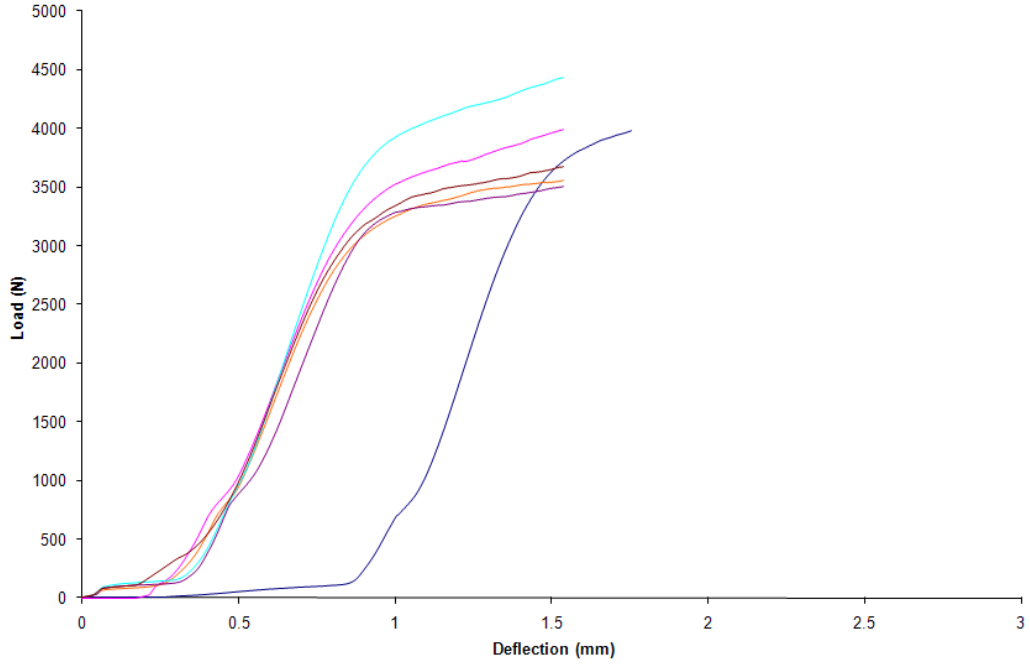

Fig. C97. Dowel Bearing load deflection diagram for PWO Control

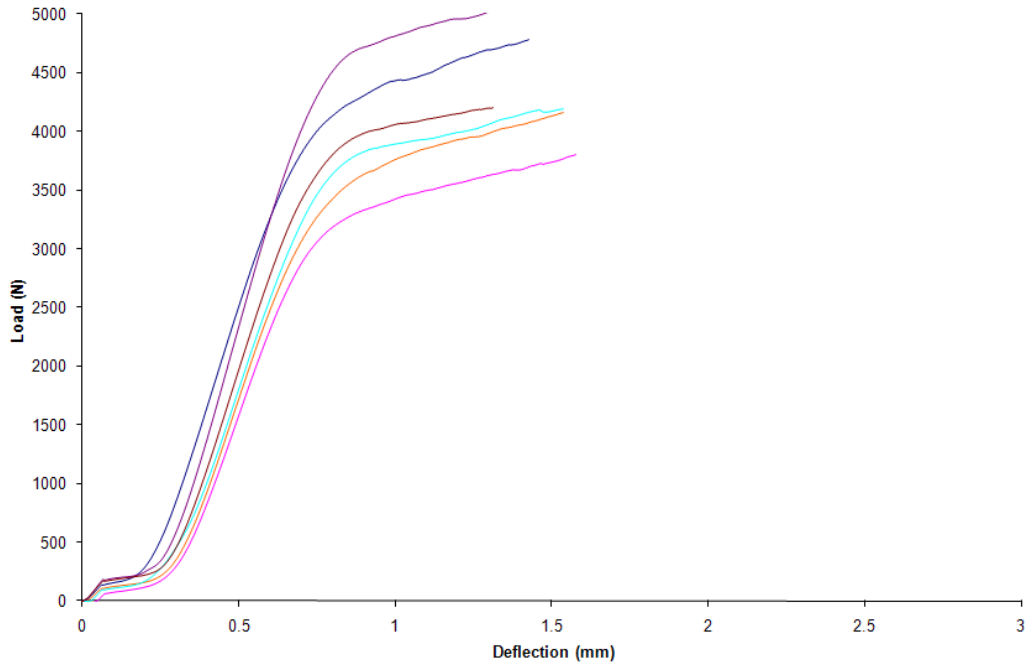

Fig. C98. Dowel Bearing load deflection diagram for PWO 100^{o}C – 1hr

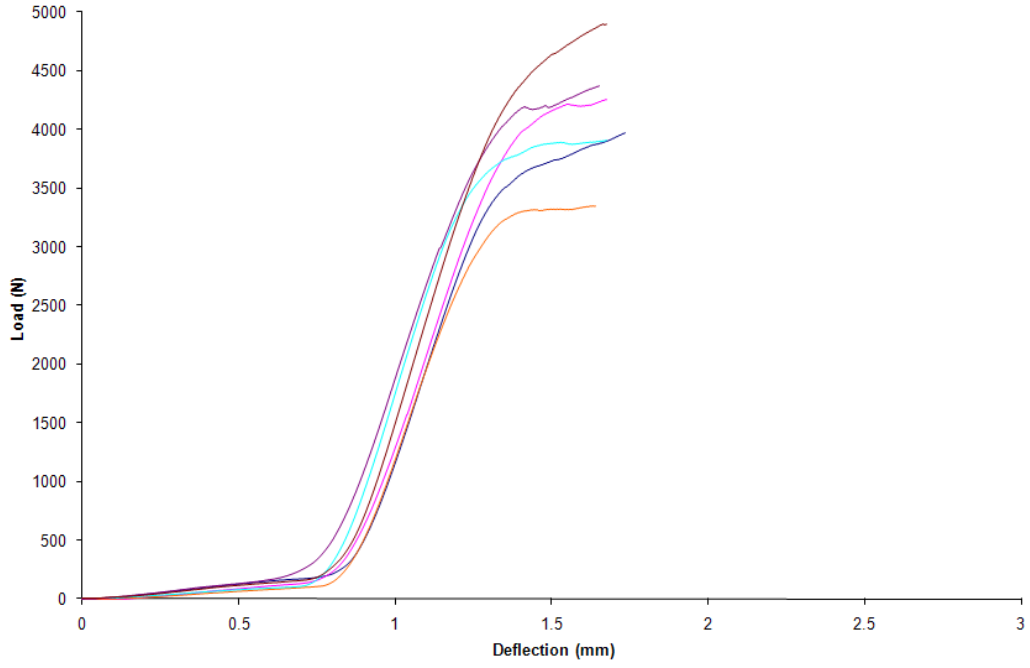

Fig. C99. Dowel Bearing load deflection diagram for PWO 100^{o}C – 2hr

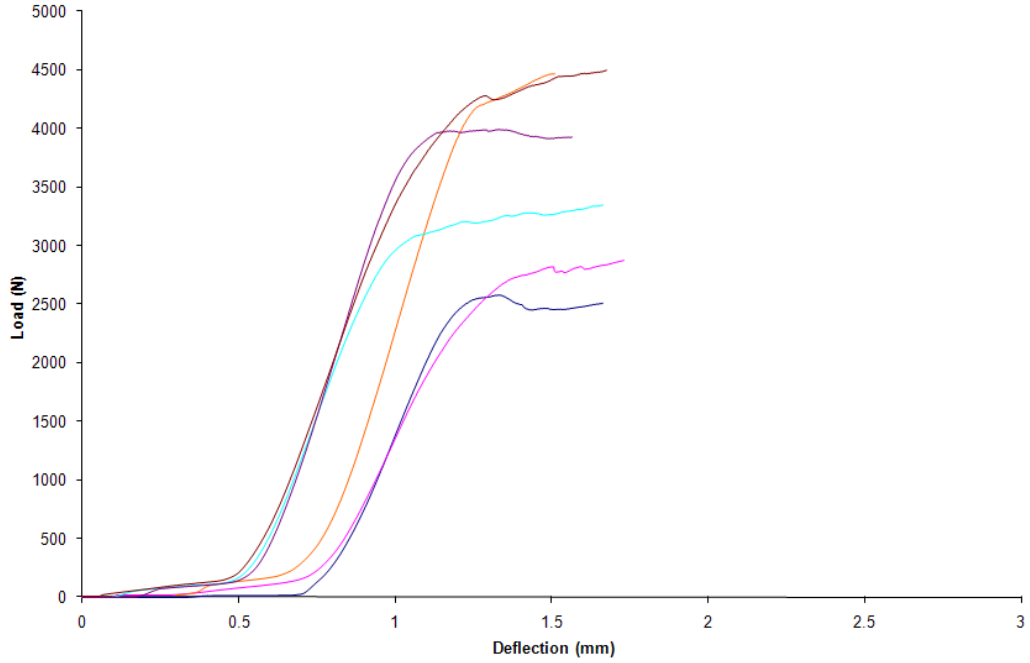

Fig. C100. Dowel Bearing load deflection diagram for PWO 200^{o}C – 1hr

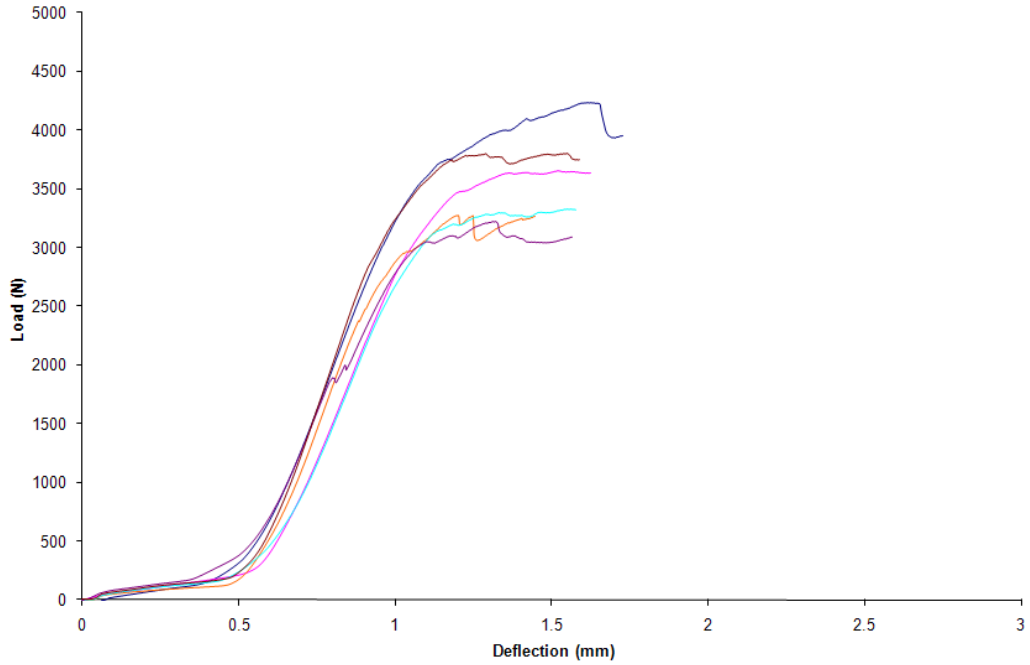

Fig. C101. Dowel Bearing load deflection diagram for PWO 200^{o}C – 2hr

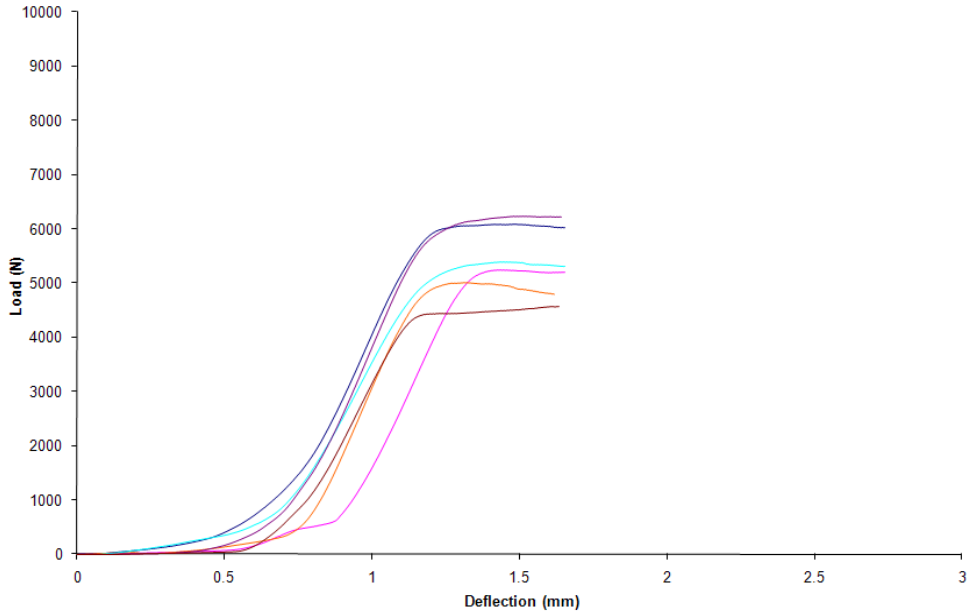

(a) Parallel to grain

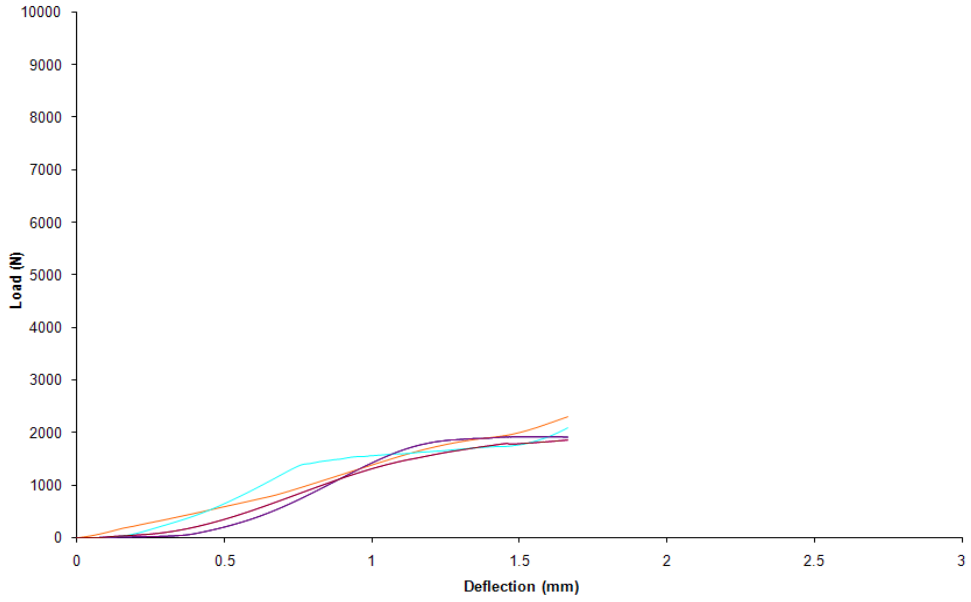

(b) Perpendicular to grain

Fig. C102. Dowel Bearing load deflection diagram for SSL Control

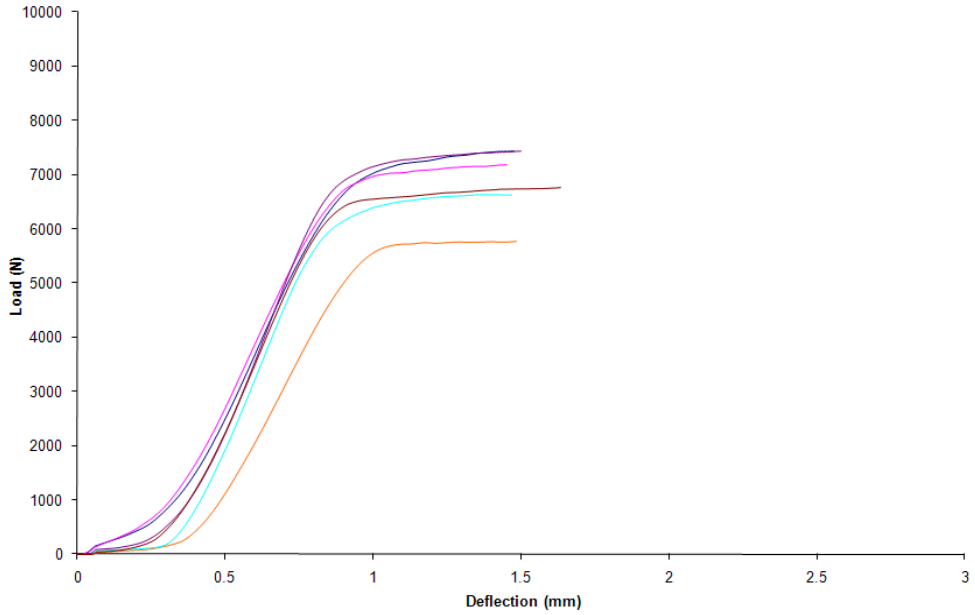

(a) Parallel to grain

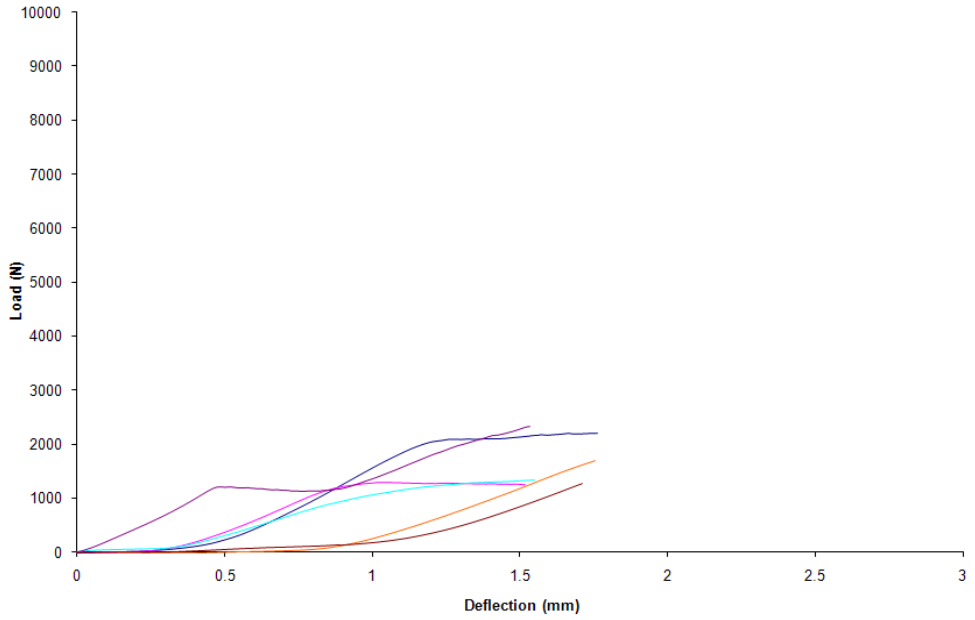

(b) Perpendicular to grain

Fig. C103. Dowel Bearing load deflection diagram for SSL 100^{o}C – 1hr

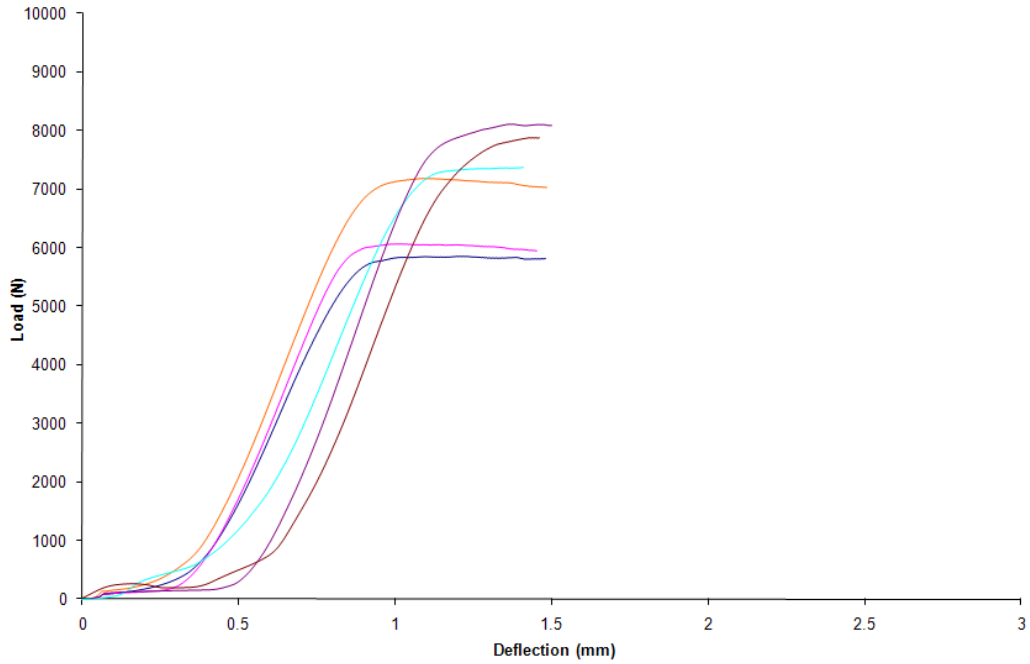

(a) Parallel to grain

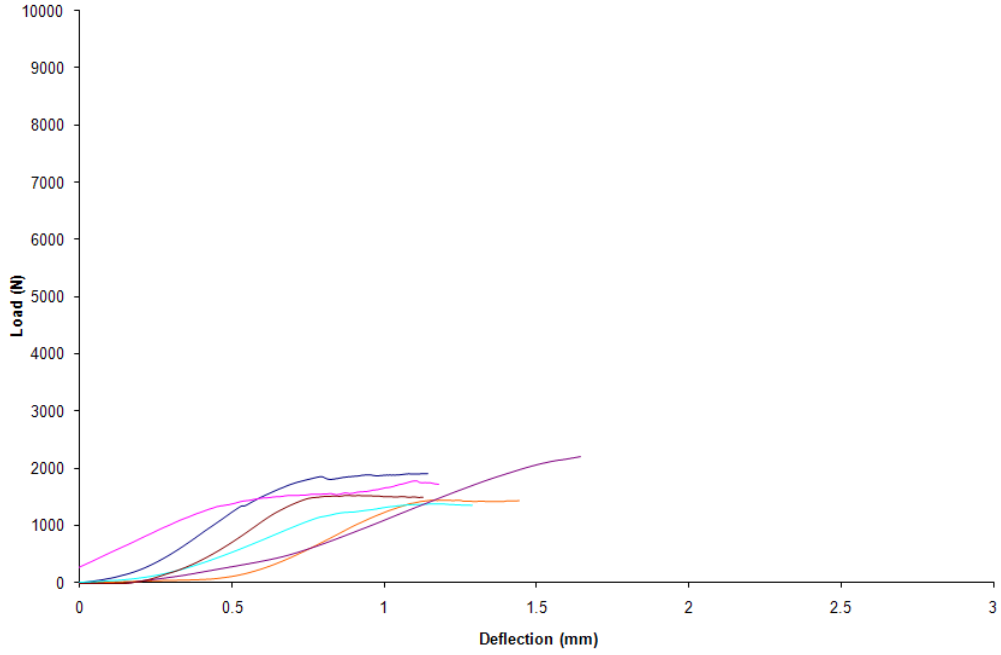

(b) Perpendicular to grain

Fig. C104. Dowel Bearing load deflection diagram for SSL 100^{o}C – 2hr

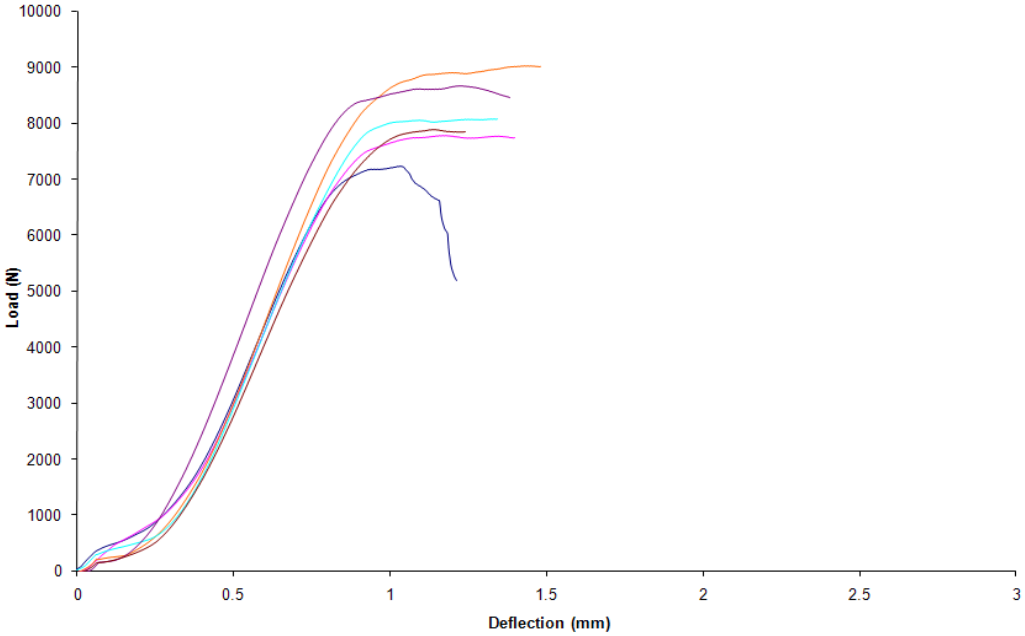

(a) Parallel to grain

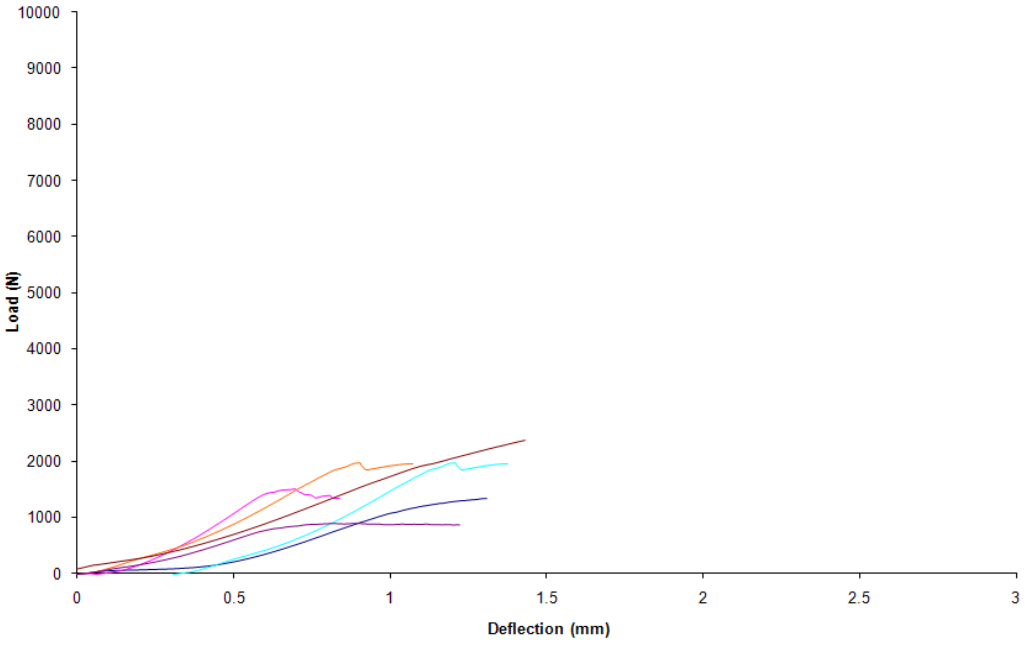

(b) Perpendicular to grain

Fig. C105. Dowel Bearing load deflection diagram for SSL 200^{o}C – 1hr

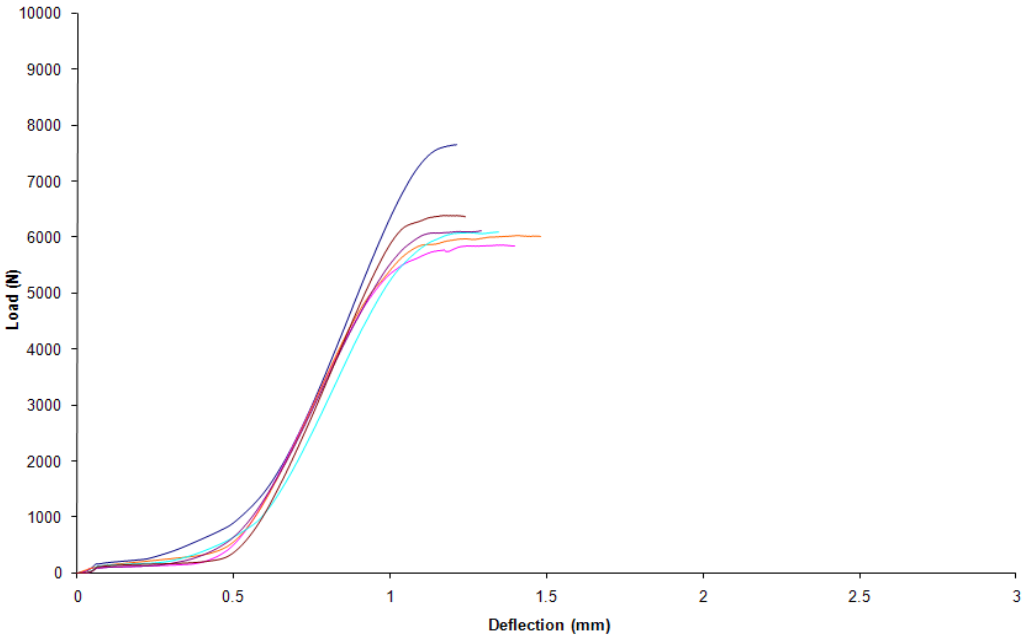

(a) Parallel to grain

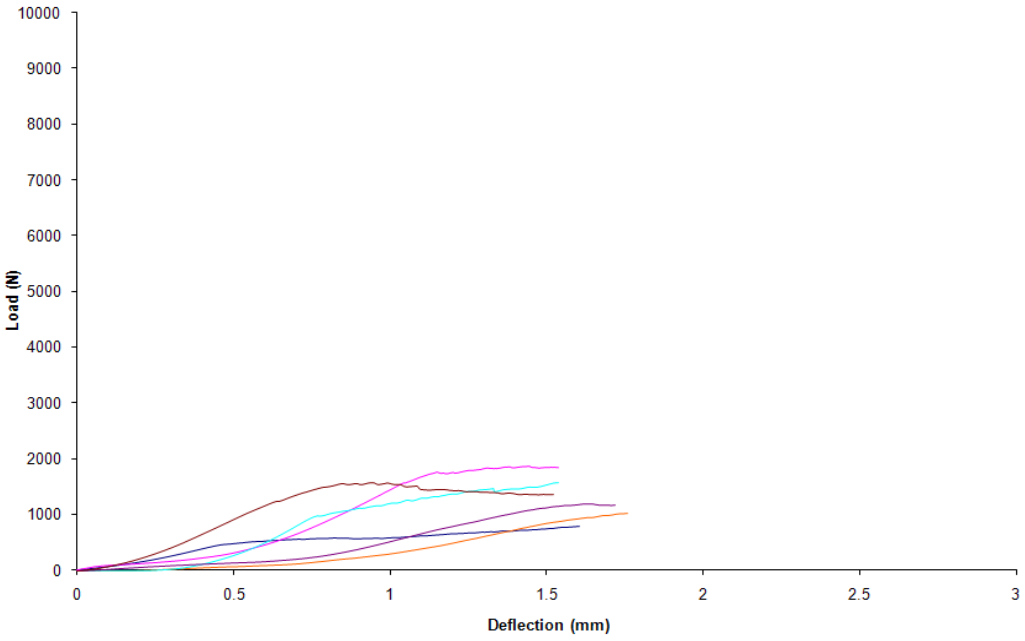

(b) Perpendicular to grain

Fig. C106. Dowel Bearing load deflection diagram for SSL 200^{o}C – 1hr

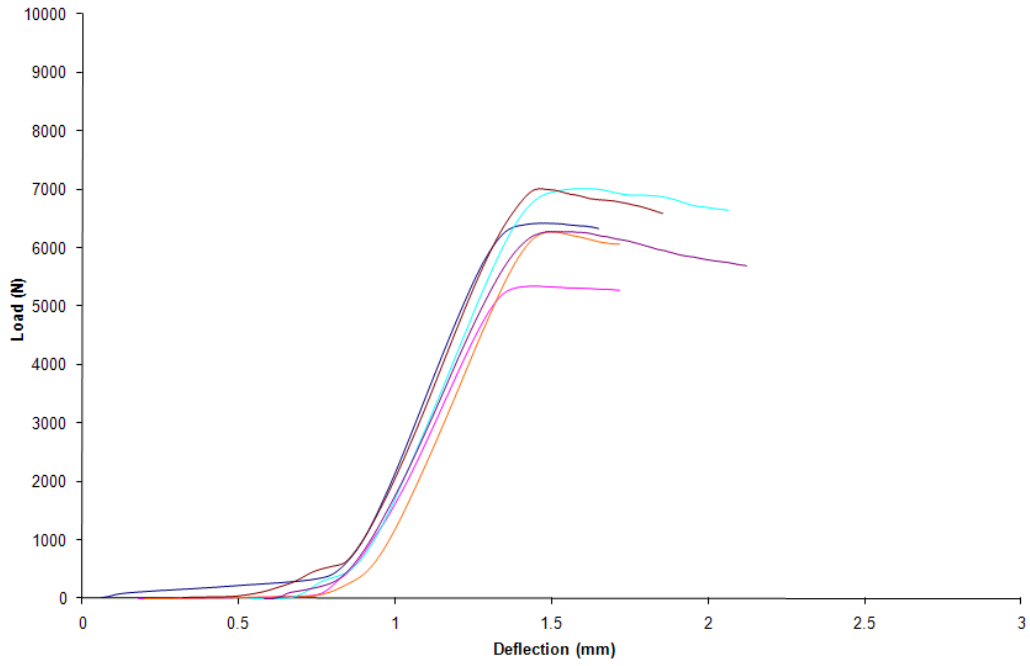

Fig. C107. Dowel Bearing load deflection diagram for LVL Control

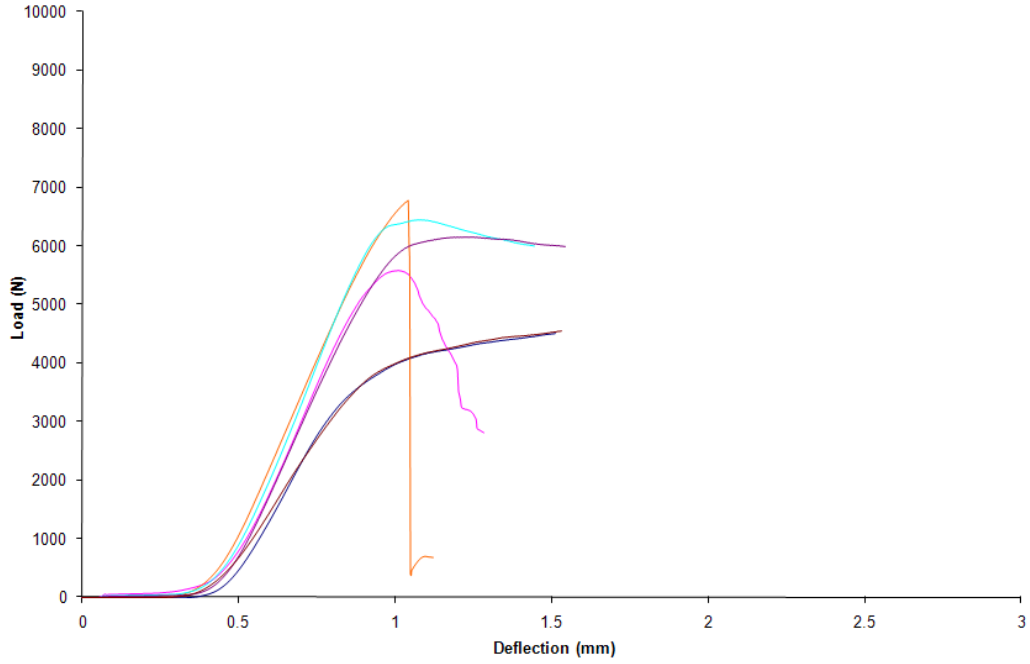

Fig. C108. Dowel Bearing load deflection diagram for LVL 100^{o}C – 1hr

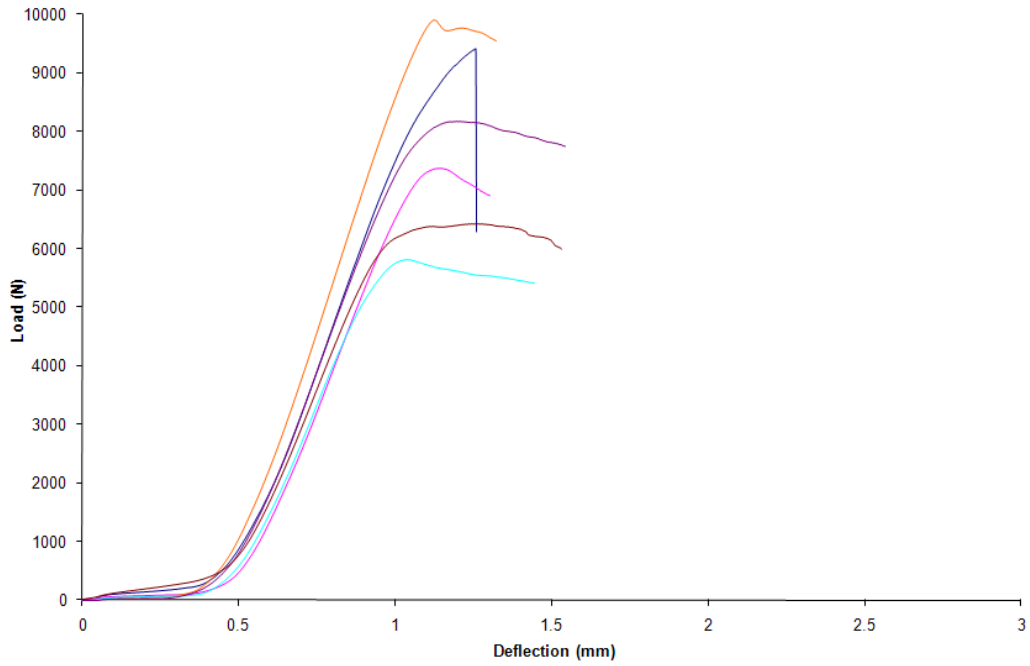

Fig. C109. Dowel Bearing load deflection diagram for LVL 100^{o}C – 2hr

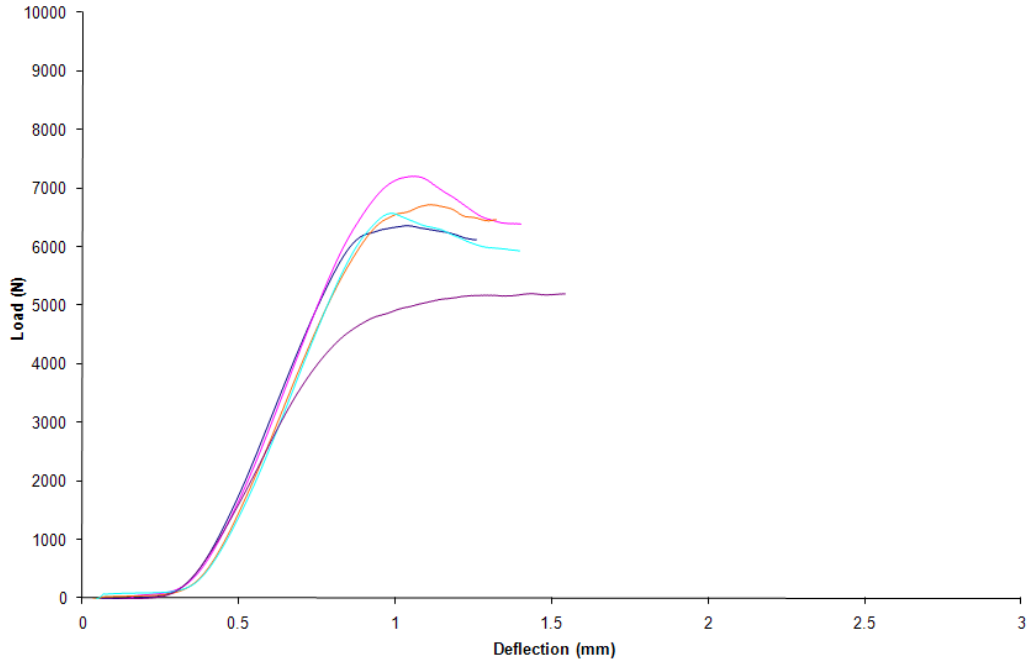

Fig. C110. Dowel Bearing load deflection diagram for LVL 200^{o}C – 1hr

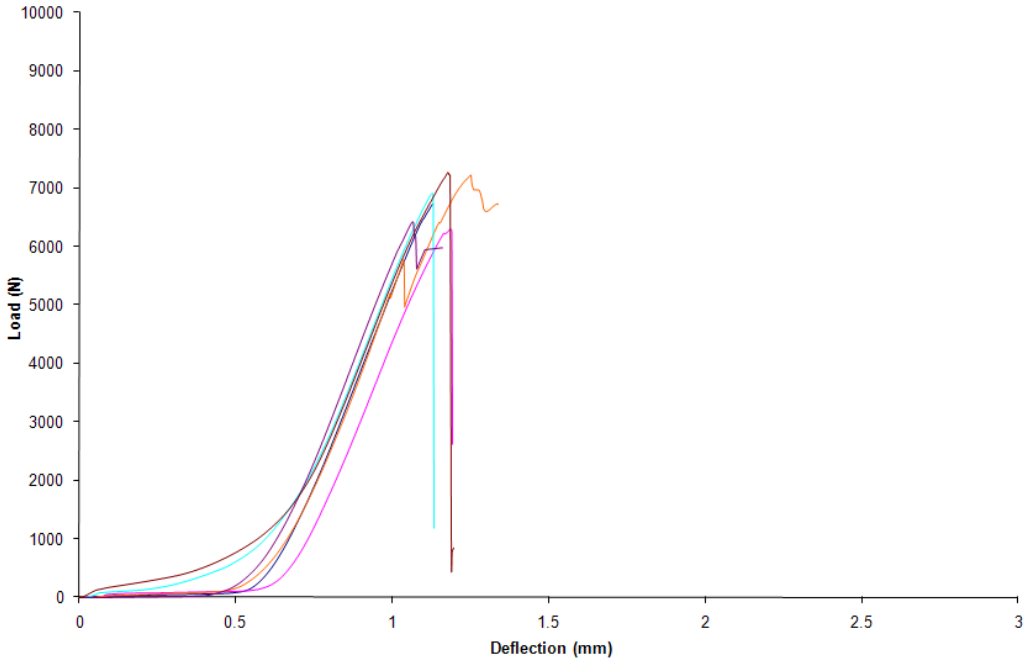

Fig. C111. Dowel Bearing load deflection diagram for LVL 200^{o}C – 2hr

Table C1. Test data for all connection using framing member SSL

Geometry	Edge				Plate			
Treatment	OSBH	OSBO	PWH	PWO	OSBH	OSBO	PWH	PWO
Control	661	682	750	1078	347	539	957	957
	712	778	734	780	446	806	856	856
	565	869	742	622	641	620	709	709
	632	566	548	667	562	740	802	802
	627	572	818	875	357	613	463	368
	865	870	674	830	564	615	712	653
100C1	623	781	482	752	420	584	575	658
	639	632	523	743	563	557	576	659
	650	668	685	856	543	630	483	638
	559	779	529	802	584	606	556	635
	555	612	652	816	439	531	607	809
	635	740	633	788	486	687	409	757
100C2	555	779	502	688	340	533	416	546
	536	702	595	725	645	541	461	438
	522	686	601	769	536	485	432	448
	684	662	593	824	444	416	627	595
	515	666	619	688	428	608	513	487
	562	823	715	696	406	558	609	579
200C1	519	606	659	644	316	576	421	659
	446	669	722	757	350	452	550	753
	403	531	604	697	358	445	220	665
	490	743	635	689	476	574	285	623
	495	655	689	678	390	459	481	609
	488	706	504	776	463	493	388	723
200C2	458	575	474	684	412	424	269	449
	432	474	553	596	512	481	232	387
	436	509	674	565	465	305	383	549
	453	575	546	741	452	501	330	550
	409	524	503	690	302	455	181	302
	614	596	533	634	332	357	358	295

Table C2. Test data for all connection using framing member LVL

Geometry	Edge				Plate			
Treatment	OSBH	OSBO	PWH	PWO	OSBH	OSBO	PWH	PWO
Control	646	710	820	652	297	539	870	638
	780	816	738	606	382	806	778	570
	645	647	765	659	549	620	645	473
	603	834	644	573	513	740	729	535
	594	699	684	625	306	613	480	358
	812	685	651	531	483	697	639	486
100C1	665	575	665	769	420	649	612	460
	512	536	593	636	563	619	768	461
	486	712	733	506	543	630	685	366
	548	833	573	482	584	606	741	379
	536	523	586	635	439	535	809	486
	546	512	546	535	403	687	665	385
100C2	645	736	634	535	525	596	498	519
	670	571	764	643	543	716	417	605
	503	588	596	676	603	572	447	407
	625	579	574	554	435	754	458	517
	548	673	526	639	446	839	549	509
	519	602	569	538	433	654	622	620
200C1	470	409	634	661	498	534	476	474
	486	429	619	717	417	639	355	349
	603	455	435	746	431	472	468	459
	401	615	521	505	458	445	389	321
	432	585	656	618	586	465	315	430
	413	526	623	649	622	439	290	389
200C2	332	457	484	597	412	424	269	449
	396	477	393	410	512	481	232	387
	295	525	318	627	465	305	383	549
	370	494	529	571	452	501	330	550
	312	450	475	359	302	455	181	302
	371	494	436	370	332	357	358	295

Table C3. Dowel Bearing Strength (MPa) Data

Dowel Bering Strength (MPa)							
Treatment	Material						
	SSL	SSL_P	OSBH	OSBO	PWH	PWO	LVL
Control	38	15	46	24	45	41	39
	51	20	43	31	52	42	41
	44	20	36	27	52	38	46
	41	16	32	30	59	47	49
	43	14	36	22	53	37	46
	50	16	32	29	51	38	42
100C1	61	18	39	37	70	40	37
	49	11	41	40	42	44	45
	48	14	37	35	61	53	42
	45	11	27	26	58	54	40
	41	19	44	30	68	44	33
	47	11	38	39	56	50	30
100C2	48	12	26	28	51	45	49
	50	11	38	26	35	35	65
	59	18	39	28	55	41	48
	61	13	44	22	68	56	58
	67	15	31	37	59	52	52
	66	16	43	21	69	42	62
200C1	54	12	43	31	52	27	47
	44	12	42	26	52	30	51
	56	16	28	31	53	47	44
	41	18	39	20	45	35	43
	65	7	44	24	58	42	50
	45	21	30	31	56	48	52
200C2	48	7	25	24	28	44	41
	30	15	20	20	32	38	48
	33	8	22	28	42	34	36
	36	13	26	26	33	35	42
	33	10	33	32	38	34	38
	34	13	26	28	35	40	44

Table C4. ANOVA table for yield strength showing all the significant main effect (R^2 =0.68).

Factors	df	Sum of Sq	F-value	p-value
TR	4	432974.9	20.42	0.0000000
G	1	177807.7	33.53	0.0000002
SM	3	13669.6	8.72	0.0000545
FM	1	38278	7.22	0.0090000
Residual	70	371149.3		

Table C5. Family-wise comparison of treatment for yield strength with lowers (LCL) and upper (UCL) confidence limits. The groups that are significantly different from each other are marked noted as yes.

Group	Estimate	LCL	UCL	Significant
CTRL-100C1hr	58	-15	130	No
CTRL-100C2hr	81	9	153	Yes
CTRL-200C1hr	134	62	206	Yes
CTRL-200C2hr	217	145	289	Yes
100C1hr-100C2hr	23	-49	95	No
100C1hr-200C1hr	77	5	149	Yes
100C1hr-200C2hr	160	88	232	Yes
100C2hr-200C1hr	54	-19	126	No
100C2hr-200C2hr	137	65	209	Yes
200C1hr-200C2hr	83	11	155	Yes

Table C6. Design Load predictions using NDS yield models equations

		Edge					
SSL		Design Load Z (N)	Adjusted Load (N)	Predicted Mode	Observed Load (N)	Observed Mode	Estimation Index
PWH	CTRL	404	646	IIIs	710	IIIs	1.10
	100C1	446	500	IIIs	584	IIIs	1.17
	100C2	447	501	IIIs	604	IIIs	1.21
	200C1	417	467	IIIs	635	IIIs	1.36
	200C2	324	363	IIIs	526	IIIs	1.45
PWO	CTRL	462	739	IV	809	IV	1.10
	100C1	693	776	IV	791	IV	1.02
	100C2	504	565	IV	731	IV	1.30
	200C1	465	521	IV	707	IV	1.36
	200C2	429	481	IV	651	IV	1.36
OSBH	CTRL	348	557	IIIs	678	IIIs	1.22
	100C1	362	405	IIIs	610	IIIs	1.51
	100C2	363	407	IIIs	569	IIIs	1.40
	200C1	360	403	IIIs	474	IIIs	1.18
	200C2	287	321	IIIs	468	Is	1.46
OSBO	CTRL	376	602	IIIs	723	IIIs	1.20
	100C1	443	496	IV	702	IIIs	1.41
	100C2	406	454	IIIs	719	IIIs	1.58
	200C1	402	451	IIIs	652	IIIs	1.45
	200C2	372	416	IIIs	542	IIIs	1.30

Table C5. Continued

		Edge					
LVL		Design Load Z (N)	Adjusted Load (N)	Predicted Mode	Observed Load (N)	Observed Mode	Estimation Index
PWH	CTRL	404	646	IIIs	717	IIIs	1.11
	100C1	423	473	IIIs	616	IIIs	1.30
	100C2	444	497	IIIs	610	IIIs	1.23
	200C1	413	463	IIIs	581	IIIs	1.26
	200C2	333	374	IIIs	437	IIIs	1.17
PWO	CTRL	462	740	IV	608	IV	0.82
	100C1	462	517	IV	593	IV	1.15
	100C2	500	560	IV	597	IV	1.07
	200C1	460	515	IV	649	IV	1.26
	200C2	445	498	IV	489	IV	0.98
OSBH	CTRL	348	558	IIIs	680	IIIs	1.22
	100C1	346	387	IIIs	549	IIIs	1.42
	100C2	361	404	IIIs	585	IIIs	1.45
	200C1	357	400	IIIs	467	IIIs	1.17
	200C2	294	329	IIIs	346	IIIs	1.05
OSBO	CTRL	376	602	IIIs	731	IV	1.21
	100C1	421	472	IV	615	IV	1.30
	100C2	404	453	IIIs	625	IIIs	1.38
	200C1	400	448	IIIs	503	IIIs	1.12
	200C2	380	425	IIIs	484	IIIs	1.14

Table C5. Continued.

PLATE							
SSL		Design Load Z (N)	Adjusted Load (N)	Predicted Mode	Observed Load (N)	Observed Mode	Estimation Index
PWH	CTRL	312	500	IIIs	749	IIIs	1.50
	100C1	314	352	IIIs	534	IIIs	1.52
	100C2	306	342	IIIs	509	IIIs	1.49
	200C1	300	336	IIIs	391	ETO	1.17
	200C2	236	264	IIIs	355	ETO	1.34
PWO	CTRL	345	552	IV	724	IV	1.31
	100C1	328	367	IV	693	IV	1.89
	100C2	327	366	IV	515	IV	1.41
	200C1	324	363	IV	672	IIIs	1.85
	200C2	292	327	IV	309	IV	0.95
OSBO	CTRL	316	506	IIIs	655	IV	1.30
	100C1	312	350	IV	599	IV	1.71
	100C2	303	340	IV	523	IV	1.54
	200C1	307	344	IV	500	IV	1.45
	200C2	278	311	IV	568	IV	1.82
OSBH	CTRL	277	444	IIIs	486	IIIs	1.10
	100C1	267	299	IIIs	506	IIIs	1.70
	100C2	262	293	IIIs	467	IIIs	1.59
	200C1	268	300	IIIs	392	ETO/IIIs	1.31
	200C2	215	241	IIIs	322	ETO	1.34

Appendix D

Fracture and Bond Classification tests

Table D1. Internal Bond Results for OSBH

OSBH									
CTRL		100C1		100C2		200C1		200C2	
Load (N)	IB (kPa)	Load (N)	IB (kPa)	Load (N)	IB (kPa)	Load (N)	IB (kPa)	Load (N)	IB (kPa)
250	97	2012	780	1562	605	1227	475	982	380
1516	587	1628	631	1206	467	704	273	1932	749
715	277	1055	409	1929	748	1814	703	1244	482
1187	460	1438	557	1159	449	681	264	268	104
1405	544	866	336	981	380	987	382	723	280
115	45	1110	430	1020	395	743	288	1814	703
1141	442	1318	511	854	331	1111	430	1212	470
1350	523	1571	609	1755	680	1135	440	1830	709
1228	476	1077	418	705	273	1887	731	1316	510
1420	550	1265	490	1920	744	1178	456	1453	563
142	55	1283	497	830	322	1403	544	506	196
1173	455	978	379	1273	493	1018	395	906	351
721	279	1606	622	1064	412	1031	400	1784	691
144	56	2095	812	780	302	1424	552	1266	491
1225	475	875	339	1267	491	1072	415	1608	623
1296	502	1294	502	894	347	697	270	1396	541
1362	528	1223	474	480	186	2255	874	1082	419
1446	560	1145	444	904	350	780	302	1197	464
1371	531	1009	391	1090	422	1716	665	1202	466
1627	631	1482	574	1530	593	1593	617	1337	518
109	42	1721	667	1415	548	717	278	639	248
1082	419	1430	554	1979	767	1483	575	1045	405
292	113	1975	765	998	387	1806	700	1923	745
696	270	1213	470	1405	544	1880	728	1367	530
1504	583	1375	533	1872	725	68	26	1680	651

ANOVA

Source of Variation	**DF**	**SS**	**MS**	**F**	**P**
Between Groups	4	299087.415	74771.854	2.452	0.050
Residual	120	3658805.126	30490.043		
Total	124	3957892.541			

Note: The only group which was different from one another was the control and 100C1.

Table D2. Internal Bond Results for OSBO

OSBO									
CTRL		100C1		100C2		200C1		200C2	
Load (N)	IB (kPa)	Load (N)	IB (kPa)	Load (N)	IB (kPa)	Load (N)	IB (kPa)	Load (N)	IB (kPa)
805	312	1227	476	850	329	645	250	698	270
754	292	728	282	549	213	341	132	1042	404
1147	444	927	359	1016	394	487	189	949	368
575	223	616	239	884	343	642	249	374	145
858	333	1026	398	827	320	915	355	21	8
815	316	304	118	981	380	352	136	1106	429
377	146	622	241	646	250	809	313	343	133
937	363	1005	389	607	235	710	275	1227	476
912	353	843	326	876	339	628	243	43	17
1112	431	994	385	554	215	400	155	438	170
711	276	1177	456	681	264	625	242	875	339
931	361	806	312	587	227	602	233	694	269
445	172	1503	582	892	345	676	262	759	294
791	307	143	55	992	384	1156	448	979	380
983	381	1074	416	724	281	359	139	772	299
957	371	513	199	1077	417	549	213	1417	549
995	386	609	236	957	371	555	215	411	159
1350	523	420	163	807	313	1089	422	680	263
1026	397	932	361	872	338	535	207	1011	392
793	307	1265	490	932	361	1143	443	598	232
439	170	840	326	679	263	1014	393	817	317
277	108	751	291	765	297	866	336	214	83
516	200	1125	436	976	378	428	166	403	156
572	222	266	103	579	224	984	381	655	254
701	272	1337	518	745	289	346	134	940	364

ANOVA

Source of Variation	**DF**	**SS**	**MS**	**F**	**P**
Between Groups	4	75479.914	18869.978	1.472	0.215
Residual	120	1537912.107	12815.934		
Total	124	1613392.021			

Table D3. Bond Classification Test results for PWH

PWH									
Control		100C1		100C2		200C1		200C2	
Load (N)	% wood failure	Load (N)	% wood failure	Load (N)	% wood failure	Load (N)	% wood failure	Load (N)	% wood failure
751	80	626.9	60	638.1	70	395.6	70	358.9	90
640.1	98	254.5	20	481.7	100	550.2	30	413.8	70
496	95	650.6	80	651.9	40	449.2	40	317.3	30
630.8	100	475	100	649.3	70	402.6	50	395.2	50
671.8	70	601.3	50	499.5	40	478.7	20	345.2	10
641.3	50	714.7	60	555.8	95	614.4	30	324.8	30
596.8	40	440.3	90	622.2	80	409.6	20	230.6	30
769.9	90	292.6	85	391.1	75	431.2	60	366.9	50
469.8	70	289.5	50	431.1	60	552.3	80	441.5	80
455.2	95	340.2	65	368.7	75	427.2	40	376.1	90
794.1	50	521.7	60	397.3	95	420	70	407	80
632.7	90	739.8	30	533.4	85	329.4	60	395.4	5
859	75	388.6	100	528.1	40	411.9	50	470.4	30
574.1	100	350.7	20	562	90	409.3	70	363.1	40
580.8	90	780.1	100	723.4	90	476.8	100	600.3	20
718.3	85	441.2	85	627.3	60	349.1	80	340.4	30
996.9	40	454.3	60	685.3	50	390	20	305.6	70
675.2	70	541.4	80	534.3	55	235	70	371.7	25
815.2	85	678	75	567.6	50	527.9	50	138.6	50
523.8	60	469.2	40	443.1	20	510.6	10	390	80
312.3	0	588.9	90	633.7	60	437	50	458.3	95
867.3	90	407.1	95	615.2	30	302.9	5	300.5	25
536.1	40	365.1	95	573.9	60	321.3	100	307.8	40
830.4	85	596.3	75	573	60	367.3	10	336.4	30
803.4	100	402.3	97	388.1	65	306.7	15	236.6	100

ANOVA:

Source of Variation	**DF**	**SS**	**MS**	**F**	**P**
Between Groups	4	1392442.770	348110.693	23.904	<0.001
Residual	120	1747520.366	14562.670		
Total	124	3139963.136			

Table D4. Bond Classification Test results for PWO

PWO									
Control		100C1		100C2		200C1		200C2	
Load (N)	% wood Failure	Load (N)	%wood failure	Load (N)	%wood failure	Load (N)	%wood failure	Load (N)	%wood failure
1342.6	90	1090.3	50	935.7	50	905.8	10	570.9	5
1687.3	62	1069.8	40	891.3	60	1464	60	380.8	10
1258.4	62	1350.8	30	1428.1	30	509.4	5	448.1	5
995.4	40	1009.7	25	1033.4	90	732.8	10	401.8	25
2080.9	50	1111.2	50	919	30	1164	75	496.9	10
1626.6	100	626.8	70	910.9	50	854.2	50	606.2	0
1222.1	20	1047.8	35	958.8	50	1324	50	645.2	5
925.8	65	946.2	70	1014.1	80	727	30	461.3	20
1122.6	40	923.8	75	1460.5	90	959.9	50	587.5	20
1249.2	50	1579	50	1253.3	55	815.8	50	660.8	90
1519.1	70	1079.6	95	1118	55	702.2	15	493.9	20
1041.3	50	1300.6	85	1277.9	95	655.6	40	529.1	10
1506.3	40	1175.9	90	1288.6	20	662.9	45	368.7	5
978.5	60	1207.2	30	622.1	55	711.6	40	514.4	10
1082.4	80	1125.6	20	1294	20	914.4	80	518.4	5
1363.8	30	1298	50	1305.6	50	695.6	30	902	15
1808.1	70	989.6	70	1538.7	95	610	95	569.3	20
1096.9	70	1487.5	70	1761.3	60	582.2	60	431.6	0
900.0	30	1034.4	50	1590.1	55	1782	40	537.2	40
625.6	40	664.5	20	1113.5	35	1155	45	560.6	5
1040.8	60	611.3	50	958.5	10	1001	30	611.3	60
1035.1	70	1059.6	50	1277.2	65	650.8	15	849.9	20
1747.5	65	1082.6	20	1053.5	40	528.3	70	397.8	25
1085.4	40	1060.6	60	925.5	60	520.9	35	687.9	5
1060.4	65	1506	75	911.9	20	980.7	30	592	35

ANOVA

Source of Variation	**DF**	**SS**	**MS**	**F**	**P**
Between Groups	4	7895706.667	1973926.667	27.152	<0.001
Residual	120	8723928.493	72699.404		
Total	124	16619635.160			

Table D5. G_{SS} (N/m) for various materials and treatment

	Treatment									
Marerial	Control		100C1		100C2		200C1		200C2	
SSL	170	220	160	175	200	230	250	160	90	130
OSH	950	950	1500	1500	1000	1600	550	1050	1250	850
LVL	1100	1000	500	500	650	900	1000	850	250	200
PWO	1100	1250	1090	1120	600	800	600	300	220	400
PWH	911	900	750	500	850	500	600		450	
OSO	400	360	300	200	325	355	421	340	150	200

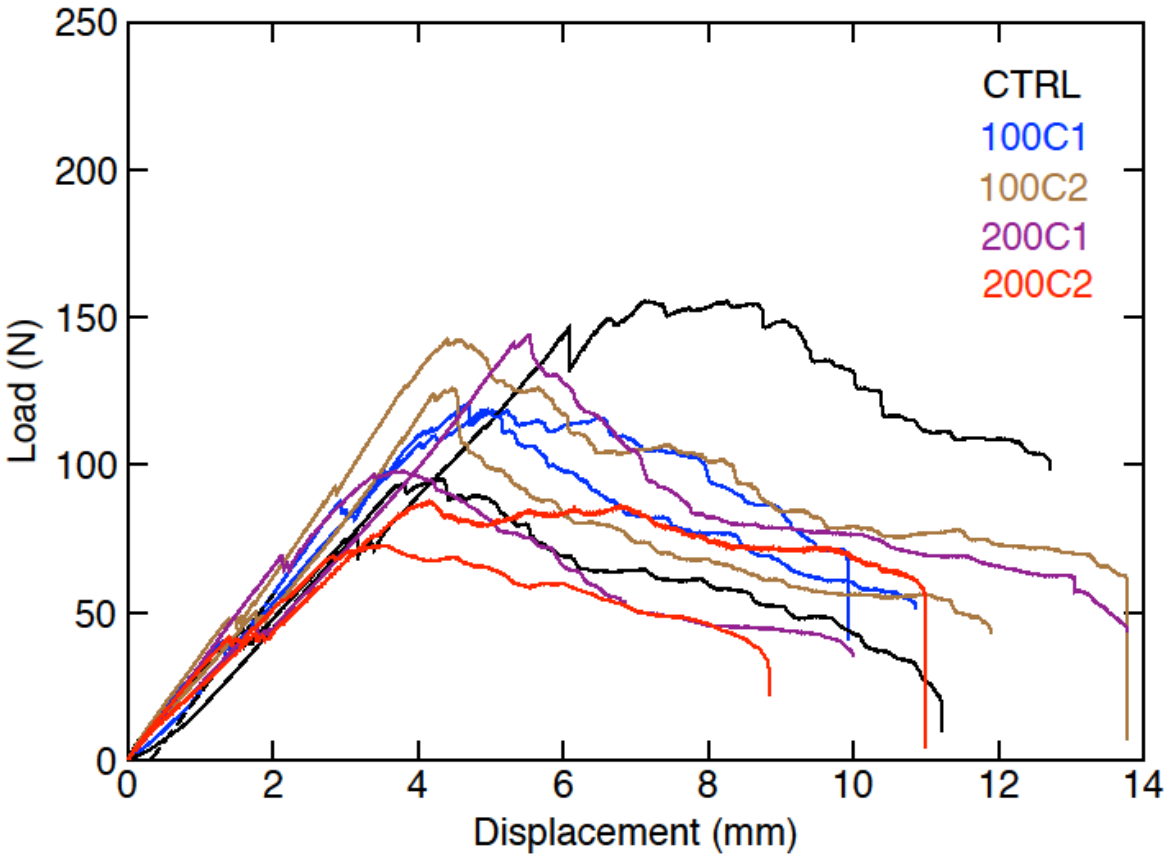

Fig. D1. Load Deflection Curves in fracture test for SSL

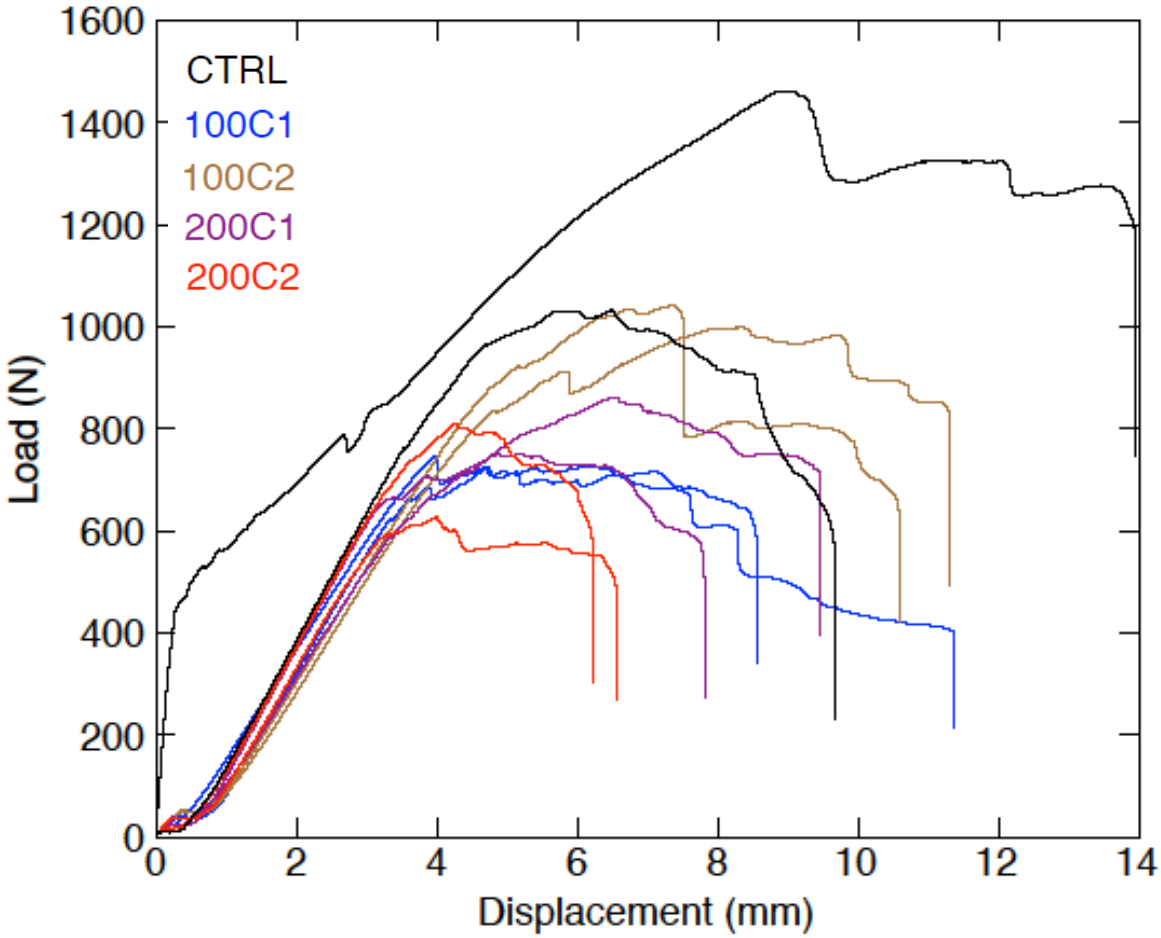

Fig. D2. Load Deflection curves in fracture tests for LVL

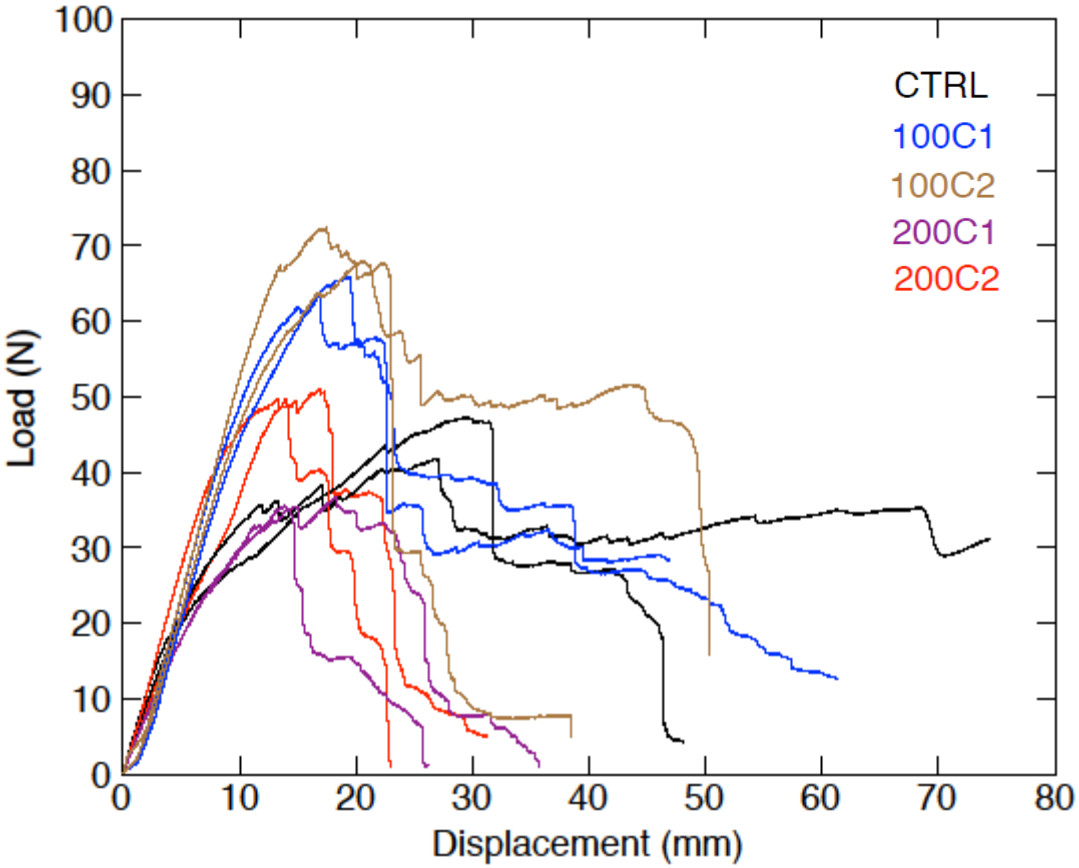

Fig. D3. Load Deflection Curves in fracture for OSBH

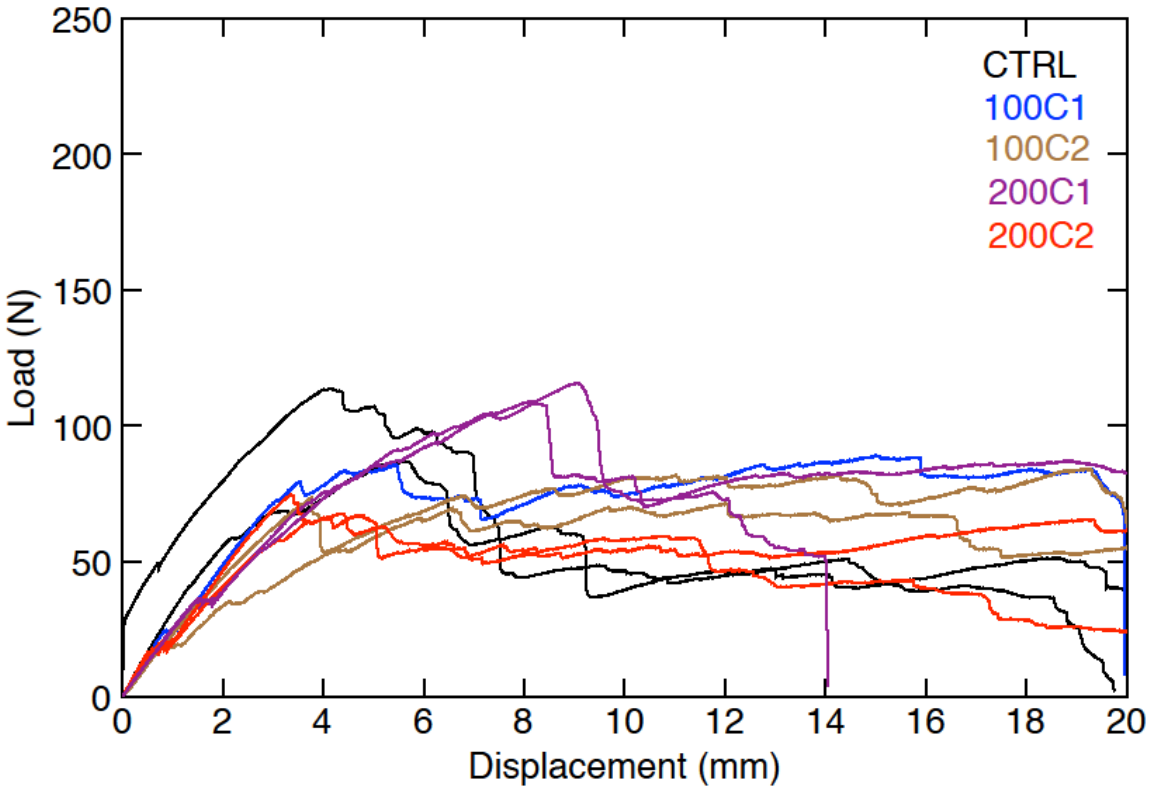

Fig. D4. Load deflection curves in fracture tests for OSBO

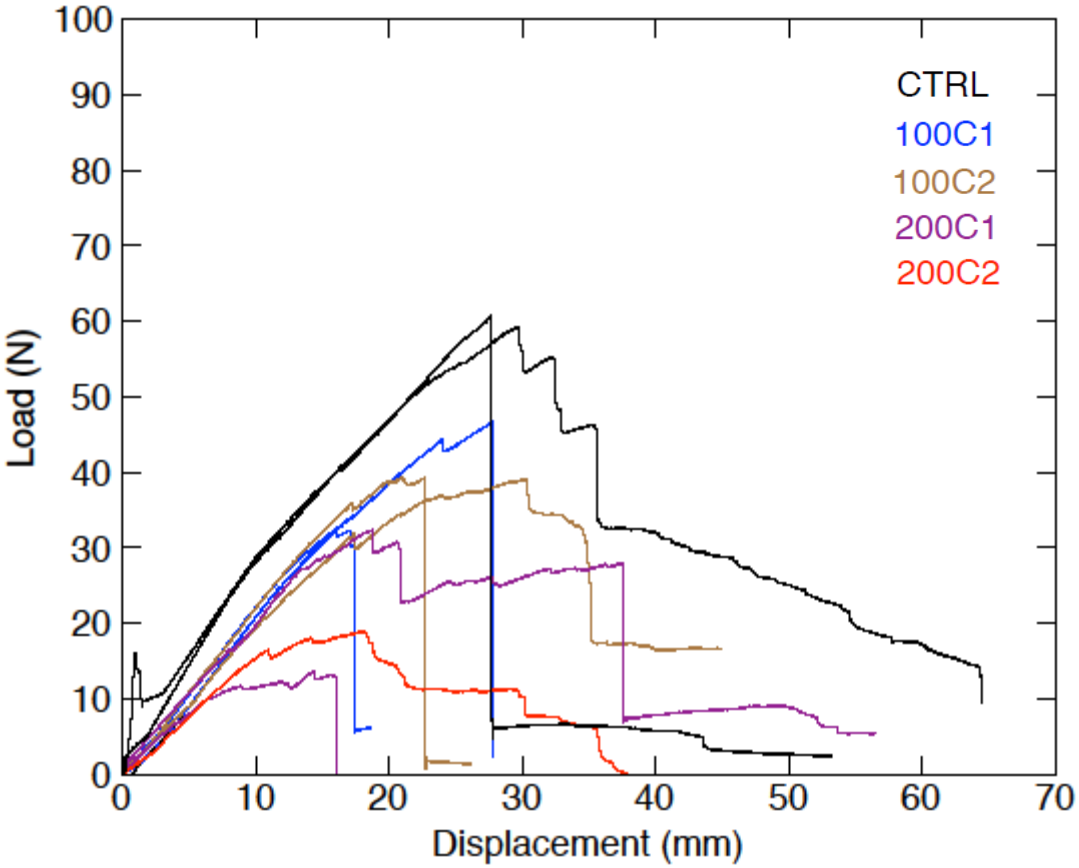

Fig. D5. Load Deflection Curves in fracture for PWH

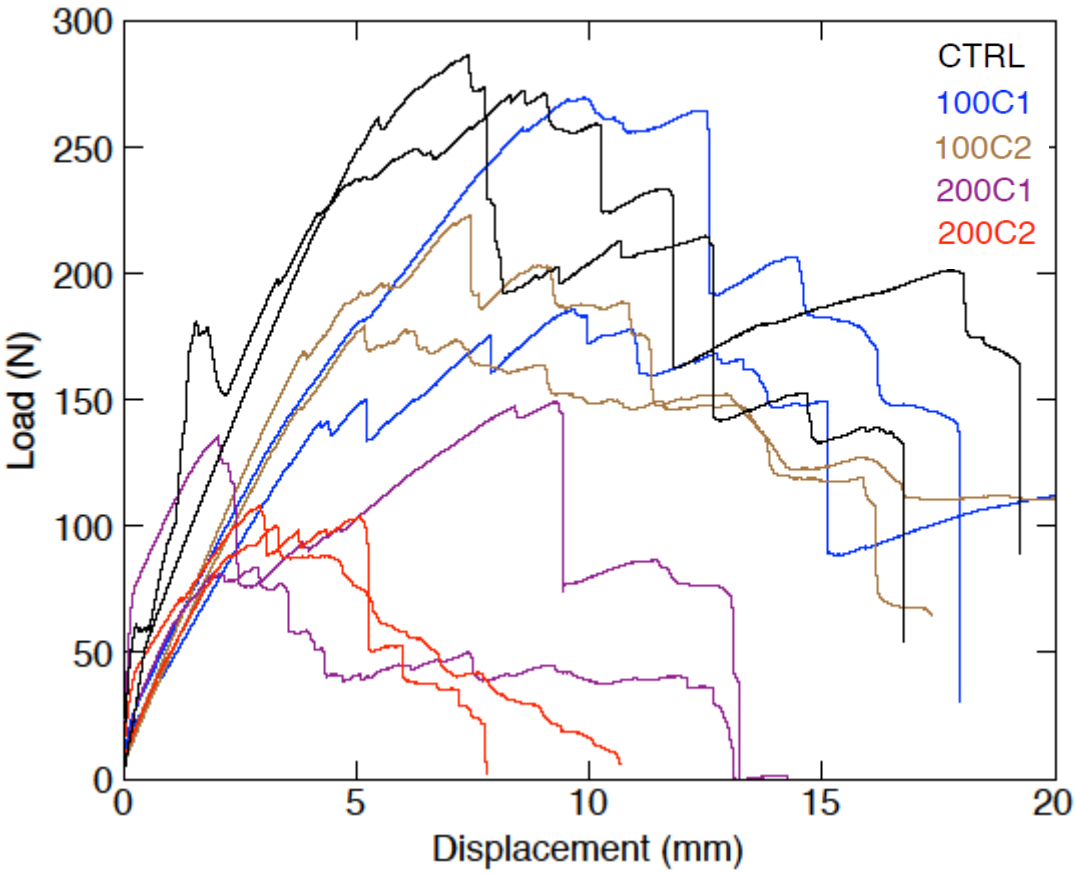

Fig. D6. Load Deflection Curves in fracture for PWO